

**Enhancing Precision Oncology: Preclinical
Assessment of Individual Drug Treatment
Susceptibility Using Patient-Derived 3D Microtumor
and Immune Cell Co-cultures**

Dissertation

der Mathematisch-Naturwissenschaftlichen Fakultät
der Eberhard Karls Universität Tübingen
zur Erlangung des Grades eines
Doktors der Naturwissenschaften
(Dr. rer. nat.)

vorgelegt von
M.Sc. Nicole Anderle
aus Sindelfingen

Tübingen
2023

Gedruckt mit Genehmigung der Mathematisch-Naturwissenschaftlichen Fakultät der
Eberhard Karls Universität Tübingen.

Tag der mündlichen Qualifikation:

09.02.2024

Dekan:

Prof. Dr. Thilo Stehle

1. Berichterstatter/-in:

Prof. Dr. Katja Schenke-Layland

2. Berichterstatter/-in:

Prof. Dr. Sara Yvonne Brucker

3. Berichterstatter/-in:

Prof. Dr. Peter Loskill

4. Berichterstatter/-in:

Prof. Dr. Robert David

Table of Contents

Abstract	I
Zusammenfassung	III
Abbreviations	V
List of Figures	VIII
List of Tables	VIII
List of Publications	IX
Contributions	XI
1 Introduction	1
1.1 The Battle Against Cancer: Are We Winning?	1
1.2 Unmasking Cancer's Complexity: A Journey Through Tumoral Heterogeneity	3
1.3 Decoding the Tumor Terrain: Exploring the Intricate Landscape of the Tumor Microenvironment	5
1.4 Tumor Heterogeneity and Therapy Resistance – a Call for Precision Oncology	9
1.4.1 Anti-cancer Therapies	9
1.4.2 Therapy Resistance Unmasked: Cracking the Code to Healing	13
1.4.3 Personalizing Oncology: Promise for a Cure?	14
1.4.4 Preclinical Models and Functional Analyses	16
2 Objectives of the Thesis	19
3 Results I: Unraveling the Heterogeneity of Ovarian Cancer: 3D Microtumors Provide Personalized Insights into Treatment Vulnerabilities	21
3.1 Comprehensive Analysis of PDM and TIL from Freshly Resected Ovarian Cancer Tissue	22
3.1.1 Promising Isolation Success and Viability Rates of Ovarian Cancer Microtumors	22
3.1.2 Unveiled Histopathologic and Immunohistochemical Tumor Profiles in Microtumors	23
3.1.3 In-depth RPPA-based Signaling Pathway Profiling of Ovarian Cancer PDM	24
3.1.4 Expanding and Phenotyping of Tumor-infiltrating, Autologous Lymphocytes	25
3.2 Individual Tumor Vulnerability to Chemo-, Targeted and Immunotherapy of PDM and PDM-TIL Co-Cultures	26
3.2.1 Examining Drug Sensitivity in Ovarian Cancer PDM for Identification of Patient-individual Treatment Responses	26
3.2.2 Specific Molecular Protein Signatures Dictate Responsiveness to Chemotherapy in Ovarian Cancer PDM	29
3.2.3 Drug Mode-of-Action Analysis in Carboplatin Treated OvCa-PDM	29
4 Results II: Harnessing Breast Cancer Patient-Derived Microtumors for Protein-Based Stratification and Functional Validation of Individualized Drug Treatment	31
4.1 In-Depth Profiling of PDM Derived from Surgically Resected BC Specimens for <i>Ex Vivo</i> BC Modeling	32
4.1.1 Isolation of Viable PDM and TIL from a Heterogeneous Population of BC Patients	32

4.1.2 Preservation of Breast Cancer Subtype Specific Histopathologic Features in NST and ILC PDM	33
4.1.3 Verification of Preserved Extracellular Matrix Composition Using Movat's Pentachrome Staining of Breast Cancer PDM and PTT.	34
4.1.4 Immunohistochemical Analysis of BC-Specific Tumor Markers and Stromal Cell Markers	35
4.1.5 DigiWest®-based Protein Profiling of BC-PDM Captures Disease Heterogeneity and Reveals Conserved Primary Molecular Tumor Profiles	37
4.1.6 Microtumors Illustrate the Pronounced Intertumoral Heterogeneity of Corresponding Primary Breast Cancer	38
4.1.7 Protein Profiling Data of TNBC-PDM	39
4.2 Combination of Protein Profiling and Functional Drug Testing Elucidates Treatment Response Mechanisms	40
4.2.1 Patient-specific Treatment Responses of <i>Ex Vivo</i> BC-PDM towards Hormonal Therapy, Chemotherapy and Targeted Therapy	40
4.2.2 Identification of Treatment Resistance and Sensitivity Marker Panels Using BC-PDM	40
5 Results III: Immune Suppression in Glioblastoma: Microtumors as a Valuable Tool for Immunotherapy Evaluation	43
5.1 Targeting the TME by CSF1R-Blockade in Glioblastoma-PDM Co-Cultured With and Without Autologous TILs	44
5.2 Characterization of Affected TIL Populations by Flow Cytometry	45
6 General Discussion and Conclusion	46
6.1 Establishment of Viable PDM and Autologous TIL: Efficacy of the Isolation Procedure	47
6.2 The Reproducibility of the Primary Tumor	48
6.2.1 Histopathologic and Immunohistologic Correlation: Preservation of Histopathological and Subtype Specific Features of the Primary Tumor in PDM	48
6.2.2 Modeling the Tumor Microenvironment	50
6.2.3 Molecular PDM Profiles: The Heterogeneity of Signal Transduction	53
6.3 Utility of PDM and TIL in Functional Testing of Therapeutic Modalities	55
6.4 Proteomic Analysis of PDM to Allow for the Identification of Patient-Specific Treatment Susceptibilities and Markers of Therapy-Response	58
6.5 Conclusion	62
References	65
Declaration	94
Appendix	95

Abstract

Despite 50 years of dedicated efforts in the "War on Cancer", the results achieved in treating cancer have been regrettably unsatisfactory. Particularly challenging are tumors characterized by high inter- and intratumoral heterogeneity and an advanced stage. These complex cancers, including ovarian, breast and glioblastoma, present significant barriers to effective therapy. Nowadays, the healthcare system faces two major issues in cancer treatment: low success rates of newly approved anti-cancer drugs and ineffective treatments leading to adverse side effects in patients. The ability to pre-select and pre-determine individualized treatment options prior to clinical care, as envisioned in the context of personalized medicine, could thus facilitate therapeutic decision making and ultimately improve patient outcomes. This will require advances in the implementation of diagnostic tools for detailed and accurate patient stratification, and advances in the prediction of patient-specific response to treatment. To enable preclinical validation of anticancer drug efficacy in personalized cancer therapy, it is crucial to develop patient-derived tumor models that mirror the unique complexity of individual tumors and account for the significant impact of the tumor microenvironment and cellular diversity on drug response. In this context, this study presents an *ex vivo* tumor model composed of patient-derived 3D microtumors (PDM) and autologous tumor-infiltrating immune cells (TIL), established and validated for ovarian cancer, breast cancer, and glioblastoma patients to identify individual tumor vulnerabilities. By limited digestion and subsequent culture in defined media, PDM and TIL cultures with high viability were successfully generated from freshly resected primary tumors. In-depth histopathological, immunohistological and proteomic analyses of PDM and corresponding primary tumors were performed and confirmed conserved subtype-specific histology, tumor marker expression, and the presence of tumor microenvironment components including extracellular matrix, tumor-associated macrophages, and cancer-associated fibroblasts. Comprehensive protein profiling of up to 200 analytes was performed in both primary tumors and PDM with limited sample material using advanced technologies such as DigiWest® and RPPA immunoassay screening. The preservation of molecular protein signatures and molecular heterogeneity of the original primary tumor in PDM was confirmed by the extensive protein data obtained. Functional drug testing on PDM and PDM-TIL co-cultures with small molecules, chemotherapeutic as well as immunotherapeutic agents identified tumors sensitive to specific treatments, enabling the prediction of individual therapeutic

susceptibility. In combination with the collected proteomic data, molecular protein signatures have been revealed that correlate with treatment response and resistance. The clinical utility of PDM is based on their efficient isolation process, time-saving generation, ethical non-animal culture conditions, patient-specific representation, preservation of tissue architecture and TME components, and compatibility with various downstream readout technologies. These combined advantages position PDM as a powerful and versatile tool that holds great promise for drug mode of action analyses, biomarker identification and personalized therapeutic sensitivity prediction.

Zusammenfassung

Trotz 50 Jahre langer, intensiver Bemühungen im "Krieg gegen den Krebs" sind die Ergebnisse der Krebstherapie leider immer noch unbefriedigend. Insbesondere Tumoren, die durch eine hohe inter- und intratumorale Heterogenität und ein fortgeschrittenes Stadium gekennzeichnet sind, stellen eine besondere Herausforderung dar. Dazu zählen unter anderem das Ovarial- und das Mammakarzinom sowie das Glioblastom. Heutzutage sieht sich das Gesundheitssystem bei der Behandlung von Krebs mit zwei Hauptproblemen konfrontiert: geringe Erfolgsraten neu zugelassener Krebsmedikamente und unwirksame Behandlungen, die zu unerwünschten Nebenwirkungen führen. Die Möglichkeit, Behandlungsoptionen vor der Behandlung vorauszuwählen und zu definieren, wie es in der personalisierten Medizin angestrebt wird, könnte daher die therapeutische Entscheidungsfindung erleichtern und letztlich die Überlebensraten verbessern. Dies erfordert Fortschritte bei der Einführung von Diagnoseinstrumenten, die eine detaillierte und genaue Stratifizierung der Patienten ermöglichen, sowie Fortschritte bei der Vorhersage des patientenspezifischen Ansprechens auf die Behandlung. Für die präklinische Validierung effektiver, personalisierter Therapien ist es unerlässlich patienten-abgeleitete Tumormodelle zu entwickeln, die die einzigartige Komplexität individueller Tumoren widerspiegeln und den signifikanten Einfluss der Mikroumgebung des Tumors und der zellulären Diversität auf das Therapieansprechen berücksichtigen. In diesem Zusammenhang wird in dieser Studie ein neues *ex vivo* Tumormodell vorgestellt, das aus patientenabgeleiteten 3D Mikrotumoren (PDM) und autologen tumorinfiltrierenden Immunzellen (TIL) besteht, das für Patienten mit Ovarialkarzinom, Mammakarzinom und Glioblastom etabliert und validiert wurde, um individuelle Tumorschwachstellen zu identifizieren. Aus frisch resezierten Primärtumoren konnten durch eingeschränkten Gewebeaufschluss und anschließende Kultivierung in definierten Medien erfolgreich PDM- und TIL-Kulturen mit hoher Viabilität gewonnen werden. Ausführliche histopathologische, immunhistologische und Proteomanalysen von PDM und den entsprechenden Primärtumoren bestätigten die tumorspezifische Histologie, die Expression von Tumormarkern und die Präsenz von Komponenten des Tumormikromilieus, wie eine extrazelluläre Matrix, tumor-assoziierte Makrophagen und tumor-assoziierte Fibroblasten. Mit fortschrittlichen Technologien wie DigiWest® und RPPA-Immunoassay-Screenings wurden umfassende Proteinprofile mit bis zu 200 Analyten

in Primärtumoren und PDM mit begrenztem Probenmaterial erstellt. Die umfangreichen Proteindaten bestätigten den Erhalt der molekularen Proteinsignaturen des ursprünglichen Primärtumors im PDM. Funktionelle Wirkstofftests an PDM- und PDM-TIL-Kokulturen mit „small molecules“, chemotherapeutischen und immuntherapeutischen Wirkstoffen konnten therapieempfindliche Tumoren identifizieren und damit eine individuelle Therapiesensitivität vorhersagen. Kombiniert mit den gesammelten Proteomdaten wurden molekulare Proteinsignaturen ermittelt, die mit Therapieansprechen und -resistenz korrelieren. Zusammenfassend lässt sich sagen, dass der klinische Nutzen von PDMs auf dem effizienten Isolierungsprozess, der zeitsparenden Herstellung, den ethischen Bedingungen einer tierfreien Kultur, der patientennahen Abbildung, der Erhaltung der ursprünglichen Gewebearchitektur und der TME-Komponenten sowie der Kompatibilität mit verschiedenen nachgeschalteten Analysen beruht. Diese Vorteile machen PDM zu einem vielversprechenden und vielseitigen Werkzeug zur Analyse der Arzneimittelwirkung, zur Identifizierung von Biomarkern und zur personalisierten Vorhersage des Therapieansprechens.

Abbreviations

2D	two-dimensional
3D	three-dimensional
AFI	averaged fluorescent intensity
BC	breast cancer
C1QBP	complement C1q binding protein
CA125	cancer antigen 125
CAFs	cancer-associated fibroblasts
CAR T	chimeric antigen receptor T cell
CD	cluster of differentiation
CK	cytokeratin
CML	chronic myelogenous leukemia
CNS	central nervous system
CPI	checkpoint inhibitor
CRC	colorectal cancer
CSF-1	colony-stimulating factor 1
CSF1R	colony-stimulating factor 1 receptor
CTL	cytotoxic T lymphocytes
DAB	3,3'-Diaminobenzidin
DCIS	ductal carcinoma <i>in situ</i>
DMSO	dimethyl sulfoxide
DNA	deoxyribonucleic acid
DTX	docetaxel
EC	endothelial cells
ECM	extracellular matrix
EGF	epidermal growth factor
EGFR	epidermal growth factor receptor
EMT	epithelial-to-mesenchymal transition
ER α	estrogen receptor α
ERBB2	receptor tyrosine-protein kinase erbB-2
ERK	extracellular signal-regulated kinase
FACS	fluorescence activated cell sorter
FAP α	fibroblast-associated protein α
FC	fold change
FDA	Food and Drug Administration
FFPE	formalin-fixed paraffin-embedded
FIGO	International Federation of Gynecology and Obstetrics
GAGs	glycosaminoglycans
GBM	glioblastoma
GIST	gastrointestinal stromal tumor
H&E	hematoxylin and eosin
HCL	hierarchical clustering
HER2	human epidermal growth factor receptor 2

HIF	hypoxia-inducible factor
HGSC	high-grade serous carcinoma
HMW	high molecular weight
HR	hormone receptor
ICB	immune checkpoint blockade
ICI	immune checkpoint inhibitors
IDC	invasive ductal carcinoma
IFN	interferon
IgG	immunoglobulin G
IHC	immunohistochemistry
ILC	invasive lobular carcinoma
IRS	immunoreactive score
ITH	intratumoral heterogeneity
LCIS	lobular carcinoma in-situ
mAb	monoclonal antibody
MAPK	mitogen-activated protein kinase
MDCS	myeloid-derived suppressor cell
MFS	metastasis-free survival
MMP	metalloproteinase
mTOR	mammalian target of rapamycin
NCI	national cancer institute
NFI	protein-normalized, background-corrected mean fluorescence intensity
NFκB	nuclear factor kappa B
NGS	next-generation sequencing
Non-R	non-responder
NST	invasive ductal carcinoma of no special type
OS	overall survival
OvCa	ovarian cancer
P _r	pearson correlation coefficient
PAB	palbociclib
PD-1	programmed cell death protein 1
PD-L1	programmed cell death 1 ligand 1
PD-L2	programmed cell death 1 ligand 1
PDGF	platelet-derived growth factor
PDM	patient-derived microtumor
PDO	patient-derived organoid
PDX	patient-derived xenograft
PGs	proteoglycans
PgR	progesterone receptor
PI3K	phosphatidylinositol 3-kinase
PTEN	phosphatase and tensin homolog
PTT	primary tumor tissue
PTX	paclitaxel
RFU	relative fluorescent units
R	responder

RNA	ribonucleic acid
RPPA	reverse-phase protein array
RTK	receptor tyrosine kinases
SERM	selective estrogen receptor modulator
SMI	small molecule inhibitor
STAT	signal transducer and activator of transcription
TAM	tamoxifen
Th1	type 1 T helper cell
TIL	tumor infiltrating lymphocytes
TGF- β	transforming growth factor beta
TME	tumor microenvironment
TNBC	triple-negative breast cancer
TP53	cellular tumour antigen p53
TR	treatment-to-control ratio
T _{reg} S	regulatory T cells
VEGF	vascular endothelial growth factor
WT1	Wilms Tumor 1

List of Figures

Figure 1: Global health estimates 2019.	2
Figure 2. “Cold” non T cell inflamed versus “hot” T cell inflamed tumors.	8
Figure 3. Immunotherapy clinical trials: Total number and active trials.	13
Figure 4. Expression of resistance markers for CDK4/6 inhibition in OvCa PDM.	28
Figure 5. Overview of precision oncology.	64

List of Tables

Table 1. FDA-approved targeted therapies for breast cancer, ovarian cancer and glioblastoma	11
---	----

List of Publications

Accepted Manuscripts

1. Przystal JM, Becker H, Canjuga D, Tsiami F, **Anderle N**, Keller A-L, Pohl A, Ries CH, Schmittnaegel M, Korinetska N, Koch M, Schittenhelm J, Tatagiba M, Schmees C, Beck SC, Tabatabai G. *Targeting CSF1R Alone or in Combination with PD-1 in Experimental Glioma*. *Cancers*. 2021; 13(10):2400.
<https://doi.org/10.3390/cancers13102400>
2. Walter, B., Canjuga, D., Yüz, S.G., Ghosh, M., Bozko, P., Przystal, J.M., Govindarajan, P., **Anderle, N.**, Keller, A.-L., Tatagiba, M., Schenke-Layland, K., Rammensee, H.-G., Stevanovic, S., Malek, N.P., Schmees, C. and Tabatabai, G., *Argyris F Treatment-Induced Vulnerabilities Lead to a Novel Combination Therapy in Experimental Glioma*. *Adv. Therap.* 2021; 4:2100078. <https://doi.org/10.1002/adtp.202100078>
3. Keller, A.-L., Binner, A., Breitmeyer, R., Vogel, S., **Anderle, N.**, Rothbauer, U., Schenke-Layland, K., Schmees, C. *Generation and characterization of the human induced pluripotent stem cell line NMI010-A from peripheral blood mononuclear cells of a healthy 49-year old male individual*. *Stem Cell Research*. 2021; 54:102427. <https://doi.org/10.1016/j.scr.2021.102427>
4. **Anderle N**, Koch A, Gierke B, Keller A-L, Staebler A, Hartkopf A, Brucker SY, Pawlak M, Schenke-Layland K, Schmees C. *A Platform of Patient-Derived Microtumors Identifies Individual Treatment Responses and Therapeutic Vulnerabilities in Ovarian Cancer*. *Cancers*. 2022; 14(12):2895.
<https://doi.org/10.3390/cancers14122895>
5. Erne E, **Anderle N**, Schmees C, Stenzl A. *Patient-derived microtumors: Potential for therapeutic response prediction-a case study*. *Urologie*. 2022; 61[2]:739-744.
<https://doi.org/10.1007/s00120-022-01851-2>

6. Ruoff F, Kersten N, **Anderle N**, Jerbi S, Stahl A, Koch A, Staebler A, Hartkopf A, Brucker SY, Hahn M, Schenke-Layland K, Schmees C, Templin MF. *Protein Profiling of Breast Carcinomas Reveals Expression of Immune-Suppressive Factors and Signatures Relevant for Patient Outcome*. *Cancers*. 2022; 14[2]:4542. <https://doi.org/10.3390/cancers14184542>
7. Dairkee SH, Moore DH, Luciani MG, **Anderle, N.**, Gerona R, Ky K, Torres SM, Marshall PV, Goodson III WH. *Reduction of daily-use parabens and phthalates reverses accumulation of cancer-associated phenotypes within disease-free breast tissue of study subjects*. *Chemosphere*. 2023; 322:138014. <https://doi.org/10.1016/j.chemosphere.2023.138014>

Submitted Manuscripts

8. Keller, A.-L., **Anderle, N.**, Schrenk, M., Greis, D., Binner, A., Visser, D., Göpfert J., Koch A., Weiss M., Brucker, S., Schenke-Layland K., Schmees C. *Co-cultures of iPSC-derived Mammary-like Organoids and Patient-derived Microtumors Model Invasive Behavior of Breast Cancer ex vivo*. PREPRINT (Version 1) available at Research Square. 2023; <https://doi.org/10.21203/rs.3.rs-2408179/v1>

Under Review

9. **Anderle, N.**, Schäfer-Ruoff, F., Staebler, A., Kersten, N., Koch, A., Önder, C., Keller, A-L., Liebscher, S., Hartkopf, A., Hahn, M., Templin, M., Brucker, SY., Schenke-Layland, K., Schmees, C. *Breast cancer patient-derived microtumors resemble tumor heterogeneity and enable protein-based stratification and functional validation of individualized drug treatment*. (PREPRINT available at Research Square, 2023; <https://doi.org/10.21203/rs.3.rs-2781727/v1>) - **Accepted**: 28 July 2023; **Published**: 18 August 2023: *J Exp Clin Cancer Res* **42**, 210 (2023). <https://doi.org/10.1186/s13046-023-02782-2>

Contributions

No.	Accepted	No. of authors	Position of candidate in list of authors	Scientific ideas by the candidate (%)	Data generation by the candidate (%)	Analysis and Interpretation by the candidate (%)	Paper writing by the candidate (%)
1	Yes	16	5	20	20	10	10
2	Yes	16	8	15	10	5	5
3	Yes	8	5	15	10	5	5
4	Yes	10	1	60	70	75	75
5	Yes	4	2	20	5	10	10
6	Yes	13	3	20	10	15	5
7	Yes	9	4	15	15	5	5
8	No	12	2	15	10	5	5
9	Yes	14	1	60	60	75	75

Chapter 1

Introduction

1 Introduction

1.1 The Battle Against Cancer: Are We Winning?

The year 2021 marked not only a year in pandemic history with the global spread of COVID 19, but also 50 years since the proclamation of the "War on Cancer" by then President of the United States of America, Richard Nixon. The signing of the National Cancer Act in 1971 led to a substantial increase of the budget of the National Cancer Institute (NCI). This financial growth initially raised the deceptive hope that cancer might soon be curable. In 1986, Bailar and Smith drew the disappointing conclusion that intensive efforts to improve cancer treatment had failed [3]. However, in recent decades, pessimism has given way to optimism, thanks to incredible advances in basic cancer research [4]. Furthermore, new initiatives, such as the Cancer Moonshot program revised by President Biden in February 2022, have been launched to accelerate progress in cancer prevention and survivorship. New goals were set to reduce cancer mortality by at least 50% over the next 25 years, with the ultimate goal of ending the "War on Cancer" [5, 6]. As a result of these investments, major advances in cancer treatment have been made over the past decades, including the development of new therapies such as targeted small molecules, monoclonal antibodies such as trastuzumab for HER2-positive breast cancer (BC), antibody-drug conjugates and immunotherapies including immune checkpoint inhibitors such as ipilimumab and chimeric antigen receptor (CAR)-T cell therapies such as idecabtagene vicleucel for myeloma patients [7].

Despite such progress, there is still no "cure" for cancer. It remains the second most common cause of death after cardiovascular diseases, with cancers of the breast, prostate, lung and colon being the most common, and lung cancer having the highest mortality rate (Figure 1). Already 100 years ago, it was described by Theodor Boveri that cancer arises from normal cells of the human body [8]. Cancer is caused by the uncontrolled growth and division of abnormal cells, which are phenotypically heterogeneous and plastic, adapting, evolving and becoming resistant to treatment. It is a puzzling set of diseases, complex and highly heterogenous with over 100 different

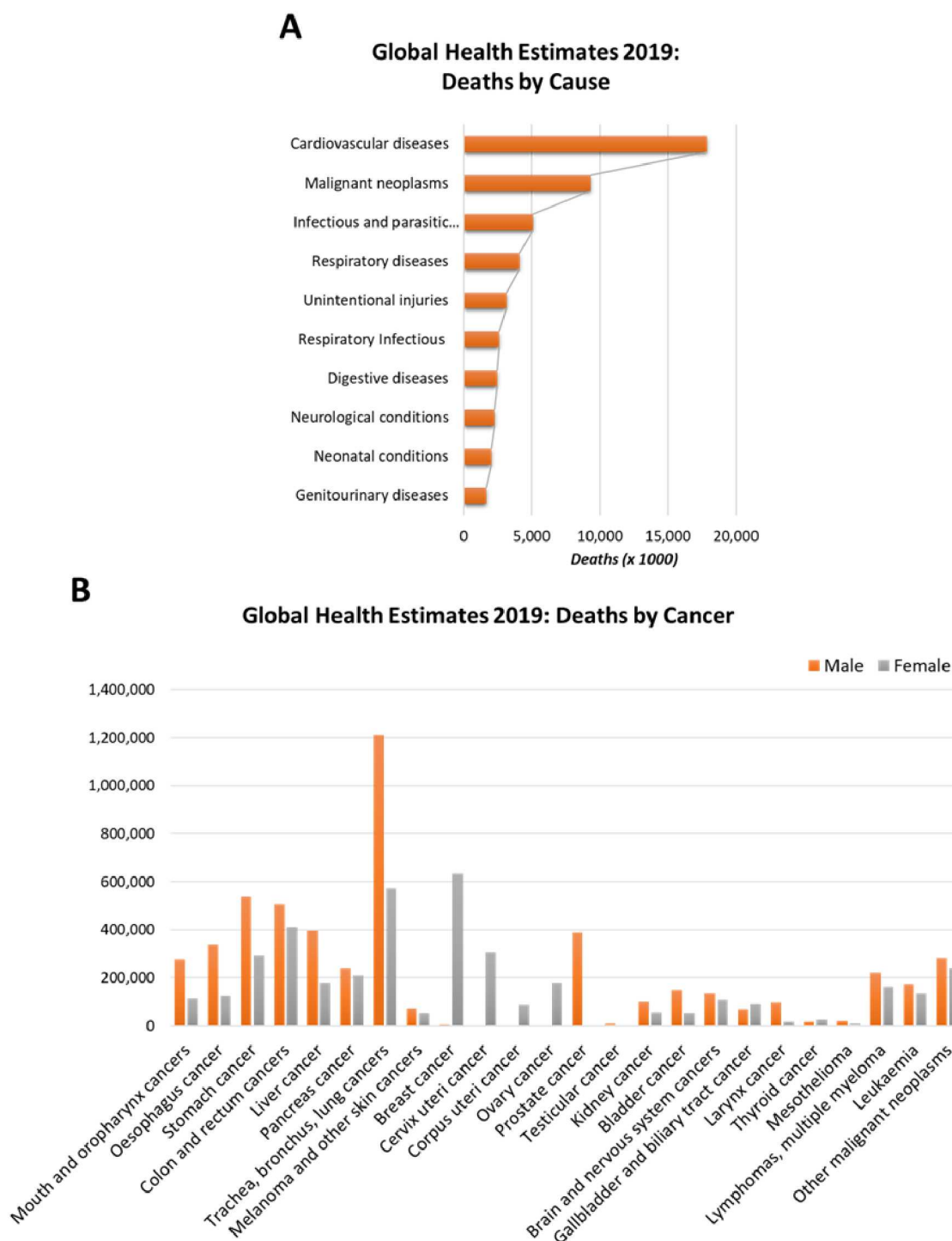


Figure 1: Global health estimates 2019. (A) General causes of death worldwide with cardiovascular diseases causing the highest mortality, followed by malignant neoplasms (cancer). (B) Cancer-related deaths in women and men worldwide. Cancer of the trachea, bronchus and lung have the highest mortality rates in men, while breast cancer is the leading cause of cancer-related death in women. Data source: Global health estimates: leading causes of death, accessed 05.07.2023. <https://www.who.int/data/gho/data/themes/mortality-and-global-health-estimates> [1].

types, located in different organs and subtissues and originating from different cell types. Understanding how cancer develops, how it wreaks havoc, and most

importantly, which factors promote or inhibit its growth, requires solving complicated biological and medical problems. As we continue to unravel the mysteries of this heterogeneous disease, it is becoming increasingly clear that cancer must be fully understood in all of its natural complexity in order to ensure successful treatment and tumor management. Well, the 'War on Cancer' is not yet over, and it's questionable whether we're going to succeed in fighting at least for a ceasefire.

1.2 Unmasking Cancer's Complexity: A Journey Through Tumoral Heterogeneity

Tumor heterogeneity reflects the complexity and diversity of cancer, referring to the observation that cancer cells can have distinct phenotypic profiles. The Darwinian selection as the basis for subclonal diversity provided the foundation for our understanding of tumor evolution: a succession of genetic alterations, each conferring one or another type of growth advantage, leads to the progressive transformation of normal human cells into cancer cells, allowing subclonal cells to spread and gain dominance in a local tissue environment [9-11]. These cells ultimately evolve into a tumor cell phenotype with eight essential tumor characteristics (cancer hallmarks): sustained proliferative signaling, evasion of growth suppressors, resistance to cell death, replicative immortality, angiogenesis induction, tissue invasion and metastasis, cellular energetics deregulation and immune destruction avoidance [9, 12]. Early observations by Gloria Heppner supported a model of nonlinear branched tumor growth in which subpopulation of cells (subclones) descended from a common ancestor eventually diverge and spread simultaneously with differing fitness. Consequently, molecularly and phenotypically distinct subclones coexist within a tumor, termed intratumoral heterogeneity (ITH) [13, 14], alongside intertumoral heterogeneity, the diversity of phenotypic profiles between two tumors of the same type [15]. The coexistence of clonal variants is determined by an interplay of genetic, epigenetic and microenvironmental factors that are intimately intertwined [16-19].

With the revolution in DNA sequencing technologies such as next generation sequencing (NGS), genetic heterogeneity has become the most studied and best understood mechanisms of ITH [20, 21]. However, it is still far from complete [22]. Genotypic variability occurs only when genetic changes manifest in the cellular phenotype, mainly as a result of genomic instability and other mechanisms such as defects in homologous recombination, chromosomal instability, chromothripsis, dysregulation of APOBEC enzymes, and drug treatment [23]. For premalignant cells

to become cancerous, they accumulate large numbers of mutations [24]. NGS has revealed an average of more than 10,000 somatic mutations within “passenger” and “driver” genes, affecting cancer-related genes that lead to activation of oncogenes and inactivation of tumor suppressor genes, and “passenger” genes [25-33]. On average, 5-15 driver mutations with selective growth advantage and 40-100 protein-coding alterations in passenger genes that may alter cell functions are found within tumors [34-36]. Due to external or internal exposure to mutagens and impaired DNA repair mechanisms, tumors increase their mutational capacity [37-40]. A large number of such aberrations arise in short bursts [41, 42] in between long periods of relative mutational equilibrium [43] as demonstrated in triple-negative breast cancer (TNBC) [44]. In particular, large-scale genomic alterations (copy number changes) associated with chromosomal instability, exert significant phenotypic effects and accelerate genomic diversification [45, 46]. Such heritable phenotypes can be acquired not only through genetic alterations, but also through non-mutational epigenetic mechanisms [47-49]. Epigenetic landscapes and gene regulatory networks directly regulate the phenotypic plasticity of tumor cells [50]. They are an illustration of the repertoire of stable (and unstable) phenotypes from the same genetic material and provide a comprehensive overview of nongenetic sources of phenotypic heterogeneity in cancer [51]. Epigenetic mechanisms, particularly DNA methylation [52], histone modifications, and regulation of non-coding RNA, directly modulate the genetic makeup of a cell. This leads to the formation of distinct, cell type-specific epigenetic profiles which influence cell fate in normal biological processes [53]. In both aging and senescence, and particularly in cancer, dysregulations and perturbations of the epigenetic machinery are frequently found altering the cell-specific epigenetic landscape and their transcriptome [54-57]. Epigenetic changes, such as epigenetic activation or silencing of driver genes (such as DNA repair genes), are more common, heritable, and reversible in cancer, and thus more influential than genetic aberrations [58]. Epigenetic landscapes of isogenic cell populations produce distinct functional states of cells e.g. differentiated cell types, stem-cell states, stressed states, activated states, each with optimized expression patterns [51]. Transient cell states of a uniform, isogenic cell population are mainly induced by gene expression noise [59] and add to the diversity of phenotypes.

In general, transitions between phenotypic states (cell types) can be triggered by oncogenic transformation, genetic perturbations, and abnormal environments, or by

changes in the "topology of the epigenetic landscape" (genetic endowment; signals from the microenvironment). Thus, environmental stress, changes in the microenvironment, and therapeutic pressure, among other stress factors, can trigger an adaptive response in cancer cells through dynamic transitions from one state to another through epigenetic and transcriptional changes (cellular plasticity) [60-62] (i.e., inflammation and therapy). The process of epithelial-mesenchymal transition (EMT) exemplifies this cellular plasticity [63] [64]. Environmental stress or microenvironmental perturbations including changes in the components, properties of stromal cells and remodeling of the EMT can exert selective pressure on cells, leading to adaptive responses, i.e. phenotypic changes [65-68]. Under normal conditions, the tissue environment provides the optimal conditions for the supply of tissue-specific cells. Alterations in these optimal tissue conditions often occur with aging and chronic inflammation, and are associated with an increased risk for tumorigenesis [69, 70]. Most importantly, perturbation of the microenvironment was found to promote tumor progression in invasive tumors or metastases [69, 70]. The stromal and epithelial disorganization translates into distinct and novel topological landscapes with spatial and temporal variability in nutrients, oxygen supply, stiffness, growth factors, inflammation and pH [68, 71], which directly links microenvironmental features to phenotypic diversification. Furthermore, the spatial distribution of genetically distinct tumor cell populations due to the presence of different microhabitats with different conditions (nutrients, oxygen, growth factors) is often associated with poor clinical outcomes [72-74].

As we continue to unravel the complexity of tumorigenesis and pathogenesis, features such as cell plasticity or non-mutational epigenetic reprogramming contribute significantly to ITH and could be incorporated into the hallmarks of cancer framework as novel cancer cell characteristics and enabling features, along with "polymorphic microbiomes" and "senescent cells" [75]. Ultimately, all these characteristics result in a high degree of phenotypic heterogeneity within the tumor and lead to a heterogeneous susceptibility of tumor cells to anticancer drugs and cytotoxic immunity, which has important implications for cancer therapy.

1.3 Decoding the Tumor Terrain: Exploring the Intricate Landscape of the Tumor Microenvironment

The tumor microenvironment (TME) is defined by a mass of cancer cells surrounded by a collection of stromal non-cancerous cells including fibroblasts/myofibroblasts,

vascular, epithelial, fat and immune cells embedded in an extracellular matrix (ECM) scaffold of connective tissue [76, 77]. While these cells are not inherently malignant, the reciprocal interaction with malignant cells and the ECM creates a dysregulated TME phenotype with altered functions that actively promotes tumor cell growth, local invasion, and metastasis [78]. Abnormal interactions result in fibroblasts and immune cells producing growth factors, cytokines and chemokines that directly stimulate tumor cell growth and progenitor recruitment, further promoting abnormal growth and proliferation.

The ECM of connective tissue mainly consists of elastic and collagen fibers, as well as so called ground substance containing glycosaminoglycans e.g. hyaluronic acid (GAGs), proteoglycans (PGs), and glycoproteins providing a scaffold for tissues and organs [79, 80]. Its biophysical characteristics determine topography, molecular density and stiffness of the connective tissue [81]. Primarily, fibroblasts as the predominant cells in the stroma, are responsible for the deposition, the maintenance and remodeling of the fibrillar ECM-type I, III and V collagen and fibronectin providing structural support of cells and maintenance of tissue integrity [82]. By secretion of type IV collagen and laminin, fibroblasts further support the formation of the basement membrane [83]. In normal tissue the dynamic process of ECM-turnover is tightly controlled by ECM protein production and fibroblast-derived matrix metalloproteinases (MMPs)-associated degradation [83, 84]. In tumors, Schor and colleagues (1986) [85] found an altered appearance of these fibroblasts, capable of driving noncancerous cells into a tumor-like state through oncogenic signaling and initiating epithelial tumor growth [86]. Tumor-associated fibroblast are usually referred to as myofibroblasts or cancer-associated fibroblasts (CAFs). CAF phenotypes are hallmarked by high proliferative index, extensive collagen deposition causing fibrillar collagen compaction [82], and increased hyaluronate and epithelial growth factor synthesis [87], often initiated by tumoral TGF β secretion [87, 88]. Further they were found to promote tumor angiogenesis, invasion and metastasis [89-91].

The complex vascular system in the human body is designed to keep our tissues oxygenated and nourished. In the case of fast-growing tumors, oxygen and nutrient supply is no longer sufficient, requiring the formation of new blood vessels and a tumor-vascular network to surpass a certain tumor size [92, 93]. Angiogenesis is induced by hypoxia-inducible factors (HIFs), which activate the transcription of angiogenic growth factor genes, including platelet-derived growth factor (PDGF), epidermal growth factor

(EGF) and vascular endothelial growth factor (VEGF), during oxygen deprivation [94]. Mainly VEGF is considered to be the master regulator of angiogenesis. It causes the attraction of endothelial cells (ECs) from nearby vessels, leading to the formation of new basement membranes and vascular spreading, a characteristic feature of tumors in response to low oxygen levels [77, 94]. In TME, these blood vessels often fail to mature, and the excessive secretion of angiogenic factors resulting from hypoxia leads to a vicious cycle in which the tumor is never reoxygenated [77, 95]. To restore tissue oxygenation during tumor growth and metastasis [96], hypoxic ECs demonstrate high adaptability [97]. Apart from this, ECs show high cellular plasticity being able to transition into CAFs through the process of EMT, promoting tumor progression. Modification of the endothelial barrier in response to tumor cell intravasation and leakiness of the blood vessels facilitates the passage of migrating cells through the vasculature and infiltration of other areas [95].

In non-malignant tissues, both the innate and adaptive immune system work hand in hand to defend the body against foreign bodies (pathogens), infections, or abnormal cells, thus mainly acting suppressive. In the dynamic process of cancer immunoeediting, complex cross-talk between transformed cells and immune cells determines if neoplastic cells get eliminated, persist or outgrow [95, 98, 99]. The presence of immune cells in the TME can have an ambivalent effect on tumor growth, either tumor promoting or tumor antagonizing. Whether neoplastic cells are eliminated or immune cells execute a pro-tumorigenic activity depends on the immune cell composition as well as the density and localization of the immune contexture within the TME, including innate (natural killer cells, macrophages, neutrophils, mast cells and dendritic cells) and adaptive (T and B cells) immune cells. The innate immune system generates an unspecialized, rapid immune response against a foreign antigen, while the adaptive immune system is activated by contact with specific antigens and uses immunological memory to evaluate the threat and amplify the immune response. In the TME, inflammatory neutrophils, M2-polarized tumor-associated macrophages (TAMs), T_H2 $CD4^+$ T cells (MDCs) were found to induce pro-tumorigenic effects supporting tumor angiogenesis, stimulate proliferation, facilitate tissue invasion and metastasis [100-103] contrary to anti-tumoral M1-macrophages, T_H1 $CD4^+$ T cells and cytotoxic $CD8^+$ cells [104]. These processes are controlled by the release of immunologically active growth factors (cytokines, chemokines, angiogenic factors, interferons) and various proteolytic enzymes [9, 105]. Distinct immune contextures of the TME in solid tumors

and the activation of adaptive immune response are associated with improved patient survival. For example, effective antigen presentation, IFN signaling and sufficient numbers of T cells correlate with better prognosis [106-110]. This has led to the implementation of the "Immunoscore" (validated for CRC) [111], which differentiates T cell-inflamed (hot) TME, composed of high levels of infiltrating T cells, from uninflamed [112] TME, characterized by low levels of infiltrating T cells, low tumor-specific (neoantigen) antigen expression and lack of IFN signal [113]. "Cold" TMEs are actively shaped by the complex interaction between tumor, stromal and immune cells.

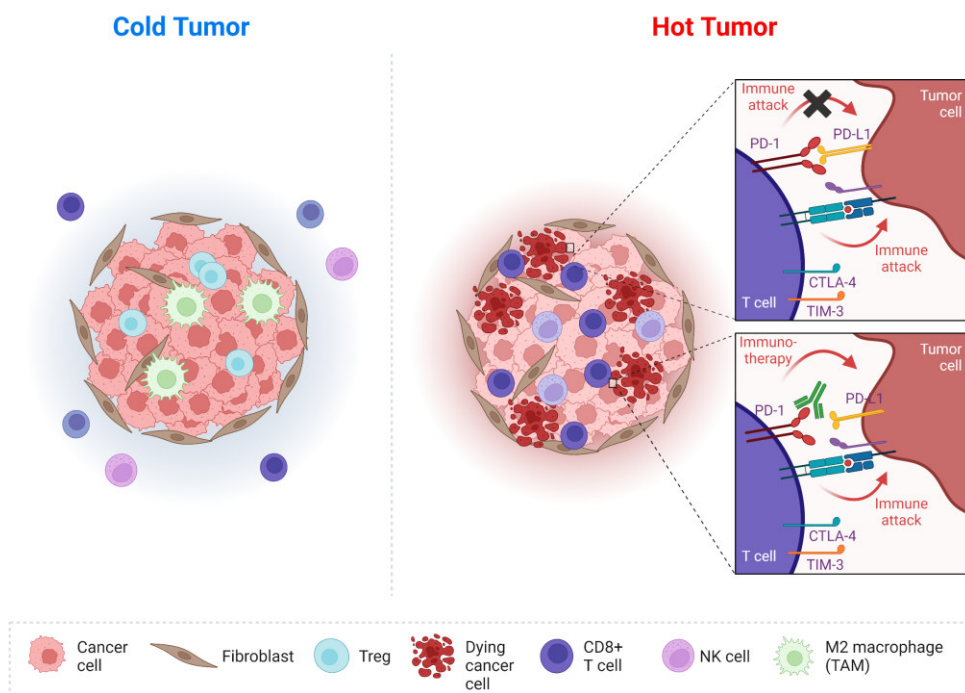


Figure 2. "Cold" non T cell inflamed versus "hot" T cell inflamed tumors. "Cold" tumors are poorly infiltrated with effector T cells, which are mostly found embedded in surrounding stroma. Further, they are often characterized by the presence of immunosuppressive cells, such as cancer-associated fibroblasts (CAFs), Treg cells or tumor-associated macrophages (TAM), which dampen the immune response and inhibit the migration of T cells into the tumor. "Hot" tumors are characterized by T cell infiltration, the production of proinflammatory cytokines and immune activation. (Figure created with Biorender)

Distinct secretomes of ECs and CAFs disrupt T cell extravasation, remodel the ECM and trap T cells within it, resulting in low levels of tumor-infiltrating lymphocytes (TIL), while encouraging the recruitment and polarization of regulatory cells and monocytes [114-116]. Other mechanisms of stromal cells are found to directly suppress anti-tumor immune responses such as the upregulation of PD-L1 [117-119]. The PD-1 (PD-L1) axis has a critical role in the maintenance of immune homeostasis. Binding of PD-L1 to PD-1 on TILs counteracts the TCR signaling cascade and inhibits the activation of

T cells, thereby preventing hyperactivation [120] and the development of autoimmune diseases [121]. Upregulation of PD-L1 on cancer cells and on cells in the TME, such as macrophages, dendritic cells, CAFs, thus creates an immunosuppressive environment that supports cancer cell growth through impaired T cell activation [122-124].

Summarized, understanding the complexity of the TME and its role in cancer progression is essential to the development of new therapeutic strategies for the treatment of this devastating disease. Recently, molecular strategies for tumor treatment have focused on the unique interplay between various aspects of the tumor and the microenvironment. By identifying and targeting specific molecular pathways involved in tumor cell-microenvironment interactions, researchers hope to develop effective treatments to halt tumor growth and metastasis. Approaches include the blockade of TAM recruitment, blockade of MDM infiltration into the TME, interference with TAM differentiation, modulation of dendritic cells and inhibition of proinflammatory cytokines [125]. Various therapies are under clinical evaluation in various tumors, including CSF1-R-inhibitors to deplete TAMs, CCL2-inhibitors to block TAM-recruitment, dendritic cell-modulating agents FLT3L and GM-CSF, or FAP-targeting agents (e.g., PT630, RO6874281, and sibrotuzumab) [125].

1.4 Tumor Heterogeneity and Therapy Resistance – a Call for Precision Oncology

1.4.1 Anti-cancer Therapies

With the advancements in deciphering molecular mechanisms of tumorigenesis and causes of tumor heterogeneity the development in clinical oncology has evolved from the radical surgical approaches towards novel cancer therapies including targeted therapies using small molecule inhibitors (SMIs) or monoclonal antibodies (mAbs), checkpoint inhibitory mAbs, adoptive T cell therapies including chimeric antigen receptor (CAR)-T cell therapy or TCR-transgenic T cell therapy, antitumor vaccines, and oncolytic viruses (OVs) [126]. Nevertheless, surgical removal remains the primary treatment for many solid cancers e.g. BC, ovarian cancer (OvCa), unless the tumor has metastasized and spread to other parts of the body [127]. In the case of aggressive tumors, it is often combined with radiation therapy, chemotherapy or targeted therapies. These treatments use high-dose radiation and/or drugs with the aim to kill rapidly dividing cells and shrink the tumor. However, the low specificity of

chemotherapies also damages proliferating healthy cells, resulting in common adverse events and toxicities [128]. Besides chemotherapy's low specificity for cancer cells, some tumors, such as glioblastoma (GBM), are usually resistant to chemotherapy, making recurrence inevitable and the tumor incurable. The relatively non-specific chemotherapy is contrasted with the targeted therapy with SMI and mAbs, which has a higher tumor specificity and general lower toxicities [129-132]. However, targeted therapies have unexpectedly a whole new set of toxicities and therefore may have similar levels of toxicity in some cases [133]. One of the reasons for the toxicity of targeted therapies is the unexpected cross-reactivity between the targets on the tumor cells and the normal cells of the host, which leads to toxicity in other organs. This is the case for EGFR targets such as afatinib and cetuximab [134] or for HER-2 targets. The fact that HER2 is also expressed on normal heart muscle cells increases the risk that HER2⁺ BC patients will develop cardiac dysfunction when they receive HER2-targeted therapy [135]. Notwithstanding some limitations, targeted therapy, in particular mAbs, represent a promising option in cancer therapy due to their low toxicity, high specificity, and scalability [136, 137], and interest in developing and using mAbs in cancer therapy has increased significantly over the past 20 years [138]. SMIs and mAbs have a molecular weight of less than 900 kDa and are capable of specifically binding to molecular targets such as growth factor receptors, oncogenes, cyclin-dependent kinases, proteasomes, and poly-ADP-ribose polymerase [139, 140]. Targeted therapies aim to reduce tumor growth by specifically inhibiting signal transduction pathways involved in cancer cell growth, proliferation, differentiation, survival and migration of cancer cells, or by altering the TME [129]. Several targeted agents are currently approved by the Food and Drug Administration and in clinical use for the treatment of various types of cancer. These are used as first-line therapy in certain cancers where druggable driver gene mutations have been identified through extensive genomic analyses. For example, in lung cancer, gefitinib or cetuximab target an EGFR aberrant gene product [141], trastuzumab and pertuzumab [142, 143] target HER2 in HER2 positive breast cancer (BC), crizotinib and ceritinib target an ALK mutation [144] non-small-cell lung cancers [145, 146], and vemurafenib or dabrafenib target a BRAF mutation in melanoma [147, 148].

Table 1. FDA-approved targeted therapies for breast cancer, ovarian cancer and glioblastoma

Tumor type	Drug (brand name)	Drug type	Target	Tumor subtype	Conditions	Treatment	Clinical trial number	FDA approval
brain cancer	bevacizumab (Avastin)	monoclonal antibody (mAb)	VEGF	GBM	recurrent GBM in adults	with lomustine (second-line treatment)	EORTC 26101 (NCT01260839), AVF37089 (NCT00345163), NCI D06-C-0064E	2009
brain cancer	dabrafenib meylate (Tafinlar)	small molecule inhibitor	BRAF	GBM	<i>BRAF</i> V600E-mutated, low grade pediatric cancer (children aged 1-18 years)	with trametinib dimethyl sulfoxide (first-line treatment)	Study CDRB436G2201 (NCT02684058)	2023
brain cancer	trametinib (Mekinist)	small molecule inhibitor	MEK	GBM	<i>BRAF</i> V600E-mutated low grade pediatric cancer (children aged 1-18 years)	with dabrafenib (first-line treatment)	Study CDRB436G2201 (NCT02684058)	2023
breast cancer	abemaciclib (Verzenio)	small molecule inhibitor	CDK4/6	HR+	HR+ HER2- advanced or metastatic BC (men or postmenopausal women)	single agent or with fulvestrant (second-line treatment)	Monarch 1 (NCT02107703) Monarch 2 (NCT02102490)	2017
	abemaciclib (Verzenio)	small molecule inhibitor	CDK4/6	HR+	HR+ HER2- advanced or metastatic BC (men or postmenopausal women)	with aromatase inhibitor (first-line treatment)	Monarch 3 (NCT02246621)	2018
breast cancer	alpelisib (Piqray)	small molecule inhibitor	PI3K	HR+	HR+ HER2- PI3KCA-mutated, advanced or metastatic BC (men and postmenopausal women)	with fulvestrant (second-line treatment)	Monarche (NCT03155697)	2023
breast cancer	everolimus (Afinitor)	small molecule inhibitor	mTOR	HR+	advanced HR+ HER2- BC (postmenopausal women)	with exemestane (second-line treatment)	Bolero 2 (NCT00863855)	2012
breast cancer	lapatinib ditosylate (Tykerb)	small molecule inhibitor	TKI	HER2+	advanced or metastatic HER2+ BC	with capecitabine (second-line treatment)	(NCT00078572)	2007
breast cancer	neratinib maleate (Mylotarg)	small molecule inhibitor	TKI	HER2+	early-stage HER2+ BC	single agent (second-line treatment)	ExelNET (NCT00878709)	2017
breast cancer	palbosiclib (Ibrance)	small molecule inhibitor	CDK4/6	HR+	HR+ HER2- advanced or metastatic BC	with aromatase inhibitor (first-line treatment)	NALA (NCT01808573)	2020
breast cancer	pembrolizumab (Keytruda)	monoclonal antibody (mAb)	PD-1	TNBC	locally recurrent unresectable or metastatic TNBC (with PD-L1 expression)	with fulvestrant (second-line treatment)	Paloma-2 (NCT01749427)	2017
breast cancer	trastuzumab (Herceptin)	monoclonal antibody (mAb)	HER2	HER2+	early-stage TNBC (high-risk of recurrence)	with chemotherapy (neoadjuvant treatment) followed by single agent (adjuvant treatment)	KEYNOTE-355 (NCT02619518)	2020
breast cancer	trastuzumab (Herceptin)	monoclonal antibody (mAb)	HER2	HER2+	metastatic HER2+ BC	with trastuzumab and docetaxel (first-line treatment)	KEYNOTE-522 (NCT03036488)	2021
breast cancer	trastuzumab (Herceptin)	monoclonal antibody (mAb)	HER2	HER2+	locally advanced, inflammatory, or early-stage HER2+ BC	with trastuzumab and chemotherapy (neoadjuvant treatment)	CLEOPATRA (NCT00567180)	2012
breast cancer	trastuzumab (Herceptin)	monoclonal antibody (mAb)	HER2	HER2+	locally advanced, inflammatory, or early-stage HER2+ BC	with trastuzumab and chemotherapy (neoadjuvant treatment)	NeoSphere (NCT00545688), TRYPHAENA (NCT00976989)	2013
breast cancer	trastuzumab (Herceptin)	monoclonal antibody (mAb)	HER2	HER2+	early-stage HER2+ BC (high-risk of recurrence)	with trastuzumab and chemotherapy (adjuvant treatment)	BERENICE (NCT02132949)	2017
breast cancer	trastuzumab (Herceptin)	monoclonal antibody (mAb)	HER2	HER2+	advanced, unresectable or metastatic HER2+ BC	single agent (second-line treatment)	APHINITY (NCT01358877)	2018
breast cancer	trastuzumab (Herceptin)	monoclonal antibody (mAb)	HER2	HER2+	germline <i>BRCA</i> -mutated metastatic HER2+ BC	with trastuzumab and capecitabine (second- or third-line treatment)	EMBRACA (NCT01945775)	2020
breast cancer	trastuzumab (Herceptin)	monoclonal antibody (mAb)	HER2	HER2-	germline <i>BRCA</i> -mutated metastatic HER2- BC	with trastuzumab and capecitabine (second- or third-line treatment)	HER2CLIMB (NCT02614794)	2020
breast cancer	trastuzumab (Herceptin)	monoclonal antibody (mAb)	HER2	HER2-	germline <i>BRCA</i> -mutated early-stage HER2- BC (high-risk of recurrence)	single agent (second-line treatment)	OlympiAD (NCT02000622)	2018
breast cancer	trastuzumab (Herceptin)	monoclonal antibody (mAb)	HER2	HER2-	recurrent and platinum-resistant cancer	single agent (second-line treatment)	Olympia (NCT02032823)	2022
ovarian cancer	bevacizumab (Avastin)	monoclonal antibody (mAb)	VEGF		platinum-sensitive, recurrent cancer stage III, stage IV or recurrent cancer	with paclitaxel, doxorubicin hydrochloride liposome, or topotecan hydrochloride	AURELIA (NCT00878911)	2014
ovarian cancer	mirvetuximab soravansine-gynx (Elahere)	monoclonal antibody (mAb)	FRα		FRα+ platinum-resistant epithelial cancer (max. 3 prior systemic treatments; bevacizumab required)	with carboplatin and paclitaxel or carboplatin and gemcitabine hydrochloride followed by single agent (second-third-line treatment)	GOG-0213 (NCT00565851) and OCEANS (NCT00434642)	2016
ovarian cancer	mirvetuximab soravansine-gynx (Elahere)	monoclonal antibody (mAb)	FRα		FRα+ platinum-resistant epithelial cancer (max. 3 prior systemic treatments; bevacizumab required)	GOG-02+H28+G31	GOG-0218 (NCT00282847)	2018
ovarian cancer	mirvetuximab soravansine-gynx (Elahere)	monoclonal antibody (mAb)	FRα		advanced epithelial cancer with partial or complete response to platinum-based chemotherapy	single agent (second-third-line therapy)	SORAYA (NCT04296890)	2022
ovarian cancer	mirvetuximab soravansine-gynx (Elahere)	monoclonal antibody (mAb)	FRα		response to first-line platinum-based chemotherapy	single agent (second maintenance treatment)	PRIMA (NCT02655016)	2017
ovarian cancer	mirvetuximab soravansine-gynx (Elahere)	monoclonal antibody (mAb)	FRα		germline <i>BRCA</i> -mutated recurrent epithelial cancer with partial or complete response to platinum-based chemotherapy	single agent (first maintenance treatment)	NOVA (NCT01847274)	2022
ovarian cancer	mirvetuximab soravansine-gynx (Elahere)	monoclonal antibody (mAb)	FRα		germline <i>BRCA</i> -mutated, advanced epithelial cancer with partial or complete response to platinum-based chemotherapy	single agent (first maintenance treatment)	SOLO-1 (NCT01844686)	2018
ovarian cancer	mirvetuximab soravansine-gynx (Elahere)	monoclonal antibody (mAb)	FRα		HRD-positive, advanced cancer with partial or complete response to platinum-based chemotherapy	with bevacizumab (first maintenance treatment)	PAOLA-1 (NCT02477644)	2020
ovarian cancer	mirvetuximab soravansine-gynx (Elahere)	monoclonal antibody (mAb)	FRα		recurrent epithelial cancer with partial or complete response to platinum-based chemotherapy	single agent (maintenance treatment)	Study-19 (NCT00763545)	2020
ovarian cancer	mirvetuximab soravansine-gynx (Elahere)	monoclonal antibody (mAb)	FRα		germline <i>BRCA</i> -mutated, recurrent epithelial cancer with partial or complete response to platinum-based chemotherapy	single agent (maintenance treatment)	ARIEL3 (NCT01968213)	2018

GBM: glioblastoma; BC: breast cancer; TNBC: triple negative breast cancer; HR+: human epidermal growth factor receptor 2 positive; FRα: folate receptor α; HRD: homologous recombination repair deficiency.

Data source: "List of Targeted Therapy Drugs Approved for Specific Types of Cancer" by the National Cancer Institute <https://www.cancer.gov/about-cancer/treatment/types/targeted-therapies/approved-drug-list#targeted-therapy-approved-for-brain-cancer>; DailyMed database <https://dailymed.nlm.nih.gov/dailymed/index.cfm>

Targeted therapies are also used to block the crosstalk between the TME and the tumor. For example, attempts are being made to suppress hypoxia-induced tumor cell angiogenic signals, such as VEGF, which lead to the formation of heterogeneous, chaotic vessels [149, 150]. The first anti-angiogenic drug approved by FDA was bevacizumab, targeting VEGF [151]. Table 1 lists a number of targeted therapies that have been approved by the FDA specifically for BC, OvCa, and GBM, and shows the success of drug development over the past two decades. It is clear from the table that fewer targeted therapies have been approved for the treatment of OvCa and GBM compared to BC. Nevertheless, there have been important developments in recent years with the approval of PARP inhibitors for *BRCA*-mutated OvCa or the approval of dabrafenib and trametinib for BRAF-V600E-mutated pediatric GBM (Table 1).

Immunotherapy, which uses the patient's own immune system to kill cancer cells and generate systemic, protective anticancer immunity, rather than reducing tumor burden (through chemotherapy), is another therapeutic option that has evolved in recent years. Immunotherapies include mAbs, checkpoint inhibitors (CPI), cytokines, vaccines and adoptive cell transfer, including chimeric antigen receptor (CAR)-T cell therapies and TCR-engineered T cell therapy. Significant progress has been made in recent years with immunological CPI as new cancer therapies, with the FDA approving 6 new CPI drugs [152]. These are primarily immune checkpoint blockade (ICB) therapies in which mAbs block/inhibit the interaction of T cell co-inhibitory receptors and their ligands. These are often over-expressed by tumors in order to evade the T cell immune response [153], which ultimately leads to increased T cell cytotoxicity. The first ICB drug to receive FDA approval was the CTLA-4 inhibitor ipilimumab in melanoma patients in 2011 [154]. Next, in 2014, the FDA approved the PD-1-targeting ICB drug nivolumab for melanoma [155] and later for first-line treatment of non-small cell lung cancer [156], renal cell carcinoma [157], urothelial carcinoma [158], Hodgkin's lymphoma [159] and others. Recent FDA-approved ICBs target PD-1 ligand PD-L1, including atezolizumab [160] and durvalumab [161]. The current status of immunotherapy clinical trials in BC, OvCa and GBM is shown in Figure 2. Many of the ongoing trials are mainly focused on testing CPIs and vaccines. In particular, across phase one to phase three clinical trials, there are an increasing number of trials

investigating the use of ICBs, CAR-T/CAR-NK and vaccines in BC. In contrast, current TCR-engineered T-cell trials are limited to OvCa studies.

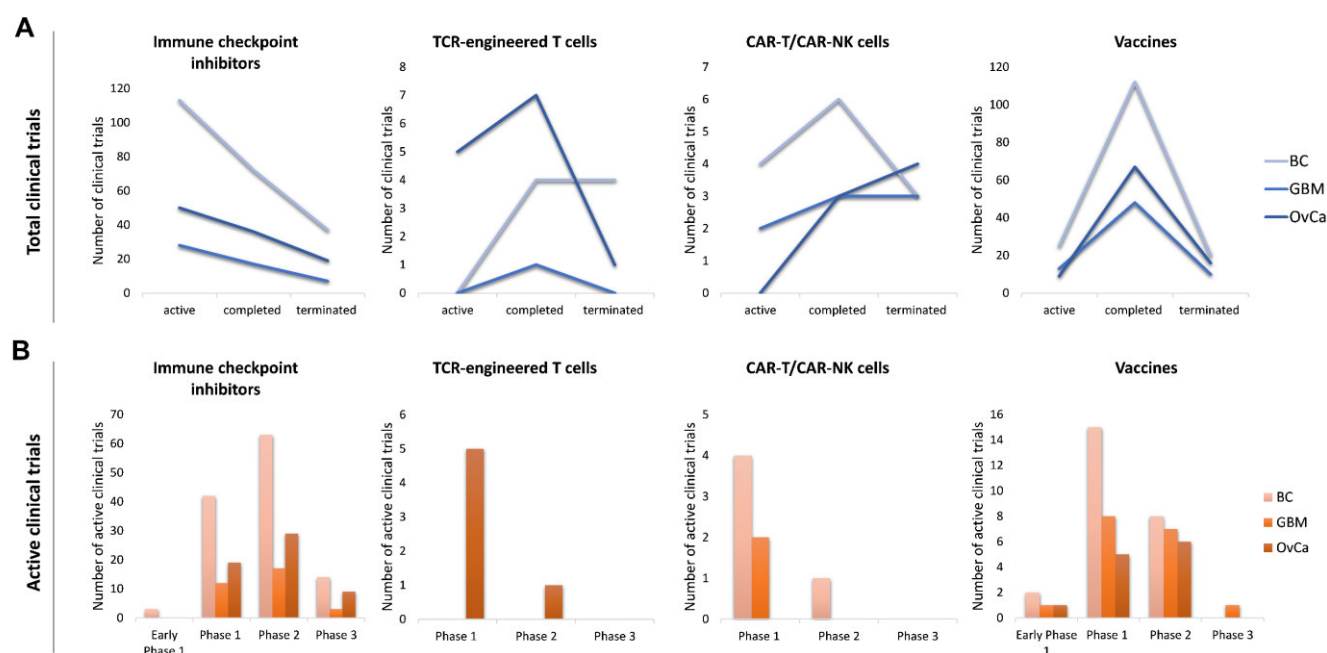


Figure 3. Immunotherapy clinical trials: Total number and active trials. (A) Number of active, completed or terminated immunotherapy clinical trials by therapy and cancer type. (B) Number of active immunotherapy clinical trials in breast cancer (BC), ovarian cancer (OvCa) and glioblastoma (GBM) by clinical trial phase. Data source: <https://www.clinicaltrials.gov/>

1.4.2 Therapy Resistance Unmasked: Cracking the Code to Healing

Despite the development of new cancer therapies such as immunotherapies and targeted therapies, drug resistance remains the greatest challenge in treating cancer. While cancer therapies often elicit a good initial response, the emergence of treatment resistance and relapse during progression or metastasis is almost inevitable in most tumors [162]. As a result, patients with advanced solid tumors continue to be faced with poor clinical outcomes. Worryingly, 75% of patients do not achieve a response regardless of the type of treatment [163-165], even when a large proportion of cancer cells are killed. One of the main reasons for high recurrence rates or resistance is the "one size fits all" approach that still prevails for many cancers, where treatments are applied based on clinical treatment guidelines and mostly without consideration of patient-individual or cohort-specific differences. Cancers with high recurrence rates include GBM with 75.3% local and 6.1% distant disease progression [166] and OvCa with 80% disease progression at advanced stages [167]. Developing new therapeutics is based on the simple approach of trying to develop effective therapies for the "average patient" [168]: Successful for some patients, but not for many. In many cases,

this oversimplified model does not lead to a successful treatment, but rather to unnecessary side effects for the patient. Current therapeutic approaches neglect inter- and intra-tumoral heterogeneity at the morphological-histological and molecular levels, which often leads to therapeutic resistance [169-172]. Following an initial response, treatment resistance can either be acquired due to somatic events/new mutations that subsequently alter signal transduction pathways [173], or it is already prevalent due to the presence of pre-existing subclones that are selected by therapy [174-176]. This was demonstrated in several tumor types [177-181]. For example, genetic alterations leading to response failure include mutations that prevent the drug from binding to the target as with imatinib in CML and GIST [182, 183], that circumvent the targeted pathway blockade as with B-RAF inhibition in resistant BRAFV600-mutant melanoma [184], or that restore the wildtype function of a protein as with BRCA2 in BRCA-mutated cancers [185]. By contrast, pre-existing chemotherapy-resistant subclones have been identified by single-cell RNA sequencing in metastatic estrogen receptor positive (ER) BC patients, as well as fulvestrant- and tamoxifen-resistant subclones in ER⁺ BC cell lines [50, 174, 186]. Resistant tumor cells arise not only from direct genetic alterations but also from non-genetic epigenetic changes that alter gene expression patterns in genetically identical cells in a semi-stable manner [50, 187-193]. In most cases, for surviving subpopulations to become fully resistant phenotypes, additional gene expression changes must occur alongside transient resistance-gene expression changes [194, 195]. Besides genetic and non-genetic changes, therapies generate a specific TME that also acts to select for specific phenotypes. For example, certain growth factors secreted by tumor cells or stromal cells in the TME [196], ECM-tumor cell interactions [197], or hypoxic, acidic, and nutritional conditions in the TME [198] influence the development of intrinsic resistance. As such, the higher the pre-existing ITH, the more likely certain tumor cell subpopulations will survive and undergo further phenotypic adaptation due to therapy-induced selection pressure, leading to a more resistant phenotype and thus likely relapse.

1.4.3 Personalizing Oncology: Promise for a Cure?

All of this points to the need for a treatment approach that takes an individualized and holistic view of the patient's tumor. In the last decade, attempts have been made to move away from the antiquated 'one-size-fits-all' approach to a patient-specific treatment approach known as 'personalized medicine' [199] and subsequently

'precision medicine' [200]. The FDA defines precision medicine as "an innovative approach to tailoring disease prevention and treatment by taking into account differences in people's characteristics, environments, and lifestyles. The goal of precision medicine is to target the right treatments to the right patients at the right time [168]". The goal of precision oncology is therefore to identify, develop, and deliver highly selective drugs against specific cancer targets to the appropriate sub-population of individual cancer types [200, 201]. In this context, oncology includes precision diagnostics that provides accurate diagnosis, classification into subtypes, and treatment stratification of each individual patient tumor [202]. A stratified medical approach with more precise and data-driven treatment strategies is enabled by the integration of molecular categorization of tumors using tumor-specific biomarkers (so-called "signatures") [203, 204]. One example is the identification of *BRCA1/2* mutations in BC, which supports individual risk stratification [205, 206]. On the other hand, precision oncology encompasses precision therapy, in which the most effective treatment is tailored to each patient on the basis of genetic and phenotypic profiling data. For some tumors, genomics has succeeded in developing tailored targeted therapies, such as the first "personalized" treatment of HER2-positive BC with trastuzumab in 1998 [207, 208] or targeting the driver mutations EGFR or ALK in lung adenocarcinoma or BRAF in melanoma, and PD-1/PD-L1 in microsatellite unstable tumors [209]. On average, 38-40% of cancer patients have detectable genetic susceptibilities. However, there are far fewer genetic alterations that can be targeted by a targeted agent, and relapsed cancers are particularly unlikely to respond, as several clinical trials have shown [210-215]. Few patients are likely to benefit from this type of personalized treatment approach, suggesting that genomic analysis alone is not sufficient to predict response to therapy. Many nongenetic and epigenetic mechanisms affecting response to therapy determine many discrete and metastatic cancer cell phenotypes [55], which must be considered in the context of precision oncology. Bridging the gap between the genotypic effects and the phenotypic manifestation may be achieved in particular with the help of multiomic techniques such as transcriptome, proteome and metabolome analyses. Many challenges remain before precision oncology can be fully integrated into mainstream care, although this approach promises to improve clinical outcomes, increase cost-effectiveness, and protect patients from unnecessary treatments.

1.4.4 Preclinical Models and Functional Analyses

Precise diagnosis and prediction of treatment outcome is one of the major hurdles to successful precision oncology. In particular, developing functional predictive biomarkers can be used to guide treatment decisions and risk stratification. On the other hand, there is a need for deep tumor profiling for tumor classification and the development of new targeted therapies. Besides multiomics analyses, this primarily requires the development of preclinical models. The use of preclinical patient-derived models capable of reflecting patients' tumors can, on the one hand, assess the sensitivity or resistance of tumor samples from affected patients to clinically approved drugs (functional precision medicine) [216] and, on the other hand, support drug discovery. Functional data from patient-derived models can be used to detect vulnerabilities, such as protein signaling pathways and epigenetic alterations and/or changes in non-genomic pathways and provide predictive data prior to the initiation of treatment. This would allow therapies to be selected individually based on their functional effectiveness. Integrated with genomic, proteomic and transcriptomic data, this "next generation" functional assay [217] promises to increase therapeutic efficiency. This would help decide which genomic aberrations are valid targets to avoid mistreatment like RAF inhibitors in BRAF V600E mutant CRC [218]. With the advent of 3D cell culture systems, new tumor models have been established in oncology over the past decade. These replace mainly 2D monolayer cultures in both *in vitro/ex vivo* drug screening and personalized functional testing [219-221]. 2D cell culture is still widely used in drug discovery due to its advantages such as expediency, simplicity, and cost-effectiveness. However, the results obtained show virtually no clinical applicability [222]. This is primarily due to the lack of essential components of the 3D tissue structures that are critical for the efficacy of the drug [223]. One is dimensionality, which provides a more relevant environment that more closely mimics the pathophysiological environment *in vivo*, allowing for dynamic cell-cell and cell-ECM interactions. The 3D matrix given by dimensionality has a strong influence on morphology, phenotypic cell states and expression profiles [224-226]. Through the spatial positioning of cells, the stiffness of the matrix, and the molecules of the ECM (including glycoproteins, ECM fibers, proteoglycans), the ECM largely affects the efficacy of a drug [227-229]. Moreover, dimensionality creates a gradient of soluble metabolites, oxygen concentration, and pH [230, 231] that contributes to ITH and influences proliferation and chemotaxis [227]. Finally, 2D tumor cell lines cannot

accurately mimic cell growth [232] and cannot represent tumor subtypes such as luminal A BC [233] and thus intertumoral heterogeneities. Today, oncologists use 47% animal models, including two-thirds mouse models, and 18% 3D cell culture systems and 3D organoids [234]. Among them, patient-derived tumor models such as patient-derived organoid (PDO) or patient-derived xenograft [235] models have been established from clinical cancer biopsies [219, 220, 236]. PDX models are generated by implantation of primary patient-derived tumor cells, biopsied tumor tissue or cultured PDO into immunodeficient mice [237-239] mostly subcutaneously or orthotopic [240]. They largely represent inter- and intratumoral tumor heterogeneity, exhibit similar structural, functional, histopathology and genetic characteristics as the primary tumor [236] and are being investigated for patient stratification [241]. Indeed, PDX models of BC have been shown to predict metastatic recurrence [242-244] and patient response to therapy [245]. PDO models, which could be developed for a variety of tumor types, also have a great potential for precision therapy [246-250]. In pancreatic and colorectal tumor models, PDO and primary tumors have been shown to correlate genotypically and phenotypically [251, 252] and may also partially predict drug response [253-256]. PDO models are generated by dissociating primary tumoral tissues containing cancer cells, adult stem cells, pluripotent stem cells or cancer stem cells, which are cultured under defined 3D culture conditions in a 3D matrix. This produces functional units (3D cell units) with tissue-specific structure, containing both differentiated cells and stem cells [257, 258]. As a testament to the current efforts in PDO culture and its promising applicability in drug screening and functional precision medicine, Y.-H. Lo et al. [2] reviewed currently established PDO cultures for various tumor types, success rates, application for drug testing, and available correlation data with patient outcomes [259]. However, the generation of reliable data and detailed evaluation of the models are critical to the clinical relevance and predictive value of such models. Several factors can significantly impact the clinical relevance of such models. For example, the temporal availability and the speed with which results can be generated are of great importance to clinicians. Furthermore, the general availability and required amount of fresh tumor tissue, which is not given in metastatic disease or needle biopsies, as well as sufficient cell yields are relevant. Major limitations of the use of PDOs in functional precision medicine include long *ex vivo* culture time (weeks/months), lack of an intrinsic tumor microenvironment, in particular the stromal and immune compartments, high cost of conditioned medium and matrices, potentially interfering growth factors in

medium, no vascularity and the variable success rates in establishing PDOs [209, 259-261]. Varying engraftment rates, low success rates for low tumor burden-cancers compared to high success rates for metastatic cancers, high cost, long periods, low scalability, host-tumor interactions, lack of functional immune system and mouse-specific selection pressure causing genetic drift are several drawbacks of PDX models [209, 261, 262]. Despite technological advances, there is a continuing need for clinically meaningful patient-derived preclinical tumor models to assess the susceptibility and treatability of individual patients. The greatest challenge remains the development of a preclinical model that reflects the phenotypic and pharmacological diversity of a tumor while preserving the TME. Disappointing success rates of 3.4% - 5.1% for the approval of new anti-cancer drugs demonstrate the limits of the translatability of current tumor models [263]. The demand for models incorporating a functional TME with an immune component is also emphasized by the emergence of promising immunotherapies. Gaps in precision medicine can be filled and decisively shaped in the near future by the establishment of more accurate, cost-effective and efficient preclinical technologies for *in vitro/ex vivo/in vivo* methods, the refinement of established models and the development of new, complementary short- and long-term models and their accurate validation. Ultimately, no single model will be able to represent a 'patient avatar'. Rather, all available models will represent complementary tools in PM, each best suited and used for specific applications.

Chapter 2

Objectives of the Thesis

2 Objectives of the Thesis

The individual response to cancer therapies and the development of resistance remains poorly understood despite the success of new methods such as the establishment of patient-derived tumor models or the genomic and transcriptomic analysis of disease determinants. There is an urgent need to address gaps in personalized cancer therapy, such as the lack of patient-derived models for all tumor types, low efficacy rates, or long culture times that hinder use in personalized medicine. The aim of this study was the development and validation of a complementary, clinically relevant, patient-derived model for highly heterogeneous and advanced tumor entities. For this purpose, a novel 3D *ex vivo* tumor model of BC, OvCa and GBM was established, consisting of patient-derived microtumors (PDM) and TILs obtained by mechanical and enzymatic dissociation of tumor tissue within maximum of 24 hours after receipt. Extensive phenotypic analysis and validation was performed using clinically relevant histological (H&E staining), immunohistochemical (DAB staining) and quantitative multiparameter flow cytometry methods. Emphasis was placed on the histopathologic comparability of PDM and corresponding patient tumor tissue, preserving tumor subtype characteristics, and intertumoral heterogeneity between individual patient tumors. Furthermore, the preservation of ECM components such as collagen and PGs/GAGs in PDM, which have been shown to influence treatment response, was evaluated using Movat's Pentachrome staining. These results were complemented by RPPA and DigiWest®-based protein signal transduction profiling by adapting proteomic technologies to small PDM sample sizes. A number of protein pathways and their functional status were recorded in a variety of PDM in order to define their molecular, patient-specific, phenotypic profiles. Subsequently, their preclinical use in parallelized drug efficacy testing was evaluated to determine individual responses to chemotherapy, targeted therapy, and immunotherapy using PDM alone and in co-culture with autologous TILs, and to novel treatment combinations. Finally, this thesis explored the integration of drug efficacy testing and protein pathway analysis to decipher molecular patterns of treatment resistance and sensitivity in order to predict treatment response. Moving from genomic profiling to proteomic profiling enables the identification of individual susceptibilities at the protein level, i.e. at the level of drug action, thereby defining more effective treatments and personalizing therapy approaches. In conclusion, the results of this thesis obtained in three distinct heterogeneous tumor types demonstrate the preclinical applicability of

PDM and autologous TILs in drug development and as a complementary *ex vivo* tumor model with the potential to support clinical decision making in personalized oncology by decoding patient-specific vulnerabilities.

Chapter 3

Results I:

Unraveling the Heterogeneity of Ovarian Cancer: 3D Microtumors Provide Personalized Insights into Treatment Vulnerabilities

The contents of this chapter are based on:

Anderle N, Koch A, Gierke B, Keller A-L, Staebler A, Hartkopf A, Brucker SY, Pawlak M, Schenke-Layland K, Schmees C. *A Platform of Patient-Derived Microtumors Identifies Individual Treatment Responses and Therapeutic Vulnerabilities in Ovarian Cancer*. *Cancers*. 2022; 14(12):2895.

3 Results I: Unraveling the Heterogeneity of Ovarian Cancer: 3D Microtumors Provide Personalized Insights into Treatment Vulnerabilities

In the future, personalizing cancer treatment and predicting treatment response will be one of the main challenges to improve therapeutic efficacy. Advances in the genomic and transcriptomic profiling of tumors have enabled a detailed investigation of the drivers of disease. This includes a major effort to unravel the intertumoral heterogeneity of cancer types with dismal rates of success in treatment, such as advanced stage OvCa [264-266]. However, OvCa is often diagnosed at a late stage due to a lack of early symptoms and diagnosis, which is associated with an advanced stage of the disease and a 5-year survival of only 31%, resulting in a high mortality rate (worldwide >185 000 in 2018) [267, 268]. To make matters worse, the high degree of molecular and genetic heterogeneity contributes to the complexity of the disease and thus to the high variability in response to first-line chemotherapy in advanced stage OvCa [269]. Yet, the principles underlying treatment response and, importantly, the development of resistance in OvCa remain poorly understood [266] highlighting the urgent need to define more effective treatments and identify individual susceptibilities. However, due to lack of efficacy and heterogeneity of response, trials of targeted therapies in OvCa often fail in clinical phase I and II studies or even at preclinical development in cell lines, calling into question the use of current preclinical OvCa tumor models [270-272]. This study describes the establishment of a novel 3D *ex vivo* model for OvCa comprised of PDM and TIL enabling parallel drug testing and the identification of appropriate treatment responses in individual patients. A modified pre-existing protocol was applied to generate a patient-specific *ex vivo* platform consisting of PDM and TIL from residual fresh OvCa tumor tissue. Clinically relevant methods such as histology, immunohistochemical staining (IHC), and flow cytometric immune cell analysis are utilized to study and characterize the obtained PDM and TIL. RPPA analysis provided a rapid, cost-effective, sensitive high-throughput method to assess the tumor heterogeneity and protein expression patterns of different OvCa *ex vivo* samples. Further, potential responders to chemotherapy, targeted therapy and immunotherapy were identified through functional drug testing. Autologous PDM-TIL co-cultures were used to assess the efficacy of CPI, and FACS analysis helped to identify differences in the TIL populations involved. Finally, RPPA pathway profiling combined with

functional drug testing identified molecular protein patterns correlating with treatment response or resistance.

3.1 Comprehensive Analysis of PDM and TIL from Freshly Resected Ovarian Cancer Tissue

3.1.1 Promising Isolation Success and Viability Rates of Ovarian Cancer Microtumors

The development of a new tumor model that allows individualization of cancer therapy through preclinical identification of patient-specific therapeutic vulnerabilities and sensitivities is a challenging task. Despite the great importance of 2D tumor cell lines and various tumor mouse models in the past, and the recent development of organoid and tumor-organoid technology and its transformative impact on cancer research, there are still many challenges that remain to be addressed. As a complement to existing PDO models for OvCa [273-275], the goal was to establish an *ex vivo* tumor model that overcomes limitations such as preservation of existing cell-cell contacts, maintenance of an intrinsic microenvironment, and most importantly, is clinically relevant for personalized cancer therapy. In this context, the main issues to be addressed are the timeframe from generation to applicability, as well as the usability for elucidating treatment-relevant molecular mechanisms together with the preservation of central features of the corresponding primary tumor tissue. To this end, PDM were isolated and generated from residual fresh ovarian tumor tissues of consenting patients as shown in Scheme I (Anderle et al. 2022, **Appendix I**, Scheme I), adapting the protocol of Kondo et al. (2011) [276]. Isolation relied on tissue dissociation by mechanical fragmentation followed by two-hour enzymatic digestion. Isolation relied on tissue dissociation by mechanical shredding followed by two-hour enzymatic digestion. The yield of dissociated viable and functionally active cells was maximized by using optimal concentrations and ratios of collagenase I, collagenase II and Dispase® in the applied research grade Liberase™DH [277]. Tumor fragments of various sizes with intact cell-cell contacts, referred to as PDM, were obtained by filtering out larger portions of digested tissue and dissociated single cells. PDM were cultured in suspension for 2-3 days before use for subsequent analyses. Further, the protocol was optimized for the parallel collection of autologous TILs, present in the single cell fraction. Residual fresh tumor specimen were obtained from n = 16 OvCa patients who underwent tumor debulking surgery. For n = 14 samples, PDM samples with varying amounts of available PDM for downstream analyses were successfully

retrieved, representing a success rate of 87.5%. Instead, 12.5% of the samples failed to recover PDM (Anderle et al. 2022, **Appendix I**, Figure 1A). The ovarian tumor specimens received were predominantly high-grade serous carcinomas (HGSC) of epithelial origin, the most common type of OvCa, one mucinous carcinoma, one low-grade serous carcinoma and one granulosa cell tumor of sex cord-stromal origin (Anderle et al. 2022, **Appendix I**, Table 1). Thereby the generation of PDM was independent of age, lymph node spread, distant cancer spread, perineural invasion or the FIGO stage (Anderle et al. 2022, **Appendix I**, Table S1). After 2-3 days of cultivation, PDM were analyzed by 3D live cell imaging and image-based quantification to quantify cell viability after isolation. Calcein-AM and Sytox™ orange were used for labeling of both viable and dead cells (Anderle et al. 2022, **Appendix I**, Figure 1B-C). With an average of $\leq 7\%$ dead cells, staining confirmed robust viability of PDM. Underscoring its potential preclinical applicability and compatibility with time frames of clinical decision making, PDM can be generated from primary OvCa tissue in a short time and have high viability across multiple samples after limited enzymatic digestion.

3.1.2 Unveiled Histopathologic and Immunohistochemical Tumor Profiles in Microtumors

In order to further assess the clinical relevance of OvCa-PDM, the PDM have been thoroughly characterized and compared to the parent tumors. Routine H&E staining, still the gold standard of clinical cancer diagnosis, was performed on both PDM-FFPE and clinically available, corresponding primary tumor tissue (PTT) cryosections for blinded histopathologic comparison by an expert pathologist (Anderle et al. 2022, **Appendix I**, Figure 2A and S1). In addition to classical histopathologic analysis, such as assessing cell changes, atypia and growth patterns in H&E sections, the scope of analysis was expanded to include IHC examination of tumor-specific markers, ECM components and immune cell markers. DAB staining of the different protein markers was evaluated semi-quantitatively (Anderle et al. 2022, **Appendix I**, Figure 2A-B and S1). Professional evaluation by a board-certified pathologist confirmed the presence of typical, distinct histopathologic features of OvCa. HGSC-derived OvCa PDM exhibited histopathologic features such as papillary growth pattern, irregular branching, cystic and glandular structures comparable to PTT, whereas the low-grade mucosal PDM model showed none of these features. Similar to routine HGSC differential histopathology [278], both p53 and Wilms' tumor 1 (WT1) proteins were analyzed by IHC, showing high concordance with corresponding primary tumors except for one

sample. Furthermore, CA125 expression confirmed ovarian origin, but somehow differed in PDM as previously reported by other studies [279, 280]. The possible presence of a TME within the PDM consisting of stromal cells (immune cells, fibroblasts) and ECM components was investigated as it influences tumor progression, metastasis, and response to therapy [281-284]. Besides ECM factors collagen I, C1QBP and FAP α , CD163⁺ TAMs were found in individual PDM samples (Anderle et al. 2022, **Appendix I**, Figure 2A, S1). In most cases, these markers, especially FAP α and C1QBP, showed the same expression in PDM as in the corresponding primary tumor. For collagen I, three samples showed differential expression between PDM and PTT. However, it should be noted that in some cases only $n = 1$ sections were considered. To conclude, the typical histologic features of the corresponding primary ovarian tumors are preserved in PDM, allowing the differentiation of different tumor subtypes. Furthermore, the TME is partially preserved in the obtained PDM, indicating that the isolation method used is advantageous in retaining intrinsic tumor microenvironmental structures.

3.1.3 In-depth RPPA-based Signaling Pathway Profiling of Ovarian Cancer PDM

RPPA enables multiplex analysis of total and post-translationally modified protein analytes in multiple biological samples using small amounts of protein lysate [285-287]. Using RPPA, protein expression patterns of $n = 7$ OvCa- and $n = 1$ BC-PDM samples were generated and provided insight into the tumor heterogeneity and differential signal transduction phenotypes. Abundances were measured using $n = 100 - 150$ PDM per sample for 116 different total and phosphorylated proteins (Anderle et al. 2022, **Appendix I**, Figure 3A). Pathways interrogated by the platform included the cell cycle, DNA damage response, apoptosis, chromatin regulation, MAPK/RTK, PI3K/Akt with mTOR, Wnt, NF κ B as well as tumor and stem-cell markers. Three PDM clusters were identified by cluster analysis of protein expression patterns distinguishing a HGSC-subtype cluster ($n = 4$) from a granulosa cell tumor cluster (OvCa #21) and a third cluster including the BC-PDM sample together with OvCa PDM #19 (Anderle et al. 2022, **Appendix I**, Figure 3A). In both the granulosa cell tumor PDM (OvCa #19) originating from the sex cord stroma and the BC-PDM, WT1 expression, a marker of epithelial OvCa [288, 289], was strongly decreased. In addition, the clusters differed in the expression of Nanog, a key stem cell marker [290], with higher protein levels in the HGSC cluster.

OvCa PDM showed a heterogeneous activation profile (Figure 3B, Table S2) when looking at the different signaling pathways. An enhanced MAPK/RTK signaling activity was found in OvCa PDM #17, 21, 23, and 24 (\log_2 NFI: 0.30; 0.38; 0.32; 0.31) compared to an attenuated signaling in the BC model (\log_2 NFI: -0.47) (Anderle et al. 2022, **Appendix I**, Figure 3B, Table S2). Up to 50% upregulation of cell cycle signaling was observed in OvCa PDM #17 and #24 in comparison to #21 (\log_2 NFI = -0.33). PDM #17 and #24 further exhibited high PI3K/Akt and #24 additionally exhibited high mTOR (\log_2 NFI = 0.54) protein abundances. A significant difference of apoptosis-related proteins was detected between BC-PDM (\log_2 NFI = 1.41) and OvCa PDM #25 (\log_2 NFI = 0.75), while tumor/stem-cell related markers were found to be significantly upregulated in OvCa PDM #17 and #23 compared to BC-PDM. To sum up, the applicability of RPPA for protein profiling of 3D *ex vivo* PDM was demonstrated and phenotypic features of different OvCa PDM with preserved OvCa-related tumor heterogeneity were identified.

3.1.4 Expanding and Phenotyping of Tumor-infiltrating, Autologous Lymphocytes

Modifying the protocol used to generate *ex vivo* PDM from OvCa residual fresh tumor tissue allowed for the additional collection of autologous TILs. In general, OvCa are considered to be immunogenic tumors, as they can become infiltrated by immune cells [291-293], but they are often functionally impaired by inhibitory receptors or an immunosuppressive environment [294]. This tumor surveillance has been shown to be mediated by different immune cell populations in OvCa [292]. Phenotypic characterization of T lymphocyte populations in TIL samples from n = 13 OvCa tumors by multicolor flow cytometry revealed that 57.8% of infiltrating cells were CD4⁺ helper T cells (Th) and had a significantly lower proportion CD8⁺ cytotoxic T cells (CTL) (Anderle et al. 2022, **Appendix I**, Figure 5A, Table S5). CD8⁺ TIL were further characterized by expression of co-inhibitory, immune-checkpoint receptors (PD-1, CTLA-4), the tumor-specificity, checkpoint and exhaustion marker CD39 [295] and the co-stimulatory activation marker CD137 (4-1BB) (Anderle et al. 2022, **Appendix I**, Figure 5A). Evidence for pre-exposure to tumor antigens (CD137⁺) and subsequent CD8 T cell activation [296] varied from 0-10% in the samples. More than 5% of positive CD8⁺CD137⁺ cells were detected in the samples of OvCa #1, 3, and 5. The frequencies of the co-inhibitory receptors PD-1 and CTLA-4, known CPI targets, were not significantly different among analyzed samples (Anderle et al. 2022, **Appendix I**, Table

S5). Exhausted CD8⁺ TIL populations showed >10% PD-1 (OvCa #3, 7, 25) or CTLA-4 expression (OvCa #5, 13, 26) (Anderle et al. 2022, **Appendix I**, Figure 5B). Furthermore, significant differences between the frequency of tumor antigen-specific, exhausted CD8⁺CD39⁺ TILs [297-299] and CD8⁺CD39⁻ bystander TILs, which mainly recognize viral antigens [300] were observed. On average, 40.5% of the measured TIL populations were CD8⁺CD39⁺, while 9.5% were CD8⁺CD39⁻ (Anderle et al. 2022, **Appendix I**, Figure 5A). While the frequency of CD8⁺ CTLs was strongly correlated with a higher frequency of CD39⁺ CTLs, the number of CD4⁺ cells was inversely correlated (Anderle et al. 2022, **Appendix I**, Figure S4B, Table S6). Among cell counts of exhausted PD-1⁺/CTLA-4⁺, tumor-specific CD39⁺ CTL were also of interest, as these could be directly targeted by immune checkpoint inhibitors (ICIs) to elicit an anti-tumor immune response. Compared with CTLA4⁺CD39⁺ CTLs, more PD-1⁺CD39⁺ CTLs were detected in these OvCa samples (Anderle et al. 2022, **Appendix I**, Figure 5A, Table S5). The exhaustion state primarily affects tumor-specific CD39⁺ CTLs, since the number of PD-1⁺ CTLs correlates with the number of CD39⁺PD-1⁺ tumor-specific CTLs (Anderle et al. 2022, **Appendix I**, Figure S4B, Table S6). These TILs are described as terminally differentiated effector cells with limited survival but immediate effector functions, as opposed to CD39⁻PD-1⁺ cells with a stem-like phenotype found in 7.3% of TILs [300, 301] (Anderle et al. 2022, **Appendix I**, Table S5). Lymph node metastasis was associated with both CD8⁺ and CD8⁺CD39⁺ TIL infiltration of tumors when correlating the presence of specific populations with clinical data (Anderle et al. 2022, **Appendix I**, Figure 5C).

3.2 Individual Tumor Vulnerability to Chemo-, Targeted and Immunotherapy of PDM and PDM-TIL Co-Cultures

3.2.1 Examining Drug Sensitivity in Ovarian Cancer PDM for Identification of Patient-individual Treatment Responses

Using patient-derived *ex vivo* tumor models to combine functional drug testing with tumor screening analysis prior to patient treatment is one approach to personalizing cancer therapy. It would allow for a direct assessment of the individual response of a tumor to a specific agent or to a range of drugs worth considering for individualized treatment. Therefore, the suitability of the PDM/TIL *ex vivo* platform to determine the individual tumor susceptibility to chemotherapy, targeted therapy and immunotherapy was evaluated. Since RPPA protein profiling of PDM samples previously revealed the greatest differences in cell cycle and MAPK/RTK signaling (Anderle et al. 2022,

Appendix I, Figure 3A-B), the drug efficacy of targeted inhibition of these pathways was evaluated with the CDK4/6 inhibitor palbociclib, the MEK1/2 inhibitor selumetinib, and the Src inhibitor saracatinib. Drug activity was compared to standard platinum-based chemotherapy (carboplatin) (Anderle et al. 2022, **Appendix I**, Figure 3C). Based on the reported C_{max} values, three different concentrations were used for each drug [302]. Individual OvCa PDM exhibited heterogeneous drug-induced cytotoxic cell death with the majority of 6 out of 7 PDM responding well to carboplatin and selumetinib. At 75 μ M carboplatin induced a high level of cytotoxicity after 72 h in OvCa #17, 24, but only at higher dose in OvCa #23,25. In all of these models, the cell cycle pathway was upregulated to a comparatively high degree, and most significantly in OvCa #17&24 (Anderle et al. 2022, **Appendix I**, Figure 3A-B). In contrast, treatment with palbociclib, which inhibits G1 cell cycle progression, failed to elicit a response in these two high cell cycle activity models. Palbociclib induced significant responses in OvCa #25 and #26, which showed a moderate level of cell cycle signaling and significant lower MAPK pathway signaling (#21 vs. #26) (Anderle et al. 2022, **Appendix I**, Figure 3B), associated with CDK4/6 inhibitor-resistance. Compared to palbociclib-resistant OvCa samples, OvCa #25 and #26 showed low CDK4 but high CDK4P-Thr127, overall low CDK6/CDK6-P-Tyr24 and moderate Cyclin E2 protein levels (Figure 4), which are markers associated with resistance [303-306]. Saracatinib had a dose-dependent and significant effect only in OvCa #26, inducing early cell death after 24 hours. Inhibiting the MAPK pathway with selumetinib caused significant cytotoxicity in OvCa #17,19, 21, 23 at 100-150 nM. The MAPK/RTK pathway was comparatively more upregulated in OvCa #21, which also showed the greatest increase in cell death.

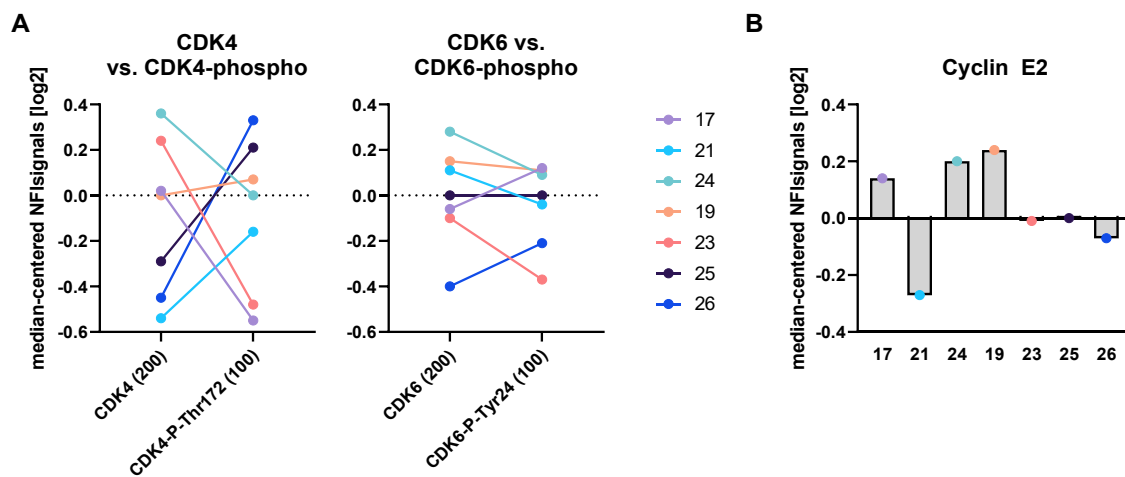


Figure 4. Expression of resistance markers for CDK4/6 inhibition in OvCa PDM. (A) Protein abundances for CDK4, CDK4-P-Thr172, CDK6 and CDK6-P-Tyr24 in OvCa PDM samples. (B) Cyclin E2 marker expression in OvCa PDM samples. Each Analyte is displayed as median-centered, log₂ transformed NFI (normalized fluorescent intensity) signal.

These heterogeneous drug responses in functional drug testing confirmed the molecular heterogeneity of OvCa PDM as determined by protein expression analysis. PDM that were resistant to standard carboplatin chemotherapy (OvCa #19, #26) instead proved sensitive to targeted therapeutic approaches.

Therapeutic efficacy of ICIs and the functional, tumor cell-killing capacity of TILs was assessed in autologous PDM-TIL co-cultures of OvCa #24 and #26 (Anderle et al. 2022, **Appendix I**, Figure 5D-F). TILs induced basal killing of PDM in both co-culture models, whereas isotype control of CPI antibodies did not affect PDM viability (Anderle et al. 2022, **Appendix I**, Figure 5E-F). Applied monotherapy failed to elicit a response in OvCa #24 PDM, while CPI combination treatment with PD-L1 and CTLA (atezolizumab and ipilimumab) significantly increased the treatment response (Anderle et al. 2022, **Appendix I**, Figure 5E). In contrast, OvCa #26 PDM responded to anti-CTLA-4 and anti-PD-L1 monotherapy but did not respond to anti-PD-1 monotherapy. The effects of the monotherapies were not additive in combination for this PDM model (Anderle et al. 2022, **Appendix I**, Figure 5F). In conclusion, either combined CPI therapy (OvCa #24) or specific anti-PD-L1 therapy (OvCa #26) enhanced TIL-specific killing of PDM. The beneficial effects of these immunotherapies may be related to the profiled TIL OvCa #24 and #26 phenotypes. The TIL populations had a greater population of CTLA-4⁺ CTLs and a lower proportion of terminally exhausted, tumor-specific (CD8⁺CD39⁺PD-1⁺) CTLs compared to other profiled models (Anderle et al. 2022, **Appendix I**, Figure 5B).

3.2.2 Specific Molecular Protein Signatures Dictate Responsiveness to Chemotherapy in Ovaria Cancer PDM

In order to investigate the specific responses to carboplatin, PDM were divided into responders and non-responders based on the results of the drug test, and their protein expression patterns were compared (Anderle et al. 2022, **Appendix I**, Figure 3C). HCL cluster analysis identified five protein clusters with differential expression between responders and non-responders (Anderle et al. 2022, **Appendix I**, Figure 4A). The proteins were sorted according to their pathway affiliation. This revealed proteins that were either up- or downregulated in the treatment response group (Anderle et al. 2022, **Appendix I**, Figure 4B). Carboplatin sensitivity was significantly associated with upregulation of cell cycle, RTK, PI3K/Akt/NFκB and apoptosis/DNA damage response pathways, including, as previously reported, increased levels of mitosis-associated proteins [307], as well as cleaved-caspase 8 and cleaved PARP (Anderle et al. 2022, **Appendix I**, Figure S2A). Sensitivity to therapy was highly correlated with p-aurora A/B/C, cyclin B1 and PCNA (Anderle et al. 2022, **Appendix I**, Table S3). Carboplatin resistance was associated with low expression of aurora A, cyclin B1, p-S6P, PDGFR and snail1, but high expression of G0/G1-related proteins. Despite the small cohort size, analysis of available clinical follow-up data of corresponding patients demonstrated a prolonged median OS of 16.2 months for tested carboplatin-responder versus 9.2 months for non-responder PDM (Anderle et al. 2022, **Appendix I**, Table S4).

3.2.3 Drug Mode-of-Action Analysis in Carboplatin Treated OvCa-PDM

Examining treatment-related changes in protein profiles of carboplatin-treated OvCa #24 PDM revealed substantial and time-dependent changes in treatment-to-control signal ratios (TR). Immediate proteomic changes occurred after 30 min of carboplatin treatment: downregulation of the cell cycle-related proteins p-CDK2, CDK1, and p-histone H3 (Ser10), affecting chromatin condensation during cell division, and induction of known stress response mechanisms [307] by upregulating the mTOR effector proteins S6RP and p-S6RP (Anderle et al. 2022, **Appendix I**, Figure 4C, Figure S3). Within the first four hours after treatment, the stress response via the PI3K/Akt/mTOR pathway was significantly increased compared to vehicle control, and the expression of p-aurora ABC and histone H3 raised. While cell cycle, PI3K/Akt/mTOR, and MAPK/RTK signaling were significantly downregulated after 72

hours of treatment, apoptosis-related signaling activity increased with elevated cleaved caspase and acetylate p53 levels. In summary, RPPA has been shown to map treatment-induced temporal changes in signaling pathways in a single PDM sample. However, it has the potential to provide insight into treatment response mechanisms.

Chapter 4

Results II:

Harnessing Breast Cancer Patient-Derived Microtumors for Protein-Based Stratification and Functional Validation of Individualized Drug Treatment

The contents of this chapter are based on

Anderle, N., Schäfer-Ruoff, F., Staebler, A., Kersten, N., Koch, A., Önder, C., Keller, A-L., Liebscher, S., Hartkopf, A., Hahn, M., Templin, M., Brucker, SY., Schenke-Layland, K., Schmees, C. *Breast cancer patient-derived microtumors resemble tumor heterogeneity and enable protein-based stratification and functional validation of individualized drug treatment.* (PREPRINT available at Research Square, 2023; <https://doi.org/10.21203/rs.3.rs-2781727/v1>) - **Accepted:** 28 July 2023;
Published: 18 August 2023: *J Exp Clin Cancer Res* **42**, 210 (2023).
<https://doi.org/10.1186/s13046-023-02782-2>

4 Results II: Harnessing Breast Cancer Patient-Derived Microtumors for Protein-Based Stratification and Functional Validation of Individualized Drug Treatment

BC remains the most common cancer and the second leading cause of death among women. It has been classified into 19 different histologic subtypes due to the great genetic, morphologic, and clinical heterogeneity of these tumors [308]. Global gene expression analyses have further classified BC into four molecular subtypes with distinct gene expression patterns: HR-related luminal A and B tumors versus HR-negative, HER2-enriched, and basal-like tumors [309-313]. These reflect distinct phenotypes with different prognoses, different treatment paradigms, and different responses to therapy [314-318]. The development of treatment resistance, side effects, and inadequate efficacy remain major treatment challenges despite advances in the clinical stratification of BC patients by H&E and IHC analysis of HRs, HER2, and Ki67 expression [194, 309-311] and the application of genetic testing including MammaPrint® and Oncotype DX® [319]. Most importantly, the enormous diversity of tumor cell profiles within a patient's tumor determined by genomic, epigenomic, proteomic alterations, the TME and other factors [320, 321], determines systemic treatment failure [194]. The development of tailored BC therapies has the potential to increase treatment efficacy and reduce side effects. However, to accurately assess the individual efficacy of potential therapies, *ex vivo* patient-derived models that closely mimic the patient's primary tumor would be of high value. In addition, protein expression profiling can provide a comprehensive understanding of treatment resistance mechanisms at the protein level by revealing information that may not be reflected in genomic mutation and gene expression analysis. For this purpose, PDM were established from a cohort of $n = 102$ residual fresh mammary carcinoma tissue samples comprising tumor cells, TME and ECM components. PDM were successfully obtained from various BC subtypes with histopathologic features and ECM components (e.g. collagen, PGs/GAGs) corresponding to those of the original primary tumor according to the blinded assessment of a certified pathologist. Heterogeneous signaling pathway activity was revealed by protein profiling of BC-PDM using the DigiWest® technology, reflecting the intertumoral heterogeneity of the disease. The expression levels of BC-related proteins and the profiles of signaling pathways were highly correlated with those of the corresponding primary tumors. Hierarchical clustering grouped BC-PDM according to classification and molecular signature of

protein expression. The combination of functional drug testing and pathway analysis was used to assess patient-specific treatment responses and identify treatment sensitivity/resistance markers in BC-PDM. This allowed for the identification of phenotypic hallmarks of treatment resistance and sensitivity in BC and thus the stratification of individualized treatment.

4.1 In-Depth Profiling of PDM Derived from Surgically Resected BC Specimens for *Ex Vivo* BC Modeling

4.1.1 Isolation of Viable PDM and TIL from a Heterogenous Population of BC Patients

The aim of the study was to extend the previously established 3D platform of PDM and TILs described in Anderle et al. (2022) [322] to investigate intra- and intertumoral heterogeneity as well as treatment response in BC. A total of $n = 102$ fresh residual BC tissue samples were obtained from debulking surgical procedures performed at the Women's Hospital in Tübingen, Germany. Patients over 18 years of age with a diagnosis of BC of any molecular subtype were eligible for participation. TIL populations were successfully isolated and expanded in >95% of samples analyzed, with average TIL viability >90% (Figure S1A-B). Heterogeneous subpopulations of regulatory and exhausted T cell populations were identified by multicolor flow cytometry analysis (Figure S1C-H). BC microtumor isolation was performed as previously described (Anderle, 2002 #512). Here, the protocol was adapted by the extension of the tissue digestion time from two hours to overnight. In this way, PDM could be successfully generated in more than 75% of the cases. 50% of the 102 tissue samples received yielded more than 100 PDM per sample (Anderle et al. 2023, **Appendix II**, Figure 1D). When correlating the available clinical data of the obtained tumor specimens with the obtained PDM specimens, there was no correlation between the success of PDM isolation and clinical features (Anderle et al. 2023, **Appendix II**, Figure 1E). High viability of freshly isolated PDM was demonstrated by live-dead cell staining with Calcein-AM and Sytox™ Orange of PDM from 27 different patients (Anderle et al. 2023, **Appendix II**, Figure 1A-B). The microtumors varied in size with a mean area of $59,261 \mu\text{m}^2$ (Anderle et al. 2023, **Appendix II**, Figure 1C, Table S2). The higher the number of single PDM recovered per patient, the more downstream analyses were performed per patient. These downstream analyses included IHC, anticancer drug efficacy testing, and/or protein profiling.

4.1.2 Preservation of Breast Cancer Subtype Specific Histopathologic Features in NST and ILC PDM

H&E staining of tissue biopsies is the most important technique in histopathologic diagnosis. It allows visualization of morphologic features and assessment of morphologic changes in tumor tissue. BCs are characterized by highly heterogeneous histopathology, with nineteen different BC subtypes distinguished by WHO [308], most commonly invasive ductal carcinoma (IDC) and invasive lobular carcinoma (ILC). FFPE sections of BC-PDM and corresponding PTT were H&E stained, imaged, and qualitatively evaluated in a blinded fashion by a board-certified pathologist at the University Women's Hospital, Tuebingen, Germany, to compare histopathologic and cytologic characteristics of BC-PDM and corresponding PTT (Anderle et al. 2023, **Appendix II**, Figure 2A-C). Pathologic evaluation revealed that PDM specimens resembled breast tumor histology in $n = 39/40$ cases and matched the histologic tumor type in 95% ($n = 36/38$) (Anderle et al. 2023, **Appendix II**, Figure 2C). A distinct and irregular growth pattern was observed in PTT sections of IDCs of no specific type (NST), with or without in situ lesions. Tumor cells formed invasive nests, clusters, cords, and sheets within the surrounding stroma. Tissue sections also showed clear ascitic structures filled with tumor cells, small tubular structures with small lumina, papillary structures, or no clear architecture. NST-PDM tumor cells resembled the solid, cohesive, papillary growth pattern with closely spaced cells clearly separated from the ECM compartment, similar to the histopathology of NST-PTT (Anderle et al. 2023, **Appendix II**, Figure 2A). In comparison, the arrangement of tumor cells in ILC-PDM mimicked that of primary infiltrating tumor lesions, which grow scattered and disjointed in the surrounding stromal tissue, similar to slender strands ("Indian files"). Alternatively, invasive cells grew concentrically around ducts or lobules in PTT sections. Meanwhile ducts and ascites of in situ lesions in PTT retained their overall structure. When comparing cellular aberrations, similar cellular atypia was observed, with some samples showing small homogeneous cells without marked nuclear aberrations common to in situ lesions, whereas most BC-PDM showed moderate to severe nuclear pleomorphism and hyperchromasia (Anderle et al. 2023, **Appendix II**, Figure 2B-C). In 59% of the samples, the BC-PDM nuclear grade was reduced by 1 degree (Anderle et al. 2023, **Appendix II**, Figure S1A). Further, a stromal compartment was found in over half of the BC-PDM (Anderle et al. 2023, **Appendix II**, Figure 2C).

These results suggest close histopathologic correspondence between BC-PDM and PTT sections.

4.1.3 Verification of Preserved Extracellular Matrix Composition Using Movat's Pentachrome Staining of Breast Cancer PDM and PTT.

The TME is defined as a composite of various cells, stroma and soluble molecules influencing tumor growth, progression, invasion and resistance to therapy [76, 323, 324]. The stroma itself is made up of a variety of cells, including fibroblasts, immune cells, blood vessels and the ECM. The ECM serves as a scaffold that surrounds the cells of the tissues and organs to provide structure, support and a reservoir for e.g. growth factors [325, 326]. The ECM consists of fibrils (e.g. collagen, elastin), glycoproteins (laminin, fibronectin), proteoglycans (PGs) and glycosaminoglycans (GAGs). The ECM of BC-PDM and corresponding BC-PTT was examined by Movat's pentachrome staining [327], highlighting major components of the BC-related ECM: PGs/GAGs in cyan/blue, collagen fibers in yellow, mucin in blue/grey and elastin in black (Anderle et al. 2023, **Appendix II**, Figure 2D). Most of the collagen fibers and PG/GAGs were overlapped, resulting in a green color. Despite enzymatic degradation (collagenase I and II, dispase) of received tumor tissue, the ECM scaffold found within PTT was not completely destroyed when PDM extracted. Thus, various PDM displayed ECM components of corresponding PTT, but to a lesser degree. The expression of collagen (yellow/green) was detected in BC-PDM #29,36,58,53,70, with a less specific arrangement than that in PTT, serving more as a backbone scaffold for the tumor cells. In PTT increased collagen deposition leads to dense collagen fibers in the vicinity of the tumor masses and causes stiffening of the tissue [326]. The collagen fibers varied in appearance in the PTTs, sometimes short and wavy, sometimes thin and straight, and sometimes thick and straight. Strikingly, the stromal areas adjacent to the in situ lesions in the PTT sections, where the collagen fibers were tightly wrapped around the tumor cell masses, showed the thickest fibers. They were either drawn at tangential angle around these lesions or at a perpendicular angle to the direction of cell invasion, as described in Provenzano et al. (2006) [328]. In addition to collagen, PGs/GAGs were conserved in BC-PDM, when their expression was found to be high in the tumor masses in corresponding PTT (e.g. #29, 31, #58). Either PG/GAGs were located within tumor masses or delineated them from tumor stroma and collagen fibers in PTT. Elastic fibers (black) were more abundant in the PTT of the ILC compared to the IDC and were mostly associated with collagen. BC-PDM #102 was the only PDM that showed elastin

in correlation with the primary tumor. Mucin was also sporadically detected as an ECM component. Mucin was secreted by PTT #31 and 86, and corresponding PDM. After the identification of various ECM components in BC-PDM, the correlation between tumor subtype and the extent of collagen deposition was investigated (Anderle et al. 2023, **Appendix II**, Figure 2E-F). Color deconvolution and evaluation of the collagen-positive %-area fraction using Image J, revealed significant higher amount of collagen fibers within ILC-PTT, as previously reported [329]. The extent of collagen deposition in the PDM was not comparable to the extent of deposition in tissues but showed a similar (non-significant) trend toward slightly higher levels in ILC-PDM. In conclusion, Movat's pentachrome staining visualized different primary tumor ECM components within BC-PDM. Compared to whole tumor masses in tumor tissue, ECM compartments in BC-PDM are less abundant and have a slightly different arrangement. Thus, PDM are similar to tumor fragments removed from the corresponding PTT, containing the central tumor cell mass along with its ECM components, but without the surrounding thick collagen fibers.

4.1.4 Immunohistochemical Analysis of BC-Specific Tumor Markers and Stromal Cell Markers

Complementary to the histologic assessment of BC-PDM, the expression of several relevant BC markers was analyzed by IHC of FFPE PDM sections and semi quantified using color deconvolution as described [330]. Beyond the histological classification of breast tumors into different subtypes, breast tumors are classified at the molecular level based on the expression of hormone receptors (HR). Expression of HER2, cytokeratins (CKs), CAFs and immune cell markers were examined in addition to ER α and PgR expression. Based on the results of pathologic examination of the associated primary tumors, the BC-PDM were classified as HR⁺ or TNBC, with TNBC being an aggressive subtype lacking HR or HER2 expression. The expression of HR and HER2 in BC-PDM was compared with the pathological classification of the corresponding primary tumors (Anderle et al. 2023, **Appendix II**, Figure 3A-B). The results showed that the expression of ER α and PgR expression in BC-PDM matched the corresponding clinical classification and was increased in HR⁺ BC-PDM compared to TNBC PDM. In contrast, HER2 expression was detected in only a few HR⁺ BC-PDM (#10 & 37) and the expression varied with respect to HER score (Anderle et al. 2023, **Appendix II**, Figure 3A).

CKs are intermediate filaments found in the cytoskeleton of epithelial cells. The luminal epithelial cells line the ducts and lobules of the breast and are surrounded by myoepithelial cells that form the basement membrane. Different CKs help to distinguish between these two cell types and are also used to classify breast tumors into basal-like CK5/6/7/14⁺ and luminal subtypes CK8/18/19⁺ [309, 325, 331-333]. The differential expression patterns between the HR⁺ and TNBC PDM as well as the ILC and NST PDM were analyzed. Both HR⁺ and TNBC PDM exhibited highly heterogeneous expression of CKs, with HR⁺ PDM expressing significantly higher levels of CK18, a marker for luminal carcinoma (Anderle et al. 2023, **Appendix II**, Figure 3C-D). Apart from TNBC PDM #38, TNBC PDM did not express CK18, but did express CK5/6 to a moderate extent. Due to the high level of CK5/6 positivity, which correlates with a worse prognosis [334], TNBC PDM #38 was considered to represent a basal-like subtype of TNBC. Four groups based on CK expression were identified within HR⁺ PDM: CK5-/CK18⁺ (luminal, differential glandular phenotype), CK5⁺ (basal), CK5/6⁺ (basal, stem cell phenotype), and CK5/6/18⁺ (intermediate glandular phenotype) [335] (Anderle et al. 2023, **Appendix II**, Figure 3C-D). Comparison of CK5/6 expression between luminal and myoepithelial subtypes revealed significantly increased expression in HR⁺ CK5⁺ PDM and HR⁺ CK5/6⁺ PDM (Anderle et al. 2023, **Appendix II**, Figure 3D). Within the CK5-CK18⁺ subgroup, CK18 was significantly enriched in comparison to CK5 or CK6. Some of the HR⁺ BC-PDM models were positive for all three of the CKs. When comparing the ILC and NST BC subtypes, the HMW CKs (CK5/6) were upregulated in the ILC PDM, whereas the luminal CK18 was elevated in the NST PDM (Anderle et al. 2023, **Appendix II**, Figure 3E).

The presence of the stromal cell and immune cell markers FAP, CD163, CD8 and PD-L1 in BC-PDM was also examined (Anderle et al. 2023, **Appendix II**, Figure 3F). FAP⁺ CAFs were found in all BC-PDM, as opposed to immune cells such as CD8⁺ T cells and CD163⁺ M2 macrophages, which were only sporadically detected. ILC PDM contained significantly more FAP⁺ CAFs compared to NST PDM (Anderle et al. 2023, **Appendix II**, Figure 3E, $p = 0.028$). In summary, BC PDM generally reflect the HR status of the corresponding PTT, and show variable expression of CKs and FAP α , which differ in HR⁺ and TNBC PDM, as well as in NST and ILC PDM.

4.1.5 DigiWest®-based Protein Profiling of BC-PDM Captures Disease Heterogeneity and Reveals Conserved Primary Molecular Tumor Profiles

In-depth quantitative protein profiling analysis was performed on 20 matched BC-PDM-PTT pairs using DigiWest® technology [336]. Protein expression and activity of key signal transduction pathways were determined by measurement of 142 total and phosphorylated proteins (Anderle et al. 2023, **Appendix II**, Table S3-4). Proteins analyzed were representative of the cell cycle, JAK/STAT, MAPK, RTK, PI3K/Akt, EMT/cytoskeleton, and Wnt/NFκB signaling pathways. To investigate the conservation of primary tumor protein expression signatures in BC-PDM, DigiWest® protein signals from $n = 20$ paired PDM and corresponding primary tumors were compared. Overall, there was a strong positive correlation ($P_r = 0.856$) between the averaged protein signals of matched BC-PDM and PTT (Anderle et al. 2023, **Appendix II**, Figure 4A). This was confirmed by similar pathway activity and breast-cancer-associated protein expression (Anderle et al. 2023, **Appendix II**, Figure 4B, Table S5). Eighteen analytes were identified as significantly differentially expressed between BC-PDM and PTT (Anderle et al. 2023, **Appendix II**, Figure 4C-D). Consistent with the findings from IHC analysis of BC-PDM, BC-PDM demonstrated elevated levels of the cytoskeletal proteins CK5 and CK6, and reduced expression of immune cell markers including CD11c, CD16, CD68, CD8 alpha, CD25, PD-1, and PD-L1. The remaining proteins were distributed in a variety of signaling pathways and had lower expression levels, including p38 MAPK-pThr180/Tyr163, PI3K p85/p55-pTyr458/199, and NFκB p65-pSer172, IKK alpha-pThr23, IKK epsilon-pSer172 (Anderle et al. 2023, **Appendix II**, Figure 4C-D). The correlation of the majority of analyzed individual protein levels between the BC-PDM and the corresponding PTT resulted in an overall positive correlation (Anderle et al. 2023, **Appendix II**, Figure 4E-F). There were strong, significant correlations between individual protein abundances of BC-PDM and PTT across pathways, including the ERα protein expression with a $P_r = 0.86$ (Anderle et al. 2023, **Appendix II**, Table S6). Summarized, at the protein level, the cellular signaling activity of the primary tumor is preserved in the PDM, as demonstrated by the correlation between BC-PDM and the corresponding PTT. Moreover, the IHC findings were confirmed: PDM are small tumor fragments with ECM components harboring some stromal cells and rare immune cell infiltration.

4.1.6 Microtumors Illustrate the Pronounced Intertumoral Heterogeneity of Corresponding Primary Breast Cancer

Valuable information on patient-specific altered protein expression, modification and interaction in key signaling pathways was obtained from the protein profiling data of $n = 42$ BC-PDM. Using hierarchical cluster linkage (HCL) analysis BC-PDM samples were classified into different sample clusters based on patient-specific signaling pathway activity (Anderle et al. 2023, **Appendix II**, Figure 5, Table S7). Samples were assigned according to the clinical classification of the corresponding PTT (Anderle et al. 2023, **Appendix II**, Table S1). Four groups of samples with different levels of expression of cell cycle related proteins, such as transcriptional activators E2F-1, E2F-2, transcriptional repressor E2F-4 and p53, were characterized (Anderle et al. 2023, **Appendix II**, Figure 5A). Elevated levels of cell cycle related proteins were found in the cluster with TNBC, HER2⁺ and some HR⁺ BC-PDM ($n = 16$). Samples with low and mixed levels of cell cycle activity were grouped into cluster 2 ($n = 8$) and 3 ($n = 17$). Further, BC-PDM exhibited distinct profiles of MAPK/RTK signaling activity, with $n = 19$ HR⁺ BC-PDM showing lower overall protein abundance and $n = 19$ TNBC, HER2⁺, and HR⁺ PDM showing high protein expression, including c-Met, RSK1-pThr573, NF1 and c-Raf (Anderle et al. 2023, **Appendix II**, Figure 5B). Comparison of PI3K/Akt pathway activity revealed two clusters of BC-PDM: one cluster with only HR⁺ BC PDM with relatively low PI3K/Akt pathway activity and the second cluster with all TNBC and HER2⁺ PDM plus additional HR⁺ PDM with high PI3K/Akt pathway activity (Anderle et al. 2023, **Appendix II**, Figure 5C). Substantial differences were noted in the expression of beta catenin, FoxO3a, Akt-pSer473, CREB, CREB-pSer133, PDK1 and IKKalpha-pThr23.

Moreover, the individual BC-PDM protein profiling data presented in box-whisker plots reflected the individuality of each PDM model at the molecular protein level (Anderle et al. 2023, **Appendix II**, Figure 5D, Table S8). Median-centered protein profiling data identified samples with increased cell cycle, MAPK/RTK, and PI3K/AKT protein abundance. Eight samples showed enhanced cell cycle activity, 11 samples showed amplified MAPK/RTK signaling, and seven samples showed upregulated PI3K/AKT pathway activity. All three pathways were upregulated in four of the BC-PDM samples (#20, #78, #92 and #96), which do not share a common histologic or molecular subtype. Other BC-PDM samples showed a simultaneous down-regulation of all pathways (#15, #18, #60, #89, #99; \log_2 AFI ≤ 1). Thus, pathway analysis in individual

BC-PDM allowed characterization of individual protein expression profiles with reproducible TNBC tumor-specific pathway activity in TNBC-PDM. In addition, with PDM samples having similar signal transduction but no common histologic or molecular subtype, the data suggest a potential subtype independence of pathway activity.

4.1.7 Protein Profiling Data of TNBC-PDM

Genetic alterations in the upstream regulators of the PI3K/Akt and MAPK/ERK pathways, including mutations in PI3K, Ras, b-Raf, and loss-of-function in PTEN, as well as EGFR overexpression, are prevalent in TNBC resulting in oncogenic signaling, cellular dysregulation and chemoresistance [337-344]. In line with this, significant alterations in the PI3K/AKT and MAPK/RTK were identified in the DigiWest® protein data of BC-PDM, allowing differentiation of TNBC from HR⁺ PDM (Anderle et al. 2023, **Appendix II**, Figure 5E). For cell cycle and NFκB/Wnt signaling, however, no significant differences were observed. Protein levels of AKT ($p = 0.022$), eIF2α-pSer51 ($p = 0.009$), eIF4E ($p = 0.049$), GSK3beta ($p = 0.006$), GSK3beta-pSer9 ($p = 0.007$), PTEN ($p = 0.040$), PTEN non-p ($p = 0.044$), p70S6K ($p = 0.009$), CREB-pSer133 ($p = 0.041$), PI3K/AKT pathway regulators associated with TNBC, were significantly upregulated. Like the PI3K/AKT pathway [345, 346], the MAPK/RTK pathway is one of the major drivers of TNBC and is associated with a high rate of disease recurrence [347]. Significantly enhanced MAPK/RTK pathway proteins in TNBC PDM included Erk1/2, MEK2, Src-pSer17 and Src-pTyr527 (Anderle et al. 2023, **Appendix II**, Figure 5F). TNBC was distinguished from HR⁺ PDM by hyperactivation of CDK2 and CDK2-pThr160, which are associated with basal BC, and increased expression of CDK4 and CDK4-pThr172, which are associated with drug resistance [347-349]. Also consistent with the increased phosphorylation of eIF2α in the TNBC PDM and the associated upregulation of aerobic glycolysis was the upregulation of metabolism-related proteins, including GLUT1 ($p = 0.029$) and IDH1 ($p = 0.029$) [350-352]. In summary, the BC-PDM protein profiling data are consistent with previous studies in TNBC and are an accurate reflection of the activation characteristics of the primary breast tumor signaling pathways.

4.2 Combination of Protein Profiling and Functional Drug Testing Elucidates Treatment Response Mechanisms

4.2.1 Patient-specific Treatment Responses of *Ex Vivo* BC-PDM towards Hormonal Therapy, Chemotherapy and Targeted Therapy

Tumor heterogeneity plays a critical role in the resistance to therapy and thus influences the response to treatment and the outcome of BC. Since patient tumor derived BC-PDM are heterogeneous in cellular composition and reflect intertumoral heterogeneity as described above, they have been used to investigate patient-specific responses to cancer therapies. Three BC treatment strategies were evaluated in a microplate-based cytotoxicity assay: hormonal therapy with the selective estrogen receptor modulator (SERM) tamoxifen (TAM), chemotherapy with the taxanes docetaxel (DTX) and paclitaxel (PTX), and targeted therapy with the CDK4/6 inhibitor palbociclib [353]. Treatment-related cell death was measured in a time series (24h, 48h and 72h) and compared to the respective vehicle control (Anderle et al. 2023, **Appendix II**, Table S9). There was no prior stratification of samples by receptor status. Based on significant or non-significant measured cell death signals (FC vehicle vs. FC treatment), samples were categorized into responder (R) and non-responder (non-R) groups. BC-PDM showed variable response to drug treatment. The most common drug response was to treatment with DTX, with $n = 9/29$ (31%) of the BC-PDMs tested found to be sensitive. $N = 6/27$ (22.2%) had a significant response to PTX treatment. $N = 4/29$ (13.8%) PDM were sensitive to TAM treatment, compared to $n = 5/26$ (19.23%) PDM sensitive to PAP treatment (Anderle et al. 2023, **Appendix II**, Figure 6A).

4.2.2 Identification of Treatment Resistance and Sensitivity Marker Panels Using BC-PDM

For each treatment, the protein expression profiles of treatment responsive and non-responsive PDM samples were compared. Resistance and sensitivity protein marker panels were generated for TAM, DTX, PTX, and PAB treatments to help discriminate between BC-PDM responders and non-responders. These panels identified proteins previously associated with therapy resistance or sensitivity, significantly differentially expressed between responder and non-responder BC-PDM or involved in therapy-related signaling pathways. Nine proteins significantly differentially expressed in responder versus non-responder BC-PDM treated with TAM were identified in both resistance and sensitivity marker panels (Anderle et al. 2023, **Appendix II**, Figure 6B,D, Table 2). Treatment-resistant BC-PDM had elevated phosphoprotein levels of

ER α -pSer167, FGFR-pTyr653/654, PI3-kinase p85/p55-pTyr458/199, and IKKepsilon-pSer172 protein levels, which were previously associated with TAM resistance [354-359]. Furthermore, cell cycle-related proteins such as CDK6 were found to be significantly differentially expressed (Anderle et al. 2023, **Appendix II**, Figure 6C) and negatively affected the likelihood of TAM response with a 50% decrease of the odds (OR = 0.5, 95% CI 0.21-0.82) (Anderle et al. 2023, **Appendix II**, Figure S4B, Table S10). Comparatively, the TAM-sensitive BC-PDM exhibited higher protein levels of ER α , the transcriptional repressor protein E2F-4, the microtubule protein α Tubulin, proteins involved in cancer cell metabolism (GLUT1, LDHA and PDK1-pSer241) and stress response (eIF2A-pSer51).

Proteins involved in the induction of EMT and in drug metabolism have previously been implicated in the resistance to DTX/PTX drugs [360, 361]. In accordance with these reports, elevated levels of vimentin-pSer56, NF κ B p100/p52, IKK ϵ -pSer172, caveolin-1, cyclin E1, and b-Raf-pSer445 contributed to DTX resistance and discriminated non-responder from responder BC-PDM. Both caveolin-1 (*p = 0.029) and b-Raf-pSer445 (**p < 0.001) were significantly enriched in non-responding BC-PDM and decreased the odds of DTX response by 44% (OR = 0.56, 95% CI: 0. 0.32-0.88) and 54% respectively (OR = 0.46, 95% CI: 0.25 to 0.72) (Anderle et al. 2023, **Appendix II**, Figure 6E-F, S4D, Table 2, S10). Moreover, the combination of elevated ER α , luminal cell marker (CK 8/18), inactive beta-catenin-pSer552 and microtubule-associated protein tau-pSer202, among others, predicted the sensitivity to DTX treatment (Anderle et al. 2023, **Appendix II**, Figure 6H). In the present panel, CK 8/18 (**p < 0.001) and tau-pSer202 (*p = 0.028) were identified as significantly enriched and associated with DTX treatment response in BC-PDM (Anderle et al. 2023, **Appendix II**, Figure 6H, S4D, Table 2, S10).

PTX resistance in BC-PDM was determined by a 9-protein panel with comparably elevated levels of caveolin-1, PgR, mTOR, phosphorylated MEK1/2 (pSer217/221) of the Erk/MAPK pathway, phosphorylated IKK α (pThr23) of the NF κ B pathway, microtubule-associated protein Tau, and the basal BC markers CK5, CK6, and vimentin-pSer56 (Anderle et al. 2023, **Appendix II**, Figure 6I-J, Table 2). Vimentin-pSer56 was significantly upregulated in responders and decreased the likelihood of response to PTX (Anderle et al. 2023, **Appendix II**, Figure S4D, Table S10). To differentiate between PTX-sensitive and resistant BC-PDM, a 13-protein panel was identified. Higher protein abundances of several cell cycle-associated proteins (e.g.

CDK1, CDK4-pThr172), luminal epithelial cell markers (e.g. E-cadherin, CK 8/18), the microtubule-forming protein tubulin (acetylated Tubulin, tubulin beta-chain), the Ras-inhibitor NF1 (neurofibromin), c-Met-pTyr1003 and beta-catenin-pSer55 affected PTX treatment sensitivity (Anderle et al. 2023, **Appendix II**, Figure 6K-L). Increased expression of GATA3 (OR=2.34, 95% CI: 1.24-6.2) and NF1 (OR=2.15, 95% CI: 1.25-4.5) doubled the odds of responding to PTX (Anderle et al. 2023, **Appendix II**, Figure 6L, S4D, Table S10). To the best of our knowledge, there have been no previous studies that have correlated the expression of these proteins with the response to PTX treatment.

As a selective inhibitor of the cyclin-dependent kinases CDK4 and CDK6, PAB prevents the cell progression through the G1 phase of the cell cycle [362]. A panel of proteins previously associated with PAB resistance has been identified in PAB-resistant BC-PDM: CDK6, cyclin E1 and FGFR [363]. Together with the basal cell markers CK6 and vimentin, the MAPK signaling protein Erk1/2- pThr202/Tyr204 and the active mTOR signaling protein eIF4E-pSer209, these proteins differentiated PAB-resistant from PAB-sensitive BC-PDM (Anderle et al. 2023, **Appendix II**, Figure 6M). In contrast, PAB-sensitivity was defined by an 8-protein panel consisting of elevated ER α , HER2, CDK2-pThr160, E-cadherin-pSer838/840, cyclin D1, c-Raf-p259, JNK/SAPK-pThr183/Tyr185 and p38MAPK-pThr180/Tyr182 (Anderle et al. 2023, **Appendix II**, Figure 6N-O). PAB response was significantly dependent on high levels of ER α (OR = 2.15, 95% CI: 1.2-5.91) [364, 365], HER2 (OR = 72.48, 95% CI: 2.36-14948598) and E-cadherin-pSer838/840 (OR = 1.84, 95% CI: 1.15 to 3.55), which more than doubled the odds of PAB response (Anderle et al. 2023, **Appendix II**, Figure S4D; Table S10). In conclusion, differential responses to multiple anticancer therapies relevant to BC could be assessed using the *ex vivo* BC-PDM platform. By analyzing the molecular protein signaling pathways in both sensitive and resistant BC-PDM, new insights into the treatment response mechanisms of BC cells were obtained while the histopathology, protein expression profiles, and heterogeneity of primary breast tumors are preserved. These findings support a role for protein markers that are already known to influence the resistance or sensitivity of a patient to therapy. However, novel markers have also been identified that were highly correlated with an individual's response to treatment in the present study.

Chapter 5

Results III:

Immune Suppression in Glioblastoma: Microtumors as a Valuable Tool for Immunotherapy Evaluation

The contents of this chapter are based on:

Przystal JM, Becker H, Canjuga D, Tsiami F, **Anderle N**, Keller A-L, Pohl A, Ries CH, Schmittnaegel M, Korinetska N, Koch M, Schittenhelm J, Tatagiba M, Schmees C, Beck SC, Tabatabai G. *Targeting CSF1R Alone or in Combination with PD-1 in Experimental Glioma*. *Cancers*. 2021; 13(10):2400.

5 Results III: Immune Suppression in Glioblastoma: Microtumors as a Valuable Tool for Immunotherapy Evaluation

Particularly GBM, the most common malignant brain tumor in adults [366] currently lacks effective therapies, which is reflected in poor overall median survival and high recurrence rates [367-371]. Despite promising preclinical studies [372-374], a plethora of phase III clinical trials have disappointingly failed [375-380], with some recent exceptions [381]. This highlights the urgent need for new therapeutic strategies to prolong the overall survival of GBM patients. Immunotherapies have been successfully used to treat several cancer types and may represent a promising treatment alternative and are currently being investigated for GBM [381-386]. Yet, they mostly failed to improve overall survival (OS) in GBM patients [379, 387-390]. Main causes are high tumoral heterogeneity and the highly immunosuppressive TME of GBM [391]. Each subtype of GBM has a distinct immunologic landscape with varying degrees of infiltration by T cells and macrophages/microglia [392]. Preclinical studies have shown that targeting the TME through inhibition of the CSF-1/CSF1R axis is a novel therapeutic option that may transform the TME into a non-tumorigenic environment [393, 394] and may be an adjunct to anti-PD-1 immunotherapy [395]. CSF1R blockade directly targets pro-tumorigenic M2 macrophages (TAMs), which are the major immunosuppressive stimuli in GBM [396, 397], inducing prolonged overall survival [394] and microenvironmental remodeling in preclinical studies [398] compared to a phase II clinical trial that showed no objective response, with the primary endpoint of 6-month progression-free survival being only 8.6% [393].

Using an autologous experimental *ex vivo* platform of PDM co-cultured with and without TIL from residual GBM tissue, this study aimed to investigate the effects of anti-CSFR1 monotherapy [399] and combination therapy with anti-PD-1. Thereby, treatment effects that directly affect or remodel the TME were investigated. Based on the transcriptomic data of Neubert et al. [2] [395], the potential additive effect of anti-CSF1R blockade to anti-PD-1 therapy in GBM was studied based on the enrichment of non-anti-PD-1-responsive CD8⁺ T cells with CSF-1. In this context, using an *ex vivo* system derived from patient material allowed capturing both tumor heterogeneity and the patient's immune system, complementing the study's *in vivo* assays.

5.1 Targeting the TME by CSF1R-Blockade in Glioblastoma-PDM Co-Cultured With and Without Autologous TILs

To study the efficacy of a novel immunotherapy strategy inhibiting the immunosuppressive TME in experimental *ex vivo* GBM, PDM and autologous TILs were isolated from fresh residual tissue of GBM resections as illustrated before [322]. Tissue dissociation was performed by mechanical shredding, enzymatic disruption, and filtration. Microtumors were successfully isolated as tumor fragments > 100 μ M in size with intact cell-cell contacts and a three-dimensional architecture (Przystal et al.2021, **Appendix III**, Figure 7A). GBM microtumors were assayed for viability after 2-3 days in culture, while patient-specific TILs were expanded using anti-CD3/CD28 stimulation and low cytokine doses after isolation (Przystal et al.2021, **Appendix III**, Figure S5A, S6C). Calcein-AM was used to stain living cells of GBM-PDM. After hydrolysis of the acetoxymethyl ester by intracellular esterases, the initially non-fluorescent calcein-AM is converted to green, fluorescent calcein. Compromised dead cells on the other hand were stained with the nucleic acid dye Sytox™ Orange. Furthermore, IHC staining confirmed targeted expression of CSF1R in PDM models #1 and #2, whereas CD68⁺CD204⁺ macrophages were identified only in PDM model 2 (Przystal et al.2021, **Appendix III**, Figure 7A, S6A). Model 1 GBM-PDM were subsequently co-cultured with autologous TILs and treated with either anti-CSF1R [399], anti-PD-1, or the combination of both at various concentrations. The cytotoxicity induced by the monotherapy was measured at 6 different concentrations after 72 hours of treatment. The addition of autologous TILs to the PDM culture in the absence of immunotherapy already resulted in the killing of the tumor cells. The addition of 1 or 5 μ g/mL of CSF1R inhibitor further enhanced this effect and resulted in significant responses relative to IgG control treatment (Przystal et al.2021, **Appendix III**, Figure 7B). At the lowest combination dose, similar treatment responses were observed with 50 μ g/mL or 125 μ g/mL of anti-PD-1 or the combination of both. These results suggest therapy induced activation of the immune system.

In order to investigate the mechanism of CSF1R or PD-1 blockade on PDM-infiltrating TAM, PDM were treated without the addition of TILs (Przystal et al.2021, **Appendix III**, Figure 7A(2), C). Treatment of PDM with either anti-CSF1R, anti-PD-1 or the combination in the absence of TILs (model 2) resulted in different outcomes. Except for the highest dose (125 μ M), monotherapies failed to induce significant cytotoxic effects (Przystal et al.2021, **Appendix III**, Figure 7C). Again, the combination of anti-

PD-1 and CSF1R treatment resulted in significant tumor cell death, with the lowest combination dose being most effective in comparison to IgG control treatment and monotherapies. To confirm the finding of combination efficacy in *ex vivo* GBM models, the immunotherapy was evaluated in a third PDM model derived from another GBM patient. Again, the strongest effect was obtained by combination treatment of the two inhibitors (Przystal et al.2021, **Appendix III**, Figure S6B). Similar to the PDM model 2, TAMs were detected in model 3 as well as high levels of CSFR1 expression (Przystal et al.2021, **Appendix III**, Figure S6A).

5.2 Characterization of Affected TIL Populations by Flow Cytometry

Different populations of T cells have different effects on the tumor. They can be immunosuppressive or immunostimulatory. For example, a high proportion of cytotoxic CD8⁺ T cells is correlated with a better prognosis in GBM [400], while Treg cells are mainly associated with recurrence and poor prognosis in GBM patients [401]. T cell populations within the TILs were characterized by multicolor flow cytometry to draw conclusions about the immunotherapy responses to anti-CSF1R and anti-PD-1 in the PDM-TIL coculture. Cytotoxic CD8⁺ T cells (55.5%) and fewer CD4⁺ helper T cells (37.7%) comprised slightly more than half of the CD3⁺ TILs (Przystal et al.2021, **Appendix III**, Figure S5). Both the CD8⁺ and the CD4⁺ TILs showed activation by the expression of CD137 and CD107, which identify antigen-stimulated T cells [402]. Thus, PDM model 1 TILs were mainly composed of tumor antigen-stimulated T cells, which were able to induce tumor-specific cell killing when added to GBM-PDM (Przystal et al.2021, **Appendix III**, Figure 7C). In summary, this study demonstrates the feasibility of investigating the therapeutic potential of immunotherapy *ex vivo* in a patient-derived platform consisting of PDM cultured with and without autologous TILs. Results from *ex vivo* cultures of three separate GBM patients suggest that parallel inhibition of TAMs and PD-1 might have the potential to increase the cytotoxic efficacy of anti-PD-1 therapy and represent a novel potential immunotherapy strategy.

Chapter 6

General Discussion and Conclusion

6 General Discussion and Conclusion

Over the past few decades, research has made great strides in the fight against cancer. Much of this has been driven by the development of new technologies, new therapies, and new preclinical models. The downside is: Tumor diseases are more complex than originally thought. The complexity of tumors is a result of inter- and intratumoral heterogeneity, which is influenced by a multitude of components, mechanisms, and signals. Recently, the impact of TME on tumor heterogeneity and its impact on drug efficacy has been elucidated [403-405]. The high recurrence rates in OvCa [267], the vast tumor heterogeneity leading to therapy resistance in BC and OvCa [265, 266, 406], and the lack of treatment options in GBM [407] underscore the need to develop new and effective treatment approaches. This includes, on the one hand, the development of new targeted therapies, including TME targeting drugs, and on the other hand, new treatment strategies that take a personalized approach. Over the past decade, personalized cancer therapy has emerged as a new approach aimed at identifying and assessing individual tumor susceptibility and subsequently tailoring treatment [199, 200]. To this end, new pre- and clinical methods are being elaborated in the context of clinical validation, sampling and histopathological analysis of tumor material, preclinical models, drug development and multiomic analysis, to enable comprehensive stratification of individual patients. These include restructuring of clinical trials from drug- to patient-oriented studies, performing genome-/transcriptome-/proteome-based biomarker analysis, developing new drug concepts and multitargeting treatment approaches, and developing more reliable preclinical tumor models [219, 220, 408-412]. Tumor models that accurately represent the complexity of a patient's tumor and that can be applied to multiple readout modalities are gaining significance. Although a number of different *ex vivo* platforms have been established, including PDO, PDX, tumor explants and others [413-415], well validated and characterized, readily available patient-derived preclinical models that fully mimic tumor heterogeneity, tumor microenvironment including connective tissue, immune and stromal compartments, are still lacking [209, 416-418]. In this sense, this study aimed to establish and validate a novel, *ex vivo* patient-derived 3D model accurately recapitulating highly heterogeneous and advanced tumors focusing on BC, OvCa and GBM. Finally, its preclinical applicability for individual patient stratification through functional testing of different cancer therapies and the identification of potential therapy resistance/sensitivity markers based on proteomic data is demonstrated.

6.1 Establishment of Viable PDM and Autologous TIL: Efficacy of the Isolation Procedure

The present study demonstrates the successful implementation and advancement of a previously reported protocol [276] for isolation of 3D tumor fragments termed microtumors and autologous TILs from primary OvCa, BC and GBM tumor specimen. Using mechanical disruption, enzymatic dissociation, and filtration, a repertoire of highly viable PDM and autologous TIL samples was successfully generated. For both OvCa (87.5%) and BC (75%), success rates for PDM generation are comparable to PDO [250, 259, 274, 419]. When the success of PDM isolation was correlated with the clinical characteristics of the tumors, no bias was observed. Concluding that the success of PDMs isolation is independent of the tumor subtype. On average, hundreds to thousands of microtumors can be isolated from fresh tissue samples for individualized in-depth multiparametric analysis and functional drug testing, based on experience with the various tumor types in this study. Successful PDM isolation is primarily determined by the tumor tissue provided and its quality. Criteria include tissue size, tumor cell density, tissue viability, and the extent of fibrosis and necrosis. Factors that also play a role in the establishment of PDO [420-422]. The good quality of the tissues obtained is confirmed by the robust and high viability of the obtained PDM. This also rules out quality problems in the transport chain as a cause for the sometimes lower numbers of PDM, as was the case in 50% of the BC samples with less than 100 PDM. To ensure optimal tissue quality for successful PDM generation, close collaboration and coordination with clinicians and surgeons is indispensable.

A limitation of this model in comparison to PDO [420] is the limited number of PDM that can be isolated from tumor tissue digestion. However, laborious procedures such as splitting larger PDM into multiple smaller ones could increase the number of PDM per sample. Conversely, as known from classical cell line culture, expansion and repeated passages in PDO generation cause genetic drift and clonal selection [259]. Although limited by the number of PDM obtained, samples with high PDM amounts are suitable for drug screening purposes in a 384-well format. This raises the question of what drug throughput can be used in PDM cultures, unlike spheroids derived from cancer cell lines or organoids that are expandable. [423-425]. Although possible, the establishment of a patient-specific functional drug test to assess patient-specific susceptibility was the primary objective of this study.

Unlike other patient-derived tumor models [420, 422, 426-428], the time from tumor tissue collection to PDM recovery is very short, less than 24 hours. The rapid availability of PDM allows immediate downstream analysis within the diagnosis-to-treatment interval, making PDM a clinically relevant tumor model for individualized functional drug testing. Furthermore, suspension culture of PDM eliminates the need for an artificial ECM matrix, thus avoiding the use of animal material such as Matrigel or chemically defined hydrogels as is required for PDO generation and expansion. Therefore, the influence of animal origin and batch-dependent differences in the composition of Matrigel on the comparability with human tumor tissue has to be considered for PDO cultures [429, 430]. However, synthetic alternatives to Matrigel are being developed. To summarize, PDM have the advantage over PDO that they can be obtained more quickly, easily and cheaply from patient tumor tissue, do not require culturing in an extracellular matrix, and are directly available for functional testing without expansion.

6.2 The Reproducibility of the Primary Tumor

6.2.1 Histopathologic and Immunohistologic Correlation: Preservation of Histopathological and Subtype Specific Features of the Primary Tumor in PDM

Detailed characterization is required for a clinically relevant, i.e. translatable, tumor model. Specifically, the *ex vivo* reproducibility of subtype specific tumor tissues must be ensured first and foremost by demonstrating histopathologic similarity to the primary tumor, which is still the gold standard and fundamental for diagnosis and patient stratification. Pathologic tumor classification is routinely performed according to specific histologic features, i.e. tissue and cell structures typical for the specific tumor type, such as degree of pleomorphism, cellular atypicality, mitotic activity, and stromal circumference. Standard H&E stains were performed and reviewed by a certified pathologist and compared to sections of the corresponding primary tumor tissue in a blinded fashion to determine these characteristics and identify differences and similarities on the obtained PDM specimens. The results of the histopathologic assessment of OvCa- and BC-PDM demonstrate retention of histopathologic and subtype specific features such as growth pattern, cellular pleomorphism and atypia of the corresponding primary tumors comparable to PDO cultures [250, 274, 419]. PDM from patients with different tumor subtypes show different expression of these features,

illustrating preservation of histopathologic tumor characteristics of primary tumors. Specifically, typical high-grade tumor characteristics such as papillary growth pattern, irregular branching, pleomorphism, and high nuclear-cytoplasmic ratio are conserved in HGSC OvCa-PDM and are distinct from low-grade mucosa-derived OvCa, a slow-growing OvCa subtype [431, 432]. Further, this study could histologically differentiate BC-PDM into NST or ILC based on preserved subtype specific tissue patterns [308, 433] found in corresponding primary tumors.

Similar to grading differences between punch biopsies and surgical specimens due to the underestimation of mitotic count [434-437], some BC-PDM were graded lower than the primary tumor. As is the case with punch biopsies, this may be attributable to ITH [438]. Histopathologic evaluation of breast tumor PDO showed a similar picture: PDO could also not be clearly assigned to a tumor status and were frequently graded lower [250]. Finally, meaningful comparison of the grading would require more PDM sections (minimum $n = 10$) per patient for accurate staging.

Besides reflecting histopathologic characteristics of the original tumor, PDM also preserve the expression of subtype-specific markers of the corresponding primary tumors as confirmed by IHC. These include CA125, p53 and WT1 expression in OvCa subtypes [278, 439], HR and CK expression in BC subtypes [309, 311, 318, 331, 332, 440], and CSF1R as a marker for glioma-associated microglia/macrophages within GBM [441]. Similar to PDO cultures [250, 274, 419], BC-PDM could be differentiated into HR⁺ and TNBC samples based on HR expression, while OvCa-PDM could be classified as HGSC on the basis of p53 and WT1 expression [442]. As determined by IHC, the pathologically determined HR status was maintained in BC-PDM. In contrast to other PDO studies [250, 443, 444], multiple CK expression profiles of BC-PDM were characterized as reported by Abd El-Rehim et al. (2004) [331]. Here, PDM were further differentiated into CK5⁺ and double-positive CK5/6-expressing PDM. Our results indicate reduced luminal CK18 levels in TNBC PDM, consistent with previous reports [331, 440]. However, contrary to findings that only 17% of the ILCs express basal CKs [445], a generally high expression level of basal CKs was found within the ILC as compared to the NST PDM. Further evaluation in a larger ILC cohort is warranted for this unexpected finding. As described in primary BC tumors [331, 335], some of the HR⁺ BC PDM were positive for all luminal and myoepithelial CKs. Unexpectedly, the overall expression of CK5 and CK6 were upregulated in BC-PDM regardless of subtype compared to the corresponding primary tumors as shown by DigiWest®

protein analysis. This discrepancy of CK5/6 levels between PDM and PTT was also observed in BC-PDO cultures [443] and may result from estrogen-deprived culture conditions or even from ECM-free cultivation, which may cause CK upregulation to support tumor sphere formation in suspension [446-448]. The possibility that the PDM culture conditions select for basal-like subclones (CK5/CK6⁺), which are frequently observed in *BRCA*-1-related BC [449, 450] and are underrepresented in the primary tumor, cannot be ruled out. This should be subject of following studies. Overall, the long-term effects of PDM culture conditions over a period of more than three weeks to several months on the stability of BC, OvCa and GBM tumor-specific markers and the underlying mechanisms are beyond the scope of this study and require further investigation.

In conclusion, PDM mimic the histopathology of the original primary tumor such as cellular atypia, morphology, and cytology, and further allow for the differentiation of tumor subtypes of BC and OvCa. As previously observed with PDO in breast tumors, tumor grade cannot be clearly determined from a few PDM sections and would need to be re-examined using more sections. Overall, PDM reflect the expression of tumor-specific markers important for tumor stratification and can be considered an equivalent tumor model to PDO in this regard [250, 274, 419, 422]. Beyond that, this study suggests that the expression of CK5/6 in *ex vivo* cultured 3D BC-models such as PDO and PDM is affected by the cultivation conditions.

6.2.2 Modeling the Tumor Microenvironment

Several processes of tumorigenesis are substantially influenced by the surrounding tissue. Reciprocal and dynamic crosstalk between tumor cells and the non-cellular/cellular components of the TME results in TME reorganization. This crosstalk controls tumor growth, progression, metastasis, clonal evolution, tumor heterogeneity, EMT, neovascularization and drug resistance to targeted, chemo- or immunotherapies in OvCa, BC and GBM [281, 282, 284, 325, 326, 451-455]. It is regulated by a intricate network of tumor cells, tumor stromal cells such as stromal fibroblasts, endothelial cells, and immune cells such as microglia, macrophages, and lymphocytes, as well as the non-cellular components of the ECM such as tissue fibers (collagen), glycoproteins (e.g. elastin, fibronectin, laminin), PGs, and GAGs, (e.g. hyaluronan) [325, 326]. The better a model represents this complexity, the better it will be able to reflect the tumor biology and therapeutic response of the patient's tumor. Pathologic examination, DAB

immunohistochemistry and Movat's pentachrome staining [327] demonstrated the presence of a native TME in PDM sections of BC, OvCa and GBM. Similar to PTT, OvCa-PDM expressed the CAF marker FAP α , which is detectable in 90% of epithelial OvCa and induces tumor progression and chemoresistance [283]. Subtype specific expression profiles have further been identified in BC-PDM. ILC PDM contained significantly more FAP-expressing CAFs compared to NST PDM, as described previously [456]. Interactions between CAFs and BC cells have been shown to promote the migration, invasion and ultimately the metastasis of cancer cells [457-460]. The roles of CAFs are diverse and include the production of ECM proteins, the induction of angiogenesis via FGF2 and VEGFa [461], and serving as a source of nutrients for tumor cells [462]. Which of these processes occur in PDM has not been investigated but should be the subject of future studies. The presence of "tumor tissue native" CAFs in PDM provides a platform with preserved tumor stroma to study cellular effects of CAFs on therapeutic response on the one hand and to evaluate the effect of CAF-targeted therapies on the other hand [463-465]. Importantly, since PDO are known to lack endogenous tumor-associated stromal components, particularly immune cells and fibroblasts, this can only be achieved in PDO models by co-culturing PDO with CAFs [466-468].

Tumor-associated connective tissue elements such as PGs, hyaluronic acid-associated GAGs and collagen fibers [329, 469], as detected by Movat's pentachrome staining or by the expression of C1QBP [470] and collagen in IHC, are retained in PDM, but collagen at comparatively lower levels than in the corresponding PTT. This may be due to enzymatic digestion of tumor tissue with collagenase I, required to isolate PDM. Tumor-specific expression patterns of these connective tissue elements, such as increased collagen deposition in ILC tumors [454], have been demonstrated in this study. Collagen deposition, fiber density and orientation induce ECM stiffening and impact tumor aggressiveness, invasiveness, therapy response, and correlate with prognosis in BC [328, 471-474]. Notably, collagen I, like FAP, promotes tumor progression and invasiveness in OvCa [321, 475, 476] and BC [328, 454, 474].

While PDM show conserved native, endogenous ECM of primary tissues, organoid models are rather simplistic as they lack native ECM and stromal cells, which are important regulators of drug responses in patients [262, 477]. Organoids consist of dissociated single tumor cells of epithelial origin that lack cell-ECM interactions and only grow in 3D when embedded in a biological or synthetic scaffold, most commonly

Matrigel, and with various exogenous growth factors [478]. Matrigel is derived from mouse sarcoma and comes with several drawbacks in this regard [429, 479] such as high batch-to-batch variability, the potential for transmission of animal pathogens due to the origin of the material [480, 481] and a composition or stiffness of the ECM that may not provide the ideal tissue-specific microenvironment [482, 483]. To overcome this limitation of organoid culture, great efforts are being made to generate natural matrices and synthetic hydrogels[484-488]. The need for extrinsic biological or synthetic ECM is easily eliminated when the intrinsic cell-cell contacts of a resected tissue are maintained, as in PDM isolation, thereby preserving non-cancerous cells, cell-cell and cell-ECM interactions on the one hand, and the 3D microarchitecture on the other.

In order to overcome the limitations of syngeneic mouse models, which only represent mouse tumors and not human tumors, PDX models have been developed for different tumor types by implantation of patient-derived tumor tissue, tumor cells or organoids into immunodeficient mice [237]. While the subcutaneous implantation of tumors in PDX is very simple and allows for little tissue damage and easy monitoring [489], the orthotopic implantation in the organ corresponding to the tumor ensures a matched anatomical microenvironment [235]. Besides the lack of a functional immune system, the use of orthotopic PDX for drug discovery is hampered by the fact that the human stroma, as part of the implanted tissue, is replaced by the mouse stroma after only a few passages, with the fastest replacement occurring with CAFs [235, 477, 490, 491]. Although PDM demonstrate preservation of tumor-derived ECM, CAFs and connective tissue, the long-term maintenance of this ECM is unknown and warrants further investigation.

Besides the influence of ECM, the presence of immunosuppressive TME is a major limitation for the success of novel therapeutic approaches such as immunotherapies in GBM [451, 452]. Therefore, the fact that GBM-PDM possess an immunosuppressive TME due to the high expression of myeloid CSF1R and infiltration with TAM (CD204⁺) [392], indicating immunologically cold tumors with multidimensional resistance mechanisms to immunotherapy [492-497], is advantageous for immunotherapy evaluation over PDO and PDX. In contrast, immunosuppressive TAM and CD8 TIL are sporadically found in PDM of OvCa and BC. Low CD8 T cell infiltrated, immunologically cold tumors are associated with poorer patient survival in OvCa [292] and BC [498, 499], and are largely unresponsive to immunotherapies [113, 500]. The low immune

cell content within the OvCa-/BC-PDM may either truly resemble immunologically cold tumors with low intratumoral TILs [501], defined as lymphocytes in direct contact with tumor cells within the tumor nests, or it may reflect the cell culture-related depletion of non-proliferating immune cells. In any case, this is also reflected in the low level of NFkB signaling in the PDM, as measured by the DigiWest®. However, since tumor tissue-isolated TILs could be cultured, expanded and characterized by flow cytometry, the presence of stromal TILs [501] located in the stroma between tumor nests without tumor cell contact can be confirmed. This allows for the direct investigation of immunotherapies in autologous PDM-TIL co-cultures. Summarized, PDM may exhibit an immune cell infiltrate, albeit varying in individual patients and between tumor entities, reflecting tumor heterogeneity. This highlights the importance of individual tumor analysis to decipher the unique immunologic tumor landscapes.

Reliable cancer models for personalized oncology and drug development, especially for immunotherapies, that preserve the key features of the native TME and molecular properties of the native tumor at the individual patient level, are highly desired as a translational tool to improve cancer research [502, 503]. PDM, mainly distinguishable from PDO and PDX by the preservation of a native TME with connective tissue and stromal cells, can serve as a novel tumor model to enable fast and effective evaluation of anti-cancer drugs, especially targeting the TME. Nevertheless, newly developed humanized PDX models with a functional immune system [504-506] will play a particularly important role in the preclinical testing of immunotherapeutics.

6.2.3 Molecular PDM Profiles: The Heterogeneity of Signal Transduction

The development of NGS has resulted in several multigene expression tests (e.g., MammaPrint™, Oncotype DX™, and Prosigna ROR™ and PAM50) [507, 508] that have been applied to characterize BC subtypes and estimate the risk of recurrence as well as the benefit of adjuvant chemotherapy [509-511]. Using such gene expression analysis, trials attempted to target specific driver mutations of tumors. Disappointingly, in the largest precision oncology trial (NCI-MATCH) [211], only a minority of patients with predicted genetic vulnerabilities - identified in 38% of patients - benefited from targeted treatment. A number of additional studies have reported similar findings [212, 213, 512-515]. This failure is illustrative of the fact that changes in DNA or RNA do not always translate into changes at the protein level, and thus into changes in cellular function and in the tumor phenotype [516]. Because cancer cell phenotypic

heterogeneity is determined by non-genomic as well as mutation-related mechanisms [55, 60, 61] genomics alone cannot fully predict therapeutic response. For this reason, treatment decisions should not be made solely on the basis of DNA/RNA profiles, especially in very aggressive cancers e.g. TNBC [517-520]. By identifying altered pathways and dysregulated proteins associated with genetic alterations [521], proteomics can resolve tumor heterogeneity [522-524]. In this way, proteomics can contribute to the identification of suitable prognostic biomarkers [525, 526], cancer diagnosis, cancer subtyping [527] and patient stratification [528], as well as the identification of new therapeutic targets [525, 526] and markers of treatment resistance [529]. Given the limitations of genomic analysis to decipher the cellular function and translation to phenotype, this study identified phenotypic tumor profiles of various PDM utilizing DigiWest® and RPPA protein profiling contrasting commonly applied genomic and transcriptomic analyses in OvCa and BC PDO [250, 274, 419, 530]. These highly sensitive and robust immunoassays allowed quantification of >110 or 142 proteins from limited OvCa-/BC-PDM sample material for relative protein expression and post-translational modifications (e.g. cleavage, phosphorylation, acetylation) [336, 531]. Both methods allowed the interrogation of key signaling transduction pathways and confirmed intertumoral heterogeneity of cellular signaling activity in PDM previously observed by IHC. Samples hierarchically clustered according to their classification and their pathway activity profiles (protein expression signatures). The data highlighted significant differences in cell cycle and MAPK/RTK pathway activity in OvCa-PDM and confirmed known TNBC protein signatures in TNBC-PDM, such as upregulated PI3K/Akt and MAPK/RTK signaling [344, 346, 347, 532], overexpressed proteins associated with stress response [533, 534], higher relapse rates, mortality [347, 535, 536], tumor growth and EMT [537-539]. Furthermore, a high correlation between PDM protein expression and corresponding primary tumors is shown not only semi quantitatively by IHC, but also quantitatively by DigiWest®. Strikingly, the detected, reduced expression of NFκB pathway proteins, which mainly regulate immune and inflammatory processes and are involved in the immune defense against transformed cells [540, 541], is comparable to the reduced expression of immune-related genes in a PDM-similar GBM model [422]. The decreased NFκB-related signals in BC-PDM likely reflect the limited presence of immune cells within BC-PDM, discussed previously in section 6.2.2.. Further, DigiWest® confirmed the elevated CK5/6 protein levels of

PDM compared to PTT as previously demonstrated by IHC staining and discussed in section 6.2.1..

In conclusions, RPPA- and DigiWest-based protein profiling allows for the identification of molecular signatures and grouping of phenotypically similar PDM. Significantly, PDM preserve key molecular profiles and the intertumoral heterogeneity of the native primary tumors. Ultimately, the combination of translational omics approaches (genomics, transcriptomics, proteomics and metabolomics), of tumors and corresponding PDM may enable stratified, patient-specific medicine, and the prediction of treatment response.

6.3 Utility of PDM and TIL in Functional Testing of Therapeutic Modalities

The ability to predict patient-specific responses to anticancer drugs prior to treatment will ultimately enable the personalization of cancer treatment. To this end, functional validation of cancer therapies in patient-derived *ex vivo* models will be required to complement the molecular and histopathological analysis of individual tumors. To date, the limited reproducibility of tumor complexity in *ex vivo* preclinical models in terms of TME and intratumoral heterogeneity has led to a large discrepancy between preclinical results and clinical success [542]. Given the preserved tumor heterogeneity and key molecular pathways of the primary tumor, PDM provide an excellent platform for the evaluation of personalized drug efficacy and drug sensitivity. The study provides proof of concept that validation of individual susceptibility of PDM to chemo-, targeted and/or immunotherapies at C_{max} drug concentrations previously reported in clinical trials [302] is feasible. Despite the relatively good response to first line cytoreductive surgery and platinum-based chemotherapy in patients with OvCa, treatment resistance and disease recurrence are prevalent [543]. Respective treatment responses to carboplatin were found in OvCa-PDM with four out of seven models being sensitive to treatment. Comparison of molecular protein profiles of PDM revealed high cell cycle signaling associated with carboplatin sensitivity. Notably, carboplatin-resistant PDM were instead sensitive to targeted therapy with the MEK inhibitor selumetinib, underscoring the importance of validated functional drug testing to identify patient-specific susceptibility and drug resistance prior to treatment. Similarly, BC-PDM showed divergent treatment responses to TAM (13.8%), PAX (22.2%) or PAB (19.25%), with DTX showing the highest response rate with 31%, consistent with its high activity as an anti-microtubule agent in the neoadjuvant and adjuvant treatment of early node-

positive, anthracycline-resistant, advanced or metastatic BC [544-546]. The differential response to anticancer drugs suggests that PDMs are a reflection of the patient-specific heterogeneity and complexity of the primary tumor and its differential sensitivity to drugs. Combined gene expression analysis and functional drug testing of PDM would further enable genotype-drug and phenotype-drug correlation to evaluate the targetability of individual gene alterations [221, 419]. For example, the patient-specific sensitivity to PARP inhibitors and the correlation with *BRCA1* and *BRCA2* mutations would be of great interest for future follow-up studies in OvCa- and BC-PDM [547-549]. This would integrate not only proteomic but also genomic evaluation into functional drug testing [217] of PDM. The capability to perform functional drug testing makes the PDM an *ex vivo* platform that can quickly and easily test patient responses to standard of care and targeted therapies in a clinically relevant timeframe. However, subsequent validation in PDX as reported in PDO [250, 273], followed by prospective validation in co-clinical studies will be required to demonstrate the comparability and the predictability of the *ex vivo* results obtained.

Due to the lack of major changes in treatment strategies for several tumor types, immunotherapy is increasingly being investigated as a new treatment approach to improve long-term remission in resistant tumors such as recurrent OvCa [550-552] and GBM [553-555]. Common preclinical models used for this purpose include syngeneic mice [556], PDX [557] and humanized PDX [558-560], each of which has its advantages and disadvantages. As a non-animal replacement for some of these models, this study demonstrates the feasibility of conducting *ex vivo* immunotherapy evaluations using OvCa- and GBM-PDM combined with autologous TILs. The immunogenicity of both tumor types [561, 562] with CD4⁺ and CD8⁺ isolated TILs as demonstrated by flow cytometry data and their correlation with progression-free survival and overall survival [291, 293, 400, 401, 563-565] are rational to pursue immuno-oncologic treatments such as ICI in these tumors. Isolated OvCa-TIL have been found to be predominantly composed of CD4⁺ TILs. This suggests a higher degree of immunosuppression, which in turn is associated with a worse prognosis of patients with OvCa [563]. Furthermore, since CD39 expression was restricted to CD8⁺PD-1⁺ TILs, our data suggest that CD8⁺ TIL levels directly correlate with the level of tumor-specific CD8⁺ CD39⁺ TIL levels and represent an exhausted, memory T cell-like phenotype [566] in OvCa patients. In general, ICI is aimed at reinvigorating exhausted, tumor antigen-specific TIL by inhibiting immune checkpoints such as PD-

1, CTLA-4, LAG-3 and TIM3 [567], thereby enhancing their effector activity. Most notably, these include successful approved monotherapies such as anti-PD-1/PD-L1 (Nivolumab/Atezolizumab) antibodies and CLTA-4 (Ipilimumab) for T cell mediated (immunologically "hot") tumors such as melanoma, NSCLC, etc. [154, 155, 568-571]. Despite being immunogenic tumors, GBM and OvCa show on average a lower T cell infiltrate compared to other tumor types [572, 573] and therefore a lower response rate to different ICIs [379, 389, 390, 574, 575]. Immunotherapeutic response is mainly dependent on the composition of the TME, the degree of infiltrating cytotoxic CD8⁺ T cells, their exhaustion state described by high PD-1 [576-578], neoantigen load and mutational burden [579-583]. These factors trigger heterogeneous, patient-specific responses to mono- and combination immunotherapies as detected in OvCa-PDM and TIL co-cultures [584], with one co-culture showing increased T cell mediated tumor killing after monotherapy with anti-CLTA-4 and anti-PD-L1, and one responding only to combination therapy with anti-PD-1/anti-PD-L1 and anti-CLTA-4. The ICI efficacy assessment was complemented by immunophenotyping of the expanded TIL populations, suggesting an association between successful anti-CTLA-4 treatment and increased presence of CTLA-4-positive CTLs combined with low proportions of terminally exhausted CD39⁺PD-1⁺ CTLs. Thus, blockade of CTLA-4 suggests enhanced activity of the tumor-specific TILs. Prospective studies using OvCa-PDM co-cultures could make an important contribution to improving the success rates of clinical interventional trials by allowing the efficacy of specific combination therapies to be pre-tested and ineffective combinations to be excluded in advance. Examples of combination therapies currently under investigation include anti-CTLA-4 with anti-PD-1 ([NCT03342417](#), [NCT02498600](#), and [NCT03355976](#)) [294], PARPi with CPIs (NCT02571725, NCT02485990, NCT03522246, NCT03642132, NCT02484404, NCT02657889, NCT03602859, NCT03737643, and NCT03740165) [294] and even CPIs with chemotherapy [353, 585].

GBM poses an even greater challenge to successful immunotherapy, as one third of the tumor mass consists of immunosuppressive TAM, as confirmed by IHC of GBM-PDM, which inhibit TIL activation [576, 586, 587]. Blocking CSF1R, a key receptor for macrophage differentiation and survival [396, 588] with an oncogenic role in gliomagenesis [589], represents a promising target in GBM to modify the immunosuppressive TME [394, 398]. The differential expression of immunosuppressive TAM and CSF1R detected in GBM-PDM allows for the

individualized evaluation of TME-targeted therapy and ICB therapy *ex vivo*. Contrary to the limited clinical success of anti-CSF1R monotherapy [393], PDM-TIL co-cultures support the potential of a combined anti-CSF1R and anti-PD-1 treatment strategy, as the combined PD-1 and CSF1R inhibition potentiated treatment-induced cytotoxicity and increased immune cell infiltration in parallel experiments in mouse models [590]. Co-culture of TILs resulted in tumor-specific cell killing mainly by activated T cells with high expression of CD137, CD107 and effector cytokines (TNF α , GranzymeB). This is supported by preclinical studies showing that combining CSF1R- and PD-1 inhibitors prolongs survival and reverses immune resistance [395, 591]. Especially the application of combination therapies holds great promise as it may prevent adaptive resistance of tumor cells to immunotherapies [592]. Optional combination with radiation or chemotherapy might further overcome resistance in GBM and would be of interest to investigate [593]. Finally, the rapid availability of PDM, the preservation of tumor heterogeneity and an intrinsic TME, together with the isolation of autologous TILs, provides an important platform for the evaluation of immunotherapy responses. PDM-TIL co-culture systems may be valuable for both the identification of potential immunotherapy biomarker and the preselection of patients most likely to benefit from immunotherapy [594, 595].

6.4 Proteomic Analysis of PDM to Allow for the Identification of Patient-Specific Treatment Susceptibilities and Markers of Therapy-Response

The need for personalized approaches to improve patient outcomes is undeniable. However, the question remains: What are the best approaches to achieve precision oncology? Genomics has been the driving force in most cases. However, with only modest objective responses in genotype-drug-matched patients, the individual predispositions identified by genomic analysis were not the precise targets hoped for [213, 596-598]. Some of the reasons for the rather disappointing results include: low matching rates of patients to drugs (5% - 49%), enrollment of patients with end-stage disease, ITH and constantly evolving genomic landscapes, the lack of available matched targeted agents, incomplete pathway inhibition, targeting of non-driver or passenger mutations, presence of other driver mutations, no obvious targetable DNA alterations and difficulties in combining targeting agents due to treatment toxicities [409, 599-602]. Proteomic methods (e.g. mass spectrometry, RPPA, DigiWest®) [286, 336, 499, 603, 604] can help to overcome some of these limitations by providing information on deregulated proteins, subtype-specific protein expression patterns

driven by genetic and non-genetic alterations, and the activity state of different pathways, thus potentially detecting aberrations that act as oncogenic drivers [521-524, 527, 605, 606]. As an innovation over PDO studies, the combination of RPPA and DigiWest® protein profiling analysis with functional drug data in 3D microtumors demonstrates a valuable way to identify mechanisms of treatment resistance and sensitivity. RPPA-based proteome profiling could assign individual OvCa-PDM drug responses to specifically up- or down-regulated pathway activities. Most importantly, PDM patterns most likely to respond to chemotherapy or targeted therapy were identified. Consistent with the ability of cytostatic drugs to induce apoptosis, particularly in actively dividing cells [607], a further correlation was found between proteins relevant to cell cycle progression through S and G2/M phases and carboplatin response of OvCa PDM. Specifically, our data suggest that elevated levels of aurora A, cyclin B1, and PCNA proteins may aid in identifying carboplatin responsive tumors. In addition, consistent with previous reports, we confirmed that reduced capacity to repair DNA damage and undergo apoptosis [608] is associated with carboplatin sensitivity in OvCa PDM, as demonstrated by increased levels of cleaved caspase-7 and cleaved PARP. By comparison of RPPA-based protein signaling pathway transduction of untreated and carboplatin-treated OvCa-PDM, previously reported therapy-induced transient protein changes as well as direct on- and off-target pathway effects [609] were determined. A rapid stress response mechanism was induced in carboplatin-sensitive PDM in addition to the concomitant degradation of cell cycle proteins and the increase in apoptosis-associated proteins. This manifests as elevated mTOR pathway activity with raised levels of S6RP and phospho-S6RP [307]. Excessive mTOR activity in combination with cellular stress and failure of cells to adapt to cellular stress can lead to p53 upregulation [610, 611] and drive cells into senescence or apoptosis [612, 613]. Similarly, in this study, n = 29 BC-PDM were tested for treatment resistance/sensitivity phenotypes using a combination of DigiWest®-based protein profiling analysis and functional drug testing of TAM, PTX, DTX and PAB. Overexpression of CDK6 has been shown to be an inhibitor of fulvestrant-mediated apoptosis and an inducer of fulvestrant-resistance [614]. Among the TAM-resistant PDM of this cohort, CDK6 levels were also elevated and shown to negatively impact the likelihood of responding to TAM treatment, suggesting similar resistance mechanisms between the two hormonal therapies. While TAM acts as a competitive inhibitor of the ER with some agonistic activity, fulvestrant acts as a selective ER degrader by inducing a conformational

change in the ER [615]. However, both of these therapies work by inhibiting the hormone-driven signaling of these receptors. Both the activation of ER α activation via Ser167 phosphorylation and the activation of FGFR may also contribute to TAM resistance [354, 358, 616], and showed increased levels in TAM-resistant PDM. Elevated total ER α levels are associated with TAM sensitivity in PDM [617], consistent with the clinical use of TAM in HR⁺ BC. Comparative PDO studies show that the functional testing of TAM has only been performed in small BCO sample cohorts, but with similarly heterogeneous responses [250, 443, 618].

The most effective treatment for BC-PDM has been found to be DTX. The chemotherapeutic agent DTX inhibits cancer cell growth by inhibiting the depolymerization of microtubules during mitosis, halting the progression of the cell cycle with the highest cell killing effect in the S phase [619, 620]. It has shown significant efficacy in the treatment of BC patients [544]. Less invasive, luminal-like CK8/18^{high} with low EMT, and ER α ^{high} BC-PDM were sensitive to treatment, in line with previous studies [621-623]. Contrary our data indicate that DTX resistance is associated with high expression of EMT-related proteins, DTX-metabolizing CYP1B1 and Caveolin-1 [360, 361, 624, 625]. Unlike this study, there are currently no reports on the effect of Tau-pSer202 or b-Raf-pSer445 on response to taxane-based treatments. As discussed by M. V. Barbolina et al. [2], it is controversial whether the expression of tau, which is thought to bind to the same microtubule target sites as taxanes, correlates with response to taxanes [620, 626]. In particular, very little is known about the function of the post-translational modifications of tau [627]. However, phosphorylation of tau results in the loss of its ability to bind microtubules [628, 629] and thus of its ability to compete with taxanes. Tau phosphorylation may therefore be a marker of taxane sensitivity. In PTX resistance, the EMT process plays a critical role in treatment resistance [630], which is in line with the resistance and sensitivity marker panel identified for BC-PDM. This panel includes EMT regulatory proteins such as vimentin-pSer56, CK5, CK6, E-cadherin, CK8/18, IKK α -pThr23, and beta-catenin-pSer55. Since, unlike DTX, increased tau levels correlate with resistance, further studies are warranted to investigate the influence of tau expression, but also phosphorylated tau, on taxane treatment response. Besides, the previously reported association between high levels of PgR and decreased PTX sensitivity was confirmed in BC-PDM [631]. Again, additional proteins not previously described to be directly linked to taxane treatment but associated with BC development were found to

significantly affect PTX sensitivity in BC-PDM: GATA3, NF1, and c-Met-pTyr1003 [632-634].

The comparison of PDM expression profiles between PAB-treated responders and non-responders, in addition to endocrine therapy and chemotherapy, provided intriguing results. PAB is approved for the treatment of ER⁺ metastatic BC in combination with fulvestrant and has been shown to prolong progression-free survival compared to fulvestrant alone [635]. Several intrinsic and acquired resistance mechanisms to CDK4/6 inhibition have been described preclinically. However, these have failed to translate to the clinic [636]. BC-PDM resistance/sensitivity panel identified multiple proteins with potential predictive value for PAB treatment response. Some of these have been implicated in PAB resistance/sensitivity in previous studies, including CDK6, cyclinE1, FGFR, cyclinD1, and ER α [636]. Surprisingly, the data also point to the expression of vimentin, CK6, CDK2-p and HER2 proteins as novel markers of responsiveness. Elevated levels of vimentin and CK6 may define a more aggressive and invasive type of tumor that is resistant to PAB, which is also reflected by the fact that two of the PAB-sensitive PDM (#20, #81) are derived from TNBC patients [637, 638]. CDK4/6 inhibitors are currently being investigated in clinical trials for the treatment of TNBC [639]. While the presence of CDK2-p, which is required for the transition from G1 to S phase, contributed to PAB sensitivity in BC-PDM, other studies have reported the opposite, as the cyclin E-CDK2 pathway can bypass the cyclin D1-CDK4/6 axis in acquired resistance [636]. One interpretation could be that the initial response to PAB is driven by pre-existing CDK2-p levels and thus active cell cycle progression. However, further upregulation during treatment could lead to acquired resistance via cyclin E-CDK2 signaling. Further studies of long-term treatment responses are warranted to decipher acquired resistance mechanisms. Differential responses to PAB treatment should also be investigated in early stage and metastatic aggressive BC-PDM.

Summarized drug responses in PDM correlate with differential treatment responses observed in cancer patients and allowed the identification of potential responder and non-responders. Furthermore, when combined with protein profiling, the results show that previously described sensitivity and resistance markers for the tested agents are also detectable in BC-PDM. This underlines the translational relevance of this model system. Besides matching known resistance/susceptibility markers, identifying new markers with possible predictive potential seems possible. Finally, PDM enable the

identification of patient vulnerabilities through the combination of functional drug testing and comprehensive molecular protein profiling. Proteomics is providing valuable insights into the complex protein networks, pathways, and processes in the heterogeneous tumor phenotypes that influence the response to treatment. While genomics allows the identification of changes in the genome, it is at the protein level that the manifestation of mutations in cellular signaling can be tracked and used to functionally classify tumors. Information about the expression levels, modifications and interactions of proteins in the pathophysiological environment is an important source of biomarkers and therapeutic targets for the individualized treatment of cancer patients [640]. Correlating these data with clinical follow-up data from respective patients will be essential to successfully implement functional testing and proteomic profiling of PDM as an *ex vivo* platform for precision oncology. In comparison, in cohorts with a limited number of cases (maximum $n < 10$), treatment responses in PDO have already been correlated with patient responses and have been shown to recapitulate patient responses to chemotherapy and targeted therapy [221, 250, 256, 419, 641]. In the analyzed OvCa cohort, carboplatin response in PDM correlated with longer median metastasis-free survival (MFS) of corresponding patients. Unfortunately, patient outcome and overall response could not be correlated as the required follow-up data was not available within the time frame of the study. Especially for BC, the patient collective consists of patients with non-metastatic disease, who received primary tumor resection and eventually adjuvant tamoxifen when ER⁺. Adjuvant tamoxifen reduces recurrence risk by one-third in the first 15 years [642], complicating comparison of patient response data with *ex vivo* functional data from PDM trials within the short study period. A focus on other patient populations, such as metastatic disease or TNBC, which have a broader therapeutic spectrum, would be more relevant for future studies to correlate patient response with PDM treatment response. Furthermore, extending the methods used to a larger cohort will increase the robustness of results.

6.5 Conclusion

To enable biomarker validation and demonstrate clinical utility for patient stratification in precision oncology, there is an undisputed need for cost-effective, reproducible preclinical models that resemble the genetic and proteomic background, the inter- and intratumoral heterogeneity, and the TME of human tumors. To lay the foundation for

successful patient stratification and treatment, it is important to develop, establish and thoroughly characterize additional *ex vivo* tumor models in addition to existing models such as PDO or PDX, which will undoubtedly remain useful in preclinical research. This study introduced and validated the establishment of PDM from freshly resected tumor specimen as complementary tumor model for heterogenous OvCa, BC and GBM. Like an ideal preclinical tumor model, PDMs mimic phenotypic and pharmacological diversity and, in contrast to PDO and PDX, preserve TME components of the native patient tumor. PDM hereby preserve healthy tumor cells within a heterogenous 3D structure including cell-cell interactions and ECM components and display histopathological and immunohistological similarities to corresponding primary tumors. Primarily, intertumoral heterogeneity is maintained within the PDM, as evidenced the levels of expression of tumor and TME markers, and the differential activity of signaling pathways that correlate with the corresponding primary tumor. Applied comprehensive protein profiling analyses and combined functional drug testing of PDM highlight the potential of identifying tumor-associated differentially expressed proteins to enable the stratification of treatment responders and non-responders. Functional drug testing in PDM identifies treatment-sensitive tumors and helps predict individual therapeutic susceptibility. Further, parallel isolation and expansion of autologous TIL allows for characterization of tumor-specific immune phenotypes as well as the assessment of immunotherapy and TME-targeting drug responses in PDM co-cultures. Clinical utility is demonstrated by isolation-efficacy, time efficiency of PDM generation, straightforward and well-established as well as animal-free culture conditions, patient-specificity, conserved tissue architecture and TME components, as well as by compatibility with a variety of downstream readout technologies. As a complement to genomic mutation analysis and standard subtype classification, the combination of individual histopathologic analysis, preclinical drug testing, and parallel protein profiling analyses of PDM may hold promise for identifying predictive markers of treatment resistance, prevent patients from receiving ineffective treatments, replace, refine and reduce the use of animals in cancer research, support clinical decision making and improve patient stratification. In the future, all available patient-derived tumor models will be complementary tools in the personalization of cancer care, each best suited and used for specific applications. For PDM, further confirmatory studies are warranted in larger sample cohorts that provide comparability with clinical follow-up data. These studies will relate functional data and protein profiles

of PDM to clinical response to treatment in individual, matched patients. Ultimately, the goal is the integration of these data with other omics data to develop an automated prediction model of treatment response for precision oncology (Figure 5). The main challenges will be the tumor complexity, the interpretation, and the integration of the generated data, especially when complemented by genomic data.

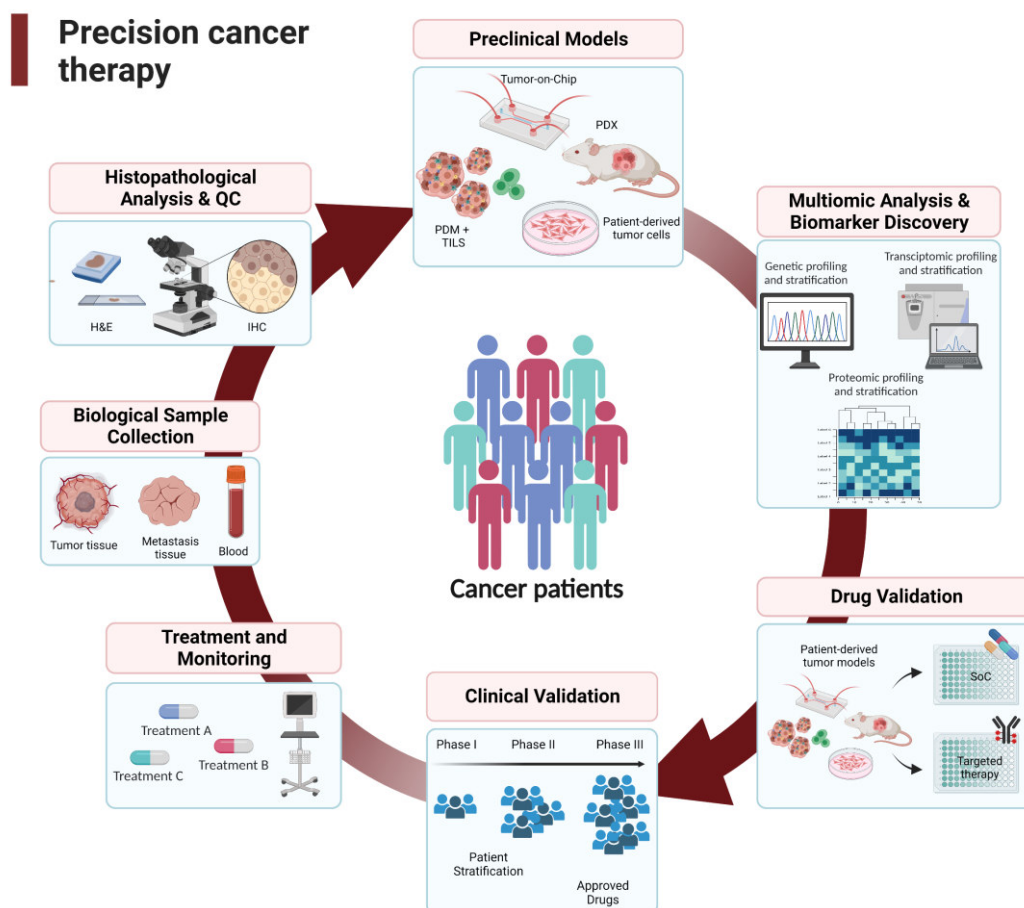


Figure 5. Overview of precision oncology. Shown is the pipeline for personalized cancer care, starting with patient sample collection, histopathology, and generation of patient-derived tumor models for multiomic analysis and drug validation. This is followed by clinical validation of novel therapies, patient treatment and monitoring of cancer patients.

References

1. World Health Organization, G., *Global Health Estimates 2019: Deaths by Cause, Age, Sex, by Country and by Region, 2000-2019*. 2020.
2. Surveillance, E., and End Results (SEER) Program (www.seer.cancer.gov) SEER*Stat Database: Incidence - SEER Research Data, 9 Registries, Nov 2020 Sub (1975-2018) - Linked To County Attributes - Time Dependent (1990-2018) Income/Rurality, 1969-2019 Counties, National Cancer Institute, DCCPS, Surveillance Research Program, released April 2021, based on the November 2020 submission. National Cancer Institute: Bethesda, MD.
3. Bailar, J.C., 3rd and E.M. Smith, *Progress against cancer?* N Engl J Med, 1986. **314**(19): p. 1226-32.
4. Kratzer, T.B., et al., *Progress Against Cancer Mortality 50 Years After Passage of the National Cancer Act*. JAMA Oncol, 2022. **8**(1): p. 156-159.
5. Sharpless, N.E. and D.S. Singer, *Progress and potential: The Cancer Moonshot*. Cancer Cell, 2021. **39**(7): p. 889-894.
6. Singer, D.S., *A new phase of the Cancer Moonshot to end cancer as we know it*. Nat Med, 2022. **28**(7): p. 1345-1347.
7. Munshi, N.C., et al., *Idecabtagene Vicleucel in Relapsed and Refractory Multiple Myeloma*. New England Journal of Medicine, 2021. **384**(8): p. 705-716.
8. Boveri, T., *Concerning the Origin of Malignant Tumours by Theodor Boveri. Translated and annotated by Henry Harris*. Journal of Cell Science, 2008. **121**(Supplement_1): p. 1-84.
9. Hanahan, D. and Robert, *Hallmarks of Cancer: The Next Generation*. Cell, 2011. **144**(5): p. 646-674.
10. Nowell, P.C., *The clonal evolution of tumor cell populations*. Science, 1976. **194**(4260): p. 23-8.
11. Vendramin, R., K. Litchfield, and C. Swanton, *Cancer evolution: Darwin and beyond*. The EMBO Journal, 2021. **40**(18): p. e108389.
12. Hanahan, D. and R.A. Weinberg, *The Hallmarks of Cancer*. Cell, 2000. **100**(1): p. 57-70.
13. Greaves, M. and C.C. Maley, *Clonal evolution in cancer*. Nature, 2012. **481**(7381): p. 306-313.
14. Heppner, G.H., *Tumor heterogeneity*. Cancer research, 1984. **44**(6): p. 2259-2265.
15. Koren, S. and M. Bentires-Alj, *Breast Tumor Heterogeneity: Source of Fitness, Hurdle for Therapy*. Mol Cell, 2015. **60**(4): p. 537-46.
16. Bakhoun, S.F. and L.C. Cantley, *The multifaceted role of chromosomal instability in cancer and its microenvironment*. Cell, 2018. **174**(6): p. 1347-1360.
17. Colotta, F., et al., *Cancer-related inflammation, the seventh hallmark of cancer: links to genetic instability*. Carcinogenesis, 2009. **30**(7): p. 1073-1081.
18. Grivennikov, S.I., F.R. Greten, and M. Karin, *Immunity, inflammation, and cancer*. Cell, 2010. **140**(6): p. 883-899.
19. Korkola, J. and J.W. Gray, *Breast cancer genomes--form and function*. Curr Opin Genet Dev, 2010. **20**(1): p. 4-14.
20. Anderson, K., et al., *Genetic variegation of clonal architecture and propagating cells in leukaemia*. Nature, 2011. **469**(7330): p. 356-61.
21. Shah, S.P., et al., *Mutational evolution in a lobular breast tumour profiled at single nucleotide resolution*. Nature, 2009. **461**(7265): p. 809-13.
22. McGranahan, N. and C. Swanton, *Biological and therapeutic impact of intratumor heterogeneity in cancer evolution*. Cancer Cell, 2015. **27**(1): p. 15-26.
23. Marusyk, A. and K. Polyak, *Tumor heterogeneity: Causes and consequences*. Biochimica et Biophysica Acta (BBA) - Reviews on Cancer, 2010. **1805**(1): p. 105-117.
24. Parmigiani, G., et al., *Design and analysis issues in genome-wide somatic mutation studies of cancer*. Genomics, 2009. **93**(1): p. 17-21.

25. Jackson, S.P. and J. Bartek, *The DNA-damage response in human biology and disease*. Nature, 2009. **461**(7267): p. 1071-8.
26. Kastan, M.B., *DNA damage responses: mechanisms and roles in human disease: 2007 GHA Clowes Memorial Award Lecture*. Molecular Cancer Research, 2008. **6**(4): p. 517-524.
27. Kinzler, K.W. and B. Vogelstein, *Gatekeepers and caretakers*. Nature, 1997. **386**(6627): p. 761-763.
28. Lane, D.P., *p53, guardian of the genome*. Nature, 1992. **358**(6381): p. 15-16.
29. Negrini, S., V.G. Gorgoulis, and T.D. Halazonetis, *Genomic instability--an evolving hallmark of cancer*. Nat Rev Mol Cell Biol, 2010. **11**(3): p. 220-8.
30. Salk, J.J., E.J. Fox, and L.A. Loeb, *Mutational heterogeneity in human cancers: origin and consequences*. Annu Rev Pathol, 2010. **5**: p. 51-75.
31. Sigal, A. and V. Rotter, *Oncogenic mutations of the p53 tumor suppressor: the demons of the guardian of the genome*. Cancer research, 2000. **60**(24): p. 6788-6793.
32. Martincorena, I. and P.J. Campbell, *Somatic mutation in cancer and normal cells*. Science, 2015. **349**(6255): p. 1483-9.
33. Olafsson, S. and C.A. Anderson, *Somatic mutations provide important and unique insights into the biology of complex diseases*. Trends in Genetics, 2021. **37**(10): p. 872-881.
34. Parsons, D.W., et al., *An integrated genomic analysis of human glioblastoma multiforme*. Science, 2008. **321**(5897): p. 1807-12.
35. Sjöblom, T., et al., *The consensus coding sequences of human breast and colorectal cancers*. Science, 2006. **314**(5797): p. 268-74.
36. Wood, L.D., et al., *The genomic landscapes of human breast and colorectal cancers*. Science, 2007. **318**(5853): p. 1108-13.
37. Alexandrov, L.B., et al., *Signatures of mutational processes in human cancer*. Nature, 2013. **500**(7463): p. 415-421.
38. Fox, E.J., M.J. Prindle, and L.A. Loeb, *Do mutator mutations fuel tumorigenesis?* Cancer and Metastasis Reviews, 2013. **32**(3): p. 353-361.
39. Kandoth, C., et al., *Mutational landscape and significance across 12 major cancer types*. Nature, 2013. **502**(7471): p. 333-339.
40. Loeb, L.A., *Mutator phenotype may be required for multistage carcinogenesis*. Cancer research, 1991. **51**(12): p. 3075-3079.
41. Stephens, P.J., et al., *Massive genomic rearrangement acquired in a single catastrophic event during cancer development*. Cell, 2011. **144**(1): p. 27-40.
42. Baca, S.C., et al., *Punctuated evolution of prostate cancer genomes*. Cell, 2013. **153**(3): p. 666-77.
43. Cross, W., T.A. Graham, and N.A. Wright, *New paradigms in clonal evolution: punctuated equilibrium in cancer*. J Pathol, 2016. **240**(2): p. 126-36.
44. Gao, R., et al., *Punctuated copy number evolution and clonal stasis in triple-negative breast cancer*. Nat Genet, 2016. **48**(10): p. 1119-30.
45. Bakhoun, S.F. and D.A. Landau, *Chromosomal Instability as a Driver of Tumor Heterogeneity and Evolution*. Cold Spring Harb Perspect Med, 2017. **7**(6).
46. Tang, Y.-C. and A. Amon, *Gene copy-number alterations: a cost-benefit analysis*. Cell, 2013. **152**(3): p. 394-405.
47. Berdasco, M. and M. Esteller, *Aberrant epigenetic landscape in cancer: how cellular identity goes awry*. Developmental cell, 2010. **19**(5): p. 698-711.
48. Esteller, M., *Cancer epigenomics: DNA methylomes and histone-modification maps*. Nature reviews genetics, 2007. **8**(4): p. 286-298.
49. Jones, P.A. and S.B. Baylin, *The epigenomics of cancer*. Cell, 2007. **128**(4): p. 683-692.
50. Hinohara, K. and K. Polyak, *Intratumor Heterogeneity: More Than Just Mutations*. Trends in Cell Biology, 2019. **29**(7): p. 569-579.

51. Huang, S., *Reconciling Non-Genetic Plasticity with Somatic Evolution in Cancer*. Trends in Cancer, 2021. **7**(4): p. 309-322.
52. Mazor, T., et al., *Intratumoral heterogeneity of the epigenome*. Cancer cell, 2016. **29**(4): p. 440-451.
53. Feinberg, A.P., *The Key Role of Epigenetics in Human Disease Prevention and Mitigation*. N Engl J Med, 2018. **378**(14): p. 1323-1334.
54. Cheung, P., et al., *Single-cell chromatin modification profiling reveals increased epigenetic variations with aging*. Cell, 2018. **173**(6): p. 1385-1397. e14.
55. Baylin, S.B. and P.A. Jones, *Epigenetic determinants of cancer*. Cold Spring Harbor perspectives in biology, 2016. **8**(9): p. a019505.
56. Xie, W., et al., *DNA methylation patterns separate senescence from transformation potential and indicate cancer risk*. Cancer cell, 2018. **33**(2): p. 309-321. e5.
57. Shen, H. and P.W. Laird, *Interplay between the cancer genome and epigenome*. Cell, 2013. **153**(1): p. 38-55.
58. Baylin, S.B. and J.G. Herman, *DNA hypermethylation in tumorigenesis: epigenetics joins genetics*. Trends in genetics, 2000. **16**(4): p. 168-174.
59. Raj, A. and A. van Oudenaarden, *Nature, Nurture, or Chance: Stochastic Gene Expression and Its Consequences*. Cell, 2008. **135**(2): p. 216-226.
60. Boumahdi, S. and F.J. de Sauvage, *The great escape: tumour cell plasticity in resistance to targeted therapy*. Nat Rev Drug Discov, 2020. **19**(1): p. 39-56.
61. Pogrebniak, K.L. and C. Curtis, *Harnessing Tumor Evolution to Circumvent Resistance*. Trends Genet, 2018. **34**(8): p. 639-651.
62. Rambow, F., J.C. Marine, and C.R. Goding, *Melanoma plasticity and phenotypic diversity: therapeutic barriers and opportunities*. Genes Dev, 2019. **33**(19-20): p. 1295-1318.
63. Nieto, M.A., et al., *EMT: 2016*. Cell, 2016. **166**(1): p. 21-45.
64. Brabletz, S., et al., *Dynamic EMT: a multi-tool for tumor progression*. The EMBO Journal, 2021. **40**(18): p. e108647.
65. da Motta, L.L., et al., *The BET inhibitor JQ1 selectively impairs tumour response to hypoxia and downregulates CA9 and angiogenesis in triple negative breast cancer*. Oncogene, 2017. **36**(1): p. 122-132.
66. Gatenby, R.A. and R.J. Gillies, *A microenvironmental model of carcinogenesis*. Nat Rev Cancer, 2008. **8**(1): p. 56-61.
67. Keren, L., et al., *A Structured Tumor-Immune Microenvironment in Triple Negative Breast Cancer Revealed by Multiplexed Ion Beam Imaging*. Cell, 2018. **174**(6): p. 1373-1387.e19.
68. Lawson, D.A., et al., *Tumour heterogeneity and metastasis at single-cell resolution*. Nat Cell Biol, 2018. **20**(12): p. 1349-1360.
69. Fane, M. and A.T. Weeraratna, *How the ageing microenvironment influences tumour progression*. Nat Rev Cancer, 2020. **20**(2): p. 89-106.
70. Fogel, O., C. Richard-Miceli, and J. Tost, *Epigenetic Changes in Chronic Inflammatory Diseases*. Adv Protein Chem Struct Biol, 2017. **106**: p. 139-189.
71. Korenchan, D.E. and R.R. Flavell, *Spatiotemporal pH Heterogeneity as a Promoter of Cancer Progression and Therapeutic Resistance*. Cancers, 2019. **11**(7): p. 1026.
72. Gillies, R.J., et al., *Eco-evolutionary causes and consequences of temporal changes in intratumoural blood flow*. Nature Reviews Cancer, 2018. **18**(9): p. 576-585.
73. Hoefflin, R., et al., *Spatial niche formation but not malignant progression is a driving force for intratumoural heterogeneity*. Nature Communications, 2016. **7**(1): p. ncomm11845.
74. Lloyd, M.C., et al., *Darwinian Dynamics of Intratumoral Heterogeneity: Not Solely Random Mutations but Also Variable Environmental Selection Forces*. Cancer Res, 2016. **76**(11): p. 3136-44.
75. Hanahan, D., *Hallmarks of Cancer: New Dimensions*. Cancer Discovery, 2022. **12**(1): p. 31-46.

76. Baghban, R., et al., *Tumor microenvironment complexity and therapeutic implications at a glance*. Cell Communication and Signaling, 2020. **18**(1): p. 59.
77. Anderson, N.M. and M.C. Simon, *The tumor microenvironment*. Current Biology, 2020. **30**(16): p. R921-R925.
78. Jahanban-Esfahlan, R., et al., *Tumor Cell Dormancy: Threat or Opportunity in the Fight against Cancer*. Cancers, 2019. **11**(8): p. 1207.
79. Lu, P., et al., *Extracellular Matrix Degradation and Remodeling in Development and Disease*. Cold Spring Harbor Perspectives in Biology, 2011. **3**(12): p. a005058-a005058.
80. Theocharis, A.D., et al., *Extracellular matrix structure*. Advanced Drug Delivery Reviews, 2016. **97**: p. 4-27.
81. Lu, P., V.M. Weaver, and Z. Werb, *The extracellular matrix: a dynamic niche in cancer progression*. Journal of cell biology, 2012. **196**(4): p. 395-406.
82. Sappino, A.P., W. Schürch, and G. Gabbiani, *Differentiation repertoire of fibroblastic cells: expression of cytoskeletal proteins as marker of phenotypic modulations*. Lab Invest, 1990. **63**(2): p. 144-61.
83. Li, H., X. Fan, and J. Houghton, *Tumor microenvironment: The role of the tumor stroma in cancer*. Journal of Cellular Biochemistry, 2007. **101**(4): p. 805-815.
84. Kim, S.-H., J. Turnbull, and S. Guimond, *Extracellular matrix and cell signalling: the dynamic cooperation of integrin, proteoglycan and growth factor receptor*. Journal of Endocrinology, 2011. **209**(2): p. 139-151.
85. Schor, S.L., et al., *Occurrence of a fetal fibroblast phenotype in familial breast cancer*. Int J Cancer, 1986. **37**(6): p. 831-6.
86. Olumi, A.F., et al., *Carcinoma-associated fibroblasts direct tumor progression of initiated human prostatic epithelium*. Cancer Res, 1999. **59**(19): p. 5002-11.
87. Bauer, E.A., et al., *Enhanced collagenase production by fibroblasts derived from human basal cell carcinomas*. Cancer Res, 1979. **39**(11): p. 4594-9.
88. Midgley, A.C., et al., *Transforming growth factor- β 1 (TGF- β 1)-stimulated fibroblast to myofibroblast differentiation is mediated by hyaluronan (HA)-facilitated epidermal growth factor receptor (EGFR) and CD44 co-localization in lipid rafts*. J Biol Chem, 2013. **288**(21): p. 14824-38.
89. Bhowmick, N.A., E.G. Neilson, and H.L. Moses, *Stromal fibroblasts in cancer initiation and progression*. Nature, 2004. **432**(7015): p. 332-337.
90. Räsänen, K. and A. Vaheri, *Activation of fibroblasts in cancer stroma*. Experimental cell research, 2010. **316**(17): p. 2713-2722.
91. Shimoda, M., K.T. Mellody, and A. Orimo. *Carcinoma-associated fibroblasts are a rate-limiting determinant for tumour progression*. in *Seminars in cell & developmental biology*. 2010. Elsevier.
92. Bouck, N., V. Stellmach, and S.C. Hsu, *How tumors become angiogenic*. Advances in cancer research, 1996. **69**: p. 135-174.
93. Hanahan, D. and J. Folkman, *Patterns and emerging mechanisms of the angiogenic switch during tumorigenesis*. cell, 1996. **86**(3): p. 353-364.
94. Krock, B.L., N. Skuli, and M.C. Simon, *Hypoxia-induced angiogenesis: good and evil*. Genes Cancer, 2011. **2**(12): p. 1117-33.
95. Casazza, A., et al., *Tumor stroma: a complexity dictated by the hypoxic tumor microenvironment*. Oncogene, 2014. **33**(14): p. 1743-1754.
96. Mazzone, M., et al., *Heterozygous deficiency of PHD2 restores tumor oxygenation and inhibits metastasis via endothelial normalization*. Cell, 2009. **136**(5): p. 839-851.
97. Polet, F. and O. Feron, *Endothelial cell metabolism and tumour angiogenesis: glucose and glutamine as essential fuels and lactate as the driving force*. Journal of internal medicine, 2013. **273**(2): p. 156-165.
98. Mittal, D., et al., *New insights into cancer immunoediting and its three component phases—elimination, equilibrium and escape*. Current opinion in immunology, 2014. **27**: p. 16-25.

99. O'Donnell, J.S., M.W. Teng, and M.J. Smyth, *Cancer immunoediting and resistance to T cell-based immunotherapy*. Nature reviews Clinical oncology, 2019. **16**(3): p. 151-167.
100. Coffelt, S.B., et al., *Elusive identities and overlapping phenotypes of proangiogenic myeloid cells in tumors*. The American journal of pathology, 2010. **176**(4): p. 1564-1576.
101. Joyce, J.A. and J.W. Pollard, *Microenvironmental regulation of metastasis*. Nature reviews cancer, 2009. **9**(4): p. 239-252.
102. Murdoch, C., et al., *The role of myeloid cells in the promotion of tumour angiogenesis*. Nature reviews cancer, 2008. **8**(8): p. 618-631.
103. Qian, B.-Z. and J.W. Pollard, *Macrophage diversity enhances tumor progression and metastasis*. Cell, 2010. **141**(1): p. 39-51.
104. Disis, M.L., *Immune regulation of cancer*. Journal of Clinical Oncology, 2010. **28**(29): p. 4531-4538.
105. Bazzichetto, C., et al., *Advances in Tumor-Stroma Interactions: Emerging Role of Cytokine Network in Colorectal and Pancreatic Cancer*. J Oncol, 2019. **2019**: p. 5373580.
106. Galon, J., et al., *Type, density, and location of immune cells within human colorectal tumors predict clinical outcome*. Science, 2006. **313**(5795): p. 1960-1964.
107. Koebel, C.M., et al., *Adaptive immunity maintains occult cancer in an equilibrium state*. Nature, 2007. **450**(7171): p. 903-907.
108. Propper, D.J., et al., *Low-dose IFN- γ induces tumor MHC expression in metastatic malignant melanoma*. Clinical Cancer Research, 2003. **9**(1): p. 84-92.
109. Rådestad, E., et al., *Immune profiling and identification of prognostic immune-related risk factors in human ovarian cancer*. Oncoimmunology, 2019. **8**(2): p. e1535730.
110. Shankaran, V., et al., *IFN γ and lymphocytes prevent primary tumour development and shape tumour immunogenicity*. Nature, 2001. **410**(6832): p. 1107-1111.
111. Pagès, F., et al., *International validation of the consensus Immunoscore for the classification of colon cancer: a prognostic and accuracy study*. The Lancet, 2018. **391**(10135): p. 2128-2139.
112. Nakachi, I., et al., *PTTG1 Levels Are Predictive of Saracatinib Sensitivity in Ovarian Cancer Cell Lines*. Clinical and Translational Science, 2016. **9**(6): p. 293-301.
113. Galon, J. and D. Bruni, *Approaches to treat immune hot, altered and cold tumours with combination immunotherapies*. Nat Rev Drug Discov, 2019. **18**(3): p. 197-218.
114. Buckanovich, R.J., et al., *Endothelin B receptor mediates the endothelial barrier to T cell homing to tumors and disables immune therapy*. Nature medicine, 2008. **14**(1): p. 28-36.
115. Erez, N., et al., *Cancer-associated fibroblasts are activated in incipient neoplasia to orchestrate tumor-promoting inflammation in an NF- κ B-dependent manner*. Cancer cell, 2010. **17**(2): p. 135-147.
116. Gok Yavuz, B., et al., *Cancer associated fibroblasts sculpt tumour microenvironment by recruiting monocytes and inducing immunosuppressive PD-1+ TAMs*. Scientific reports, 2019. **9**(1): p. 3172.
117. Dieterich, L.C., et al., *Tumor-associated lymphatic vessels upregulate PDL1 to inhibit T-cell activation*. Frontiers in immunology, 2017. **8**: p. 66.
118. Gorchs, L., et al., *Human pancreatic carcinoma-associated fibroblasts promote expression of co-inhibitory markers on CD4+ and CD8+ T-cells*. Frontiers in immunology, 2019. **10**: p. 847.
119. Rodig, N., et al., *Endothelial expression of PD-L1 and PD-L2 down-regulates CD8+ T cell activation and cytotoxicity*. European journal of immunology, 2003. **33**(11): p. 3117-3126.
120. Ahmadzadeh, M., et al., *Tumor antigen-specific CD8 T cells infiltrating the tumor express high levels of PD-1 and are functionally impaired*. Blood, The Journal of the American Society of Hematology, 2009. **114**(8): p. 1537-1544.
121. Latchman, Y.E., et al., *PD-L1-deficient mice show that PD-L1 on T cells, antigen-presenting cells, and host tissues negatively regulates T cells*. Proc Natl Acad Sci U S A, 2004. **101**(29): p. 10691-6.

122. Jiang, X., et al., *Role of the tumor microenvironment in PD-L1/PD-1-mediated tumor immune escape*. Mol Cancer, 2019. **18**(1): p. 10.
123. Qin, W., et al., *The Diverse Function of PD-1/PD-L Pathway Beyond Cancer*. Frontiers in Immunology, 2019. **10**.
124. Akinleye, A. and Z. Rasool, *Immune checkpoint inhibitors of PD-L1 as cancer therapeutics*. J Hematol Oncol, 2019. **12**(1): p. 92.
125. Bejarano, L., M.J.C. Jordão, and J.A. Joyce, *Therapeutic Targeting of the Tumor Microenvironment*. Cancer Discovery, 2021. **11**(4): p. 933-959.
126. **Schirmacher, V.**, *Quo vadis cancer therapy ?Fascinating discoveries of the last 60 years*. 2017: Lambert Academic Publishing (LAP). 360.
127. Miller, K.D., et al., *Cancer treatment and survivorship statistics, 2022*. CA: A Cancer Journal for Clinicians, 2022. **72**(5): p. 409-436.
128. Malhotra, V. and M.C. Perry, *Classical chemotherapy: mechanisms, toxicities and the therapeutic window*. Cancer biology & therapy, 2003. **2**(sup1): p. 1-3.
129. Zhong, L., et al., *Small molecules in targeted cancer therapy: advances, challenges, and future perspectives*. Signal Transduction and Targeted Therapy, 2021. **6**(1): p. 201.
130. Ferguson, F.M. and N.S. Gray, *Kinase inhibitors: the road ahead*. Nature reviews Drug discovery, 2018. **17**(5): p. 353-377.
131. Oh, D.-Y. and Y.-J. Bang, *HER2-targeted therapies—a role beyond breast cancer*. Nature Reviews Clinical Oncology, 2020. **17**(1): p. 33-48.
132. Tariman, J.D., *Changes in cancer treatment: Mabs, mibs, mids, nabs, and nibs*. Nursing Clinics, 2017. **52**(1): p. 65-81.
133. Keefe, D.M.K. and E.H. Bateman, *Potential Successes and Challenges of Targeted Cancer Therapies*. J Natl Cancer Inst Monogr, 2019. **2019**(53).
134. Lucchini, E., et al., *Targeting the epidermal growth factor receptor in solid tumors: focus on safety*. Expert opinion on drug safety, 2014. **13**(5): p. 535-549.
135. Sandoo, A., G.D. Kitas, and A.R. Carmichael, *Breast cancer therapy and cardiovascular risk: focus on trastuzumab*. Vasc Health Risk Manag, 2015. **11**: p. 223-8.
136. Asnacios, A., S. Naveau, and G. Perlemuter, *Gastrointestinal toxicities of novel agents in cancer therapy*. Eur J Cancer, 2009. **45 Suppl 1**: p. 332-42.
137. Strelvel, E.L. and L.L. Siu, *Cardiovascular toxicity of molecularly targeted agents*. Eur J Cancer, 2009. **45 Suppl 1**: p. 318-31.
138. Lee, Y.T., Y.J. Tan, and C.E. Oon, *Molecular targeted therapy: Treating cancer with specificity*. European journal of pharmacology, 2018. **834**: p. 188-196.
139. Sawyers, C., *Targeted cancer therapy*. Nature, 2004. **432**(7015): p. 294-297.
140. Xie, Y.H., Y.X. Chen, and J.Y. Fang, *Comprehensive review of targeted therapy for colorectal cancer*. Signal Transduct Target Ther, 2020. **5**(1): p. 22.
141. Wong, S.F., *Cetuximab: an epidermal growth factor receptor monoclonal antibody for the treatment of colorectal cancer*. Clin Ther, 2005. **27**(6): p. 684-94.
142. Esteva, F.J., *Monoclonal antibodies, small molecules, and vaccines in the treatment of breast cancer*. Oncologist, 2004. **9 Suppl 3**: p. 4-9.
143. Ishii, K., N. Morii, and H. Yamashiro, *Pertuzumab in the treatment of HER2-positive breast cancer: an evidence-based review of its safety, efficacy, and place in therapy*. Core Evid, 2019. **14**: p. 51-70.
144. Soda, M., et al., *Identification of the transforming EML4-ALK fusion gene in non-small-cell lung cancer*. Nature, 2007. **448**(7153): p. 561-6.
145. Shaw, A.T., et al., *Ceritinib in ALK-rearranged non-small-cell lung cancer*. N Engl j med, 2014. **370**: p. 1189-1197.
146. Zhang, J., P.L. Yang, and N.S. Gray, *Targeting cancer with small molecule kinase inhibitors*. Nature reviews cancer, 2009. **9**(1): p. 28-39.
147. Davies, H., et al., *Mutations of the BRAF gene in human cancer*. Nature, 2002. **417**(6892): p. 949-54.

148. Goldinger, S.M., et al., *Targeted therapy in melanoma – the role of BRAF, RAS and KIT mutations*. European Journal of Cancer Supplements, 2013. **11**(2): p. 92-96.
149. De Palma, M., D. Biziato, and T.V. Petrova, *Microenvironmental regulation of tumour angiogenesis*. Nat Rev Cancer, 2017. **17**(8): p. 457-474.
150. Klein, D., *The Tumor Vascular Endothelium as Decision Maker in Cancer Therapy*. Frontiers in Oncology, 2018. **8**.
151. Fukumura, D. and R.K. Jain, *Tumor microenvironment abnormalities: Causes, consequences, and strategies to normalize*. Journal of Cellular Biochemistry, 2007. **101**(4): p. 937-949.
152. Hargadon, K.M., C.E. Johnson, and C.J. Williams, *Immune checkpoint blockade therapy for cancer: An overview of FDA-approved immune checkpoint inhibitors*. Int Immunopharmacol, 2018. **62**: p. 29-39.
153. Mellman, I., G. Coukos, and G. Dranoff, *Cancer immunotherapy comes of age*. Nature, 2011. **480**(7378): p. 480-489.
154. Hodi, F.S., et al., *Improved survival with ipilimumab in patients with metastatic melanoma*. N Engl J Med, 2010. **363**(8): p. 711-23.
155. Weber, J.S., et al., *Nivolumab versus chemotherapy in patients with advanced melanoma who progressed after anti-CTLA-4 treatment (CheckMate 037): a randomised, controlled, open-label, phase 3 trial*. Lancet Oncol, 2015. **16**(4): p. 375-84.
156. Brahmer, J., et al., *Nivolumab versus Docetaxel in Advanced Squamous-Cell Non–Small-Cell Lung Cancer*. New England Journal of Medicine, 2015. **373**(2): p. 123-135.
157. Motzer, R.J., et al., *Nivolumab versus Everolimus in Advanced Renal-Cell Carcinoma*. New England Journal of Medicine, 2015. **373**(19): p. 1803-1813.
158. Sharma, P., et al., *Nivolumab in metastatic urothelial carcinoma after platinum therapy (CheckMate 275): a multicentre, single-arm, phase 2 trial*. Lancet Oncol, 2017. **18**(3): p. 312-322.
159. Ansell, S.M., et al., *PD-1 Blockade with Nivolumab in Relapsed or Refractory Hodgkin's Lymphoma*. New England Journal of Medicine, 2014. **372**(4): p. 311-319.
160. Powles, T., et al., *Atezolizumab (atezo) vs. chemotherapy (chemo) in platinum-treated locally advanced or metastatic urothelial carcinoma (mUC): Immune biomarkers, tumor mutational burden (TMB), and clinical outcomes from the phase III IMvigor211 study*. Journal of Clinical Oncology, 2018. **36**(6_suppl): p. 409-409.
161. Antonia, S.J., et al., *Durvalumab after Chemoradiotherapy in Stage III Non–Small-Cell Lung Cancer*. New England Journal of Medicine, 2017. **377**(20): p. 1919-1929.
162. Marusyk, A., M. Janiszewska, and K. Polyak, *Intratumor Heterogeneity: The Rosetta Stone of Therapy Resistance*. Cancer Cell, 2020. **37**(4): p. 471-484.
163. Kisor, D. and M. Ehret, *The personalized medicine report 2020. Opportunity, Challenges, and the Future*. 2020, PMC Personalized Medicine Coalition. p. 72.
164. Krzyszczyk, P., et al., *The growing role of precision and personalized medicine for cancer treatment*. TECHNOLOGY, 2018. **06**(03n04): p. 79-100.
165. Chen, E.Y., V. Raghunathan, and V. Prasad, *An Overview of Cancer Drugs Approved by the US Food and Drug Administration Based on the Surrogate End Point of Response Rate*. JAMA Internal Medicine, 2019. **179**(7): p. 915-921.
166. Jiang, H., et al., *Classification of Progression Patterns in Glioblastoma: Analysis of Predictive Factors and Clinical Implications*. Frontiers in Oncology, 2020. **10**.
167. Garzon, S., et al., *Secondary and tertiary ovarian cancer recurrence: what is the best management?* Gland Surg, 2020. **9**(4): p. 1118-1129.
168. *Precision medicine*. 2018 09/27/2018 [cited 2023 06.07.2023]; Available from: <https://www.fda.gov/medical-devices/in-vitro-diagnostics/precision-medicine>.
169. Biswas, S. and C.M. Rao, *Epigenetics in cancer: Fundamentals and Beyond*. Pharmacology & Therapeutics, 2017. **173**: p. 118-134.

170. Dietz, S., et al., *Spatial distribution of EGFR and KRAS mutation frequencies correlates with histological growth patterns of lung adenocarcinomas*. International Journal of Cancer, 2017. **141**(9): p. 1841-1848.
171. Kim, K.H. and C.W.M. Roberts, *Targeting EZH2 in cancer*. Nature Medicine, 2016. **22**(2): p. 128-134.
172. Turner, N.C. and J.S. Reis-Filho, *Genetic heterogeneity and cancer drug resistance*. The Lancet Oncology, 2012. **13**(4): p. e178-e185.
173. Engelman, J.A. and J. Settleman, *Acquired resistance to tyrosine kinase inhibitors during cancer therapy*. Curr Opin Genet Dev, 2008. **18**(1): p. 73-9.
174. Brady, S.W., et al., *Combating subclonal evolution of resistant cancer phenotypes*. Nat Commun, 2017. **8**(1): p. 1231.
175. Kim, C., et al., *Chemoresistance Evolution in Triple-Negative Breast Cancer Delineated by Single-Cell Sequencing*. Cell, 2018. **173**(4): p. 879-893.e13.
176. Mullighan, C.G., et al., *Genomic analysis of the clonal origins of relapsed acute lymphoblastic leukemia*. Science, 2008. **322**(5906): p. 1377-80.
177. Diaz, L.A., Jr., et al., *The molecular evolution of acquired resistance to targeted EGFR blockade in colorectal cancers*. Nature, 2012. **486**(7404): p. 537-40.
178. Johnson, B.E., et al., *Mutational analysis reveals the origin and therapy-driven evolution of recurrent glioma*. Science, 2014. **343**(6167): p. 189-193.
179. Kosaka, T., et al., *Analysis of epidermal growth factor receptor gene mutation in patients with non-small cell lung cancer and acquired resistance to gefitinib*. Clin Cancer Res, 2006. **12**(19): p. 5764-9.
180. Liegl, B., et al., *Heterogeneity of kinase inhibitor resistance mechanisms in GIST*. J Pathol, 2008. **216**(1): p. 64-74.
181. Turke, A.B., et al., *Preexistence and clonal selection of MET amplification in EGFR mutant NSCLC*. Cancer Cell, 2010. **17**(1): p. 77-88.
182. Deininger, M., *Resistance to imatinib: mechanisms and management*. J Natl Compr Canc Netw, 2005. **3**(6): p. 757-68.
183. Kelly, C.M., L. Gutierrez Sainz, and P. Chi, *The management of metastatic GIST: current standard and investigational therapeutics*. Journal of Hematology & Oncology, 2021. **14**(1): p. 2.
184. Nazarian, R., et al., *Melanomas acquire resistance to B-RAF(V600E) inhibition by RTK or N-RAS upregulation*. Nature, 2010. **468**(7326): p. 973-7.
185. Edwards, S.L., et al., *Resistance to therapy caused by intragenic deletion in BRCA2*. Nature, 2008. **451**(7182): p. 1111-1115.
186. Hinohara, K., et al., *KDM5 Histone Demethylase Activity Links Cellular Transcriptomic Heterogeneity to Therapeutic Resistance*. Cancer Cell, 2018. **34**(6): p. 939-953.e9.
187. Glasspool, R.M., J.M. Teodoridis, and R. Brown, *Epigenetics as a mechanism driving polygenic clinical drug resistance*. Br J Cancer, 2006. **94**(8): p. 1087-92.
188. Jänne, P.A., N. Gray, and J. Settleman, *Factors underlying sensitivity of cancers to small-molecule kinase inhibitors*. Nat Rev Drug Discov, 2009. **8**(9): p. 709-23.
189. Knoechel, B., et al., *An epigenetic mechanism of resistance to targeted therapy in T cell acute lymphoblastic leukemia*. Nat Genet, 2014. **46**(4): p. 364-70.
190. Risom, T., et al., *Differentiation-state plasticity is a targetable resistance mechanism in basal-like breast cancer*. Nat Commun, 2018. **9**(1): p. 3815.
191. Sharma, S.V., et al., *A Chromatin-Mediated Reversible Drug-Tolerant State in Cancer Cell Subpopulations*. Cell, 2010. **141**(1): p. 69-80.
192. Liao, B.B., et al., *Adaptive chromatin remodeling drives glioblastoma stem cell plasticity and drug tolerance*. Cell stem cell, 2017. **20**(2): p. 233-246. e7.
193. Shu, S., et al., *Response and resistance to BET bromodomain inhibitors in triple-negative breast cancer*. Nature, 2016. **529**(7586): p. 413-417.
194. Hong, S.P., et al., *Single-cell transcriptomics reveals multi-step adaptations to endocrine therapy*. Nature Communications, 2019. **10**(1): p. 3840.

195. Shaffer, S.M., et al., *Rare cell variability and drug-induced reprogramming as a mode of cancer drug resistance*. *Nature*, 2017. **546**(7658): p. 431-435.
196. Wilson, T.R., et al., *Widespread potential for growth-factor-driven resistance to anticancer kinase inhibitors*. *Nature*, 2012. **487**(7408): p. 505-509.
197. Hirata, E., et al., *Intravital Imaging Reveals How BRAF Inhibition Generates Drug-Tolerant Microenvironments with High Integrin β 1/FAK Signaling*. *Cancer Cell*, 2015. **27**(4): p. 574-588.
198. Gillies, R.J., D. Verduzco, and R.A. Gatenby, *Evolutionary dynamics of carcinogenesis and why targeted therapy does not work*. *Nature Reviews Cancer*, 2012. **12**(7): p. 487-493.
199. Hamburg, M.A. and F.S. Collins, *The path to personalized medicine*. *N Engl J Med*, 2010. **363**(4): p. 301-4.
200. Collins, F.S. and H. Varmus, *A new initiative on precision medicine*. *N Engl J Med*, 2015. **372**(9): p. 793-5.
201. Ashley, E.A., *The precision medicine initiative: a new national effort*. *Jama*, 2015. **313**(21): p. 2119-2120.
202. Shin, S.H., A.M. Bode, and Z. Dong, *Addressing the challenges of applying precision oncology*. *npj Precision Oncology*, 2017. **1**(1): p. 28.
203. Borrebaeck, C.A.K., *Precision diagnostics: moving towards protein biomarker signatures of clinical utility in cancer*. *Nature Reviews Cancer*, 2017. **17**(3): p. 199-204.
204. Dienstmann, R., et al., *Consensus molecular subtypes and the evolution of precision medicine in colorectal cancer*. *Nat Rev Cancer*, 2017. **17**(2): p. 79-92.
205. Miki, Y., et al., *A strong candidate for the breast and ovarian cancer susceptibility gene BRCA1*. *Science*, 1994. **266**(5182): p. 66-71.
206. Wooster, R., et al., *Identification of the breast cancer susceptibility gene BRCA2*. *Nature*, 1995. **378**(6559): p. 789-92.
207. Cobleigh, M.A., et al., *Multinational study of the efficacy and safety of humanized anti-HER2 monoclonal antibody in women who have HER2-overexpressing metastatic breast cancer that has progressed after chemotherapy for metastatic disease*. *J Clin Oncol*, 1999. **17**(9): p. 2639-48.
208. Mates, M., et al., *Systemic targeted therapy for her2-positive early female breast cancer: a systematic review of the evidence for the 2014 Cancer Care Ontario systemic therapy guideline*. *Curr Oncol*, 2015. **22**(Suppl 1): p. S114-22.
209. Letai, A., P. Bholra, and A.L. Welm, *Functional precision oncology: Testing tumors with drugs to identify vulnerabilities and novel combinations*. *Cancer Cell*, 2022. **40**(1): p. 26-35.
210. Le Tourneau, C., et al., *Molecularly targeted therapy based on tumour molecular profiling versus conventional therapy for advanced cancer (SHIVA): a multicentre, open-label, proof-of-concept, randomised, controlled phase 2 trial*. *The Lancet Oncology*, 2015. **16**(13): p. 1324-1334.
211. Flaherty, K.T., et al., *Molecular Landscape and Actionable Alterations in a Genomically Guided Cancer Clinical Trial: National Cancer Institute Molecular Analysis for Therapy Choice (NCI-MATCH)*. *J Clin Oncol*, 2020. **38**(33): p. 3883-3894.
212. Chen, A.P., et al., *Molecular Profiling-Based Assignment of Cancer Therapy (NCI-MPACT): A Randomized Multicenter Phase II Trial*. *JCO Precision Oncology*, 2021(5): p. 133-144.
213. Massard, C., et al., *High-Throughput Genomics and Clinical Outcome in Hard-to-Treat Advanced Cancers: Results of the MOSCATO 01 Trial*. *Cancer Discov*, 2017. **7**(6): p. 586-595.
214. Prasad, V., *Perspective: The precision-oncology illusion*. *Nature*, 2016. **537**(7619): p. S63-S63.
215. Prasad, V. and A. Vandross, *Characteristics of Exceptional or Super Responders to Cancer Drugs*. *Mayo Clinic Proceedings*, 2015. **90**(12): p. 1639-1649.
216. Letai, A., *Functional precision cancer medicine-moving beyond pure genomics*. *Nat Med*, 2017. **23**(9): p. 1028-1035.

-
217. Friedman, A.A., et al., *Precision medicine for cancer with next-generation functional diagnostics*. *Nat Rev Cancer*, 2015. **15**(12): p. 747-56.
218. Prahallad, A., et al., *Unresponsiveness of colon cancer to BRAF(V600E) inhibition through feedback activation of EGFR*. *Nature*, 2012. **483**(7387): p. 100-3.
219. Liu, L., et al., *Patient-derived organoid (PDO) platforms to facilitate clinical decision making*. *J Transl Med*, 2021. **19**(1): p. 40.
220. Tuveson, D. and H. Clevers, *Cancer modeling meets human organoid technology*. *Science*, 2019. **364**(6444): p. 952-955.
221. Vlachogiannis, G., et al., *Patient-derived organoids model treatment response of metastatic gastrointestinal cancers*. *Science*, 2018. **359**(6378): p. 920-926.
222. Law, A.M.K., et al., *Advancements in 3D Cell Culture Systems for Personalizing Anti-Cancer Therapies*. *Frontiers in Oncology*, 2021. **11**.
223. Lv, D., et al., *Three-dimensional cell culture: A powerful tool in tumor research and drug discovery*. *Oncol Lett*, 2017. **14**(6): p. 6999-7010.
224. Birgersdotter, A., R. Sandberg, and I. Ernberg, *Gene expression perturbation in vitro--a growing case for three-dimensional (3D) culture systems*. *Semin Cancer Biol*, 2005. **15**(5): p. 405-12.
225. Hakkinen, K.M., et al., *Direct comparisons of the morphology, migration, cell adhesions, and actin cytoskeleton of fibroblasts in four different three-dimensional extracellular matrices*. *Tissue Eng Part A*, 2011. **17**(5-6): p. 713-24.
226. Tibbitt, M.W. and K.S. Anseth, *Hydrogels as extracellular matrix mimics for 3D cell culture*. *Biotechnology and bioengineering*, 2009. **103**(4): p. 655-663.
227. Langhans, S.A., *Three-Dimensional in Vitro Cell Culture Models in Drug Discovery and Drug Repositioning*. *Front Pharmacol*, 2018. **9**: p. 6.
228. Lovitt, C.J., T.B. Shelper, and V.M. Avery, *Doxorubicin resistance in breast cancer cells is mediated by extracellular matrix proteins*. *BMC Cancer*, 2018. **18**(1).
229. Sun, Y., *Tumor microenvironment and cancer therapy resistance*. *Cancer Lett*, 2016. **380**(1): p. 205-15.
230. Di Paolo, A. and G. Bocci, *Drug distribution in tumors: mechanisms, role in drug resistance, and methods for modification*. *Curr Oncol Rep*, 2007. **9**(2): p. 109-14.
231. Minchinton, A.I. and I.F. Tannock, *Drug penetration in solid tumours*. *Nat Rev Cancer*, 2006. **6**(8): p. 583-92.
232. Sharma, S.V., D.A. Haber, and J. Settleman, *Cell line-based platforms to evaluate the therapeutic efficacy of candidate anticancer agents*. *Nature Reviews Cancer*, 2010. **10**(4): p. 241-253.
233. Sajjad, H., et al., *Cancer models in preclinical research: A chronicle review of advancement in effective cancer research*. *Animal Model Exp Med*, 2021. **4**(2): p. 87-103.
234. Fosse, V., et al., *Evaluating Translational Methods for Personalized Medicine—A Scoping Review*. *Journal of Personalized Medicine*, 2022. **12**(7): p. 1177.
235. Hidalgo, M., et al., *Patient-Derived Xenograft Models: An Emerging Platform for Translational Cancer Research*. *Cancer Discovery*, 2014. **4**(9): p. 998-1013.
236. Woo, X.Y., et al., *Conservation of copy number profiles during engraftment and passaging of patient-derived cancer xenografts*. *Nat Genet*, 2021. **53**(1): p. 86-99.
237. Abdolahi, S., et al., *Patient-derived xenograft (PDX) models, applications and challenges in cancer research*. *Journal of Translational Medicine*, 2022. **20**(1): p. 206.
238. Invrea, F., et al., *Patient-derived xenografts (PDXs) as model systems for human cancer*. *Current opinion in biotechnology*, 2020. **63**: p. 151-156.
239. Kijima, N. and Y. Kanemura, *Mouse Models of Glioblastoma*, in *Glioblastoma*, S. De Vleeschouwer, Editor. 2017, Codon Publications
- Copyright: The Authors.: Brisbane (AU).
240. Dobrolecki, L.E., et al., *Patient-derived xenograft (PDX) models in basic and translational breast cancer research*. *Cancer and Metastasis Reviews*, 2016. **35**: p. 547-573.

-
241. Shi, J., et al., *The fidelity of cancer cells in PDX models: Characteristics, mechanism and clinical significance*. *Int J Cancer*, 2020. **146**(8): p. 2078-2088.
242. DeRose, Y.S., et al., *Tumor grafts derived from women with breast cancer authentically reflect tumor pathology, growth, metastasis and disease outcomes*. *Nat Med*, 2011. **17**(11): p. 1514-20.
243. du Manoir, S., et al., *Breast tumor PDXs are genetically plastic and correspond to a subset of aggressive cancers prone to relapse*. *Mol Oncol*, 2014. **8**(2): p. 431-43.
244. Garrido-Laguna, I., et al., *Tumor engraftment in nude mice and enrichment in stroma-related gene pathways predict poor survival and resistance to gemcitabine in patients with pancreatic cancer*. *Clin Cancer Res*, 2011. **17**(17): p. 5793-800.
245. Byrne, A.T., et al., *Interrogating open issues in cancer medicine with patient-derived xenografts*. *Nat Rev Cancer*, 2017. **17**(10): p. 632.
246. Broutier, L., et al., *Human primary liver cancer-derived organoid cultures for disease modeling and drug screening*. *Nat Med*, 2017. **23**(12): p. 1424-1435.
247. Drost, J., et al., *Organoid culture systems for prostate epithelial and cancer tissue*. *Nat Protoc*, 2016. **11**(2): p. 347-58.
248. Kim, M., et al., *Patient-derived lung cancer organoids as in vitro cancer models for therapeutic screening*. *Nat Commun*, 2019. **10**(1): p. 3991.
249. Mullenders, J., et al., *Mouse and human urothelial cancer organoids: A tool for bladder cancer research*. *Proc Natl Acad Sci U S A*, 2019. **116**(10): p. 4567-4574.
250. Sachs, N., et al., *A Living Biobank of Breast Cancer Organoids Captures Disease Heterogeneity*. *Cell*, 2018. **172**(1): p. 373-386.e10.
251. Gendoo, D.M.A., et al., *Whole genomes define concordance of matched primary, xenograft, and organoid models of pancreas cancer*. *PLoS Comput Biol*, 2019. **15**(1): p. e1006596.
252. Larsen, B.M., et al., *A pan-cancer organoid platform for precision medicine*. *Cell Rep*, 2021. **36**(4): p. 109429.
253. Bruun, J., et al., *Patient-Derived Organoids from Multiple Colorectal Cancer Liver Metastases Reveal Moderate Intra-patient Pharmacotranscriptomic Heterogeneity*. *Clin Cancer Res*, 2020. **26**(15): p. 4107-4119.
254. Narasimhan, V., et al., *Medium-throughput Drug Screening of Patient-derived Organoids from Colorectal Peritoneal Metastases to Direct Personalized Therapy*. *Clin Cancer Res*, 2020. **26**(14): p. 3662-3670.
255. Nuciforo, S., et al., *Organoid Models of Human Liver Cancers Derived from Tumor Needle Biopsies*. *Cell Rep*, 2018. **24**(5): p. 1363-1376.
256. Tiriach, H., et al., *Organoid Profiling Identifies Common Responders to Chemotherapy in Pancreatic Cancer*. *Cancer Discov*, 2018. **8**(9): p. 1112-1129.
257. Pauli, C., et al., *Personalized In Vitro and In Vivo Cancer Models to Guide Precision Medicine*. *Cancer Discov*, 2017. **7**(5): p. 462-477.
258. Shamir, E.R. and A.J. Ewald, *Three-dimensional organotypic culture: experimental models of mammalian biology and disease*. *Nat Rev Mol Cell Biol*, 2014. **15**(10): p. 647-64.
259. Lo, Y.-H., K. Karlsson, and C.J. Kuo, *Applications of organoids for cancer biology and precision medicine*. *Nature Cancer*, 2020. **1**(8): p. 761-773.
260. Veninga, V. and E.E. Voest, *Tumor organoids: Opportunities and challenges to guide precision medicine*. *Cancer Cell*, 2021. **39**(9): p. 1190-1201.
261. Bae, J., et al., *The Patient-Derived Cancer Organoids: Promises and Challenges as Platforms for Cancer Discovery*. *Cancers*, 2022. **14**(9): p. 2144.
262. Wu, T. and Y. Dai, *Tumor microenvironment and therapeutic response*. *Cancer Letters*, 2017. **387**: p. 61-68.
263. Wong, C.H., K.W. Siah, and A.W. Lo, *Estimation of clinical trial success rates and related parameters*. *Biostatistics*, 2019. **20**(2): p. 273-286.
264. Bell, D., et al., *Integrated genomic analyses of ovarian carcinoma*. *Nature*, 2011. **474**(7353): p. 609-615.

265. Izar, B., et al., *A single-cell landscape of high-grade serous ovarian cancer*. *Nat Med*, 2020. **26**(8): p. 1271-1279.
266. Zhang, H., et al., *Integrated Proteogenomic Characterization of Human High-Grade Serous Ovarian Cancer*. *Cell*, 2016. **166**(3): p. 755-765.
267. Bray, F., et al., *Global cancer statistics 2018: GLOBOCAN estimates of incidence and mortality worldwide for 36 cancers in 185 countries*. *CA Cancer J Clin*, 2018. **68**(6): p. 394-424.
268. Institute, N.C., *Surveillance, Epidemiology, and End Results (SEER) 17 registries*. 2022.
269. Cunnea, P., et al., *Spatial and temporal intra-tumoral heterogeneity in advanced HGSOC: Implications for surgical and clinical outcomes*. *Cell Reports Medicine*, 2023. **4**(6).
270. Farley, J., et al., *Selumetinib in women with recurrent low-grade serous carcinoma of the ovary or peritoneum: an open-label, single-arm, phase 2 study*. *The Lancet Oncology*, 2013. **14**(2): p. 134-140.
271. Iyengar, M., et al., *CDK4/6 inhibition as maintenance and combination therapy for high grade serous ovarian cancer*. *Oncotarget*, 2018. **9**(21): p. 15658-15672.
272. McGivern, N., et al., *Activation of MAPK signalling results in resistance to saracatinib (AZD0530) in ovarian cancer*. *Oncotarget*, 2018. **9**(4): p. 4722-4736.
273. De Witte, C.J., et al., *Patient-Derived Ovarian Cancer Organoids Mimic Clinical Response and Exhibit Heterogeneous Inter- and Inpatient Drug Responses*. *Cell Reports*, 2020. **31**(11): p. 107762.
274. Kopper, O., et al., *An organoid platform for ovarian cancer captures intra- and interpatient heterogeneity*. *Nature Medicine*, 2019. **25**(5): p. 838-849.
275. Phan, N., et al., *A simple high-throughput approach identifies actionable drug sensitivities in patient-derived tumor organoids*. *Commun Biol*, 2019. **2**(1): p. 78.
276. Kondo, J., et al., *Retaining cell-cell contact enables preparation and culture of spheroids composed of pure primary cancer cells from colorectal cancer*. *Proc Natl Acad Sci U S A*, 2011. **108**(15): p. 6235-40.
277. Najar, M., et al., *Mesenchymal stromal cells from the foreskin: Tissue isolation, cell characterization and immunobiological properties*. *Cytotherapy*, 2016. **18**(3): p. 320-335.
278. Köbel, M., et al., *An Immunohistochemical Algorithm for Ovarian Carcinoma Typing*. *International Journal of Gynecological Pathology*, 2016. **35**(5): p. 430-441.
279. Kriplani, D. and M.M. Patel, *Immunohistochemistry: A diagnostic aid in differentiating primary epithelial ovarian tumors and tumors metastatic to the ovary*. *South Asian Journal of Cancer*, 2013. **02**(04): p. 254-258.
280. Neunteufel, W. and G. Breitenecker, *Tissue expression of CA 125 in benign and malignant lesions of ovary and fallopian tube: a comparison with CA 19-9 and CEA*. *Gynecol Oncol*, 1989. **32**(3): p. 297-302.
281. Bhat, R. and M.J. Bissell, *Of plasticity and specificity: dialectics of the microenvironment and macroenvironment and the organ phenotype*. *WIREs Developmental Biology*, 2014. **3**(2): p. 147-163.
282. Cox, T.R., *The matrix in cancer*. *Nature Reviews Cancer*, 2021. **21**(4): p. 217-238.
283. Mhaweche-Fauceglia, P., et al., *Stromal Expression of Fibroblast Activation Protein Alpha (FAP) Predicts Platinum Resistance and Shorter Recurrence in patients with Epithelial Ovarian Cancer*. *Cancer Microenvironment*, 2015. **8**(1): p. 23-31.
284. Roskelley, C.D. and M.J. Bissell, *The dominance of the microenvironment in breast and ovarian cancer*. *Seminars in Cancer Biology*, 2002. **12**(2): p. 97-104.
285. Kresbach, G.M. and M. Pawlak, *High Precision RPPA: Concept, Features, and Application Performance of the Integrated Zeptosens Platform*. *Adv Exp Med Biol*, 2019. **1188**: p. 31-59.
286. Pawlak, M. and N.O. Carragher, *Reverse Phase Protein Arrays elucidate mechanisms-of-action and phenotypic response in 2D and 3D models*. *Drug Discovery Today: Technologies*, 2017. **23**: p. 7-16.

287. Pawlak, M., et al., *Zeptosens' protein microarrays: A novel high performance microarray platform for low abundance protein analysis*. *PROTEOMICS*, 2002. **2**(4): p. 383-393.
288. Yamamoto, S., et al., *Clinicopathological significance of WT1 expression in ovarian cancer: a possible accelerator of tumor progression in serous adenocarcinoma*. *Virchows Archiv*, 2007. **451**: p. 27-35.
289. Taube, E.T., et al., *Wilms tumor protein 1 (WT1)—not only a diagnostic but also a prognostic marker in high-grade serous ovarian carcinoma*. *Gynecologic oncology*, 2016. **140**(3): p. 494-502.
290. Vasefifar, P., et al., *Nanog, as a key cancer stem cell marker in tumor progression*. *Gene*, 2022. **827**: p. 146448.
291. Hamanishi, J., et al., *Programmed cell death 1 ligand 1 and tumor-infiltrating CD8+ T lymphocytes are prognostic factors of human ovarian cancer*. *Proc Natl Acad Sci U S A*, 2007. **104**(9): p. 3360-5.
292. Sato, E., et al., *Intraepithelial CD8+ tumor-infiltrating lymphocytes and a high CD8+/regulatory T cell ratio are associated with favorable prognosis in ovarian cancer*. *Proc Natl Acad Sci U S A*, 2005. **102**(51): p. 18538-43.
293. Zhang, L., et al., *Intratumoral T Cells, Recurrence, and Survival in Epithelial Ovarian Cancer*. *New England Journal of Medicine*, 2003. **348**(3): p. 203-213.
294. Kandalaft, L.E., K. Odunsi, and G. Coukos, *Immune Therapy Opportunities in Ovarian Cancer*. *American Society of Clinical Oncology Educational Book*, 2020(40): p. e228-e240.
295. Liu, Y., et al., *Review immune response of targeting CD39 in cancer*. *Biomarker Research*, 2023. **11**(1): p. 63.
296. Ye, Q., et al., *CD137 Accurately Identifies and Enriches for Naturally Occurring Tumor-Reactive T Cells in Tumor*. *Clinical Cancer Research*, 2014. **20**(1): p. 44-55.
297. Canale, F.P., et al., *CD39 Expression Defines Cell Exhaustion in Tumor-Infiltrating CD8+T Cells*. *Cancer Research*, 2018. **78**(1): p. 115-128.
298. Duhon, T., et al., *Co-expression of CD39 and CD103 identifies tumor-reactive CD8 T cells in human solid tumors*. *Nat Commun*, 2018. **9**(1): p. 2724.
299. Simoni, Y., et al., *Bystander CD8+ T cells are abundant and phenotypically distinct in human tumour infiltrates*. *Nature*, 2018. **557**(7706): p. 575-579.
300. Jansen, C.S., et al., *An intra-tumoral niche maintains and differentiates stem-like CD8 T cells*. *Nature*, 2019. **576**(7787): p. 465-470.
301. Zehn, D., et al., *'Stem-like' precursors are the fount to sustain persistent CD8+ T cell responses*. *Nature Immunology*, 2022. **23**(6): p. 836-847.
302. Liston, D.R. and M. Davis, *Clinically Relevant Concentrations of Anticancer Drugs: A Guide for Nonclinical Studies*. *Clin Cancer Res*, 2017. **23**(14): p. 3489-3498.
303. Cen, L., et al., *p16-Cdk4-Rb axis controls sensitivity to a cyclin-dependent kinase inhibitor PD0332991 in glioblastoma xenograft cells*. *Neuro-Oncology*, 2012. **14**(7): p. 870-881.
304. de Leeuw, R., et al., *MAPK Reliance via Acquired CDK4/6 Inhibitor Resistance in Cancer*. *Clinical Cancer Research*, 2018. **24**(17): p. 4201-4214.
305. Finn, R.S., et al., *Biomarker Analyses of Response to Cyclin-Dependent Kinase 4/6 Inhibition and Endocrine Therapy in Women with Treatment-Naïve Metastatic Breast Cancer*. *Clinical Cancer Research*, 2020. **26**(1): p. 110-121.
306. Yang, C., et al., *Acquired CDK6 amplification promotes breast cancer resistance to CDK4/6 inhibitors and loss of ER signaling and dependence*. *Oncogene*, 2017. **36**(16): p. 2255-2264.
307. Aramburu, J., et al., *Transcriptional regulation of the stress response by mTOR*. *Science Signaling*, 2014. **7**(332): p. re2.
308. Lakhani, S.R., et al., *WHO Classification of Tumours of the Breast*. 2012.
309. Perou, C.M., et al., *Molecular portraits of human breast tumours*. *nature*, 2000. **406**(6797): p. 747-752.
310. Sørlie, T., et al., *Gene expression patterns of breast carcinomas distinguish tumor subclasses with clinical implications*. *Proc Natl Acad Sci U S A*, 2001. **98**(19): p. 10869-74.

311. Sorlie, T., et al., *Repeated observation of breast tumor subtypes in independent gene expression data sets*. Proc Natl Acad Sci U S A, 2003. **100**(14): p. 8418-23.
312. Caswell-Jin, J.L., C. Lorenz, and C. Curtis, *Molecular Heterogeneity and Evolution in Breast Cancer*. Annual Review of Cancer Biology, 2021. **5**(1): p. 79-94.
313. Lehmann, B.D., et al., *Identification of human triple-negative breast cancer subtypes and preclinical models for selection of targeted therapies*. Journal of Clinical Investigation, 2011. **121**(7): p. 2750-2767.
314. Carey, L.A., et al., *The triple negative paradox: primary tumor chemosensitivity of breast cancer subtypes*. Clin Cancer Res, 2007. **13**(8): p. 2329-34.
315. Glück, S., et al., *TP53 genomics predict higher clinical and pathologic tumor response in operable early-stage breast cancer treated with docetaxel-capecitabine ± trastuzumab*. Breast Cancer Res Treat, 2012. **132**(3): p. 781-91.
316. Martin, M., et al., *Genomic predictors of response to doxorubicin versus docetaxel in primary breast cancer*. Breast Cancer Res Treat, 2011. **128**(1): p. 127-36.
317. Rouzier, R., et al., *Breast cancer molecular subtypes respond differently to preoperative chemotherapy*. Clinical cancer research, 2005. **11**(16): p. 5678-5685.
318. Tsang, J.Y.S. and G.M. Tse, *Molecular Classification of Breast Cancer*. Adv Anat Pathol, 2020. **27**(1): p. 27-35.
319. Cardoso, F., et al., *Early breast cancer: ESMO Clinical Practice Guidelines for diagnosis, treatment and follow-up*. Annals of Oncology, 2019. **30**(8): p. 1194-1220.
320. Glajcar, A., et al., *The relationship between breast cancer molecular subtypes and mast cell populations in tumor microenvironment*. Virchows Arch, 2017. **470**(5): p. 505-515.
321. Natarajan, S., et al., *Collagen Remodeling in the Hypoxic Tumor-Mesothelial Niche Promotes Ovarian Cancer Metastasis*. Cancer Research, 2019. **79**(9): p. 2271-2284.
322. Anderle, N., et al., *A Platform of Patient-Derived Microtumors Identifies Individual Treatment Responses and Therapeutic Vulnerabilities in Ovarian Cancer*. Cancers, 2022. **14**(12): p. 2895.
323. Correia, A.L. and M.J. Bissell, *The tumor microenvironment is a dominant force in multidrug resistance*. Drug Resistance Updates, 2012. **15**(1): p. 39-49.
324. Park, C.C., M.J. Bissell, and M.H. Barcellos-Hoff, *The influence of the microenvironment on the malignant phenotype*. Molecular Medicine Today, 2000. **6**(8): p. 324-329.
325. Klimonda, Z., et al., *Breast-lesions characterization using Quantitative Ultrasound features of peritumoral tissue*. Scientific Reports, 2019. **9**(1).
326. Lepucki, A., et al., *The Role of Extracellular Matrix Proteins in Breast Cancer*. Journal of Clinical Medicine, 2022. **11**(5): p. 1250.
327. Movat, H.Z., *Demonstration of all connective tissue elements in a single section; pentachrome stains*. AMA Arch Pathol, 1955. **60**(3): p. 289-95.
328. Provenzano, P.P., et al., *Collagen density promotes mammary tumor initiation and progression*. BMC Medicine, 2008. **6**(1): p. 11.
329. Natal, R.d.A., et al., *Exploring Collagen Parameters in Pure Special Types of Invasive Breast Cancer*. Scientific Reports, 2019. **9**(1): p. 7715.
330. Ruifrok, A.C. and D.A. Johnston, *Quantification of histochemical staining by color deconvolution*. Anal Quant Cytol Histol, 2001. **23**(4): p. 291-9.
331. Abd El-Rehim, D.M., et al., *Expression of luminal and basal cytokeratins in human breast carcinoma*. The Journal of Pathology, 2004. **203**(2): p. 661-671.
332. Taylor-Papadimitriou, J., et al., *Keratin expression in human mammary epithelial cells cultured from normal and malignant tissue: relation to in vivo phenotypes and influence of medium*. J Cell Sci, 1989. **94 (Pt 3)**: p. 403-13.
333. Wetzels, R., et al., *Basal cell-specific and hyperproliferation-related keratins in human breast cancer*. The American journal of pathology, 1991. **138**(3): p. 751.

-
334. Rodríguez-Pinilla, S.M., et al., *Prognostic significance of basal-like phenotype and fascin expression in node-negative invasive breast carcinomas*. Clin Cancer Res, 2006. **12**(5): p. 1533-9.
335. Böcker, W., et al., *Common adult stem cells in the human breast give rise to glandular and myoepithelial cell lineages: a new cell biological concept*. Laboratory investigation, 2002. **82**(6): p. 737-746.
336. Treindl, F., et al., *A bead-based western for high-throughput cellular signal transduction analyses*. Nature Communications, 2016. **7**(1): p. 12852.
337. Cossu-Rocca, P., et al., *Analysis of PIK3CA Mutations and Activation Pathways in Triple Negative Breast Cancer*. PLOS ONE, 2015. **10**(11): p. e0141763.
338. Liu, T., et al., *Combinatorial Effects of Lapatinib and Rapamycin in Triple-Negative Breast Cancer Cells*. Molecular Cancer Therapeutics, 2011. **10**(8): p. 1460-1469.
339. LoPiccolo, J., et al., *Targeting the PI3K/Akt/mTOR pathway: effective combinations and clinical considerations*. Drug Resist Updat, 2008. **11**(1-2): p. 32-50.
340. McCubrey, J.A., et al., *Therapeutic resistance resulting from mutations in Raf/MEK/ERK and PI3K/PTEN/Akt/mTOR signaling pathways*. J Cell Physiol, 2011. **226**(11): p. 2762-81.
341. Ooms, L.M., et al., *The Inositol Polyphosphate 5-Phosphatase PIPP Regulates AKT1-Dependent Breast Cancer Growth and Metastasis*. Cancer Cell, 2015. **28**(2): p. 155-69.
342. Stephens, P., et al., *Lung cancer: intragenic ERBB2 kinase mutations in tumours*. Nature, 2004. **431**(7008): p. 525-6.
343. The Cancer Genome Atlas, N., *Comprehensive molecular portraits of human breast tumours*. Nature, 2012. **490**(7418): p. 61-70.
344. Zhao, J.J., et al., *The oncogenic properties of mutant p110alpha and p110beta phosphatidylinositol 3-kinases in human mammary epithelial cells*. Proc Natl Acad Sci U S A, 2005. **102**(51): p. 18443-8.
345. Steelman, L.S., et al., *Suppression of PTEN function increases breast cancer chemotherapeutic drug resistance while conferring sensitivity to mTOR inhibitors*. Oncogene, 2008. **27**(29): p. 4086-95.
346. Umemura, S., et al., *Increased phosphorylation of Akt in triple-negative breast cancers*. Cancer Sci, 2007. **98**(12): p. 1889-92.
347. Eralp, Y., et al., *MAPK overexpression is associated with anthracycline resistance and increased risk for recurrence in patients with triple-negative breast cancer*. Ann Oncol, 2008. **19**(4): p. 669-74.
348. Hamilton, E. and J.R. Infante, *Targeting CDK4/6 in patients with cancer*. Cancer Treat Rev, 2016. **45**: p. 129-38.
349. Sviderskiy, V.O., et al., *Hyperactive CDK2 Activity in Basal-like Breast Cancer Imposes a Genome Integrity Liability that Can Be Exploited by Targeting DNA Polymerase ϵ* . Molecular Cell, 2020. **80**(4): p. 682-698.e7.
350. Alluri, P. and L.A. Newman, *Basal-like and triple-negative breast cancers: searching for positives among many negatives*. Surg Oncol Clin N Am, 2014. **23**(3): p. 567-77.
351. Pelicano, H., et al., *Mitochondrial dysfunction in some triple-negative breast cancer cell lines: role of mTOR pathway and therapeutic potential*. Breast Cancer Res, 2014. **16**(5): p. 434.
352. Warburg, O., F. Wind, and E. Negelein, *THE METABOLISM OF TUMORS IN THE BODY*. J Gen Physiol, 1927. **8**(6): p. 519-30.
353. Shu, C.A., et al., *Neoadjuvant atezolizumab and chemotherapy in patients with resectable non-small-cell lung cancer: an open-label, multicentre, single-arm, phase 2 trial*. Lancet Oncol, 2020. **21**(6): p. 786-795.
354. Campbell, R.A., et al., *Phosphatidylinositol 3-Kinase/AKT-mediated Activation of Estrogen Receptor β : A NEW MODEL FOR ANTI-ESTROGEN RESISTANCE **. Journal of Biological Chemistry, 2001. **276**(13): p. 9817-9824.

-
355. Ghayad, S.E., et al., *Endocrine resistance associated with activated ErbB system in breast cancer cells is reversed by inhibiting MAPK or PI3K/Akt signaling pathways*. International Journal of Cancer, 2010. **126**(2): p. 545-562.
356. Guo, J.P., et al., *IKKepsilon phosphorylation of estrogen receptor alpha Ser-167 and contribution to tamoxifen resistance in breast cancer*. J Biol Chem, 2010. **285**(6): p. 3676-3684.
357. Kastrati, I., et al., *The NF-κB Pathway Promotes Tamoxifen Tolerance and Disease Recurrence in Estrogen Receptor–Positive Breast Cancers*. Molecular Cancer Research, 2020. **18**(7): p. 1018-1027.
358. Lv, Q., et al., *FGFR1 Is Associated With Tamoxifen Resistance and Poor Prognosis of ER-Positive Breast Cancers by Suppressing ER Protein Expression*. Technology in Cancer Research & Treatment, 2021. **20**: p. 15330338211004935.
359. Wang, W., S.A. Nag, and R. Zhang, *Targeting the NFκB signaling pathways for breast cancer prevention and therapy*. Curr Med Chem, 2015. **22**(2): p. 264-89.
360. Ashrafizadeh, M., et al., *New insight towards development of paclitaxel and docetaxel resistance in cancer cells: EMT as a novel molecular mechanism and therapeutic possibilities*. Biomed Pharmacother, 2021. **141**: p. 111824.
361. McFadyen, M.C., et al., *Cytochrome P450 CYP1B1 protein expression: a novel mechanism of anticancer drug resistance*. Biochem Pharmacol, 2001. **62**(2): p. 207-12.
362. Eggersmann, T.K., et al., *CDK4/6 Inhibitors Expand the Therapeutic Options in Breast Cancer: Palbociclib, Ribociclib and Abemaciclib*. BioDrugs, 2019. **33**(2): p. 125-135.
363. Álvarez-Fernández, M. and M. Malumbres, *Mechanisms of Sensitivity and Resistance to CDK4/6 Inhibition*. Cancer Cell, 2020. **37**(4): p. 514-529.
364. Finn, R.S., et al., *PD 0332991, a selective cyclin D kinase 4/6 inhibitor, preferentially inhibits proliferation of luminal estrogen receptor-positive human breast cancer cell lines in vitro*. Breast Cancer Res, 2009. **11**(5): p. R77.
365. Wander, S.A., et al., *The Genomic Landscape of Intrinsic and Acquired Resistance to Cyclin-Dependent Kinase 4/6 Inhibitors in Patients with Hormone Receptor–Positive Metastatic Breast Cancer*. Cancer Discovery, 2020. **10**(8): p. 1174-1193.
366. Ostrom, Q.T., et al., *CBTRUS statistical report: primary brain and central nervous system tumors diagnosed in the United States in 2008-2012*. Neuro-oncology, 2015. **17**(suppl_4): p. iv1-iv62.
367. Ostrom, Q.T., et al., *The epidemiology of glioma in adults: a “state of the science” review*. Neuro-oncology, 2014. **16**(7): p. 896-913.
368. Campos, B., et al., *A comprehensive profile of recurrent glioblastoma*. Oncogene, 2016. **35**(45): p. 5819-5825.
369. Stupp, R., et al., *Radiotherapy plus concomitant and adjuvant temozolomide for glioblastoma*. New England journal of medicine, 2005. **352**(10): p. 987-996.
370. Jackson, C.M., J. Choi, and M. Lim, *Mechanisms of immunotherapy resistance: lessons from glioblastoma*. Nature Immunology, 2019. **20**(9): p. 1100-1109.
371. Prados, M.D., et al., *Toward precision medicine in glioblastoma: the promise and the challenges*. Neuro-oncology, 2015. **17**(8): p. 1051-1063.
372. Allen, E., et al., *Combined antiangiogenic and anti–PD-L1 therapy stimulates tumor immunity through HEV formation*. Science translational medicine, 2017. **9**(385): p. eaak9679.
373. Verreault, M., et al., *Preclinical Efficacy of the MDM2 Inhibitor RG7112 in MDM2-Amplified and TP53 Wild-type Glioblastomas* Preclinical Efficacy of RG7112 in Glioblastoma. Clinical Cancer Research, 2016. **22**(5): p. 1185-1196.
374. Wu, A., et al., *Combination anti-CXCR4 and anti-PD-1 immunotherapy provides survival benefit in glioblastoma through immune cell modulation of tumor microenvironment*. Journal of Neuro-Oncology, 2019. **143**: p. 241-249.
375. Bagley, S.J., et al., *Glioblastoma Clinical Trials: Current Landscape and Opportunities for Improvement*. Clin Cancer Res, 2022. **28**(4): p. 594-602.

376. Liao, L.M., et al., *First results on survival from a large Phase 3 clinical trial of an autologous dendritic cell vaccine in newly diagnosed glioblastoma*. Journal of translational medicine, 2018. **16**(1): p. 1-9.
377. Lim, M., et al., *Current state of immunotherapy for glioblastoma*. Nature reviews Clinical oncology, 2018. **15**(7): p. 422-442.
378. Wen, P.Y., et al., *A Randomized Double-Blind Placebo-Controlled Phase II Trial of Dendritic Cell Vaccine ICT-107 in Newly Diagnosed Patients with Glioblastoma* ICT-107 Vaccine for Newly Diagnosed Glioblastoma. Clinical Cancer Research, 2019. **25**(19): p. 5799-5807.
379. Reardon, D.A., et al., *Effect of nivolumab vs bevacizumab in patients with recurrent glioblastoma: the CheckMate 143 phase 3 randomized clinical trial*. JAMA oncology, 2020. **6**(7): p. 1003-1010.
380. Sprooten, J., et al., *Trial watch: dendritic cell vaccination for cancer immunotherapy*. Oncoimmunology, 2019. **8**(11): p. 1638212.
381. Liao, L.M., et al., *Association of Autologous Tumor Lysate-Loaded Dendritic Cell Vaccination With Extension of Survival Among Patients With Newly Diagnosed and Recurrent Glioblastoma: A Phase 3 Prospective Externally Controlled Cohort Trial*. JAMA Oncology, 2023. **9**(1): p. 112-121.
382. Brudno, J.N. and J.N. Kochenderfer, *Chimeric antigen receptor T-cell therapies for lymphoma*. Nature reviews Clinical oncology, 2018. **15**(1): p. 31-46.
383. Hellmann, M.D., et al., *Nivolumab plus ipilimumab in advanced non-small-cell lung cancer*. New England Journal of Medicine, 2019. **381**(21): p. 2020-2031.
384. Hucks, G. and S.R. Rheingold, *The journey to CAR T cell therapy: the pediatric and young adult experience with relapsed or refractory B-ALL*. Blood cancer journal, 2019. **9**(2): p. 10.
385. Larkin, J., et al., *Five-year survival with combined nivolumab and ipilimumab in advanced melanoma*. New England Journal of Medicine, 2019. **381**(16): p. 1535-1546.
386. Wolchok, J.D., et al., *Overall survival with combined nivolumab and ipilimumab in advanced melanoma*. New England Journal of Medicine, 2017. **377**(14): p. 1345-1356.
387. Lim, M., et al., *Phase III trial of chemoradiotherapy with temozolomide plus nivolumab or placebo for newly diagnosed glioblastoma with methylated MGMT promoter*. Neuro Oncol, 2022. **24**(11): p. 1935-1949.
388. Woroniecka, K. and P.E. Fecci, *Immuno-synergy? Neoantigen vaccines and checkpoint blockade in glioblastoma*. Neuro Oncol, 2020. **22**(9): p. 1233-1234.
389. Nayak, L., et al., *Randomized Phase II and Biomarker Study of Pembrolizumab plus Bevacizumab versus Pembrolizumab Alone for Patients with Recurrent Glioblastoma* Pembrolizumab±Bevacizumab for Recurrent GBM. Clinical Cancer Research, 2021. **27**(4): p. 1048-1057.
390. Omuro, A., et al., *Nivolumab with or without ipilimumab in patients with recurrent glioblastoma: results from exploratory phase I cohorts of CheckMate 143*. Neuro-oncology, 2018. **20**(5): p. 674-686.
391. Nduom, E.K., M. Weller, and A.B. Heimberger, *Immunosuppressive mechanisms in glioblastoma*. Neuro-oncology, 2015. **17**(suppl_7): p. vii9-vii14.
392. Wang, Q., et al., *Tumor evolution of glioma-intrinsic gene expression subtypes associates with immunological changes in the microenvironment*. Cancer cell, 2017. **32**(1): p. 42-56. e6.
393. Butowski, N., et al., *Orally administered colony stimulating factor 1 receptor inhibitor PLX3397 in recurrent glioblastoma: an Ivy Foundation Early Phase Clinical Trials Consortium phase II study*. Neuro Oncol, 2016. **18**(4): p. 557-64.
394. Quail, D.F., et al., *The tumor microenvironment underlies acquired resistance to CSF-1R inhibition in gliomas*. Science, 2016. **352**(6288): p. aad3018.
395. Neubert, N.J., et al., *T cell-induced CSF1 promotes melanoma resistance to PD1 blockade*. Sci Transl Med, 2018. **10**(436).

396. Coniglio, S.J., et al., *Microglial stimulation of glioblastoma invasion involves epidermal growth factor receptor (EGFR) and colony stimulating factor 1 receptor (CSF-1R) signaling*. *Molecular medicine*, 2012. **18**: p. 519-527.
397. De, I., et al., *CSF1 Overexpression Promotes High-Grade Glioma Formation without Impacting the Polarization Status of Glioma-Associated Microglia and Macrophages*. *Cancer research*, 2016. **76**(9): p. 2552-2560.
398. Yan, D., et al., *Inhibition of colony stimulating factor-1 receptor abrogates microenvironment-mediated therapeutic resistance in gliomas*. *Oncogene*, 2017. **36**(43): p. 6049-6058.
399. Ries, C.H., et al., *Targeting tumor-associated macrophages with anti-CSF-1R antibody reveals a strategy for cancer therapy*. *Cancer Cell*, 2014. **25**(6): p. 846-59.
400. Yang, I., et al., *CD8+ T-cell infiltrate in newly diagnosed glioblastoma is associated with long-term survival*. *Journal of Clinical Neuroscience*, 2010. **17**(11): p. 1381-1385.
401. Sayour, E.J., et al., *Increased proportion of FoxP3+ regulatory T cells in tumor infiltrating lymphocytes is associated with tumor recurrence and reduced survival in patients with glioblastoma*. *Cancer Immunology, Immunotherapy*, 2015. **64**(4): p. 419-427.
402. Ye, Q., et al., *CD137 Accurately Identifies and Enriches for Naturally Occurring Tumor-Reactive T Cells in Tumor*. *Clinical Cancer Research*, 2014. **20**(1): p. 44-55.
403. Cao, D., et al., *Potential Strategies to Improve the Effectiveness of Drug Therapy by Changing Factors Related to Tumor Microenvironment*. *Frontiers in Cell and Developmental Biology*, 2021. **9**.
404. Jin, M.-Z. and W.-L. Jin, *The updated landscape of tumor microenvironment and drug repurposing*. *Signal Transduction and Targeted Therapy*, 2020. **5**(1): p. 166.
405. Dagogo-Jack, I. and A.T. Shaw, *Tumour heterogeneity and resistance to cancer therapies*. *Nature reviews Clinical oncology*, 2018. **15**(2): p. 81-94.
406. Burstein, H.J., *Unmet challenges in systemic therapy for early stage breast cancer*. *The Breast*, 2022. **62**: p. S67-S69.
407. Rong, L., N. Li, and Z. Zhang, *Emerging therapies for glioblastoma: current state and future directions*. *Journal of Experimental & Clinical Cancer Research*, 2022. **41**(1): p. 142.
408. Dupont, C.A., et al., *Druggable genome and precision medicine in cancer: current challenges*. *The FEBS Journal*, 2021. **288**(21): p. 6142-6158.
409. Tsimberidou, A.M., et al., *Review of precision cancer medicine: Evolution of the treatment paradigm*. *Cancer Treatment Reviews*, 2020. **86**.
410. Malaney, P., S.V. Nicosia, and V. Davé, *One mouse, one patient paradigm: New avatars of personalized cancer therapy*. *Cancer Letters*, 2014. **344**(1): p. 1-12.
411. Nair, R.R., et al., *Uses for humanised mouse models in precision medicine for neurodegenerative disease*. *Mammalian Genome*, 2019. **30**: p. 173-191.
412. Sontheimer-Phelps, A., B.A. Hassell, and D.E. Ingber, *Modelling cancer in microfluidic human organs-on-chips*. *Nature Reviews Cancer*, 2019. **19**(2): p. 65-81.
413. Foo, M.A., et al., *Clinical translation of patient-derived tumour organoids- bottlenecks and strategies*. *Biomarker Research*, 2022. **10**(1): p. 10.
414. He, L. and C. Deng, *Recent advances in organotypic tissue slice cultures for anticancer drug development*. *Int J Biol Sci*, 2022. **18**(15): p. 5885-5896.
415. Templeton, A.R., et al., *Patient-Derived Explants as a Precision Medicine Patient-Proximal Testing Platform Informing Cancer Management*. *Front Oncol*, 2021. **11**: p. 767697.
416. Voskoglou-Nomikos, T., J.L. Pater, and L. Seymour, *Clinical predictive value of the in vitro cell line, human xenograft, and mouse allograft preclinical cancer models*. *Clin Cancer Res*, 2003. **9**(11): p. 4227-39.
417. Ben-David, U., et al., *Patient-derived xenografts undergo mouse-specific tumor evolution*. *Nature genetics*, 2017. **49**(11): p. 1567-1575.
418. Ellis, L.M. and I.J. Fidler, *Finding the tumor copycat: therapy fails, patients don't*. *Nature medicine*, 2010. **16**(9): p. 974-975.

-
419. Hill, S.J., et al., *Prediction of DNA Repair Inhibitor Response in Short-Term Patient-Derived Ovarian Cancer Organoids*. *Cancer Discov*, 2018. **8**(11): p. 1404-1421.
420. Porter, R.J., G.I. Murray, and M.H. McLean, *Current concepts in tumour-derived organoids*. *British Journal of Cancer*, 2020. **123**(8): p. 1209-1218.
421. Li, X., et al., *Organoid cultures recapitulate esophageal adenocarcinoma heterogeneity providing a model for clonality studies and precision therapeutics*. *Nature communications*, 2018. **9**(1): p. 2983.
422. Jacob, F., et al., *A Patient-Derived Glioblastoma Organoid Model and Biobank Recapitulates Inter- and Intra-tumoral Heterogeneity*. *Cell*, 2020. **180**(1): p. 188-204.e22.
423. Phan, N., et al., *A simple high-throughput approach identifies actionable drug sensitivities in patient-derived tumor organoids*. *Communications Biology*, 2019. **2**(1): p. 78.
424. Du, Y., et al., *Development of a miniaturized 3D organoid culture platform for ultra-high-throughput screening*. *Journal of Molecular Cell Biology*, 2020. **12**(8): p. 630-643.
425. Hou, S., et al., *Advanced Development of Primary Pancreatic Organoid Tumor Models for High-Throughput Phenotypic Drug Screening*. *SLAS Discovery*, 2018. **23**(6): p. 574-584.
426. Clevers, H., *Modeling Development and Disease with Organoids*. *Cell*, 2016. **165**(7): p. 1586-1597.
427. Fatehullah, A., S.H. Tan, and N. Barker, *Organoids as an in vitro model of human development and disease*. *Nature Cell Biology*, 2016. **18**(3): p. 246-254.
428. Huszthy, P.C., et al., *In vivo models of primary brain tumors: pitfalls and perspectives*. *Neuro-oncology*, 2012. **14**(8): p. 979-993.
429. Aisenbrey, E.A. and W.L. Murphy, *Synthetic alternatives to Matrigel*. *Nat Rev Mater*, 2020. **5**(7): p. 539-551.
430. Kozlowski, M.T., C.J. Crook, and H.T. Ku, *Towards organoid culture without Matrigel*. *Commun Biol*, 2021. **4**(1): p. 1387.
431. Babaier, A. and P. Ghatage, *Mucinous Cancer of the Ovary: Overview and Current Status*. *Diagnostics (Basel)*, 2020. **10**(1).
432. Lisio, M.A., et al., *High-Grade Serous Ovarian Cancer: Basic Sciences, Clinical and Therapeutic Standpoints*. *Int J Mol Sci*, 2019. **20**(4).
433. McCart Reed, A.E., et al., *Invasive lobular carcinoma of the breast: the increasing importance of this special subtype*. *Breast Cancer Res*, 2021. **23**(1): p. 6.
434. Andrade, V.P. and H. Gobbi, *Accuracy of typing and grading invasive mammary carcinomas on core needle biopsy compared with the excisional specimen*. *Virchows Arch*, 2004. **445**(6): p. 597-602.
435. Badoual, C., et al., *Pathological prognostic factors of invasive breast carcinoma in ultrasound-guided large core biopsies-correlation with subsequent surgical excisions*. *Breast*, 2005. **14**(1): p. 22-7.
436. Burge, C.N., H.R. Chang, and S.K. Apple, *Do the histologic features and results of breast cancer biomarker studies differ between core biopsy and surgical excision specimens?* *Breast*, 2006. **15**(2): p. 167-72.
437. Harris, G.C., et al., *Correlation of histologic prognostic factors in core biopsies and therapeutic excisions of invasive breast carcinoma*. *Am J Surg Pathol*, 2003. **27**(1): p. 11-5.
438. Rakha, E.A. and I.O. Ellis, *An overview of assessment of prognostic and predictive factors in breast cancer needle core biopsy specimens*. *J Clin Pathol*, 2007. **60**(12): p. 1300-6.
439. Tornos, C., et al., *Expression of WT1, CA 125, and GCDFFP-15 as useful markers in the differential diagnosis of primary ovarian carcinomas versus metastatic breast cancer to the ovary*. *Am J Surg Pathol*, 2005. **29**(11): p. 1482-9.
440. Korsching, E., et al., *Cytogenetic Alterations and Cytokeratin Expression Patterns in Breast Cancer: Integrating a New Model of Breast Differentiation into Cytogenetic Pathways of Breast Carcinogenesis*. *Laboratory Investigation*, 2002. **82**(11): p. 1525-1533.

-
441. Barca, C., et al., *The Colony Stimulating Factor-1 Receptor (CSF-1R)-Mediated Regulation of Microglia/Macrophages as a Target for Neurological Disorders (Glioma, Stroke)*. *Frontiers in Immunology*, 2021. **12**.
442. Acs, G., T. Pasha, and P.J. Zhang, *WT1 is differentially expressed in serous, endometrioid, clear cell, and mucinous carcinomas of the peritoneum, fallopian tube, ovary, and endometrium*. *Int J Gynecol Pathol*, 2004. **23**(2): p. 110-8.
443. Campaner, E., et al., *Breast Cancer Organoids Model Patient-Specific Response to Drug Treatment*. *Cancers (Basel)*, 2020. **12**(12).
444. Chen, P., et al., *Patient-Derived Organoids Can Guide Personalized-Therapies for Patients with Advanced Breast Cancer*. *Adv Sci (Weinh)*, 2021. **8**(22): p. e2101176.
445. Fadare, O., S.A. Wang, and D. Hileeto, *The expression of cytokeratin 5/6 in invasive lobular carcinoma of the breast: evidence of a basal-like subset?* *Hum Pathol*, 2008. **39**(3): p. 331-6.
446. McGinn, O., et al., *Cytokeratin 5 alters β -catenin dynamics in breast cancer cells*. *Oncogene*, 2020. **39**(12): p. 2478-2492.
447. Fetting, L.M., et al., *Cross talk between progesterone receptors and retinoic acid receptors in regulation of cytokeratin 5-positive breast cancer cells*. *Oncogene*, 2017. **36**(44): p. 6074-6084.
448. Kabos, P., et al., *Cytokeratin 5 positive cells represent a steroid receptor negative and therapy resistant subpopulation in luminal breast cancers*. *Breast Cancer Res Treat*, 2011. **128**(1): p. 45-55.
449. Foulkes, W.D., et al., *The Prognostic Implication of the Basal-Like (Cyclin Ehigh/p27low/p53+/Glomeruloid-Microvascular-Proliferation+) Phenotype of BRCA1-Related Breast Cancer*. *Cancer Research*, 2004. **64**(3): p. 830-835.
450. Foulkes, W.D., et al., *Germline BRCA1 Mutations and a Basal Epithelial Phenotype in Breast Cancer*. *JNCI: Journal of the National Cancer Institute*, 2003. **95**(19): p. 1482-1485.
451. Adhikaree, J., et al., *Resistance mechanisms and barriers to successful immunotherapy for treating glioblastoma*. *Cells*, 2020. **9**(2): p. 263.
452. Razavi, S.-M., et al., *Immune evasion strategies of glioblastoma*. *Frontiers in surgery*, 2016. **3**: p. 11.
453. Henke, E., R. Nandigama, and S. Ergün, *Extracellular matrix in the tumor microenvironment and its impact on cancer therapy*. *Frontiers in molecular biosciences*, 2020. **6**: p. 160.
454. Nissen, N.I., M. Karsdal, and N. Willumsen, *Collagens and Cancer associated fibroblasts in the reactive stroma and its relation to Cancer biology*. *J Exp Clin Cancer Res*, 2019. **38**(1): p. 115.
455. Yu, G. and J. Wang, *Significance of hyaluronan binding protein (HABP1/P32/gC1qR) expression in advanced serous ovarian cancer patients*. 2013. **94**(1): p. 210-215.
456. Park, C.K., W.H. Jung, and J.S. Koo, *Expression of cancer-associated fibroblast-related proteins differs between invasive lobular carcinoma and invasive ductal carcinoma*. *Breast Cancer Res Treat*, 2016. **159**(1): p. 55-69.
457. Dang, T.T., A.M. Prechtel, and G.W. Pearson, *Breast cancer subtype-specific interactions with the microenvironment dictate mechanisms of invasion*. *Cancer research*, 2011. **71**(21): p. 6857-6866.
458. Gaggioli, C., et al., *Fibroblast-led collective invasion of carcinoma cells with differing roles for RhoGTPases in leading and following cells*. *Nature cell biology*, 2007. **9**(12): p. 1392-1400.
459. Goetz, J.G., et al., *Biomechanical remodeling of the microenvironment by stromal caveolin-1 favors tumor invasion and metastasis*. *Cell*, 2011. **146**(1): p. 148-163.
460. Matisse, L.A., et al., *Lack of transforming growth factor- β signaling promotes collective cancer cell invasion through tumor-stromal crosstalk*. *Breast cancer research*, 2012. **14**(4): p. 1-18.
461. Wang, F.T., et al., *Cancer-associated fibroblast regulation of tumor neo-angiogenesis as a therapeutic target in cancer*. *Oncology letters*, 2019. **17**(3): p. 3055-3065.

462. Lisanti, M.P., et al., *Understanding the "lethal" drivers of tumor-stroma co-evolution: emerging role (s) for hypoxia, oxidative stress and autophagy/mitophagy in the tumor microenvironment*. *Cancer biology & therapy*, 2010. **10**(6): p. 537-542.
463. Kraman, M., et al., *Suppression of antitumor immunity by stromal cells expressing fibroblast activation protein- α* . *Science*, 2010. **330**(6005): p. 827-830.
464. Mercier, I., et al., *Caveolin-1 and accelerated host aging in the breast tumor microenvironment: chemoprevention with rapamycin, an mTOR inhibitor and anti-aging drug*. *The American journal of pathology*, 2012. **181**(1): p. 278-293.
465. Quail, D.F. and J.A. Joyce, *Microenvironmental regulation of tumor progression and metastasis*. *Nat Med*, 2013. **19**(11): p. 1423-37.
466. Tsai, S., et al., *Development of primary human pancreatic cancer organoids, matched stromal and immune cells and 3D tumor microenvironment models*. *BMC cancer*, 2018. **18**(1): p. 1-13.
467. Tsang, S.I., et al., *Experimental models for ovarian cancer research*. *Experimental Cell Research*, 2022: p. 113150.
468. Watters, K.M., P. Bajwa, and H.A. Kenny, *Organotypic 3D models of the ovarian cancer tumor microenvironment*. *Cancers*, 2018. **10**(8): p. 265.
469. Troup, S., et al., *Reduced expression of the small leucine-rich proteoglycans, lumican, and decorin is associated with poor outcome in node-negative invasive breast cancer*. *Clin Cancer Res*, 2003. **9**(1): p. 207-14.
470. Saha, P. and K. Datta, *Multi-functional, multicompartmental hyaluronan-binding protein 1 (HABP1/p32/gC1qR): implication in cancer progression and metastasis*. *Oncotarget*, 2018. **9**(12): p. 10784-10807.
471. Bergamaschi, A., et al., *Extracellular matrix signature identifies breast cancer subgroups with different clinical outcome*. *The Journal of pathology*, 2008. **214**(3): p. 357-367.
472. Conklin, M.W., et al., *Aligned Collagen Is a Prognostic Signature for Survival in Human Breast Carcinoma*. *The American Journal of Pathology*, 2011. **178**(3): p. 1221-1232.
473. Riaz, M., et al., *High TWIST1 mRNA expression is associated with poor prognosis in lymph node-negative and estrogen receptor-positive human breast cancer and is co-expressed with stromal as well as ECM related genes*. *Breast Cancer Research*, 2012. **14**(5): p. 1-15.
474. Walsh, A.J., et al., *Collagen density and alignment in responsive and resistant trastuzumab-treated breast cancer xenografts*. *Journal of biomedical optics*, 2015. **20**(2): p. 026004.
475. Kauppila, S., et al., *Cross-linked telopeptides of type I and III collagens in malignant ovarian tumours in vivo*. *British Journal of Cancer*, 1999. **81**(4): p. 654-661.
476. Ricciardelli, C. and R.J. Rodgers. *Extracellular matrix of ovarian tumors*. in *Seminars in reproductive medicine*. 2006. Copyright© 2006 by Thieme Medical Publishers, Inc., 333 Seventh Avenue, New
477. Sajjad, H., et al., *Cancer models in preclinical research: A chronicle review of advancement in effective cancer research*. *Animal Models and Experimental Medicine*, 2021. **4**(2): p. 87-103.
478. Yang, R. and Y. Yu, *Patient-derived organoids in translational oncology and drug screening*. *Cancer Letters*, 2023. **562**: p. 216180.
479. Kleinman, H.K. and G.R. Martin. *Matrigel: basement membrane matrix with biological activity*. in *Seminars in cancer biology*. 2005. Elsevier.
480. Peterson, N.C., *From bench to cageside: risk assessment for rodent pathogen contamination of cells and biologics*. *ILAR journal*, 2008. **49**(3): p. 310-315.
481. Hofer, M. and M.P. Lutolf, *Engineering organoids*. *Nature Reviews Materials*, 2021. **6**(5): p. 402-420.
482. Ammann, C.G., et al., *Lactate dehydrogenase-elevating virus induces systemic lymphocyte activation via TLR7-dependent IFN α responses by plasmacytoid dendritic cells*. *PLoS One*, 2009. **4**(7): p. e6105.
483. Riley, V., et al., *The LDH virus: an interfering biological contaminant*. *Science*, 1978. **200**(4338): p. 124-126.

484. Broguiere, N., et al., *Growth of epithelial organoids in a defined hydrogel*. *Advanced Materials*, 2018. **30**(43): p. 1801621.
485. Cruz-Acuña, R., et al., *Synthetic hydrogels for human intestinal organoid generation and colonic wound repair*. *Nature cell biology*, 2017. **19**(11): p. 1326-1335.
486. Jabaji, Z., et al., *Type I collagen as an extracellular matrix for the in vitro growth of human small intestinal epithelium*. *PLoS one*, 2014. **9**(9): p. e107814.
487. Lindborg, B.A., et al., *Rapid induction of cerebral organoids from human induced pluripotent stem cells using a chemically defined hydrogel and defined cell culture medium*. *Stem Cells Translational Medicine*, 2016. **5**(7): p. 970-979.
488. Mollica, P.A., et al., *3D bioprinted mammary organoids and tumoroids in human mammary derived ECM hydrogels*. *Acta biomaterialia*, 2019. **95**: p. 201-213.
489. Cho, S.Y., *Patient-derived xenografts as compatible models for precision oncology*. *Lab Anim Res*, 2020. **36**: p. 14.
490. Liu, Y., et al., *Patient-derived xenograft models in cancer therapy: technologies and applications*. *Signal Transduction and Targeted Therapy*, 2023. **8**(1): p. 160.
491. Delitto, D., et al., *Patient-derived xenograft models for pancreatic adenocarcinoma demonstrate retention of tumor morphology through incorporation of murine stromal elements*. *Am J Pathol*, 2015. **185**(5): p. 1297-303.
492. Alban, T.J., et al., *Global immune fingerprinting in glioblastoma patient peripheral blood reveals immune-suppression signatures associated with prognosis*. *JCI insight*, 2018. **3**(21).
493. Fecci, P.E., et al., *Increased regulatory T-cell fraction amidst a diminished CD4 compartment explains cellular immune defects in patients with malignant glioma*. *Cancer research*, 2006. **66**(6): p. 3294-3302.
494. Gielen, P.R., et al., *Elevated levels of polymorphonuclear myeloid-derived suppressor cells in patients with glioblastoma highly express S100A8/9 and arginase and suppress T cell function*. *Neuro Oncol*, 2016. **18**(9): p. 1253-64.
495. Chongsathidkiet, P., et al., *Sequestration of T cells in bone marrow in the setting of glioblastoma and other intracranial tumors*. *Nat Med*, 2018. **24**(9): p. 1459-1468.
496. Thorsson, V., et al., *The Immune Landscape of Cancer*. *Immunity*, 2018. **48**(4): p. 812-830.e14.
497. Woroniecka, K., et al., *T-Cell Exhaustion Signatures Vary with Tumor Type and Are Severe in Glioblastoma*. *Clin Cancer Res*, 2018. **24**(17): p. 4175-4186.
498. Jin, Y.W. and P. Hu, *Tumor-Infiltrating CD8 T Cells Predict Clinical Breast Cancer Outcomes in Young Women*. *Cancers*, 2020. **12**(5): p. 1076.
499. Ruoff, F., et al., *Protein Profiling of Breast Carcinomas Reveals Expression of Immune-Suppressive Factors and Signatures Relevant for Patient Outcome*. *Cancers*, 2022. **14**(18): p. 4542.
500. Darvin, P., et al., *Immune checkpoint inhibitors: recent progress and potential biomarkers*. *Experimental & Molecular Medicine*, 2018. **50**(12): p. 1-11.
501. Salgado, R., et al., *The evaluation of tumor-infiltrating lymphocytes (TILs) in breast cancer: recommendations by an International TILs Working Group 2014*. *Annals of Oncology*, 2015. **26**(2): p. 259-271.
502. Dhandapani, M. and A. Goldman, *Preclinical Cancer Models and Biomarkers for Drug Development: New Technologies and Emerging Tools*. *J Mol Biomark Diagn*, 2017. **8**(5).
503. Jackson, S.J. and G.J. Thomas, *Human tissue models in cancer research: looking beyond the mouse*. *Dis Model Mech*, 2017. **10**(8): p. 939-942.
504. Zhao, Y., et al., *Development of a new patient-derived xenograft humanised mouse model to study human-specific tumour microenvironment and immunotherapy*. *Gut*, 2018. **67**(10): p. 1845-1854.
505. Rongvaux, A., et al., *Development and function of human innate immune cells in a humanized mouse model*. *Nature biotechnology*, 2014. **32**(4): p. 364-372.

-
506. Zeleniak, A., et al., *De novo construction of T cell compartment in humanized mice engrafted with iPSC-derived thymus organoids*. *Nature methods*, 2022. **19**(10): p. 1306-1319.
507. Parker, J.S., et al., *Supervised risk predictor of breast cancer based on intrinsic subtypes*. *J Clin Oncol*, 2009. **27**(8): p. 1160-7.
508. Wallden, B., et al., *Development and verification of the PAM50-based Prosigna breast cancer gene signature assay*. *BMC Med Genomics*, 2015. **8**: p. 54.
509. Duffy, M.J., et al., *Clinical use of biomarkers in breast cancer: Updated guidelines from the European Group on Tumor Markers (EGTM)*. *Eur J Cancer*, 2017. **75**: p. 284-298.
510. Harris, L.N., et al., *Use of Biomarkers to Guide Decisions on Adjuvant Systemic Therapy for Women With Early-Stage Invasive Breast Cancer: American Society of Clinical Oncology Clinical Practice Guideline*. *J Clin Oncol*, 2016. **34**(10): p. 1134-50.
511. Wallden, B., et al., *Development and verification of the PAM50-based Prosigna breast cancer gene signature assay*. *BMC medical genomics*, 2015. **8**(1): p. 1-14.
512. Le Tourneau, C., et al., *Molecularly targeted therapy based on tumour molecular profiling versus conventional therapy for advanced cancer (SHIVA): a multicentre, open-label, proof-of-concept, randomised, controlled phase 2 trial*. *Lancet Oncol*, 2015. **16**(13): p. 1324-34.
513. Middleton, G., et al., *The National Lung Matrix Trial of personalized therapy in lung cancer*. *Nature*, 2020. **583**(7818): p. 807-812.
514. Sicklick, J.K., et al., *Molecular profiling of cancer patients enables personalized combination therapy: the I-PREDICT study*. *Nat Med*, 2019. **25**(5): p. 744-750.
515. van Tilburg, C.M., et al., *The Pediatric Precision Oncology INFORM Registry: Clinical Outcome and Benefit for Patients with Very High-Evidence Targets*. *Cancer Discov*, 2021. **11**(11): p. 2764-2779.
516. Doll, S., F. Gnad, and M. Mann, *The Case for Proteomics and Phospho-Proteomics in Personalized Cancer Medicine*. *Proteomics Clin Appl*, 2019. **13**(2): p. e1800113.
517. Curtis, C., et al., *The genomic and transcriptomic architecture of 2,000 breast tumours reveals novel subgroups*. *Nature*, 2012. **486**(7403): p. 346-52.
518. Hoadley, K.A., et al., *Multiplatform analysis of 12 cancer types reveals molecular classification within and across tissues of origin*. *Cell*, 2014. **158**(4): p. 929-944.
519. Shah, S.P., et al., *The clonal and mutational evolution spectrum of primary triple-negative breast cancers*. *Nature*, 2012. **486**(7403): p. 395-9.
520. Stephens, P.J., et al., *The landscape of cancer genes and mutational processes in breast cancer*. *Nature*, 2012. **486**(7403): p. 400-4.
521. Clark, D.J., et al., *Integrated proteogenomic characterization of clear cell renal cell carcinoma*. *Cell*, 2019. **179**(4): p. 964-983. e31.
522. Chang, L., et al., *Identification of protein biomarkers and signaling pathways associated with prostate cancer radioresistance using label-free LC-MS/MS proteomic approach*. *Scientific Reports*, 2017. **7**(1): p. 41834.
523. Nanjundan, M., et al., *Proteomic profiling identifies pathways dysregulated in non-small cell lung cancer and an inverse association of AMPK and adhesion pathways with recurrence*. *J Thorac Oncol*, 2010. **5**(12): p. 1894-904.
524. Posadas, E., et al., *Proteomic analysis for the early detection and rational treatment of cancer—realistic hope?* *Annals of oncology*, 2005. **16**(1): p. 16-22.
525. Faria, S.S., et al., *A timely shift from shotgun to targeted proteomics and how it can be groundbreaking for cancer research*. *Frontiers in Oncology*, 2017. **7**: p. 13.
526. Lin, Y.-H., et al., *Self-assembled STrap for global proteomics and salivary biomarker discovery*. *Journal of proteome research*, 2019. **18**(4): p. 1907-1915.
527. Dou, Y., et al., *Proteogenomic characterization of endometrial carcinoma*. *Cell*, 2020. **180**(4): p. 729-748. e26.
528. Mun, D.-G., et al., *Proteogenomic characterization of human early-onset gastric cancer*. *Cancer cell*, 2019. **35**(1): p. 111-124. e10.

529. Kwon, Y.W., et al., *Application of Proteomics in Cancer: Recent Trends and Approaches for Biomarkers Discovery*. Front Med (Lausanne), 2021. **8**: p. 747333.
530. Chen, H., et al., *Short-term organoid culture for drug sensitivity testing of high-grade serous carcinoma*. Gynecol Oncol, 2020. **157**(3): p. 783-792.
531. Coarfa, C., et al., *Reverse-Phase Protein Array: Technology, Application, Data Processing, and Integration*. J Biomol Tech, 2021. **32**(1): p. 15-29.
532. Bartholomeusz, C., et al., *High ERK protein expression levels correlate with shorter survival in triple-negative breast cancer patients*. Oncologist, 2012. **17**(6): p. 766-74.
533. Bai, X., et al., *Activation of the eIF2 α /ATF4 axis drives triple-negative breast cancer radioresistance by promoting glutathione biosynthesis*. Redox Biol, 2021. **43**: p. 101993.
534. Sonenberg, N. and A.G. Hinnebusch, *Regulation of translation initiation in eukaryotes: mechanisms and biological targets*. Cell, 2009. **136**(4): p. 731-45.
535. Bhat, M., et al., *Targeting the translation machinery in cancer*. Nature Reviews Drug Discovery, 2015. **14**(4): p. 261-278.
536. Flowers, A., et al., *Eukaryotic initiation factor 4E overexpression in triple-negative breast cancer predicts a worse outcome*. Surgery, 2009. **146**(2): p. 220-6.
537. McCawley, L.J., et al., *Sustained activation of the mitogen-activated protein kinase pathway. A mechanism underlying receptor tyrosine kinase specificity for matrix metalloproteinase-9 induction and cell migration*. J Biol Chem, 1999. **274**(7): p. 4347-53.
538. Wei, Y., et al., *CDK1-dependent phosphorylation of EZH2 suppresses methylation of H3K27 and promotes osteogenic differentiation of human mesenchymal stem cells*. Nat Cell Biol, 2011. **13**(1): p. 87-94.
539. Yang, C.C., et al., *Phosphorylation of EZH2 at T416 by CDK2 contributes to the malignancy of triple negative breast cancers*. Am J Transl Res, 2015. **7**(6): p. 1009-20.
540. Chen, F. and V. Castranova, *Nuclear Factor- κ B, an Unappreciated Tumor Suppressor*. Cancer Research, 2007. **67**(23): p. 11093-11098.
541. Oeckinghaus, A. and S. Ghosh, *The NF- κ B family of transcription factors and its regulation*. Cold Spring Harb Perspect Biol, 2009. **1**(4): p. a000034.
542. Sun, D., et al., *Why 90% of clinical drug development fails and how to improve it?* Acta Pharmaceutica Sinica B, 2022. **12**(7): p. 3049-3062.
543. Lheureux, S., et al., *Epithelial ovarian cancer*. The Lancet, 2019. **393**(10177): p. 1240-1253.
544. Nowak, A.K., et al., *Systematic review of taxane-containing versus non-taxane-containing regimens for adjuvant and neoadjuvant treatment of early breast cancer*. The Lancet Oncology, 2004. **5**(6): p. 372-380.
545. Amat, S., et al., *Neoadjuvant docetaxel for operable breast cancer induces a high pathological response and breast-conservation rate*. British Journal of Cancer, 2003. **88**(9): p. 1339-1345.
546. Marry, M., et al., *Prospects with docetaxel in the treatment of patients with breast cancer*. European Journal of Cancer, 1997. **33**: p. S26-S29.
547. Coleman, R.L., et al., *Rucaparib maintenance treatment for recurrent ovarian carcinoma after response to platinum therapy (ARIEL3): a randomised, double-blind, placebo-controlled, phase 3 trial*. The Lancet, 2017. **390**(10106): p. 1949-1961.
548. Ledermann, J., et al., *Olaparib Maintenance Therapy in Platinum-Sensitive Relapsed Ovarian Cancer*. New England Journal of Medicine, 2012. **366**(15): p. 1382-1392.
549. Mirza, M.R., et al., *Niraparib Maintenance Therapy in Platinum-Sensitive, Recurrent Ovarian Cancer*. New England Journal of Medicine, 2016. **375**(22): p. 2154-2164.
550. Bukowski, R.M., R.F. Ozols, and M. Markman, *The management of recurrent ovarian cancer*. Semin Oncol, 2007. **34**(2 Suppl 2): p. S1-15.
551. Disis, M.L., et al., *Efficacy and Safety of Avelumab for Patients With Recurrent or Refractory Ovarian Cancer: Phase 1b Results From the JAVELIN Solid Tumor Trial*. JAMA Oncology, 2019. **5**(3): p. 393-401.

-
552. Varga, A., et al., *Pembrolizumab in patients with programmed death ligand 1-positive advanced ovarian cancer: Analysis of KEYNOTE-028*. *Gynecologic Oncology*, 2019. **152**(2): p. 243-250.
553. An, J., Y. Chen, and Z. Huang, *Critical upstream signals of cytochrome C release induced by a novel Bcl-2 inhibitor*. *J Biol Chem*, 2004. **279**(18): p. 19133-40.
554. Kouri, F.M., S.A. Jensen, and A.H. Stegh, *The role of Bcl-2 family proteins in therapy responses of malignant astrocytic gliomas: Bcl2L12 and beyond*. *ScientificWorldJournal*, 2012. **2012**: p. 838916.
555. Singh, R., A. Letai, and K. Sarosiek, *Regulation of apoptosis in health and disease: the balancing act of BCL-2 family proteins*. *Nat Rev Mol Cell Biol*, 2019. **20**(3): p. 175-193.
556. Day, C.P., G. Merlino, and T. Van Dyke, *Preclinical mouse cancer models: a maze of opportunities and challenges*. *Cell*, 2015. **163**(1): p. 39-53.
557. Salinas, R.D., J.S. Durgin, and D.M. O'Rourke, *Potential of glioblastoma-targeted chimeric antigen receptor (CAR) T-cell therapy*. *Cns Drugs*, 2020. **34**(2): p. 127-145.
558. Lin, S., et al. *Establishment of peripheral blood mononuclear cell-derived humanized lung cancer mouse models for studying efficacy of PD-L1/PD-1 targeted immunotherapy*. in *MABs*. 2018. Taylor & Francis.
559. Pandey, V., et al., *Anti-ovarian tumor response of donor peripheral blood mononuclear cells is due to infiltrating cytotoxic NK cells*. *Oncotarget*, 2016. **7**(6): p. 7318.
560. Spranger, S., B. Frankenberger, and D.J. Schendel, *NOD/scid IL-2R β null mice: a preclinical model system to evaluate human dendritic cell-based vaccine strategies in vivo*. *Journal of Translational Medicine*, 2012. **10**(1): p. 30.
561. Anadon, C.M., et al., *Ovarian cancer immunogenicity is governed by a narrow subset of progenitor tissue-resident memory T cells*. *Cancer Cell*, 2022. **40**(5): p. 545-557.e13.
562. Blankenstein, T., et al., *The determinants of tumour immunogenicity*. *Nature Reviews Cancer*, 2012. **12**(4): p. 307-313.
563. Curiel, T.J., et al., *Specific recruitment of regulatory T cells in ovarian carcinoma fosters immune privilege and predicts reduced survival*. *Nat Med*, 2004. **10**(9): p. 942-9.
564. Webb, J.R., K. Milne, and B.H. Nelson, *PD-1 and CD103 Are Widely Coexpressed on Prognostically Favorable Intraepithelial CD8 T Cells in Human Ovarian Cancer*. 2015. **3**(8): p. 926-935.
565. Hwang, W.-T., et al., *Prognostic significance of tumor-infiltrating T cells in ovarian cancer: A meta-analysis*. *Gynecologic Oncology*, 2012. **124**(2): p. 192-198.
566. Leem, G., et al., *4-1BB co-stimulation further enhances anti-PD-1-mediated reinvigoration of exhausted CD39⁺ CD8 T cells from primary and metastatic sites of epithelial ovarian cancers*. *Journal for ImmunoTherapy of Cancer*, 2020. **8**(2): p. e001650.
567. Nirschl, C.J. and C.G. Drake, *Molecular Pathways: Coexpression of Immune Checkpoint Molecules: Signaling Pathways and Implications for Cancer Immunotherapy*. *Clinical Cancer Research*, 2013. **19**(18): p. 4917-4924.
568. Schmid-Bindert, G. and T. Jiang, *First-line nivolumab (anti-PD-1) monotherapy in advanced NSCLC: the story of immune checkpoint inhibitors and "the sorcerers apprentice"*. *Transl Lung Cancer Res*, 2015. **4**(3): p. 215-6.
569. Pardoll, D.M., *The blockade of immune checkpoints in cancer immunotherapy*. *Nature Reviews Cancer*, 2012. **12**(4): p. 252-264.
570. Quirk, S.K., A.K. Shure, and D.K. Agrawal, *Immune-mediated adverse events of anticytotoxic T lymphocyte-associated antigen 4 antibody therapy in metastatic melanoma*. *Translational Research*, 2015. **166**(5): p. 412-424.
571. Sullivan, R.J. and K.T. Flaherty, *Anti-PD-1 therapies—a new first-line option in advanced melanoma*. *Nature Reviews Clinical Oncology*, 2015. **12**(11): p. 625-626.
572. Klemm, F., et al., *Interrogation of the Microenvironmental Landscape in Brain Tumors Reveals Disease-Specific Alterations of Immune Cells*. *Cell*, 2020. **181**(7): p. 1643-1660.e17.

573. Quail, D.F. and J.A. Joyce, *The Microenvironmental Landscape of Brain Tumors*. *Cancer Cell*, 2017. **31**(3): p. 326-341.
574. Blanc-Durand, F., et al., *Distribution of novel immune-checkpoint targets in ovarian cancer tumor microenvironment: A dynamic landscape*. *Gynecol Oncol*, 2021. **160**(1): p. 279-284.
575. Liu, Y.L., et al., *Subsequent therapies and survival after immunotherapy in recurrent ovarian cancer*. *Gynecol Oncol*, 2019. **155**(1): p. 51-57.
576. Bloch, O., et al., *Gliomas promote immunosuppression through induction of B7-H1 expression in tumor-associated macrophages*. *Clin Cancer Res*, 2013. **19**(12): p. 3165-75.
577. Buchbinder, E.I. and A. Desai, *CTLA-4 and PD-1 Pathways: Similarities, Differences, and Implications of Their Inhibition*. *Am J Clin Oncol*, 2016. **39**(1): p. 98-106.
578. Hussain, S.F., et al., *The role of human glioma-infiltrating microglia/macrophages in mediating antitumor immune responses*. *Neuro Oncol*, 2006. **8**(3): p. 261-79.
579. Hodges, T.R., et al., *Mutational burden, immune checkpoint expression, and mismatch repair in glioma: implications for immune checkpoint immunotherapy*. *Neuro Oncol*, 2017. **19**(8): p. 1047-1057.
580. McGranahan, N., et al., *Clonal neoantigens elicit T cell immunoreactivity and sensitivity to immune checkpoint blockade*. *Science*, 2016. **351**(6280): p. 1463-9.
581. Fan, S., et al., *Association between tumor mutation burden and immune infiltration in ovarian cancer*. *Int Immunopharmacol*, 2020. **89**(Pt A): p. 107126.
582. Maleki Vareki, S., *High and low mutational burden tumors versus immunologically hot and cold tumors and response to immune checkpoint inhibitors*. *J Immunother Cancer*, 2018. **6**(1): p. 157.
583. Martin, S.D., et al., *Low Mutation Burden in Ovarian Cancer May Limit the Utility of Neoantigen-Targeted Vaccines*. *PLoS One*, 2016. **11**(5): p. e0155189.
584. Hamanishi, J., et al., *Safety and Antitumor Activity of Anti-PD-1 Antibody, Nivolumab, in Patients With Platinum-Resistant Ovarian Cancer*. *Journal of Clinical Oncology*, 2015. **33**(34): p. 4015-4022.
585. Gandhi, L., et al., *Pembrolizumab plus Chemotherapy in Metastatic Non-Small-Cell Lung Cancer*. *New England Journal of Medicine*, 2018. **378**(22): p. 2078-2092.
586. Andersen, B.M., et al., *Glial and myeloid heterogeneity in the brain tumour microenvironment*. *Nat Rev Cancer*, 2021. **21**(12): p. 786-802.
587. Sørensen, M.D., et al., *Tumour-associated microglia/macrophages predict poor prognosis in high-grade gliomas and correlate with an aggressive tumour subtype*. *Neuropathol Appl Neurobiol*, 2018. **44**(2): p. 185-206.
588. Pyonteck, S.M., et al., *CSF-1R inhibition alters macrophage polarization and blocks glioma progression*. *Nat Med*, 2013. **19**(10): p. 1264-72.
589. De, I., et al., *CSF1 Overexpression Promotes High-Grade Glioma Formation without Impacting the Polarization Status of Glioma-Associated Microglia and Macrophages*. *Cancer Res*, 2016. **76**(9): p. 2552-60.
590. Przystal, J.M., et al., *Targeting CSF1R Alone or in Combination with PD1 in Experimental Glioma*. *Cancers*, 2021. **13**(10): p. 2400.
591. Antonios, J.P., et al., *Immunosuppressive tumor-infiltrating myeloid cells mediate adaptive immune resistance via a PD-1/PD-L1 mechanism in glioblastoma*. *Neuro Oncol*, 2017. **19**(6): p. 796-807.
592. Medikonda, R., et al., *A review of glioblastoma immunotherapy*. *J Neurooncol*, 2021. **151**(1): p. 41-53.
593. Dunn-Pirio, A.M. and G. Vlahovic, *Immunotherapy approaches in the treatment of malignant brain tumors*. *Cancer*, 2017. **123**(5): p. 734-750.
594. Davis, A.A. and V.G. Patel, *The role of PD-L1 expression as a predictive biomarker: an analysis of all US Food and Drug Administration (FDA) approvals of immune checkpoint inhibitors*. *J Immunother Cancer*, 2019. **7**(1): p. 278.
595. Pujade-Lauraine, E., et al., *Avelumab alone or in combination with chemotherapy versus chemotherapy alone in platinum-resistant or platinum-refractory ovarian cancer (JAVELIN*

- Ovarian 200*): an open-label, three-arm, randomised, phase 3 study. *The Lancet Oncology*, 2021. **22**(7): p. 1034-1046.
596. Meric-Bernstam, F., et al., *Feasibility of large-scale genomic testing to facilitate enrollment onto genomically matched clinical trials*. *Journal of clinical oncology*, 2015. **33**(25): p. 2753.
597. Stockley, T.L., et al., *Molecular profiling of advanced solid tumors and patient outcomes with genotype-matched clinical trials: the Princess Margaret IMPACT/COMPACT trial*. *Genome medicine*, 2016. **8**(1): p. 1-12.
598. Pezo, R.C., et al., *Impact of multi-gene mutational profiling on clinical trial outcomes in metastatic breast cancer*. *Breast Cancer Res Treat*, 2018. **168**(1): p. 159-168.
599. Tannock, I.F. and J.A. Hickman, *Molecular screening to select therapy for advanced cancer?* *Annals of Oncology*, 2019. **30**(5): p. 661-663.
600. Zardavas, D., J. Baselga, and M. Piccart, *Emerging targeted agents in metastatic breast cancer*. *Nat Rev Clin Oncol*, 2013. **10**(4): p. 191-210.
601. Park, S.R., et al., *Safety and feasibility of targeted agent combinations in solid tumours*. *Nature reviews Clinical oncology*, 2013. **10**(3): p. 154-168.
602. González-Silva, L., L. Quevedo, and I. Varela, *Tumor functional heterogeneity unraveled by scRNA-seq technologies*. *Trends in cancer*, 2020. **6**(1): p. 13-19.
603. Zhang, B., et al., *Clinical potential of mass spectrometry-based proteogenomics*. *Nature Reviews Clinical Oncology*, 2019. **16**(4): p. 256-268.
604. Pirnia, F., et al., *Novel functional profiling approach combining reverse phase protein microarrays and human 3-D ex vivo tissue cultures: expression of apoptosis-related proteins in human colon cancer*. *Proteomics*, 2009. **9**(13): p. 3535-48.
605. Rodriguez, H., et al., *The next horizon in precision oncology: Proteogenomics to inform cancer diagnosis and treatment*. *Cell*, 2021. **184**(7): p. 1661-1670.
606. Mertins, P., et al., *Proteogenomics connects somatic mutations to signalling in breast cancer*. *Nature*, 2016. **534**(7605): p. 55-62.
607. Valeriote, F. and L. van Putten, *Proliferation-dependent cytotoxicity of anticancer agents: a review*. *Cancer Res*, 1975. **35**(10): p. 2619-30.
608. Vasey, P.A., *Resistance to chemotherapy in advanced ovarian cancer: mechanisms and current strategies*. *British Journal of Cancer*, 2003. **89**(S3): p. 23-28.
609. Lu, Y., et al., *Using reverse-phase protein arrays as pharmacodynamic assays for functional proteomics, biomarker discovery, and drug development in cancer*. *Semin Oncol*, 2016. **43**(4): p. 476-83.
610. Lee, C.H., et al., *Constitutive mTOR activation in TSC mutants sensitizes cells to energy starvation and genomic damage via p53*. *Embo j*, 2007. **26**(23): p. 4812-23.
611. Vadysirisack, D.D., et al., *Feedback control of p53 translation by REDD1 and mTORC1 limits the p53-dependent DNA damage response*. *Mol Cell Biol*, 2011. **31**(21): p. 4356-65.
612. Astle, M.V., et al., *AKT induces senescence in human cells via mTORC1 and p53 in the absence of DNA damage: implications for targeting mTOR during malignancy*. *Oncogene*, 2012. **31**(15): p. 1949-62.
613. Leontieva, O.V. and M.V. Blagosklonny, *DNA damaging agents and p53 do not cause senescence in quiescent cells, while consecutive re-activation of mTOR is associated with conversion to senescence*. *Aging (Albany NY)*, 2010. **2**(12): p. 924-35.
614. Alves, C.L., et al., *High CDK6 Protects Cells from Fulvestrant-Mediated Apoptosis and is a Predictor of Resistance to Fulvestrant in Estrogen Receptor-Positive Metastatic Breast Cancer*. *Clinical Cancer Research*, 2016. **22**(22): p. 5514-5526.
615. Nathan, M.R. and P. Schmid, *A Review of Fulvestrant in Breast Cancer*. *Oncology and Therapy*, 2017. **5**(1): p. 17-29.
616. Yamnik, R.L., et al., *S6 Kinase 1 Regulates Estrogen Receptor α 1; in Control of Breast Cancer Cell Proliferation* *. *Journal of Biological Chemistry*, 2009. **284**(10): p. 6361-6369.
617. Early Breast Cancer Trialists' Collaborative, G., *Relevance of breast cancer hormone receptors and other factors to the efficacy of adjuvant tamoxifen: patient-level meta-analysis of randomised trials*. *The Lancet*, 2011. **378**(9793): p. 771-784.

618. Walsh, A.J., et al., *Quantitative Optical Imaging of Primary Tumor Organoid Metabolism Predicts Drug Response in Breast Cancer*. *Cancer Research*, 2014. **74**(18): p. 5184-5194.
619. Hennequin, C., N. Giocanti, and V. Favaudon, *S-phase specificity of cell killing by docetaxel (Taxotere) in synchronised HeLa cells*. *Br J Cancer*, 1995. **71**(6): p. 1194-8.
620. Barbolina, M.V., *Dichotomous role of microtubule associated protein tau as a biomarker of response to and a target for increasing efficacy of taxane treatment in cancers of epithelial origin*. *Pharmacological Research*, 2021. **168**: p. 105585.
621. Kim, K., Z. Lu, and E.D. Hay, *DIRECT EVIDENCE FOR A ROLE OF β -CATENIN/LEF-1 SIGNALING PATHWAY IN INDUCTION OF EMT*. *Cell Biology International*, 2002. **26**(5): p. 463-476.
622. Shi, R., et al., *Downregulation of cytokeratin 18 induces cellular partial EMT and stemness through increasing EpCAM expression in breast cancer*. *Cellular Signalling*, 2020. **76**: p. 109810.
623. Tham, Y.-L., et al., *Clinical response to neoadjuvant docetaxel predicts improved outcome in patients with large locally advanced breast cancers*. *Breast Cancer Research and Treatment*, 2005. **94**(3): p. 279-284.
624. Marín-Aguilera, M., et al., *Epithelial-to-Mesenchymal Transition Mediates Docetaxel Resistance and High Risk of Relapse in Prostate Cancer EMT Role in Docetaxel Resistance*. *Molecular cancer therapeutics*, 2014. **13**(5): p. 1270-1284.
625. Yang, C.-P.H., et al., *Upregulation of caveolin-1 and caveolae organelles in Taxol-resistant A549 cells*. *FEBS Letters*, 1998. **439**(3): p. 368-372.
626. Pusztai, L., et al., *Evaluation of Microtubule-Associated Protein-Tau Expression As a Prognostic and Predictive Marker in the NSABP-B 28 Randomized Clinical Trial*. *Journal of Clinical Oncology*, 2009. **27**(26): p. 4287-4292.
627. Guo, T., W. Noble, and D.P. Hanger, *Roles of tau protein in health and disease*. *Acta Neuropathologica*, 2017. **133**(5): p. 665-704.
628. Gu, J., et al., *Truncation of Tau selectively facilitates its pathological activities*. *Journal of Biological Chemistry*, 2020. **295**(40): p. 13812-13828.
629. Li, T. and H.K. Paudel, *14-3-3 ζ Mediates Tau Aggregation in Human Neuroblastoma M17 Cells*. *PLOS ONE*, 2016. **11**(8): p. e0160635.
630. Ashrafizadeh, M., et al., *New insight towards development of paclitaxel and docetaxel resistance in cancer cells: EMT as a novel molecular mechanism and therapeutic possibilities*. *Biomedicine & Pharmacotherapy*, 2021. **141**: p. 111824.
631. Schmidt, M., et al., *Role of the progesterone receptor for paclitaxel resistance in primary breast cancer*. *British Journal of Cancer*, 2007. **96**(2): p. 241-247.
632. Edakuni, G., et al., *Expression of the hepatocyte growth factor/c-Met pathway is increased at the cancer front in breast carcinoma*. *Pathology International*, 2001. **51**(3): p. 172-178.
633. Mehra, R., et al., *Identification of GATA3 as a Breast Cancer Prognostic Marker by Global Gene Expression Meta-analysis*. *Cancer Research*, 2005. **65**(24): p. 11259-11264.
634. Pearson, A., et al., *Inactivating NF1 Mutations Are Enriched in Advanced Breast Cancer and Contribute to Endocrine Therapy Resistance*. *Clinical Cancer Research*, 2020. **26**(3): p. 608-622.
635. Turner, N.C., et al., *Palbociclib in Hormone-Receptor-Positive Advanced Breast Cancer*. *New England Journal of Medicine*, 2015. **373**(3): p. 209-219.
636. Pandey, K., et al., *Molecular mechanisms of resistance to CDK4/6 inhibitors in breast cancer: A review*. *International Journal of Cancer*, 2019. **145**(5): p. 1179-1188.
637. Gravdal, K., et al., *A Switch from E-Cadherin to N-Cadherin Expression Indicates Epithelial to Mesenchymal Transition and Is of Strong and Independent Importance for the Progress of Prostate Cancer*. *Clinical Cancer Research*, 2007. **13**(23): p. 7003-7011.
638. Woelfle, U., et al., *Down-Regulated Expression of Cytokeratin 18 Promotes Progression of Human Breast Cancer*. *Clinical Cancer Research*, 2004. **10**(8): p. 2670-2674.
639. Saleh, L., C. Wilson, and I. Holen, *CDK4/6 inhibitors: A potential therapeutic approach for triple negative breast cancer*. *MedComm*, 2021. **2**(4): p. 514-530.

-
640. Gonzalez-Angulo, A.M., B.T.J. Hennessy, and G.B. Mills, *Future of Personalized Medicine in Oncology: A Systems Biology Approach*. Journal of Clinical Oncology, 2010. **28**(16): p. 2777-2783.
641. Ganesh, K., et al., *A rectal cancer organoid platform to study individual responses to chemoradiation*. Nat Med, 2019. **25**(10): p. 1607-1614.
642. Group, E.B.C.T.C., *Relevance of breast cancer hormone receptors and other factors to the efficacy of adjuvant tamoxifen: patient-level meta-analysis of randomised trials*. The lancet, 2011. **378**(9793): p. 771-784.

Declaration

Ich erkläre hiermit, dass ich die zur Promotion eingereichte Arbeit mit dem Titel: *”Enhancing Precision Oncology: Preclinical Assessment of Individual Drug Treatment Susceptibility Using Patient-Derived 3D Microtumor and Immune Cell Co-cultures”* selbständig verfasst, nur die angegebenen Quellen und Hilfsmittel benutzt und wörtlich oder inhaltlich übernommene Zitate als solche gekennzeichnet habe. Ich erkläre, dass die Richtlinien zur Sicherung guter wissenschaftlicher Praxis der Universität Tübingen beachtet wurden. Ich versichere an Eides statt, dass diese Angaben wahr sind und dass ich nichts verschwiegen habe. Mir ist bekannt, dass die falsche Angabe einer Versicherung an Eides statt mit Freiheitsstrafe bis zu drei Jahren oder mit Geldstrafe bestraft wird.

Tübingen, 29.03.2024

Nicole Anderle

Appendix

Appendix I:

Anderle N, Koch A, Gierke B, Keller A-L, Staebler A, Hartkopf A, Brucker SY, Pawlak M, Schenke-Layland K, Schmees C. *A Platform of Patient-Derived Microtumors Identifies Individual Treatment Responses and Therapeutic Vulnerabilities in Ovarian Cancer*. *Cancers*. 2022; 14(12):2895.

Article

A Platform of Patient-Derived Microtumors Identifies Individual Treatment Responses and Therapeutic Vulnerabilities in Ovarian Cancer

Nicole Anderle ^{1,*}, André Koch ², Berthold Gierke ³, Anna-Lena Keller ¹, Annette Staebler ⁴, Andreas Hartkopf ^{2,5}, Sara Y. Brucker ^{2,6}, Michael Pawlak ³, Katja Schenke-Layland ^{1,2,6,7,8} and Christian Schmees ^{1,*}

¹ NMI Natural and Medical Sciences Institute, The University of Tuebingen, 72770 Reutlingen, Germany; anna-lena.keller@nmi.de (A.-L.K.); katja.schenke-layland@nmi.de (K.S.-L.)

² Department of Women's Health, Eberhard Karls University Tuebingen, 72076 Tuebingen, Germany; andre.koch@med.uni-tuebingen.de (A.K.); andreas.hartkopf@med.uni-tuebingen.de (A.H.); sara.brucker@med.uni-tuebingen.de (S.Y.B.)

³ NMI Technologie Transfer GmbH, Pharmaservices Protein Profiling, 72770 Reutlingen, Germany; berthold.gierke@nmi.de (B.G.); michael.pawlak@nmi.de (M.P.)

⁴ Institute of Pathology and Neuropathology, Eberhard Karls University Tuebingen, 72076 Tuebingen, Germany; annette.staebler@med.uni-tuebingen.de

⁵ Department of Gynecology and Obstetrics, University Hospital of Ulm, 89081 Ulm, Germany

⁶ Cluster of Excellence iFIT (EXC2180) "Image-Guided and Functionally Instructed Tumor Therapies", Eberhard Karls University Tuebingen, 72076 Tuebingen, Germany

⁷ Department of Biomedical Engineering, Eberhard Karls University Tuebingen, 72076 Tuebingen, Germany

⁸ Department of Medicine/Cardiology, Cardiovascular Research Laboratories, David Geffen School of Medicine at UCLA, Los Angeles, CA 90095, USA

* Correspondence: nicole.anderle@nmi.de (N.A.); christian.schmees@nmi.de (C.S.)



Citation: Anderle, N.; Koch, A.; Gierke, B.; Keller, A.-L.; Staebler, A.; Hartkopf, A.; Brucker, S.Y.; Pawlak, M.; Schenke-Layland, K.; Schmees, C. A Platform of Patient-Derived Microtumors Identifies Individual Treatment Responses and Therapeutic Vulnerabilities in Ovarian Cancer. *Cancers* **2022**, *14*, 2895. <https://doi.org/10.3390/cancers14122895>

Academic Editors: Maria Flavia Di Renzo and Simona Corso

Received: 20 April 2022

Accepted: 10 June 2022

Published: 12 June 2022

Publisher's Note: MDPI stays neutral with regard to jurisdictional claims in published maps and institutional affiliations.



Copyright: © 2022 by the authors. Licensee MDPI, Basel, Switzerland. This article is an open access article distributed under the terms and conditions of the Creative Commons Attribution (CC BY) license (<https://creativecommons.org/licenses/by/4.0/>).

Simple Summary: For personalized oncology, it is crucial to develop appropriate patient-derived tumor models that allow individualized validation of the most effective cancer therapy. The objective of this study was to develop and characterize a new patient-derived ovarian cancer tumor model composed of patient-derived microtumors (PDM) and autologous tumor-infiltrating lymphocytes (TIL). In contrast to other preclinical tumor models, such as patient-derived organoids, PDM are generated within 24 h from fresh ovarian tumor samples. From immunohistochemical comparison with the original primary tumor, we conclude that the histopathological features of the original tumor are essentially preserved. Importantly, we successfully identified treatment-sensitive and treatment-resistant tumor models for standard platinum-based therapy by reverse-phase protein array (RPPA) analysis of PDM. Furthermore, we were able to evaluate the efficacy of cancer immunotherapy by co-culturing PDM and autologous TILs. PDM and TILs may therefore serve as a preclinical platform to identify individualized, tailored cancer treatments in the future.

Abstract: In light of the frequent development of therapeutic resistance in cancer treatment, there is a strong need for personalized model systems representing patient tumor heterogeneity, while enabling parallel drug testing and identification of appropriate treatment responses in individual patients. Using ovarian cancer as a prime example of a heterogeneous tumor disease, we developed a 3D preclinical tumor model comprised of patient-derived microtumors (PDM) and autologous tumor-infiltrating lymphocytes (TILs) to identify individual treatment vulnerabilities and validate chemo-, immuno- and targeted therapy efficacies. Enzymatic digestion of primary ovarian cancer tissue and cultivation in defined serum-free media allowed rapid and efficient recovery of PDM, while preserving histopathological features of corresponding patient tumor tissue. Reverse-phase protein array (RPPA)-analyses of >110 total and phospho-proteins enabled the identification of patient-specific sensitivities to standard, platinum-based therapy and thereby the prediction of potential treatment-responders. Co-cultures of PDM and autologous TILs for individual efficacy testing of immune checkpoint inhibitor treatment demonstrated patient-specific enhancement of cytotoxic TIL activity by this therapeutic approach. Combining protein pathway analysis and drug efficacy

testing of PDM enables drug mode-of-action analyses and therapeutic sensitivity prediction within a clinically relevant time frame after surgery. Follow-up studies in larger cohorts are currently under way to further evaluate the applicability of this platform to support clinical decision making.

Keywords: patient-derived tumor model; ovarian cancer; anti-cancer drug sensitivity; RPPA protein profiling; cancer immunotherapy

1. Introduction

In the context of personalized medicine, patient-derived model systems are expected to play an important role in order to identify suitable and effective therapies for the individual patient as well as existing therapeutic resistances of the patient's tumor. Especially for cancer types with dismal treatment success rates such as ovarian cancer (OvCa), these model systems will be valuable for future cancer therapy. OvCa is among the most lethal gynecological diseases in women, with >185,000 deaths worldwide in 2018 [1]. Late diagnosis and disease complexity characterized by strong molecular and genetic heterogeneity are causative for its poor survival rates and varying treatment response to first-line therapy. Substantial efforts have been made to resolve the complexity of OvCa, especially for high-grade serous carcinomas (HGSC) [2–4]. Despite the application of genomics and transcriptomics in elucidating disease determinants, the principles of responsiveness to therapy are still poorly understood [4]. The establishment of patient-derived tumor organoids (PDO) allowed addressing a number of these challenges for example by in-depth genetic and phenotypic tumor characterization and analysis of intra-tumoral heterogeneity in PDOs side-by-side with corresponding tumor tissue [5–8]. Even though recent studies have described the combination of PDO cultures with components of the tumor microenvironment including fibroblasts, endothelial cells and immune cells [9], PDOs do not fully reflect the original composition of primary tumor tissue in terms of extracellular matrix, tumor-associated fibroblasts, tumor-infiltrating lymphocytes (TILs), macrophages (TAMs), and tumor endothelial cells. Another challenge of current PDO models in terms of applicability for individualized drug response testing relates to the required establishment time of 1–3 months with a corresponding impact on the timeframe to obtain drug testing results [10]. Using OvCa as a prime model of a heterogeneous tumor disease, we introduce a three-dimensional (3D) preclinical ex vivo model composed of patient-derived microtumors (PDM) as well as autologous tumor-infiltrating lymphocytes (TILs) extracted from primary OvCa tissue specimen in a clinically relevant time-frame. Importantly, PDM recapitulate a 3D histo-architecture with retained cell–cell contacts and native intra-tumoral heterogeneity featuring the corresponding primary tumor microenvironment (including extracellular matrix proteins, stromal fibroblasts and immune cells). In combination with functional compound efficacy testing and multiplexed TILs phenotyping, we demonstrate the correlation of individual OvCa PDM responses to chemotherapeutic as well as immunotherapeutic treatment approaches using OvCa PDM alone and in co-culture with autologous TILs, respectively. We apply reverse-phase protein array (RPPA) analysis to map protein-signaling pathways of PDM and to measure on- and off-target drug effects in compound treated PDM. Albeit based on a small patient cohort the available clinical follow-up data suggests a correlation of obtained treatment responses in OvCa PDM models and corresponding patients indicating prolonged metastasis-free survival of identified carboplatin responders as compared to non-responders.

Based on the data presented here, we envision that our preclinical assay system combining PDM, autologous TILs and protein signaling pathway profiling could aid clinical decision making in the future and assist in the pre-selection of a personalized clinical treatment strategy for OvCa.

2. Materials and Methods

2.1. Human Specimens

Ovarian tumor samples were obtained from nineteen patients diagnosed with ovarian cancer undergoing surgery at the Center for Women's Health, University Hospital Tuebingen. Written informed consent was obtained from all participants. The tumors were classified according to International Federation of Gynecology and Obstetrics (FIGO) grading system. Tumor samples were delivered on the day of operation. The research project was approved by the ethics committee (IRB#275/2017BO2 and IRB#788/2018BO2).

2.2. Isolation and Cultivation of Patient-Derived Microtumors and Tumor-Infiltrating Lymphocytes

The procedure was adapted from Kondo et al. (2011) [11] and modified as follows. Tumor specimens were washed in HBSS (Gibco, Thermo Fisher Scientific, Waltham, MA, USA), minced with forceps, and digested with Liberase™ DH [12] for 2 h at 37 °C. Digested tissue was centrifuged ($300 \times g$, 5 min), washed with HBSS and filtered through a stainless 500 μm steel mesh (VWR). The flow-through was again filtered through a 40 μm cell strainer (Corning, Corning, NY, USA). The filtrate containing the TIL fraction was resuspended in Advanced RPMI 1640 (Gibco) supplemented with 2 mM Glutamine (Gibco), 1% MEM Vitamins (Gibco), 5% human serum (Sigma-Aldrich, St. Louis, MO, USA) and 100 $\mu\text{g}/\text{mL}$ primocin (Invivogen, San Diego, CA, USA). IL-2 (100 U/mL), IL-7 (10 U/mL) and IL-15 (23.8 U/mL) (Peprotech, East Windsor, NJ, USA) were freshly added to culture media. For expansion, CD3/CD28 dynabeads were added (Milteny Biotech, Auburn, CA, USA). PDM, held back by cell strainer, were washed in HBSS and cultured in suspension in StemPro® hESC SFM (Gibco) supplemented with 8 ng/mL FGF-basic (Gibco), 0.1 mM β -mercaptoethanol (Gibco), 1.8% BSA (Gibco) and 100 $\mu\text{g}/\text{mL}$ primocin (Invivogen) within cell-repellent culture dish (60 \times 15 mm) (Corning).

2.3. RPPA and Protein Data Analysis

Detailed methods of sample preparation and RPPA processing are provided in SI Materials. RPPA protein analysis and protein data processing was applied as reported before [13–16]. From the arrays, PDM sample signals were extracted as protein-normalized, background-corrected mean fluorescence intensity (NFI), as measured from two technical sample replicates. NFI signals, median-centered for each protein over all measured samples (including OvCa PDM and BC PDM samples) and \log_2 transformed, reflect a measure for relative protein abundance. Small NFI protein signals at around blank assay level (0.02 NFI) were as a limiting quality criterion excluded from further analysis; otherwise, all NFI signals were used for further protein data analysis. Protein heat maps were generated and cluster analysis (HCL) performed using the freely available MultiExperiment Viewer (MeV) software. For the comparison of protein profiles of treatment responders and non-responders (defined by functional compound testing), only proteins with a >20% difference between the means were used for analysis. On- and off-target pathway effects were evaluated from one biological and two technical replicate samples per model at three different treatment times (0.5, 4 and 72 h). Treated sample to respective DMSO vehicle control NFI ratios (TR) were calculated for each treatment condition and \log_2 -transformed. A treatment-specific threshold of protein change (carboplatin: minimum 50% difference) was set. Only proteins showing treatment effects above the threshold were shown.

2.4. Efficacy of Compounds Validated in PDM Cultures

Efficacy of compounds was validated by applying the real-time CellTox™ Green Cytotoxicity assay (Promega). Assays were performed according to manufacturer's protocol. PDM were cultured a maximum of 1–2 weeks in PDM culture medium prior testing. Per treatment, three to eight replicates were performed using $n = 15$ PDM per replicate in a total volume of 150 μL phenol-red free PDM culture medium. Cell death was measured as relative fluorescent unit (RFU) (485–500 nm Excitation/520–530 nm Emission), relative to the number of dead, permeable cells after 24 h, 48 h and 72 h with the Envision Multilabel

Plate Reader 2102 and Tecan Spark Multimode Plate Reader. RFU values were normalized to DMSO control according to used drug solvent. Treatment effects were measured as fold change (FC) compared to control. Differences between treated PDM and untreated PDM were calculated as fold change values separately for each time point. Statistical significance was evaluated by two-way ANOVA multiple comparison test. Outliers were identified with the Iglewicz and Hoaglin's robust test for multiple outliers applying a recommended Z-score of ≥ 3.5 [17].

2.5. FACS Analysis

To characterize lymphocyte populations within autologous TIL, cells were harvested (up to 1×10^6 cells/staining depending on available number of cells), washed $2 \times$ with PBS (200 rpm, 5 min at 4°C), resuspended in staining buffer (PBS plus 10% FBS) and plated in a 96-well V-bottom plate (100 μL /well) (Corning). To verify $>90\%$ cell viability, cells were counted with a Nucleocounter (Chemotec) before plating. For each panel staining, an unstained control and, if necessary, a FMO control were prepared. For extracellular staining, cells were incubated with antibodies (see SI Materials) for 30 min at 4°C in the dark. For subsequent intracellular staining, cells were washed 2–3 times (200 rpm, 5 min at 4°C) in eBioscience™ Permeabilization buffer (250 μL /well) (Invitrogen) and resuspended in eBioscience™ Fixation/Permeabilization solution (Invitrogen) for 20 min at 4°C . After 2–3 washing steps (200 rpm, 5 min at 4°C), cells were incubated with antibodies (30 min, 4°C in dark) (see SI Materials). After the staining process, cells were washed 2–3 times and analyzed with a BD FACS Melody machine (BD Biosciences, Franklin Lakes, NJ, USA).

2.6. Co-Culture of PDM and Autologous TILs

To measure if the expanded, autologous TILs are able to kill corresponding PDM, we performed endpoint killing assays in a 96-well format with an image-based analysis using Imaris 8.0 software. First, PDM were pretreated with $\text{IFN}\gamma$ (200 ng/mL) for 24 h to stimulate antigen presentation. In parallel, 96-well plates were coated with 5 g/mL of anti-CD28 antibody (Biolegend) o/n at 4°C to provide a co-stimulatory signal during co-culture. On the next day, coated plates were washed $3 \times$ with PBS. PDM were washed in HBSS, centrifuged and resuspended in co-culture assay media consisting of RPMI 1640 phenol red free (GIBCO) supplemented with 2 mM Glutamin (Gibco), 5% human serum (Sigma-Aldrich, St. Louis, MO, USA), $1 \times$ MEM Vitamins (Gibco) and 100 $\mu\text{g}/\text{mL}$ Primocin (Invivogen). Prior to assembling the co-culture, TILs were labeled with CellTracker™ Deep Red Dye (Thermo Fisher Scientific, Waltham, MA, USA) to differentiate between PDM and TILs. Labeled TILs were then co-cultured with PDM and in the presence of selected checkpoint immune inhibitors (CPIs: Pembrolizumab, Atezolizumab, Ipilimumab; Selleck Chemicals GmbH) or control anti-IgG4 antibody with an E:T ratio of 4:1. Thereby we counted 200 cells per single PDM. Per condition, we prepared triplicates each with 15 PDM and 12,000 TILs per well. After 92 h, cells were incubated with a staining solution consisting of live cell stain Calcein-AM (Thermo Fisher Scientific) and Sytox™ Orange dead cell stain (Thermo Fisher Scientific). After 1 h, Z-stacks of $n = 3$ PDM per well were imaged using a spinning disk microscope (ZEISS CellObserver Z1). Only viable PDM were positively stained by Calcein-AM, while all dead cells were stained by Sytox™ Orange. TILs were filtered by CellTracker™ Deep Red signal. Using the Imaris 8.0 software, we applied three masks, one for dead cells, one for dead TILs and one for live PDMs. For each mask, the total sum of all fluorescent intensities (FI) was calculated and the following ratio determined:

$$\% \text{ ratio dead vs. viable PDM [FI]} = \frac{\text{total dead [FI]} - \text{dead TIL [FI]}}{\text{viable PDM [FI]}} \quad (1)$$

2.7. Statistical Analysis

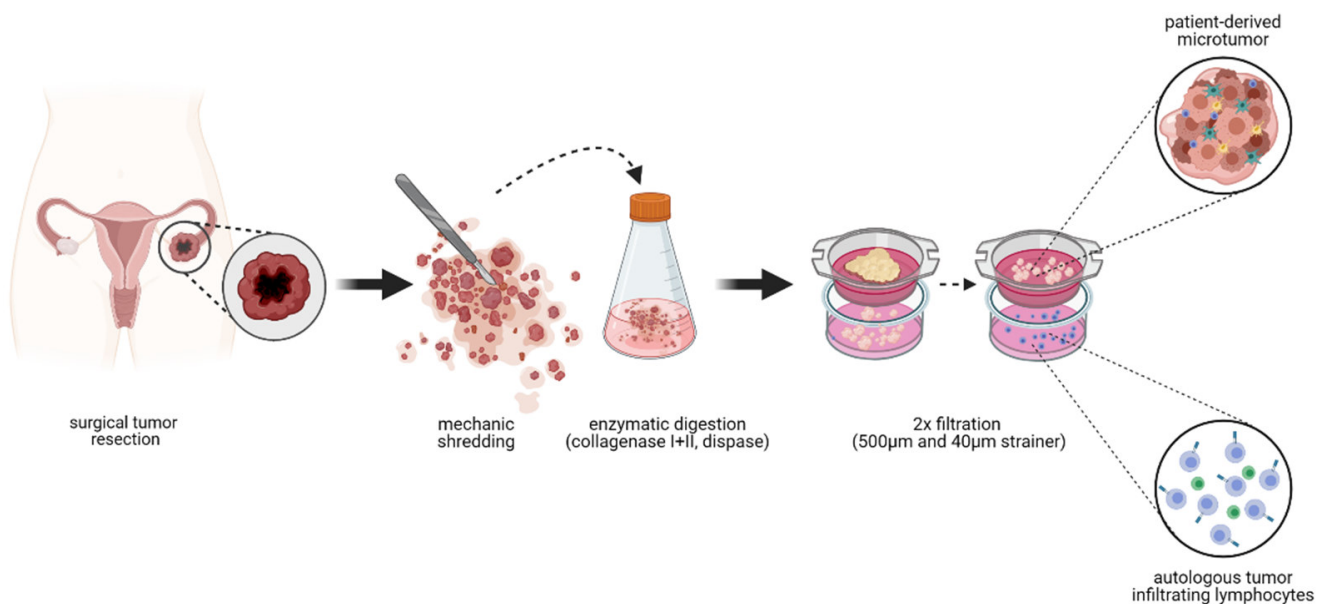
Statistical analysis was performed using GraphPad Prism. For Boxplot data, whiskers represent quartiles with minimum and maximum values and the median. Datasets with no

clear normal distribution were analyzed with unpaired, two-tailed Mann–Whitney–*U*-test, otherwise as indicated. Correlation data were evaluated by Spearman’s rank correlation. For all analyses, p values < 0.05 were considered statistically significant. Recommended post hoc tests were applied for multiple comparisons.

3. Results

3.1. Isolation of Patient-Derived Microtumors with High Viability from Primary OvCa Tissue Specimen by Limited Enzymatic Digestion

Residual fresh tumor tissue samples were collected from $n = 16$ OvCa patients undergoing primary tumor debulking surgery. The PDM and TIL isolation procedure (further developed from Kondo et al. 2011) [11] was performed on freshly excised tumor tissue specimen (Scheme 1).



Scheme 1. PDM and TIL isolation from OvCa tumor samples within 3 h after receipt of the tumor sample. Tumor tissue derived from surgical tumor resection is kept in culture media for transportation. Immediately after receipt of the sample, the tissue is mechanically disrupted into smaller pieces and enzymatically digested for 2 h. Afterwards, the digested tissue gets filtered twice using cell strainers. Within the first filtrate, tumor-infiltrating lymphocytes are obtained and are ready for culturing or cryopreservation. From the residue of the second strainer, PDMs are gained and are ready for culturing or cryopreservation. (Created with Biorender.com).

Available anonymized clinico-pathological characteristics including International Federation of Gynecology and Obstetrics (FIGO) staging and pathological TNM-classification of respective individuals are summarized in Table 1. Overall, 2/19 patients (OvCa #4 and OvCa #18) received neoadjuvant treatment with carboplatin/paclitaxel chemotherapy. The majority of included samples ($n = 15$) were derived from the most common type of OvCa, i.e., epithelial OvCa, with a majority of high-grade serous carcinomas (HGSC). One sample was classified as sex cord–stromal ovarian carcinoma that is either non-malignant or at a low stage.

Table 1. Clinical patient data from OvCa tumor specimen included into the study with successful PDM isolation and/or TIL expansion.

Sample OvCa #	Age at Surgery	Histopathological Classification	Cellular Origin	Grade	FIGO Stage	T	N	M	L	V	Pn	R	Isolated PDM	Expanded TIL
#1	53	HGSC	epithelial	HG	III	pT3c (liver/splenic capsule)	pN1a (2/14)	Mx	L1	V1	Pn1	Rx	yes	yes
#3	88	HGSC	epithelial	HG	IIB	pT2b (peritoneum douglas)	Nx	Mx	L0	V0	Pn0	Rx	yes	yes
#4	54	HGSC	epithelial	HG/ G3	IIIC	ypT3c	ypN0	Mx	L0	V0	Pn0	Rx	yes	yes
#5	59	HGSC	epithelial	HG/ G3	IIIC	pT3c	pN1a (2/18)	Mx	L0	V0	Pn0	Rx	no	yes
#7	67	HGSC	epithelial/peritoneal	HG	IVa	Tx	Nx	Mx	Lx	Vx	Pnx	Rx	yes	yes
#8	44	MC	epithelial	LG	Ia	T1a	Nx	Mx	Lx	Vx	Pnx	Rx	yes	no
#13	71	LGSC	epithelial	LG/G2	IIIC	pT3c	pN0	Mx	L0	V0	Pn0	Rx	yes	yes
#17	62	HGSC	epithelial	HG	IIIC	pT3c	pN0	Mx	L1	V0	Pn0	Rx	yes	yes
#18	61	HGSC	epithelial	HG/ G3	IIIC	ypT3c	ypN0	cM0	L0	V0	Pnx	R0	yes	yes
#19	60	HGSC	epithelial	HG/ G3	IIIB	pT3b	pN0	cM0	L0	V0	Pn0	R0	yes	no
#20	66	HGSC	epithelial	HG	IVa	pT3c (pleural effusion)	pN1a	pM1a	L0	V0	Pn0	Rx	no	yes
#21	74	adult-type GCT	sex cord-stromal	-	IA	pT1a	pNx	cM0	L0	V0	Pn0	R0	yes	no
#23	71	HGSC	epithelial	HG/ G3	IIIC	pT3c (Omentum metastasis)	pN1a	pMx	L1	V0	Pn0	Rx	yes	yes
#24	73	HGSC	epithelial	HG	IIIC	pT3c	pN1b (58/75)	Mx	L1	V0	Pnx	R0	yes	yes
#25	54	HGSC	epithelial	HG	IIA	pT2a (tube)	pN0	cM0	L0	V0	Pn0	cR0	yes	yes
#26	67	HGSC	epithelial	HG/ G3	IIIC	pT3c	pNx	Mx	L1	V0	Pn0	cR0	yes	yes

GCT, granulosa cell tumor; HGSC, high grade serous carcinoma; LGSC, low grade serous carcinoma; MC: mucinous carcinoma T: extent (size) of the tumor; N: spread to nearby lymph nodes; M: spread to distant sites; L, lymphatic invasion; V, venous invasion; Pn, perineural invasion; R, residual tumor; p, pathological state; c, clinical stage; y, restaged after neoadjuvant therapy; x, not assessed.

Isolation of PDM was successful in 87.5% (14/16) of the tumor samples (Figure 1A) with varying amounts of available PDM for downstream analyses such as live–dead staining, immunohistochemical characterization, protein signaling pathway analyses and efficacy drug testing of standard-of-care therapy as well as immunotherapy. PDMs were cultured in suspension in the absence of serum for a maximum of three weeks. No correlation was observed between successful isolation of PDM and available clinical patient data such as age, lymph node spread, distant cancer spread, perineural invasion or FIGO stage (Table S1). PDM viability was assessed by parallel staining with Calcein-AM and SYTOX™ Orange (Figure 1B). The 2D projections of 3D images displayed highly viable PDM with few dead cells. Dead PDM cells (according to nuclear SYTOX™ Orange staining) detached from PDM and thus observed mostly as single cells floating in the culture media. The quantification of the viable cell volume and dead cell volume in 3D projections of four exemplary OvCa PDM models are shown in Figure 1C. In each analyzed model, $\leq 7\%$ of the total PDM cell mass represented dead cells confirming robust PDM viability.

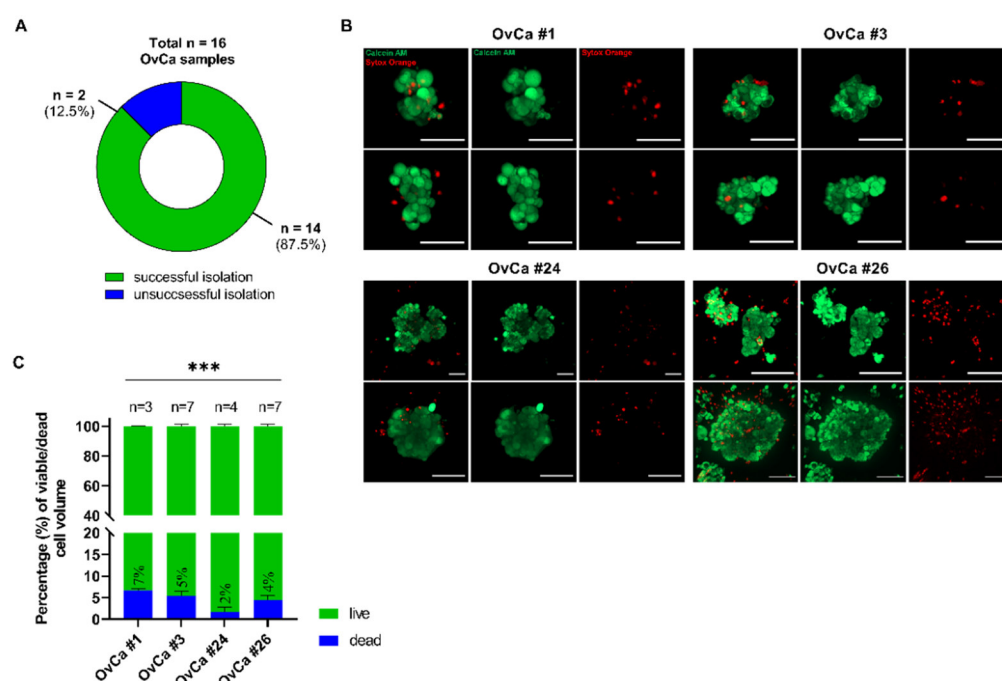


Figure 1. Patient-derived 3D microtumors (PDM) derived from primary OvCa tumor specimen show high viability. (A) Efficiency of isolating OvCa PDM from a total of $n = 16$ fresh primary OvCa tumor tissues samples. PDM were successfully isolated from $n = 14$ specimen with a success rate of 87.5%. (B) Viability of OvCa PDM models. Exemplary 2D images from 3D projections of $n = 4$ OvCa PDM models confirm high viability according to Calcein-AM (viable cells) and SYTOX™ Orange (dead cells) staining. (C) Percentage of viable and dead cells in OvCa PDM. Viability was assessed by an image-based analysis (see SI Methods) in $n = 4$ OvCa PDM models shown in (B). Data are shown as mean values with SEM from at least $n = 3$ PDM of each model. *** $p < 0.001$, multiple paired t -test with Holm–Šidák’s post hoc test. Scale bar 50 μm .

3.2. OvCa PDM Sections Display Histopathological Characteristics Comparable to the Corresponding Primary Tumor Tissue (PTT)

We next performed Hematoxylin and Eosin staining (H&E) of FFPE- and cryo-sections, respectively, derived from OvCa PDM and corresponding primary tumor tissue sections (PTT) for histopathological comparison. Professional assessment of PDM by a certified pathologist, confirmed the presence of typical, distinct histopathological characteristics of OvCa in respective PDM (Figures 2 and S1). HGSC derived PDM reflected architectural patterns such as papillary growth, irregular branching, cystic and glandular structures (Figure 2 OvCa #17–23; Figure S1, OvCa #24, 26) comparable to the corresponding PTT

specimen. Pleomorphic nuclei/cells, high nucleus:cytoplasm ratio as well as hyperchromasia were similar in PDM and corresponding PTT sections reflecting the high-grade of analyzed HGSC tumors. These tumor features were not detected within OvCa PDM #8 (Figure S1), which originated from low-grade mucosal OvCa known for slow tumor growth. Instead, OvCa #8 PDM displayed a unicellular epithelium and mostly stromal remains. In summary, histopathological analyses of PDM confirmed structural and cellular similarities to the corresponding primary tumor specimen and the conservation of typical histological features of ovarian carcinomas.

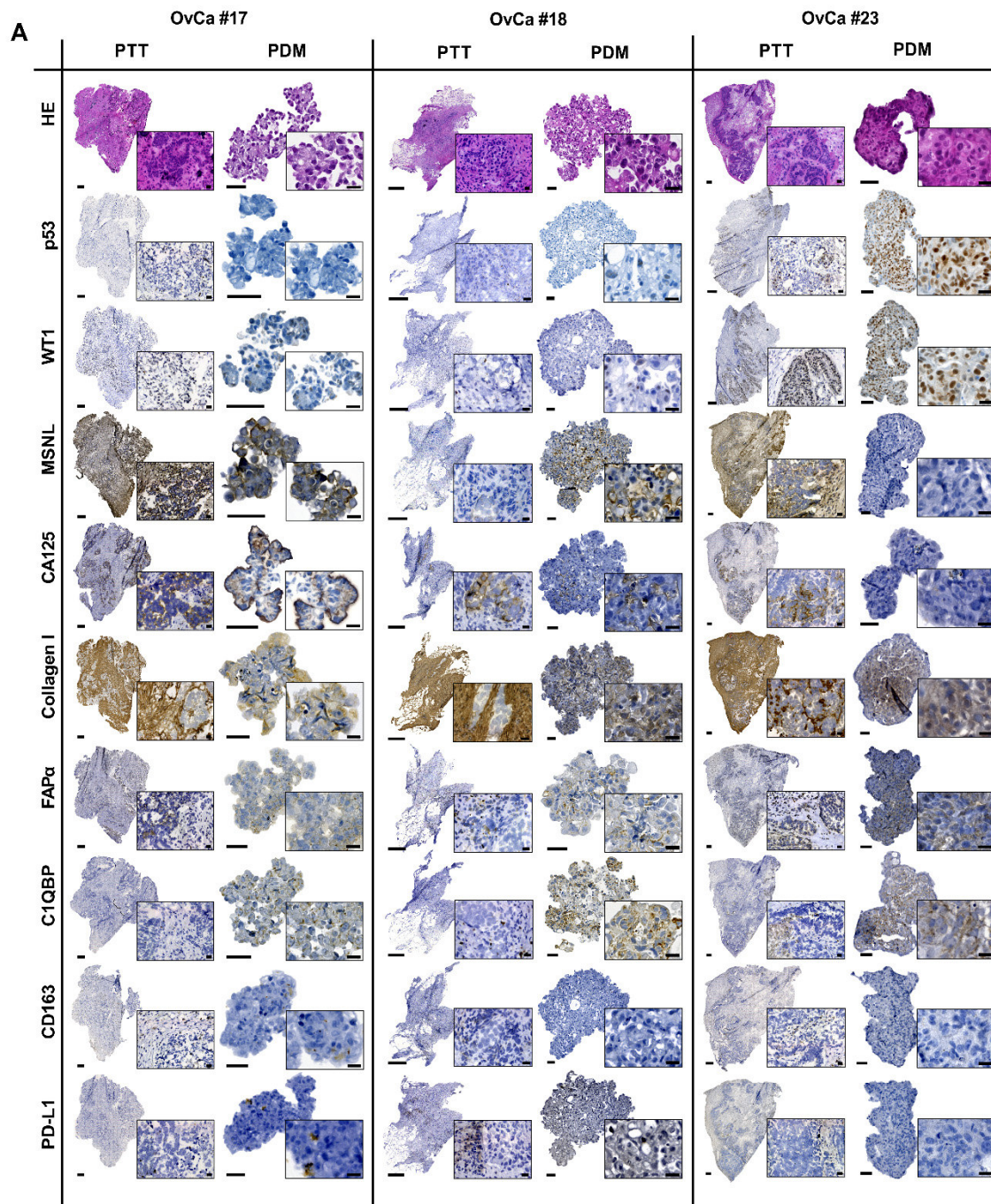


Figure 2. Cont.

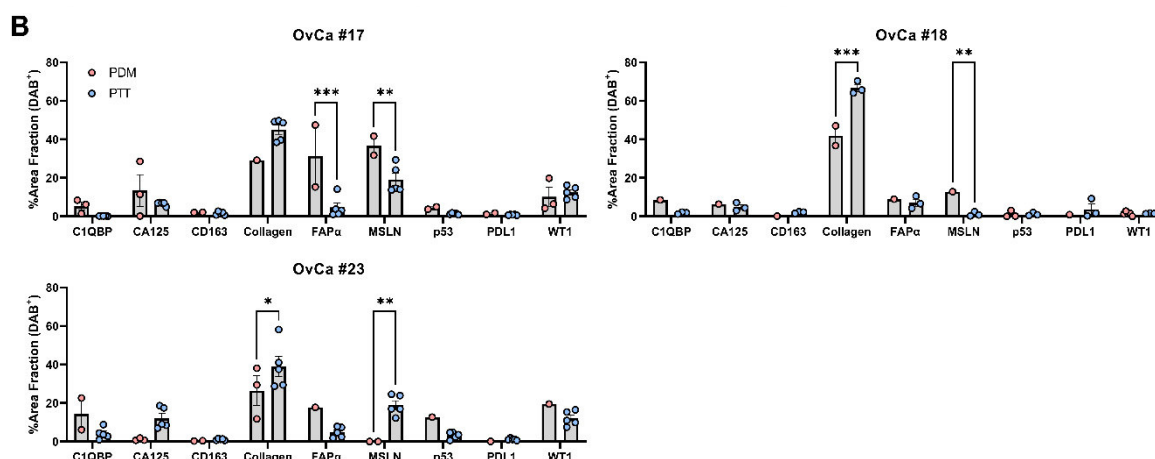


Figure 2. OvCa PDM show histopathological features comparable to corresponding primary tumor tissue. (A) Hematoxylin and Eosin (H&E) as well as immunohistochemical DAB staining of OvCa PDM (FPPE, 3 μ m) and corresponding primary tumor tissue (PTT) (Cryosections, 4–6 μ m) sections. H&E stainings revealed features of malignant cells (including giant cells with more than one nucleolus, hyperchromatic cells with dark nuclei and high nuclei:cytoplasm ratio) confirming the cancerous origin. Expression of OvCa histotype specific markers (p53, WT1), tumor markers (CA125, MSLN), tumor-associated macrophages (CD163), immune/tumor marker (PD-L1), cancer-associated fibroblasts (FAP α) and extracellular matrix components (Hyaluronan C1QBP, Collagen I) is shown. Scale bars indicate 500 μ m for PTT; 50 μ m for PDM; 20 μ m for magnifications (PTT and PDM). (B) Quantification of IHC stainings for indicated markers within OvCa #17, #18 and #23 PDM and corresponding PTT sections. Shown is the %Area Fraction of positive DAB-stain. For PTT, a minimum of 3 representative regions of interest from tumor areas were used for quantification. * $p < 0.1$, ** $p < 0.01$, *** $p < 0.001$, Two-way ANOVA analysis with Šidák's multiple comparisons test ($\alpha = 0.05$). FAP α , cancer-associated fibroblast protein alpha; C1QBP, hyaluronan binding protein; WT1, wilms tumor 1; MSLN, mesothelin.

3.3. Immunohistochemical Staining of PDM Identifies Expression of Histopathological OvCa Markers and Patterns of Extracellular Matrix and Tumour Microenvironment Components Comparable to Corresponding Primary Tumour Tissue Sections

For further characterization of histological similarities and differences between OvCa PDM and corresponding PTT, the expression of histotype specific markers together with tumor cell-, extracellular matrix- and immune cell-markers were assessed by immunohistochemistry. The degree of marker-specific staining patterns in obtained images of PDM and PTT sections was quantified by image-based analysis (Figures 2 and S1). In the clinics, immunohistochemical staining of p53 and Wilms Tumor 1 (WT1) is applied for differential diagnosis of HGSCs [18]. These two markers are the only ones examined in routine histopathology. In-depth histopathological assessment by a certified pathologist revealed that the HGSC phenotype of the original tumor persists in the corresponding PDM (see above). In line with this, expression of WT1/p53 in PDM corresponded well with either low-to-moderate (OvCa #17, #18 and #25) or strong expression (OvCa #23, #24 and #26) in respective PTT sections (Figures 2 and S1). Except for OvCa #24, where PDM showed significantly pronounced p53 staining as compared to corresponding PTT, image-based analysis did not show significant differences between PDM and PTT for WT1.

Mesothelin (MSLN) and CA125 (MUC16) were investigated as additional OvCa markers.

Mesothelin, known to be over-expressed on the cell surface in OvCa [19–21], was found to be differentially expressed in four out of seven analyzed PDM models as compared to corresponding PTT sections, with OvCa PDM #17 and #18 displaying higher and OvCa PDM #23 and #26 showing lower MSLN expression as compared to respective PTT sections (Figures 2B and S1B).

For CA125, no significant difference in expression between PDM and PTT sections of the OvCa models studied here was observed. CA125 expression has previously been described as an immunohistochemical marker to confirm ovarian origin of the tumor [22]. As shown before [23,24], expression of CA125 in OvCa sections can vary within one type and between the different OvCa tumor types. Accordingly, PTT sections derived from non-HGSC displayed no CA125 expression (OvCa #8) in contrast to HGSC-derived tumor sections (OvCa #18 and #24). CA125 expression was low or not detectable within the other PDM models studied here. As the tumor microenvironment is known to play a major role in tumor progression and metastasis [25–27], we analyzed the presence of extracellular matrix (ECM) and stromal components in OvCa PDM and corresponding PTT. Sections were stained for FAP α (Fibroblast associated protein alpha), a marker of cancer-associated fibroblasts (CAFs). FAP α expression in tumor stroma is observed in 90% of human cancers of epithelial origin and has been described to induce tumor progression and chemoresistance [28]. FAP α expression was detectable in 7 out of 11 OvCa PDM models studied. The observed FAP α staining pattern did not significantly differ between PDM and corresponding PTT sections from 5 of 7 OvCa models analyzed in our study (Figures 2 and S1). OvCa PDM #17 displayed a significantly higher expression of FAP α as compared to the corresponding PTT sections. In contrast, for OvCa PDM #25 a lower degree of FAP α expression compared to respective PTT sections was observed.

Expression of the ECM component Collagen I, known to promote invasiveness and tumor progression in epithelial OvCa [29], was also prominent within OvCa PDM. Except for OvCa #18, #23 and #25, where a lower expression of Collagen I was observed in PDM as compared to corresponding PTT, the observed Collagen I staining pattern in PDM did not significantly differ from respective PTT sections.

In addition, we observed a correlation of the expression of another ECM component (Hyaluronan Binding Protein 1 (C1QBP)) in PDM and corresponding PTT for the majority of analyzed samples except for OvCa #25, where PDM expressed significantly lower levels of this marker as compared to respective PTT sections (Figures 2 and S1). C1QBP is known to interact with the major ECM component hyaluronan [30].

In summary, the analyzed stromal and ECM components were found to be expressed in the majority of generated OvCa PDM models. In most cases, the observed expression pattern of respective markers in PDM did not significantly differ from expression in corresponding PTT sections.

To further examine tumor microenvironment (TME) components of PDM, we studied the infiltration with tumor-associated macrophages (TAMs) via CD163 expression together with the expression of the inhibitory checkpoint receptor ligand PD-L1. IHC analyses rarely detected M2-like TAMs (CD163+) within PTT and PDM sections and if so, mostly in stromal tissue parts of PTT. While macrophages were abundant in OvCa #24 PTT, they were not detected in the corresponding PDM (Figure S1). In contrast, for OvCa #17, CD163+ TAMs were detected in both PDM and PTT sections (Figure 2). Immune checkpoint receptor ligands are known to be expressed on tumor and/or immune cells of the tumor microenvironment. Here, PD-L1 expression was mostly absent in OvCa PTT and corresponding PDM sections.

In conclusion, parallel immunohistochemical staining of OvCa PDM and corresponding PTT sections showed their comparability for the majority of samples with PDM regarding features of the original tumor including presence of ECM and TME components together with expression of p53 and WT1 as markers important for the histopathological assessment of OvCa. In comparison with corresponding PTT sections, pure stromal areas were mostly absent from stained PDM sections, which might explain abovementioned differences in marker expression observed between PDM and corresponding PTT with regard to immune cell infiltration and degree of expression of stromal components. Moreover, in PTT, expression of CA125 and MSLN appeared to be mostly restricted to tumor cells at the margin of the stroma, which are less detectable within PDM.

3.4. Protein Signaling Pathway Profiling of OvCa PDM by RPPA

After initial immunohistochemical characterization of the 3D OvCa PDM that confirmed the presence of TME components in PDM similar to corresponding PTT, we performed an in-depth examination of the heterogeneity and molecular composition of different OvCa PDM models by generating signaling pathway protein profiles using RPPA. Protein abundances of 116 different proteins (including total and post-translationally modified forms) were measured in OvCa PDM samples each with a sample size of $n = 100$ – 150 per individual PDM (Figure 3A). One further PDM sample derived from human BC (breast cancer) was included to scale up the protein sample data and for comparison as both cancer types are known to share molecular and microenvironmental similarities (26, 30). Obtained protein-normalized, background-corrected mean fluorescence intensity (NFI) signals were median-centered to all samples ($n = 8$) and \log_2 transformed. Protein profiles of PDM samples covered signaling pathways such as for cell cycle, DNA damage response, apoptosis, chromatin regulation, MAPK/RTK, PI3K/AKT with mTOR, Wnt and NF κ B, as well as OvCa tumor/stem cell markers. By hierarchical clustering (HCL), PDM samples were grouped according to their similarities in relative protein signal intensity (Figure 3A). Data analysis revealed three clusters: (1) OvCa #21 (OvCa granulosa cell tumor) and #23 (HGSC), with the most distinct protein profiles as compared to the other PDM analyzed; (2) OvCa #19 (HGSC) and the BC PDM shared more similarities than OvCa #19 with the other OvCa PDM models; (3). The remaining PDM samples resembled the third cluster with the most similar protein expression profiles containing exclusively HGSC models. Long distances of the sample dendrogram further underlines the proteomic heterogeneity of similar histopathological OvCa tumor types.

To compare protein abundances within different signaling pathways as well as of tumor/stem cell markers, proteins with impact on pathway activity were sorted according to their pathway affiliation (Figure 3B, Table S2). Significant differences between PDM models were observed for the cell cycle pathway and the MAPK/RTK pathway. Highest cell cycle activity was found in OvCa #17 and #24 with almost 50% higher median NFI signals compared to OvCa #21 with the lowest median signals (median NFI = $-0.33 \log_2$) resembling a different histopathological tumor type compared to the other PDM models analyzed. MAPK/RTK pathway signaling was increased in OvCa #21 (median NFI = $0.38 \log_2$), #23 (median NFI = $0.32 \log_2$), #24 (median NFI = $0.31 \log_2$) and #17 (median NFI = $0.30 \log_2$). The BC PDM model was characterized by decreased median NFI signals of MAPK/RTK proteins (median NFI = $-0.47 \log_2$). Proteins related to PI3K/AKT pathway and of associated pathways were more abundant in OvCa #17 and #24. The mTOR pathway levels were elevated in OvCa #24 (median NFI = $0.54 \log_2$) in other OvCa PDM this pathway showed comparable activity. Median NFI signals from apoptosis-related proteins were significantly different between OvCa #25 (median NFI = $0.75 \log_2$) and BC PDM (median NFI = $1.41 \log_2$). OvCa tumor/stem cell marker protein abundance was significantly upregulated in both OvCa #17 and #23 compared to BC PDM. Thus, RPPA protein profiling analysis demonstrated the heterogeneous activity of several signaling pathways within different OvCa PDM. Apoptosis-related proteins and OvCa tumor/stem cell marker proteins indicated the strongest differences between OvCa PDM models and the BC PDM model.

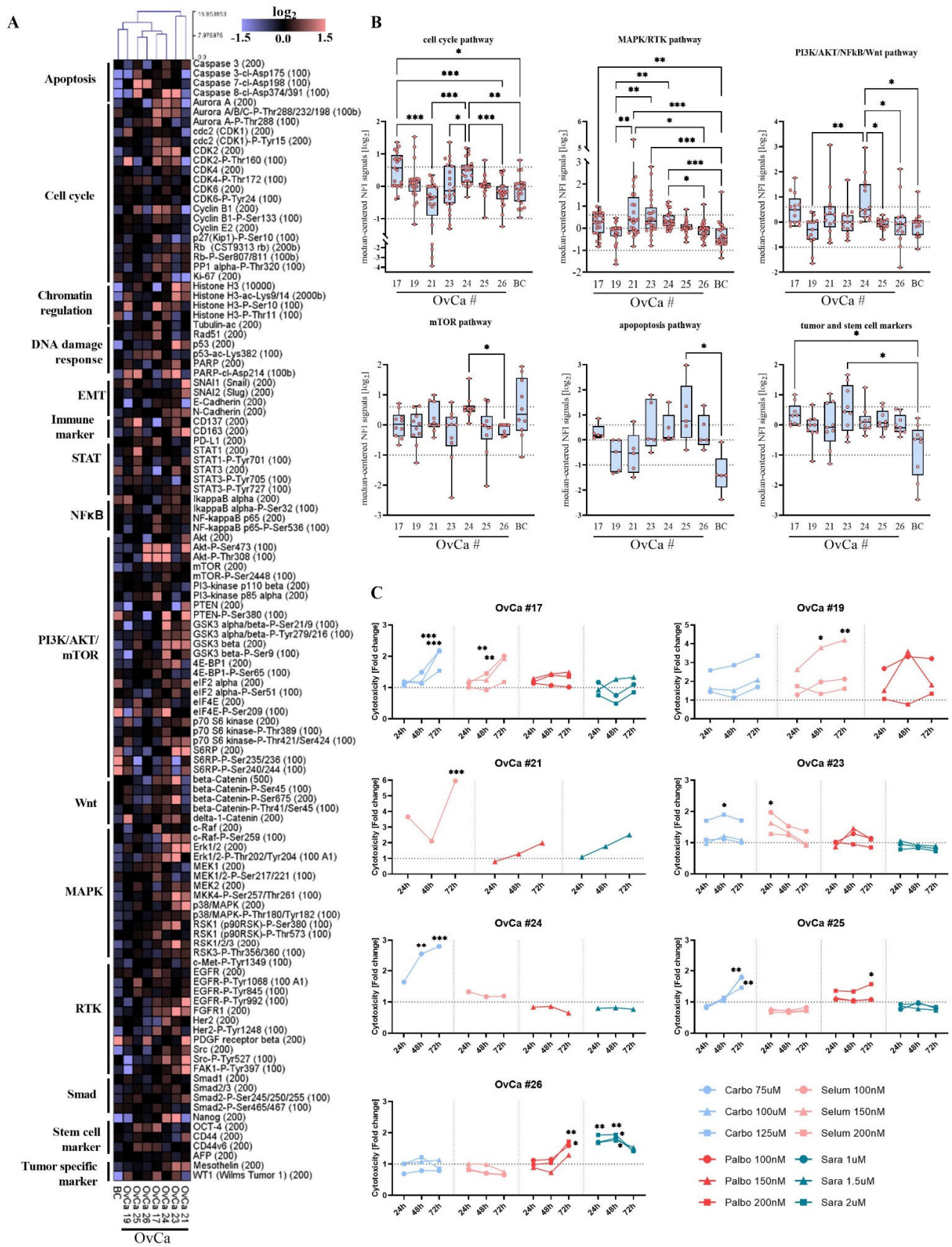


Figure 3. RPPA protein profiling of OvCa PDM identifies significant differences in active protein signaling pathways as molecular basis for OvCa PDM drug treatment responses. **(A)** Protein heat map

covering 116 analytes analyzed in OvCa PDM ($n = 7$) and BC PDM ($n = 1$) generated from sample sizes of $n = 100$ – 150 PDM. Protein abundances for each analyte are displayed as median-centered, \log_2 -transformed NFI signals. Samples were subjected to hierarchical clustering using Euclidean distance (complete linkage). (B) Activation state of different pathways in the different OvCa PDM models. Proteins related to an “active” pathway were selected for each of the plotted pathways (see Table S4). Protein signals are shown as median-centered, \log_2 transformed NFI signals. Dotted lines indicate \log_2 values of $+0.6$ (fold change of $+1.5$) and $-1 \log_2$ (fold change of -0.5). Data are shown as box and whiskers plots with minimum and maximum range. * $p < 0.05$, ** $p < 0.01$, *** $p < 0.001$, Kruskal–Wallis test with Dunn’s post hoc test. (C) Cytotoxicity measurement of OvCa PDM treated with standard platinum-based chemotherapy (carbo 75–125 μM) and/or targeted therapy (selum 100–200 nM, palbo 100–200 nM, sara 1–2 μM). Four replicates per treatment with $n = 15$ PDM per well were performed and measured after 24 h, 48 h and 72 h. Signals were measured as RFU (Relative Fluorescent Unit), background corrected and normalized to vehicle control (DMSO). In case of palbociclib to H_2O control. Data are shown as mean values. Statistical significances compared to vehicle control or H_2O are shown. * $p < 0.05$, ** $p < 0.01$, *** $p < 0.001$, Two-way ANOVA with Dunnett’s multiple comparison test. Carbo: carboplatin; Selum: selumetinib; Palbo: palbociclib; Sara: saracatinib.

3.5. Heterogeneous Treatment Responses towards Chemo- and Targeted Therapy Assessed by Functional Compound Testing in OvCa PDM

Studies of targeted therapies in OvCa are often limited to clinical phase I and II or even cell-line-based preclinical studies [31–33], as treatment efficacies are heterogeneous and mostly not beneficial compared to standard chemotherapy. However, targeting specific signaling pathways could demonstrate a treatment alternative for individual OvCa patients either as first-line or recurrent cancer therapy. As we have discovered that protein abundances differed the most in the cell cycle and MAPK/RTK pathway in OvCa PDM (Figure 3A,B), we investigated efficacy of targeted inhibition of these pathways with the CDK4/6 inhibitor palbociclib, the MEK1/2 inhibitor selumetinib, as well as the Src-inhibitor saracatinib and compared these treatments to standard platinum-based chemotherapy (Figure 3C). PDM were treated with respective drugs, each at three different concentrations, chosen according to previously reported C_{max} concentrations [34]. Treatment efficacy in OvCa PDM—as measured by cytotoxicity—was heterogeneous among individual PDM models, with some specifically responding to carboplatin and others to targeted therapy. Carboplatin induced the most significant cytotoxic effects at the lowest dose (75 μM) at longest duration $t = 72$ h in OvCa #17 and #24 (Figure 3C). On the molecular level, RPPA protein profiling revealed significantly increased cell cycle activity in both models (Figure 3B), which might be associated with the stronger carboplatin response observed in OvCa PDM #17 and #24. Two additional PDM models were also carboplatin sensitive, but responded to treatment at higher dose (OvCa #23, #25). Accordingly, both had shown intermediate cell cycle activity in protein profiling analyses (Figure 3A,B). Selumetinib induced significant cell death in OvCa #17, #19, #21 and #23 at a final concentration of 100–150 nM (Figure 3C). The strongest effect was observed for OvCa #21, which displayed comparatively high MAPK/RTK pathway activity (Figure 3B). Palbociclib, an inhibitor of G1-cell cycle progression, caused significant cytotoxicity in OvCa #26, which had shown moderate cell cycle activity compared to the other models in RPPA protein analysis (Figure 3B). PDM models with significantly higher cell cycle activity as measured by RPPA (OvCa #17, #24), did not respond to palbociclib treatment. Inhibition of the Src-pathway by saracatinib caused significant and dose-dependent killing effects in OvCa #26. Saracatinib triggered rapid PDM death already after 24–48 h of treatment. In conclusion, functional compound testing further confirmed the molecular heterogeneity of studied OvCa PDM models identified by protein profiling. Interestingly, PDM models showing resistance to standard chemotherapy with carboplatin were instead sensitive towards targeted therapeutic approaches.

3.6. Correlation of Carboplatin Treatment Response and Activation State of Protein Signaling Pathways

With a focus on platinum-based standard-of-care chemotherapy, we next related the analyzed protein signaling pathways of untreated OvCa PDM to observed treatment responses. Therefore, protein NFI signals of PDM were grouped into responder and non-responder profiles according to significant carboplatin treatment effects from previously shown functional compound testing (Figure 3C). Mean protein signals (NFI) with >20% difference between responder and non-responder were plotted as a heat map, and significant differences between pathway signaling were analyzed. Further, we examined the on- and off-target pathway effects within different OvCa PDM models by RPPA to assess drug mode-of-action. For this aim, OvCa PDM were treated at one compound concentration and compared to vehicle (DMSO) control. Treatment-to-control signal ratios (TR) were determined from protein NFI signals of treated PDM samples and DMSO vehicle controls at three different time points for each treatment: immediate (30 min), early (4 h) and late (72 h). This enabled the exploration of fast and late treatment response based on changes of protein abundances within a given time frame.

3.6.1. Carboplatin Treatment Sensitivity of OvCa PDM Correlates with High Protein Abundance of G2-M Cell Cycle Proteins

HCL clustering of PDM protein NFI signals led to five clusters that distinguish carboplatin sensitive and resistant PDM models (Figure 4A). To analyze significant differences related to activation or inactivation of signal transduction pathways, proteins from the HCL clustering were sorted according to their pathway affiliation and according to upregulation or downregulation in responder PDM models. Carboplatin-responder PDM models showed significantly increased cell cycle activity ($p < 0.001$; Figure 4B) with upregulated protein abundance observed for Aurora A kinase (mean NFI = 0.74 log₂), CDK2 (mean NFI = 0.8 log₂), Cyclin B1 (mean NFI = 0.84 log₂), PCNA (mean NFI = 0.84 log₂), and acetylated Tubulin (mean NFI = 0.1 log₂) (Figure S2A), which are mostly related to “mitosis” (35, 36). Phospho-Aurora A/B/C (Spearman’s $r = 0.8827$, $p = 0.044$), Cyclin B1 (Spearman’s $r = 0.971$, $p = 0.011$) and PCNA (Spearman’s $r = 0.8827$, $p = 0.044$) significantly correlated with carboplatin treatment sensitivity (Table S3), which was graded according to recorded significance levels from “0–3” (“0”: $p > 0.05$; “1”: $p < 0.05$; “2”: $p < 0.01$; “3”: $p < 0.001$; Figure 3C). At the same time, carboplatin non-responder PDM models showed higher abundance of CDK1 (mean NFI = 0.38 log₂), phospho-CDK2 (mean NFI = 0.77 log₂) and phospho-CDK4 (mean NFI = 0.37 log₂) (Figure S2B), which are more related to the G0/G1 cell cycle phase. In addition, the apoptosis/DNA damage response pathway was significantly upregulated in carboplatin-responder compared to non-responder PDM models ($p = 0.021$; Figure 4B), especially with high abundance of cleaved caspase-8 and cleaved PARP (Figure S2A). Additional significant differences between carboplatin-responder and non-responder OvCa PDM were detected within the RTK and the PI3K/AKT/NFκB signaling pathways ($p < 0.001$; Figure 4B). These pathways were downregulated in the carboplatin non-responder group. Higher EMT/tumor/CSC marker abundance was significantly associated with the carboplatin responder group (Figure 4B) including protein markers Mesothelin, Nanog, STAT1, and E-Cadherin (Figure S2A). In contrast, there were few proteins found, which were downregulated in the carboplatin responder group. Collectively, this panel of down-regulated proteins differed significantly compared to the carboplatin non-responder group (Figure 4B). It contained early cell cycle markers, e.g., Aurora A and Cyclin B1, the mTOR pathway effector phospho-S6RP, PDGFR and SNAI1. We further assessed metastasis-free-survival (MFS) between the described carboplatin-responder (OvCa #17, #23–25) and non-responder (OvCa #19, #26) PDM models (Table S4). Metastasis-free-survival (MFS) analyses of available clinical follow-up patient data revealed prolonged median MFS of 16.2 months in carboplatin responder vs. versus 9.2 months in carboplatin non-responder models.

In summary, the activation state of different signaling pathways composed of proteins with >20% difference in abundance, allowed us to significantly distinguish carboplatin-

responder from non-responder OvCa PDM models. Importantly, these protein signaling response profiles were well in line with results from functional compound efficacy testing assays using those OvCa PDM models.

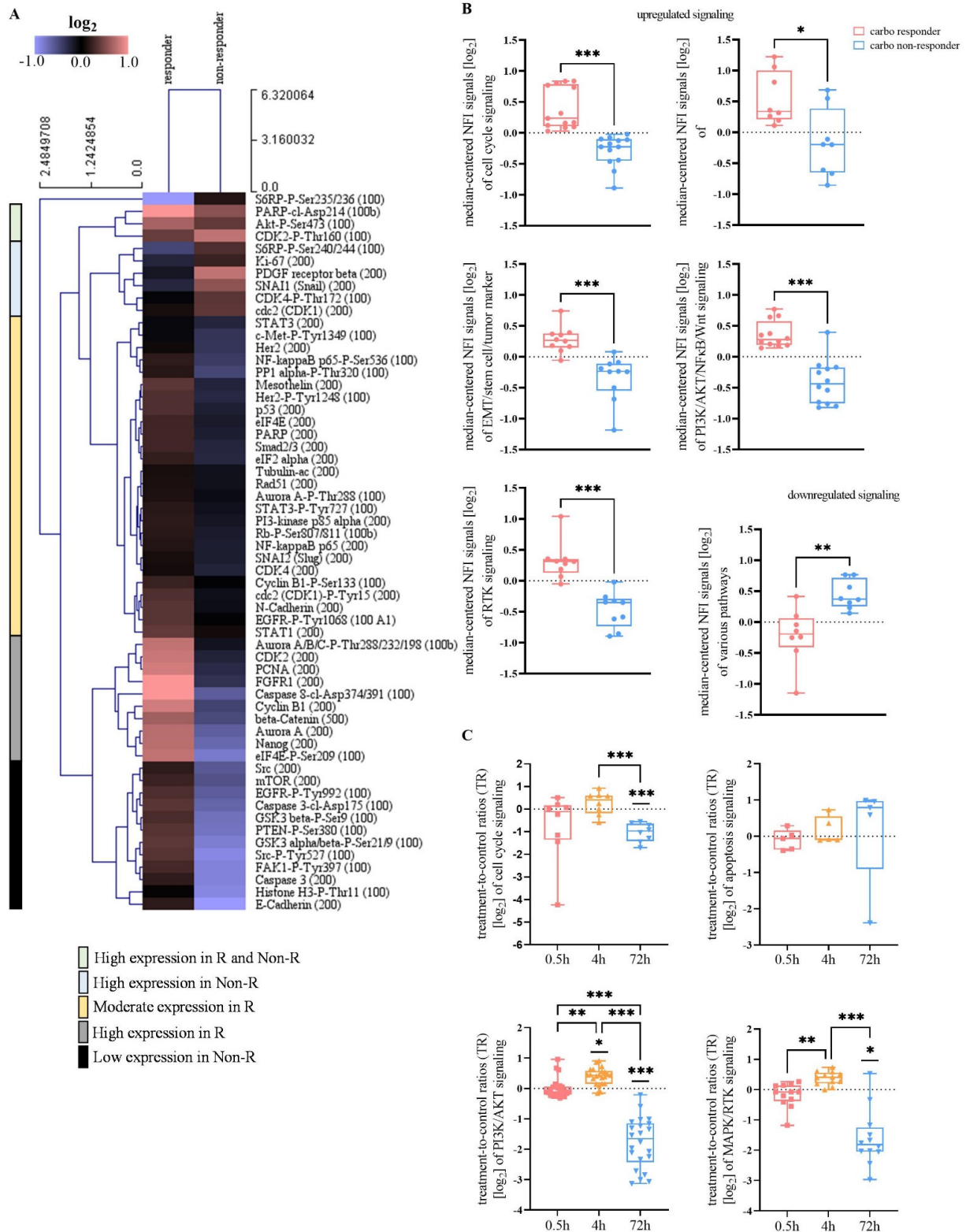


Figure 4. Carboplatin drug response in OvCa PDM correlates with the activity of diverse signaling pathways. (A) Heat map of protein abundances (calculated from median-centered NFI values) averaged over carboplatin-responder (R) and non-responder (Non-R) OvCa PDM. Carboplatin responders and

non-responders were grouped according to significant treatment effects from functional compound testing (Figure 3C). Only proteins with >20% increased or decreased abundance between responder and non-responder group were selected. Data was HCL clustered with Euclidean distance (average linkage). (B) Signaling pathway activation in carboplatin-responder vs. non-responder OvCa PDM. Proteins were sorted according to their pathway affiliation and according to upregulation or downregulation within responder group. * $p < 0.05$, ** $p < 0.01$, *** $p < 0.001$, Mann–Whitney- U -test. (C) Proteomic on- and off-target pathway effects in carboplatin-treated (75 μ M) OvCa #24 PDM analyzed by RPPA. Treated PDM were analyzed from an immediate (0.5 h), an early (4 h) and a late (72 h) treatment time. For each time point, protein values are displayed as \log_2 -transformed treatment-to-control signal ratios (TR) calculated from NFI signals of treated PDM and corresponding vehicle control (DMSO). Only proteins with >50% differential protein abundance compared to vehicle control were selected. Straight lines above plots indicate statistical significances compared to vehicle control. * $p < 0.05$, ** $p < 0.01$, *** $p < 0.001$, One-way ANOVA using nonparametric Kruskal–Wallis with Dunn’s ad hoc test.

3.6.2. Carboplatin Treatment Is Associated with Early Induction of Stress Response and Late Apoptosis

Next, we sought to investigate the carboplatin drug mode-of-action within OvCa PDM. Therefore, the carboplatin-responding OvCa PDM #24 was treated with carboplatin at a concentration of 75 μ M, which had significantly induced PDM cytotoxicity in this model (see Figure 3C). Protein NFI signals were measured at three different time points and normalized to vehicle control. Proteins revealing >50% difference in TR signals (Figure S3) were selected to focus on the strongest changes in abundance. Cell cycle progression proteins (phospho-CDK2, CDK1) and phospho-Histone H3 (Ser10), affecting chromatin condensation during cell division, were downregulated quickly within 30 min (Figure 4C). After 4 h of treatment, TR signals of phospho-Aurora A/B/C protein and Histone H3 was strongly increased (Figure S3). Longer incubation with carboplatin (72 h) resulted in strong downregulation of these proteins (Figure 4C). Diminished abundance of cell cycle proteins after 72 h of carboplatin treatment differed significantly from vehicle control ($p < 0.001$) and from early treatment (4 h; $p < 0.001$). While levels of cell cycle-related proteins decreased over time, apoptotic markers such as cleaved caspases as well as acetylated p53 were elevated after 72 h (Figure S3). Induction of apoptosis-related proteins was already observed after 4 h of treatment (Figure 4C) with increasing abundances of cleaved caspase-7 and acetylated p53 (Figure S3). Focusing on down-stream PI3K/AKT/mTOR/Wnt pathway regulation, the abundances of mTOR effector proteins (S6RP, S6RP-phospho) were quickly upregulated after immediate (0.5 h) carboplatin treatment (Figure S3), which is in line with previous reports about transcriptional regulation of stress response by the mTOR pathway [35]. We also observed additional elevation of mTOR pathway-related proteins after 4 h of carboplatin treatment. Furthermore, overactive mTOR signaling might have resulted in increased p53 activation through upregulated acetylated p53 levels (Figure S3) as described before [35]. The PI3K/AKT/mTOR pathway was significantly upregulated within 4 h of carboplatin treatment compared to vehicle control ($p = 0.021$; Figure 4C). Similar to proteins related to cell cycle, this pathway was completely abrogated as compared to vehicle control after 72 h of treatment ($p < 0.001$; Figure 4C). Changes in protein abundance differed significantly during all three measured time points (0.5 h vs. 4 h: $p = 0.003$; 4 h vs. 72 h and 0.5 h vs. 72 h: $p < 0.001$ Figure 4C). Pronounced, significant downregulation of MAPK/RTK pathway occurred after 72 h of treatment ($p = 0.017$; Figure 4C). The observed proteomic changes within MAPK/RTK-related proteins over time were significant (0.5 h vs. 4 h: $p = 0.009$; 4 h vs. 72 h: $p < 0.001$; Figure 4C). Thus, carboplatin treatment of OvCa #24 illustrated substantial and time-dependent changes in TR signals. Short treatment with carboplatin apparently triggered the induction of stress responses while longer treatment duration caused the induction of apoptosis.

3.7. Characterization of Tumor-Infiltrating Lymphocyte Populations from Primary OvCa Tissue Samples

Our established procedure of tissue processing and PDM isolation enabled us to obtain single-cell suspensions containing tumor-infiltrating lymphocytes (TILs) from respective OvCa tumor specimen. This allowed for expansion of these autologous TILs in the presence of low-dosed cytokines and antigenic stimulation in order to investigate immuno-phenotypes of respective patient samples. The immunogenicity of OvCa has been demonstrated in prior studies and is confirmed by the frequent infiltration of ovarian tumors with TILs [36–38]. As reported by Sato et al. (2005), different T cell populations diversely influence tumor immunosurveillance in OvCa. High intraepithelial CD8⁺/CD4⁺ T cell ratios in patients were associated with improved survival as CD4⁺ T cells executed immunosuppressive functions. To determine the composition of the isolated immune cell infiltrate within our sample cohort, we characterized the phenotype of autologous TIL populations by multi-color flow cytometry (Figure S4A). Within isolated and expanded OvCa TIL populations from different specimen, we found that the proportion of CD4⁺ TILs was 57.8% and significantly more abundant than CD8⁺ TILs with 33.5% ($p = 0.003$ **, Figure 5A, Table S5).

3.7.1. Isolated CD8⁺ OvCa TILs Are Composed of Tumor-Specific CD39⁺, Stem-like CD39⁻PD1⁺ and Terminally Differentiated CD39⁺PD1⁺ Populations

Within the isolated CD8⁺ TIL populations, we identified different phenotypes according to expression of the co-inhibitory receptors PD-1 and CTLA-4, the tumor-antigen specificity marker CD39 and the activation marker CD137 (Figure 5A). To investigate the activation status of CD8⁺ TILs, cells were examined for co-expression of the co-stimulatory receptor CD137 (4-1BB). CD137 is upregulated in activated T cells and has been suggested to be a marker for antigen-activated T cells [39]. The mean percentage of CD8⁺ CD137⁺ TILs was 3.1% and varied between 0–10% (Table S5), and >5% of the CD8⁺ cytotoxic T-cells (CTLs) from OvCa #1, #3 and #5 (Figure 5B) co-expressed CD137, indicating their pre-exposure to tumor antigens. Expression of co-inhibitory receptors PD-1 and CTLA-4 on CD8⁺ TILs did not differ significantly among analyzed TIL populations but tended to higher PD-1 expression levels (mean 6.9% vs. 3.4%; Table S5). TILs from OvCa #3, #7 and #25 as well as #5, #13 and #26 were among those displaying an exhausted phenotype with >10% of CD8⁺PD-1⁺ or CD8⁺CTLA-4⁺ TILs (Figure 5B). Moreover, in recent reports CD39 expression in CD8⁺ TILs was described as a marker for tumor-antigen specific TILs that have undergone tumor-antigen-driven clonal expansion, exhibit resident memory T cell-like phenotypes and express a variety of co-stimulatory and co-inhibitory receptors [40–42]. Here, CD39⁺ CTLs (mean 40.5%; range 4.4–96.8%, Table S5) were significantly more abundant than CD39⁻ CTLs (mean 9.5%; range 0–48.3%, Table S5), so-called ‘bystander TILs’, known to recognize mostly viral antigens (43) ($p < 0.001$, Figure 5A). The amount of CD39⁺ TILs strongly correlated with the amount of CD8⁺ TILs (Spearman $r = 0.88$, Figure S4B; $p < 0.001$, Table S6) and conversely with the amount of CD4⁺ TILs (Spearman $r = -0.80$, Figure S4B; $p = 0.002$, Table S6). Thus, the abundance of CD4⁺ and CD8⁺ TILs appeared to significantly determine the amount of CD39⁺ CTLs. In addition, CD39 expression was largely limited to CD8⁺ TILs. As co-inhibitory receptors play a role in T cell exhaustion and are important targets for immune checkpoint-inhibition, we analyzed PD-1 and CTLA-4 expression on the tumor-specific CD39⁺ CTL population. PD1⁺CD39⁺ were more frequent than CTLA-4⁺ CD39⁺ (15.7% vs. 5.4% Figure 5A, Table S5). The total amount of CD8⁺PD1⁺ TILs thereby correlated with the amount of CD8⁺CD39⁺PD1⁺ TILs (Spearman $r = 0.79$, Figure S4B; $p = 0.002$, Table S6) of a PDM model. Thus, CD39 expression was limited to tumor-antigen-stimulated and -exhausted TILs (e.g., OvCa #7, #17 and #25; Figure 5B). In contrast to ‘terminally differentiated cells’ [43], OvCa TILs with a ‘stem cell-like’ CD39⁻PD1⁺ phenotype were found in 7.3% of the CTLs (Table S5). This population showed the highest proportional variability with a maximum of 50.5% cells vs. a minimum of 0% as compared to other CD8⁺ TIL populations (CV 208%). The frequency of CD8⁺CD39⁺ and stem cell-like CD8⁺CD39⁻PD1⁺ was negatively correlated

(Spearman $r = -0.63$, Figure S4B; $p = 0.024$, Table S6). These results confirm the feasibility of extracting and expanding TIL populations from fresh OvCa tissue samples and identify heterogeneous, patient-specific immuno-phenotypes with potential relevance for immuno-oncological treatment approaches.

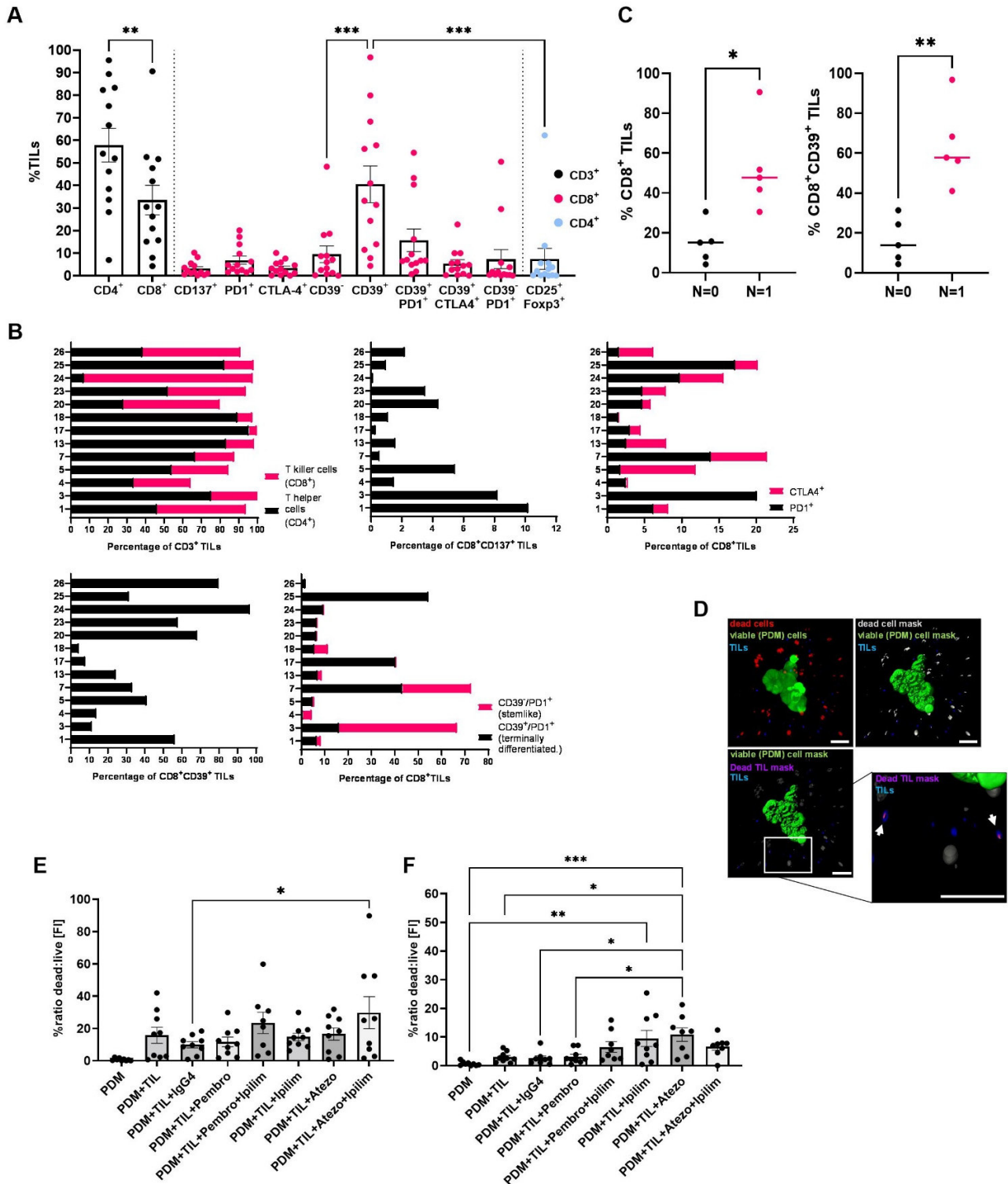


Figure 5. CPI treatment in OvCa PDM-TIL co-cultures increased functional TIL killing capacity. Autologous TIL populations were isolated and expanded from OvCa tissue specimen. (A) Percentages of different TIL populations within CD3⁺, CD8⁺ and CD4⁺ positive T cells of different models were quantified by multicolor flow cytometry. Data are shown as means \pm SEM of at least $n = 10$ OvCa

samples. * $p < 0.05$, ** $p < 0.01$, *** $p < 0.001$, ANOVA with Holm-Šidák's post hoc test. (B) Phenotypes of extracted TIL populations shown separately for each OvCa model. (C) Percentages of CD8⁺ and CD8⁺CD39⁺ TILs in OvCa patients with lymph node spread ($n = 1$) and without lymph node spread ($n = 0$). All points with median are shown. * $p < 0.05$, ** $p < 0.01$, Mann-Whitney-*U*-test. (D) PDM killing effects were measured in an image-based assay format as ratio of fluorescent intensities (FI) of dead cells vs. viable PDM cells. Per treatment $n = 3$ PDM in three replicates were analyzed. Masks for viable PDM (Calcein-AM staining), dead cells (SYTOX™ Orange dead cell staining) and TILs (CellTracker™ Deep Red staining) were applied using Imaris 8.0 software. Scale bars indicate 50 μm . FI from TILs were subtracted from the total dead FI. (E,F) Killing effects of autologous TILs on corresponding PDM in co-cultures treated with immune checkpoint inhibitors (CPI). TILs of OvCa #24 (E) and #26 (F) were co-cultured with $n = 15$ PDM using an E:T ratio of 4:1. * $p < 0.05$, ** $p < 0.01$, *** $p < 0.001$, ANOVA with Holm-Šidák's post hoc test. Pembrolizumab 60 $\mu\text{g}/\text{mL}$; Ipilimumab 50 $\mu\text{g}/\text{mL}$; Atezo: atezolizumab 50 $\mu\text{g}/\text{mL}$.

3.7.2. Specific TIL Phenotypes Isolated from OvCa Tumor Specimen Correlate with Regional Lymph Node Metastasis

We further analyzed the correlation between specific TIL populations and clinical follow-up patient data. OvCa patients with regional lymph node metastasis ($n = 1$) tended to present with significantly more extensive CD8⁺ TIL infiltration in their tumors than those with no lymph node metastasis ($n = 0$) ($p = 0.016$) (Figure 5C). Moreover, the frequency of CD8⁺ TILs appeared to significantly correlate with that of CD8⁺CD39⁺ TILs in OvCa (Figure 5C). Despite a small sample size, our data implicate a significant correlation between lymph node spread ($n = 1$) and the presence of a CD8⁺CD39⁺ population ($p = 0.008$).

3.8. OvCa PDM Killing by Autologous TIL Populations Is Enhanced by Immune Checkpoint Inhibitor Treatment

To evaluate the functional, tumor cell killing capacity of autologous TILs on OvCa PDM and the corresponding treatment efficacy of established immune checkpoint inhibitors (CPI), we subjected co-cultures of TILs and PDM from OvCa #24 and #26 to image-based analysis of CPI-treatment response. A total of nine PDM were imaged per treatment (three PDM per well in triplicates) and a dead:live PDM ratio was calculated according to the sum of measured fluorescent intensities (FI) (Figure 5D–F). Addition of TILs to autologous PDM induced a basal killing effect in PDM in both models analyzed in the absence of CPI treatment (Figure 5E,F). As the addition of matched isotype controls showed no additional effect in both co-culture models, we excluded the possibility of unspecific killing effects of CPI antibodies. TIL killing effects in OvCa #24 co-cultures were observed in response to treatment with either the combination of anti-PD1 and anti-CTLA-4 (pembrolizumab + ipilimumab) or anti-PD-L1 and anti-CTLA-4 (atezolizumab + ipilimumab) ($p = 0.039$) compared to isotype control treatment (Figure 5E). Single agents induced no significant increase in PDM killing. In OvCa #26 CPI treatment almost doubled PDM killing (Figure 5F). In comparison, co-cultures treated with ipilimumab ($p = 0.004$) or atezolizumab ($p < 0.001$) showed significant PDM killing compared to untreated PDM. The killing effect of TILs was significantly amplified by atezolizumab treatment compared to co-culture controls (PDM + TIL: $p = 0.021$; PDM + TIL + IgG4: $p = 0.018$; Figure 5F). In line with this observation, respective OvCa PDM models showed weakly positive PD-L1 staining (Figure S1). Further, atezolizumab treatment significantly increased the TIL killing effect towards PDM as compared to pembrolizumab ($p = 0.026$). Autologous CD8 TILs from both tested OvCa PDM models were composed of high amounts of tumor-specific, non-terminally differentiated CD8⁺CD39⁺ TIL populations as compared to other OvCa TILs (Figures 5B and S5). Moreover, these CD8 TILs were prominently positive for CTLA-4, which might explain the observed increase in PDM killing in response to ipilimumab (Anti-CTLA4) treatment (Figures 5B and S5). Thus, the co-culture of autologous TILs and PDM offers the possibility to extent compound efficacy testing

beyond chemotherapeutic compounds to immune oncological treatment approaches in a patient-specific setting.

4. Discussion

Recently, we could show the establishment of PDM from human glioblastoma tissue specimen containing important components of the tumor stroma (e.g., tumor-associated macrophages), and their application for the assessment of responses towards CSF1R- and PD1-targeting antibodies as well as the small molecule inhibitor Argyrin F [44,45]. In the present study, we have now further extended this approach to a patient-derived model system composed of PDM and autologous TILs extracted from a panel of primary OvCa tissue specimen and their in-depth characterization by immunohistochemistry, protein profiling, immune cell phenotyping and focused compound efficacy testing. Our results show an 87.5% success rate for isolation of PDM with robust viability and in suitable amounts for further, multi-parametric downstream analyses. In-depth histopathological assessment of PDM sections by a certified pathologist confirmed the conservation of typical histological features of respective OvCa types by this model system. Importantly, the complexity of the ovarian cancer TME with respect to the presence of cancer-associated fibroblasts and extracellular matrix components including collagen and hyaluronan-binding protein observed in primary OvCa tissue sections was conserved and did not differ significantly in the majority of PDM models generated in our study. The presence of these TME components has previously been correlated with tumor stage, prognosis, and progression and shown to substantially influence treatment responses [29,46,47]. Moreover, our data show that PDM and corresponding PTT express similar levels of markers important for histopathological assessment of ovarian cancer such as p53, WT1 and CA125. Interestingly, we could also identify immune cell infiltration within a subset of OvCa PDM, reflecting the immunogenicity of OvCa as previously reported [36,37,48]. We also identified differences in protein expression between PDM and PTT (e.g., MSLN, Collagen or FAP α). This could be explained at least in part by the low proportion of pure stromal areas within PDM as compared to PTT.

While OvCa patient-derived organoids (PDO) were often studied by genomic and transcriptomic sequencing [6–8], we were the first (to our knowledge) to investigate inter-tumoral heterogeneity and differential drug response mechanisms by RPPA-based protein profiling in a patient-derived 3D OvCa preclinical cell model. Here, analyses of a panel of >110 phospho- and total proteins allowed for the clustering of histologically similar OvCa PDM models, pathway activity profiling and investigation of on- and off target drug effects. Obtained RPPA protein profiles confirmed the heterogeneity of OvCa PDM observed via immunohistochemistry and previously reported for HGSC, the most common type of OvCa. Our work identified significant differences in the activity of cell cycle and MAPK/RTK pathways within analyzed OvCa PDM and enabled their distinction from a breast cancer derived PDM model by differential expression of OvCa tumor and stem cell markers as well as apoptosis-related proteins.

Seven OvCa PDM models were applied for individualized compound efficacy testing using a panel of clinically approved drugs at C_{max} drug concentrations previously reported in clinical trials. For analyzed OvCa PDM models, we observed patient-specific heterogeneity of response towards chemotherapy and targeted therapy. Correlation with RPPA protein profiling data allowed the allocation of individual PDM drug responses to specifically up- or down-regulated signaling pathway activities and, importantly, enabled the prediction of PDM models with high probability of response towards chemotherapy or targeted therapy. In accordance with the ability of cytostatic drugs to induce apoptosis especially in actively dividing cells [49], our work identified additional correlation between proteins relevant for S and G2/M cell cycle phase progression and carboplatin response. Specifically, our data implicate that elevated abundances of Aurora A, Cyclin B1 and PCNA proteins may allow for identification of carboplatin treatment response. Furthermore and in line with previous reports, we confirmed that decreased DNA damage repair and the

ability to undergo apoptosis [50] is associated with carboplatin treatment sensitivity in OvCa. This was illustrated by increased levels of cleaved caspase-7 and cleaved PARP. Our results did not identify a correlation of carboplatin resistance and markers of cancer stem cells (CSCs) [51,52] or epithelial-to-mesenchymal transition (EMT) [53,54]. Instead, we found the cancer stem cell-related protein Nanog as well N-Cadherin strongly upregulated in carboplatin-responding PDM. These differing results might arise from the fact that above-mentioned previous studies were performed in adherent cell lines and not within a patient-derived 3D tumor model. Importantly, we identified protein signatures of OvCa PDM allowing for the identification and prediction of PDM models with high probability of response towards chemotherapy or targeted therapy. The correlation of our results with clinical data indicated a significant correlation of carboplatin treatment response with prolonged metastasis-free survival of respective patients. Given the small sample cohort analyzed here, these results need to be interpreted with caution but warrant further investigation.

We further assessed proteomic changes upon PDM treatment such as effects on protein abundance, directed on- and off-target pathway effects and drug mechanism-of-action within OvCa PDM. In a carboplatin sensitive PDM model, we observed a time-dependent decrease in cell cycle- and an increase in apoptosis-inducing protein abundance. In parallel, we found a fast stress response upon treatment as indicated by an activated mTOR pathway with high S6RP and active phospho-S6RP levels [35]. Overactive mTOR in combination with cell stress and the inability of cells to adapt to cellular stress might be responsible for p53 elevation [55,56] and driving cells into senescence or apoptosis [57,58].

Apart from testing the response of OvCa PDM to conventional chemotherapy, we sought to investigate the applicability of this model system for efficacy assessment of immuno-oncological treatment approaches. For this aim, we applied immunophenotyping of autologous TIL populations followed by their co-culture with respective PDM in the presence and absence of immunotherapeutic mono- and combination treatment schedules. Immunosurveillance of cancer strongly depends on the composition of tumor-infiltrated immune cells and the degree of tumor tissue infiltration and is known to influence treatment efficacies. As a result, the idea of an immunoscore, identifying a patient's immunophenotype, emerged [59]. Our work uncovered several immunophenotypes within expanded TILs from OvCa patients by multicolor flow cytometry compared to previous immunohistochemistry-based analysis [60]. As described by Sato et al. (2005) [36] and Zhang et al. (2003) [37] high numbers of intraepithelial CD8⁺ TILs are associated with better prognosis in OvCa. We found that OvCa TILs were largely composed of CD4⁺ rather than CD8⁺ TILs. In this regard, OvCa models with high amounts of suppressive CD4⁺ TILs and low numbers of CD8⁺ TILs are suggested to have worse prognosis [61]. In line with previous reports [62], we identified expression of CD39 in OvCa TIL populations, a marker that distinguishes between tumor-specific CTLs (CD39⁺) and bystander TILs (CD39⁻) [40,41]. Interestingly, we found that CD8⁺ TIL amounts correlated with that of CD8⁺ CD39⁺ TILs, and could confirm that these tumor-specific T cells constitute an exhausted, memory T cell-like phenotype, as CD39 expression was limited to CD8⁺PD-1⁺ TILs. Importantly, our results further demonstrated that co-cultures of PDM and autologous TILs could be applied to assess the treatment effect of CPIs in a preclinical and patient-specific setting. Such PDM-TIL co-culture systems could potentially be used to identify OvCa patients, who would most likely benefit from immunotherapies. In the limited OvCa tumor tissue cohort investigated here, OvCa tumors with regional lymph node metastasis contained higher numbers of CD8⁺ and CD8⁺CD39⁺ TILs. The co-culture models tested in our study for response towards CPI treatment were derived from lymph-node spreading primary tumors, which might suggest that immunogenicity of OvCa increases upon metastasis.

Our work illustrates several advantages of PDM over patient-derived cancer organoid (PDO) models. First, once the tissue sample is processed, PDM can be isolated within 2 days and used for various types of analyses including those we used here. In contrast, a period of weeks to months is usually required to establish a PDO line. Another advantage of PDM

is their cellular composition and complexity with the presence of components of the ECM as well as the TME (including Collagen, C1QBP, tumor-associated fibroblasts), which is more similar to the patient tumor than PDO, which are lacking these components [63]. Moreover, PDM are cultured in suspension, whereas PDO are usually cultured in ECM matrix from mouse tumors (Matrigel). Influences of animal origin and batch-dependent differences in the composition of matrigel on comparability with human tumor tissue need to be considered for PDO [64,65]. In contrast, PDM are cultured in defined medium without the addition of animal components.

Limitations of our PDM model are currently the restricted number of PDM available from digestion of individual tumor tissue samples. From experience with different tumor types, an average of several hundred to several thousand microtumors can be isolated from fresh tissue samples. This number depends on the amount of tissue available for PDM isolation as well as tissue composition (including degree of fibrosis and necrosis). PDMs are therefore presently not suitable for high-throughput drug screening approaches, but for focused drug testing in late preclinical and translational drug development as well as in the context of precision oncology. For our study, only a limited amount of corresponding primary tumor tissue was available for comparative analyses with isolated PDM. Comparative, RPPA-based analyses between PDM and PTT were not feasible here due to this limitation. Furthermore, the limitation of our present study with regard to sample size should be noted.

5. Conclusions

In conclusion, patient-derived microtumors isolated from OvCa tumor specimen represent a novel *ex vivo* tumor model for OvCa displaying histopathological similarities to corresponding primary patient tumors and revealing intertumoral heterogeneity as evidenced by immunohistochemical and protein profiling analyses. The combination of functional drug testing with analyses of protein signaling pathways and drug-mode of action enabled the identification of PDM models susceptible to platinum-based treatment and allowed for the prediction of individual therapeutic sensitivity. Parallel isolation and culturing of autologous TILs further allowed for the characterization of patient-individual immune-phenotypes as well as the assessment of responses towards immunotherapy in PDM-TIL co-cultures. While the rapid PDM/TIL extraction procedure and quick availability of resulting datasets within 3–4 weeks is in good accordance with timelines of clinical decision making, we plan to confirm our findings in future studies with larger sample cohorts.

Supplementary Materials: The following supporting information can be downloaded at: <https://www.mdpi.com/article/10.3390/cancers14122895/s1>, SI Methods: IHC/FACS/RPPA antibody lists; Figure S1: Histology and immunohistochemistry of OvCa microtumors and corresponding primary tumor tissue; Figure S2: Up- and downregulated proteins in carboplatin-responder and non-responder OvCa PDM; Figure S3: Time-dependent alterations of signaling pathways in carboplatin sensitive OvCa PDM; Figure S4: Gating schemes of expanded TILs, the correlation of TIL populations and their comparison between different OvCa models; Figure S5: Gating schemes of expanded OvCa TILs #24 and #26; Table S1: Correlation of PDM isolation-success and clinical patient-data; Table S2: Log₂-transformed, median-centered NFI signals of signaling pathway proteins from OvCa and BC PDM from RPPA analysis; Table S3: Spearman correlation of carboplatin-treatment sensitivity and protein abundances of OvCa PDM models; Table S4: Significant difference in metastasis-free-survival between OvCa PDM carboplatin responder and non-responder. Table S5: Descriptive statistics of analyzed OvCa TIL populations; Table S6: Correlation of TIL phenotypes (Spearman correlation, *p*-values). Reference [66] is cited in the supplementary materials.

Author Contributions: Conceptualization and design of the study, N.A., C.S., M.P., K.S.-L., S.Y.B. and A.H.; data collection, data analysis, investigation and interpretation, N.A., B.G., M.P., A.K., A.-L.K., A.S., S.Y.B. and C.S.; writing—original draft, N.A. and C.S.; writing—review and editing, N.A., C.S., M.P., A.-L.K., K.S.-L., A.K., S.Y.B., A.H. and A.S.; visualization, N.A., C.S. and S.Y.B.; supervision, C.S. and A.K.; project administration: N.A., C.S. and A.K. All authors have read and agreed to the published version of the manuscript.

Funding: This work received financial support from the Ministry of Baden-Wuerttemberg for Economic Affairs, Labor and Tourism (grant 3-4332.62-HSG/84).

Institutional Review Board Statement: The study was conducted in accordance with the Declaration of Helsinki, and approved by the Institutional Review Board (or Ethics Committee) of the University Hospital Tuebingen, Germany (protocol code IRB#275/2017BO2 and IRB#788/2018BO2).

Informed Consent Statement: The use of human samples was approved by the local Ethics Commission at the Medical Faculty of Tuebingen under the reference numbers IRB#275/2017BO2 and IRB#788/2018BO2. All patients enrolled gave their informed consent to participate in the study.

Data Availability Statement: All data needed to evaluate the conclusions of the paper are included in this published article and its supplementary information file. Material and further data are available upon request after signature of an MTA from the corresponding authors.

Acknowledgments: We gratefully acknowledge the Department of Women's Health, Women's University Hospital, Tuebingen University Hospital for excellent support, helpful discussions and providing fresh tumor tissue biopsies and corresponding FFPE material. We thank all patients and healthy volunteers enrolled for giving their informed consent for secondary use of residual tissue, respectively.

Conflicts of Interest: AH received consulting and speaking fees from GSK, AstraZeneca and Clovis. N.A., A.K., B.G., A.-L.K., A.S., S.Y.B., M.P., K.S.-L. and C.S. declare no competing interest.

References

1. Bray, F.; Ferlay, J.; Soerjomataram, I.; Siegel, R.L.; Torre, L.A.; Jemal, A. Global cancer statistics 2018: Globocan estimates of incidence and mortality worldwide for 36 cancers in 185 countries. *CA Cancer J. Clin.* **2018**, *68*, 394–424. [[CrossRef](#)] [[PubMed](#)]
2. Izar, B.; Tirosh, I.; Stover, E.H.; Wakiro, I.; Cuoco, M.S.; Alter, I.; Rodman, C.; Leeson, R.; Su, M.J.; Shah, P.; et al. A single-cell landscape of high-grade serous ovarian cancer. *Nat. Med.* **2020**, *26*, 1271–1279. [[CrossRef](#)] [[PubMed](#)]
3. The Cancer Genome Atlas Research Network. Integrated genomic analyses of ovarian carcinoma. *Nature* **2011**, *474*, 609–615. [[CrossRef](#)] [[PubMed](#)]
4. Zhang, H.; Liu, T.; Zhang, Z.; Payne, S.H.; Zhang, B.; McDermott, J.E.; Zhou, J.-Y.; Petyuk, V.A.; Chen, L.; Ray, D.; et al. Integrated proteogenomic characterization of human high-grade serous ovarian cancer. *Cell* **2016**, *166*, 755–765. [[CrossRef](#)]
5. Verduin, M.; Hoeben, A.; De Ruyscher, D.; Vooijs, M. Patient-derived cancer organoids as predictors of treatment response. *Front. Oncol.* **2021**, *11*, 641980. [[CrossRef](#)]
6. Chen, H.; Gotimer, K.; De Souza, C.; Tepper, C.G.; Karnezis, A.N.; Leiserowitz, G.S.; Chien, J.; Smith, L.H. Short-term organoid culture for drug sensitivity testing of high-grade serous carcinoma. *Gynecol. Oncol.* **2020**, *157*, 783–792. [[CrossRef](#)]
7. Kopper, O.; De Witte, C.J.; Lohmussaar, K.; Valle-Inclan, J.E.; Hami, N.; Kester, L.; Balgobind, A.V.; Korving, J.; Proost, N.; Begthel, H.; et al. An organoid platform for ovarian cancer captures intra- and interpatient heterogeneity. *Nat. Med.* **2019**, *25*, 838–849. [[CrossRef](#)]
8. Hill, S.J.; Decker, B.; Roberts, E.A.; Horowitz, N.S.; Muto, M.G.; Worley, M.J., Jr.; Feltmate, C.M.; Nucci, M.R.; Swisher, E.M.; Nguyen, H.; et al. Prediction of DNA repair inhibitor response in short-term patient-derived ovarian cancer organoids. *Cancer Discov.* **2018**, *8*, 1404–1421. [[CrossRef](#)]
9. Neal, J.T.; Li, X.; Zhu, J.; Giangarra, V.; Grzeskowiak, C.L.; Ju, J.; Liu, I.H.; Chiou, S.-H.; Salahudeen, A.A.; Smith, A.R.; et al. Organoid modeling of the tumor immune microenvironment. *Cell* **2018**, *175*, 1972–1988.e1916. [[CrossRef](#)]
10. Wensink, G.E.; Elias, S.G.; Mullenders, J.; Koopman, M.; Boj, S.F.; Kranenburg, O.W.; Roodhart, J.M.L. Patient-derived organoids as a predictive biomarker for treatment response in cancer patients. *NPJ Precis. Oncol.* **2021**, *5*, 30. [[CrossRef](#)]
11. Kondo, J.; Endo, H.; Okuyama, H.; Ishikawa, O.; Iishi, H.; Tsujii, M.; Ohue, M.; Inoue, M. Retaining cell-cell contact enables preparation and culture of spheroids composed of pure primary cancer cells from colorectal cancer. *Proc. Natl. Acad. Sci. USA* **2011**, *108*, 6235–6240. [[CrossRef](#)] [[PubMed](#)]
12. Shuford, S.; Wilhelm, C.; Rayner, M.; Elrod, A.; Millard, M.; Mattingly, C.; Lotstein, A.; Smith, A.M.; Guo, Q.J.; O'Donnell, L.; et al. Prospective validation of an ex vivo, patient-derived 3d spheroid model for response predictions in newly diagnosed ovarian cancer. *Sci. Rep.* **2019**, *9*, 11153. [[CrossRef](#)] [[PubMed](#)]
13. Pirnia, F.; Pawlak, M.; Thallinger, G.G.; Gierke, B.; Templin, M.F.; Kappeler, A.; Betticher, D.C.; Gloor, B.; Borner, M.M. Novel functional profiling approach combining reverse phase protein microarrays and human 3-d ex vivo tissue cultures: Expression of apoptosis-related proteins in human colon cancer. *Proteomics* **2009**, *9*, 3535–3548. [[CrossRef](#)] [[PubMed](#)]
14. Pawlak, M.; Carragher, N.O. Reverse phase protein arrays elucidate mechanisms-of-action and phenotypic response in 2d and 3d models. *Drug Discov. Today Technol.* **2017**, *23*, 7–16. [[CrossRef](#)]
15. Kresbach, G.M.; Pawlak, M. High precision rppa: Concept, features, and application performance of the integrated zeptosens platform. *Adv. Exp. Med. Biol.* **2019**, *1188*, 31–59.
16. Pawlak, M.; Schick, E.; Bopp, M.A.; Schneider, M.J.; Oroszlan, P.; Ehrat, M. Zeptosens' protein microarrays: A novel high performance microarray platform for low abundance protein analysis. *Proteomics* **2002**, *2*, 383–393. [[CrossRef](#)]

17. Iglewicz, B.; Hoaglin, D.C. *How to Detect and Handle Outliers*; ASQC Quality Press: Milwaukee, WI, USA, 1993; p. ix. 87p.
18. Köbel, M.; Rahimi, K.; Rambau, P.F.; Naugler, C.; Le Page, C.; Meunier, L.; De Ladurantaye, M.; Lee, S.; Leung, S.; Goode, E.L.; et al. An immunohistochemical algorithm for ovarian carcinoma typing. *Int. J. Gynecol. Pathol.* **2016**, *35*, 430–441. [[CrossRef](#)]
19. Hilliard, T. The impact of mesothelin in the ovarian cancer tumor microenvironment. *Cancers* **2018**, *10*, 277. [[CrossRef](#)]
20. Hassan, R.; Kreitman, R.J.; Pastan, I.; Willingham, M.C. Localization of mesothelin in epithelial ovarian cancer. *Appl. Immunohistochem. Mol. Morphol.* **2005**, *13*, 243–247. [[CrossRef](#)]
21. Chang, M.-C.; Chen, C.-A.; Chen, P.-J.; Chiang, Y.-C.; Chen, Y.-L.; Mao, T.-L.; Lin, H.-W.; Lin Chiang, W.-H.; Cheng, W.-F. Mesothelin enhances invasion of ovarian cancer by inducing mmp-7 through mapk/erk and jnk pathways. *Biochem. J.* **2012**, *442*, 293–302. [[CrossRef](#)]
22. Tornos, C.; Soslow, R.; Chen, S.; Akram, M.; Hummer, A.J.; Abu-Rustum, N.; Norton, L.; Tan, L.K. Expression of wt1, ca 125, and gcdfp-15 as useful markers in the differential diagnosis of primary ovarian carcinomas versus metastatic breast cancer to the ovary. *Am. J. Surg. Pathol.* **2005**, *29*, 1482–1489. [[CrossRef](#)] [[PubMed](#)]
23. Kriplani, D.; Patel, M.M. Immunohistochemistry: A diagnostic aid in differentiating primary epithelial ovarian tumors and tumors metastatic to the ovary. *S. Asian J. Cancer* **2013**, *2*, 254–258. [[CrossRef](#)] [[PubMed](#)]
24. Neunteufel, W.; Breiteneker, G. Tissue expression of ca 125 in benign and malignant lesions of ovary and fallopian tube: A comparison with ca 19-9 and cea. *Gynecol. Oncol.* **1989**, *32*, 297–302. [[CrossRef](#)]
25. Cox, T.R. The matrix in cancer. *Nat. Rev. Cancer* **2021**, *21*, 217–238. [[CrossRef](#)] [[PubMed](#)]
26. Bhat, R.; Bissell, M.J. Of plasticity and specificity: Dialectics of the microenvironment and macroenvironment and the organ phenotype. *WIREs Dev. Biol.* **2014**, *3*, 147–163. [[CrossRef](#)]
27. Roskelley, C.D.; Bissell, M.J. The dominance of the microenvironment in breast and ovarian cancer. *Semin. Cancer Biol.* **2002**, *12*, 97–104. [[CrossRef](#)]
28. Mhawech-Fauceglia, P.; Yan, L.; Sharifian, M.; Ren, X.; Liu, S.; Kim, G.; Gayther, S.A.; Pejovic, T.; Lawrenson, K. Stromal expression of fibroblast activation protein alpha (fap) predicts platinum resistance and shorter recurrence in patients with epithelial ovarian cancer. *Cancer Microenviron.* **2015**, *8*, 23–31. [[CrossRef](#)]
29. Nissen, N.I.; Karsdal, M.; Willumsen, N. Collagens and cancer associated fibroblasts in the reactive stroma and its relation to cancer biology. *J. Exp. Clin. Cancer Res.* **2019**, *38*, 115. [[CrossRef](#)]
30. Saha, P.; Datta, K. Multi-functional, multicompartamental hyaluronan-binding protein 1 (habp1/p32/gc1qr): Implication in cancer progression and metastasis. *Oncotarget* **2018**, *9*, 10784–10807. [[CrossRef](#)]
31. Iyengar, M.; O'Hayer, P.; Cole, A.; Sebastian, T.; Yang, K.; Coffman, L.; Buckanovich, R.J. Cdk4/6 inhibition as maintenance and combination therapy for high grade serous ovarian cancer. *Oncotarget* **2018**, *9*, 15658–15672. [[CrossRef](#)]
32. Farley, J.; Brady, W.E.; Vathipadiekal, V.; Lankes, H.A.; Coleman, R.; Morgan, M.A.; Mannel, R.; Yamada, S.D.; Mutch, D.; Rodgers, W.H.; et al. Selumetinib in women with recurrent low-grade serous carcinoma of the ovary or peritoneum: An open-label, single-arm, phase 2 study. *Lancet Oncol.* **2013**, *14*, 134–140. [[CrossRef](#)]
33. McGivern, N.; El-Helali, A.; Mullan, P.; McNeish, I.A.; Paul Harkin, D.; Kennedy, R.D.; McCabe, N. Activation of mapk signalling results in resistance to saracatinib (azd0530) in ovarian cancer. *Oncotarget* **2018**, *9*, 4722–4736. [[CrossRef](#)] [[PubMed](#)]
34. Liston, D.R.; Davis, M. Clinically relevant concentrations of anticancer drugs: A guide for nonclinical studies. *Clin. Cancer Res.* **2017**, *23*, 3489–3498. [[CrossRef](#)]
35. Aramburu, J.; Ortells, M.C.; Tejedor, S.; Buxadé, M.; López-Rodríguez, C. Transcriptional regulation of the stress response by mtor. *Sci. Signal.* **2014**, *7*, re2. [[CrossRef](#)] [[PubMed](#)]
36. Sato, E.; Olson, S.H.; Ahn, J.; Bundy, B.; Nishikawa, H.; Qian, F.; Jungbluth, A.A.; Frosina, D.; Gnjatic, S.; Ambrosone, C.; et al. Intraepithelial cd8+ tumor-infiltrating lymphocytes and a high cd8+/regulatory t cell ratio are associated with favorable prognosis in ovarian cancer. *Proc. Natl. Acad. Sci. USA* **2005**, *102*, 18538–18543. [[CrossRef](#)] [[PubMed](#)]
37. Zhang, L.; Conejo-Garcia, J.R.; Katsaros, D.; Gimotty, P.A.; Massobrio, M.; Regnani, G.; Makrigiannakis, A.; Gray, H.; Schlienger, K.; Liebman, M.N.; et al. Intratumoral t cells, recurrence, and survival in epithelial ovarian cancer. *N. Engl. J. Med.* **2003**, *348*, 203–213. [[CrossRef](#)] [[PubMed](#)]
38. Hamanishi, J.; Mandai, M.; Iwasaki, M.; Okazaki, T.; Tanaka, Y.; Yamaguchi, K.; Higuchi, T.; Yagi, H.; Takakura, K.; Minato, N.; et al. Programmed cell death 1 ligand 1 and tumor-infiltrating cd8+ t lymphocytes are prognostic factors of human ovarian cancer. *Proc. Natl. Acad. Sci. USA* **2007**, *104*, 3360–3365. [[CrossRef](#)]
39. Ye, Q.; Song, D.G.; Poussin, M.; Yamamoto, T.; Best, A.; Li, C.; Coukos, G.; Powell, D.J. Cd137 accurately identifies and enriches for naturally occurring tumor-reactive t cells in tumor. *Clin. Cancer Res.* **2014**, *20*, 44–55. [[CrossRef](#)]
40. Duhon, T.; Duhon, R.; Montler, R.; Moses, J.; Moudgil, T.; de Miranda, N.F.; Goodall, C.P.; Blair, T.C.; Fox, B.A.; McDermott, J.E.; et al. Co-expression of cd39 and cd103 identifies tumor-reactive cd8 t cells in human solid tumors. *Nat. Commun.* **2018**, *9*, 2724. [[CrossRef](#)]
41. Simoni, Y.; Becht, E.; Fehlings, M.; Loh, C.Y.; Koo, S.-L.; Teng, K.W.W.; Yeong, J.P.S.; Nahar, R.; Zhang, T.; Kared, H.; et al. Bystander cd8+ t cells are abundant and phenotypically distinct in human tumour infiltrates. *Nature* **2018**, *557*, 575–579. [[CrossRef](#)]
42. Canale, F.P.; Ramello, M.C.; Nuñez, N.; Furlan, C.L.A.; Bossio, S.N.; Serrán, M.G.; Boari, J.T.; Del Castillo, A.; Ledesma, M.; Sedlik, C.; et al. Cd39 expression defines cell exhaustion in tumor-infiltrating cd8+t cells. *Cancer Res.* **2018**, *78*, 115–128. [[CrossRef](#)] [[PubMed](#)]

43. Jansen, C.S.; Prokhnevskaya, N.; Master, V.A.; Sanda, M.G.; Carlisle, J.W.; Bilen, M.A.; Cardenas, M.; Wilkinson, S.; Lake, R.; Sowalsky, A.G.; et al. An intra-tumoral niche maintains and differentiates stem-like cd8 t cells. *Nature* **2019**, *576*, 465–470. [[CrossRef](#)]
44. Przystal, J.M.; Becker, H.; Canjuga, D.; Tsiami, F.; Anderle, N.; Keller, A.-L.; Pohl, A.; Ries, C.H.; Schmittnaegel, M.; Korinetska, N.; et al. Targeting csf1r alone or in combination with pd1 in experimental glioma. *Cancers* **2021**, *13*, 2400. [[CrossRef](#)] [[PubMed](#)]
45. Walter, B.; Canjuga, D.; Yüz, S.G.; Ghosh, M.; Bozko, P.; Przystal, J.M.; Govindarajan, P.; Anderle, N.; Keller, A.L.; Tatagiba, M.; et al. Argyrin f treatment-induced vulnerabilities lead to a novel combination therapy in experimental glioma. *Adv. Ther.* **2021**, *4*, 2100078. [[CrossRef](#)]
46. Yu, G.; Wang, J. Significance of hyaluronan binding protein (hbabp1/p32/gc1qr) expression in advanced serous ovarian cancer patients. *Exp. Mol. Pathol.* **2013**, *94*, 210–215. [[CrossRef](#)] [[PubMed](#)]
47. Yu, H.; Liu, Q.; Xin, T.; Xing, L.; Dong, G.; Jiang, Q.; Lv, Y.; Song, X.; Teng, C.; Huang, D.; et al. Elevated expression of hyaluronic acid binding protein 1 (hbabp1)/p32/c1qbp is a novel indicator for lymph node and peritoneal metastasis of epithelial ovarian cancer patients. *Tumor Biol.* **2013**, *34*, 3981–3987. [[CrossRef](#)] [[PubMed](#)]
48. Barnett, B.; Kryczek, I.; Cheng, P.; Zou, W.; Curiel, T.J. Regulatory t cells in ovarian cancer: Biology and therapeutic potential. *Am. J. Reprod. Immunol.* **2005**, *54*, 369–377. [[CrossRef](#)]
49. Valeriote, F.; van Putten, L. Proliferation-dependent cytotoxicity of anticancer agents: A review. *Cancer Res.* **1975**, *35*, 2619–2630.
50. Vasey, P.A. Resistance to chemotherapy in advanced ovarian cancer: Mechanisms and current strategies. *Br. J. Cancer* **2003**, *89*, 23–28. [[CrossRef](#)]
51. Haygood, C.L.W. Ovarian cancer stem cells: Can targeted therapy lead to improved progression-free survival? *World J. Stem Cells* **2014**, *6*, 441. [[CrossRef](#)]
52. Bapat, S.A.; Mali, A.M.; Koppikar, C.B.; Kurrey, N.K. Stem and progenitor-like cells contribute to the aggressive behavior of human epithelial ovarian cancer. *Cancer Res.* **2005**, *65*, 3025–3029. [[CrossRef](#)] [[PubMed](#)]
53. Deng, J.; Wang, L.; Chen, H.; Hao, J.; Ni, J.; Chang, L.; Duan, W.; Graham, P.; Li, Y. Targeting epithelial-mesenchymal transition and cancer stem cells for chemoresistant ovarian cancer. *Oncotarget* **2016**, *7*, 55771–55788. [[CrossRef](#)]
54. Liu, S.; Sun, J.; Cai, B.; Xi, X.; Yang, L.; Zhang, Z.; Feng, Y.; Sun, Y. Nanog regulates epithelial-mesenchymal transition and chemoresistance through activation of the stat3 pathway in epithelial ovarian cancer. *Tumor Biol.* **2016**, *37*, 9671–9680. [[CrossRef](#)] [[PubMed](#)]
55. Lee, C.H.; Inoki, K.; Karbowiczek, M.; Petroulakis, E.; Sonenberg, N.; Henske, E.P.; Guan, K.L. Constitutive mtor activation in tsc mutants sensitizes cells to energy starvation and genomic damage via p53. *EMBO J.* **2007**, *26*, 4812–4823. [[CrossRef](#)]
56. Vadysirisack, D.D.; Baenke, F.; Ory, B.; Lei, K.; Ellisen, L.W. Feedback control of p53 translation by redd1 and mtorc1 limits the p53-dependent DNA damage response. *Mol. Cell. Biol.* **2011**, *31*, 4356–4365. [[CrossRef](#)] [[PubMed](#)]
57. Leontieva, O.V.; Blagosklonny, M.V. DNA damaging agents and p53 do not cause senescence in quiescent cells, while consecutive re-activation of mtor is associated with conversion to senescence. *Aging* **2010**, *2*, 924–935. [[CrossRef](#)] [[PubMed](#)]
58. Astle, M.V.; Hannan, K.M.; Ng, P.Y.; Lee, R.S.; George, A.J.; Hsu, A.K.; Haupt, Y.; Hannan, R.D.; Pearson, R.B. Akt induces senescence in human cells via mtorc1 and p53 in the absence of DNA damage: Implications for targeting mtor during malignancy. *Oncogene* **2012**, *31*, 1949–1962. [[CrossRef](#)] [[PubMed](#)]
59. Gajewski, T.F.; Schreiber, H.; Fu, Y.-X. Innate and adaptive immune cells in the tumor microenvironment. *Nat. Immunol.* **2013**, *14*, 1014–1022. [[CrossRef](#)]
60. Hwang, W.T.; Adams, S.F.; Tahirovic, E.; Hagemann, I.S.; Coukos, G. Prognostic significance of tumor-infiltrating t cells in ovarian cancer: A meta-analysis. *Gynecol. Oncol.* **2012**, *124*, 192–198. [[CrossRef](#)]
61. Curiel, T.J.; Coukos, G.; Zou, L.; Alvarez, X.; Cheng, P.; Mottram, P.; Evdemon-Hogan, M.; Conejo-Garcia, J.R.; Zhang, L.; Burow, M.; et al. Specific recruitment of regulatory t cells in ovarian carcinoma fosters immune privilege and predicts reduced survival. *Nat. Med.* **2004**, *10*, 942–949. [[CrossRef](#)]
62. Leem, G.; Park, J.; Jeon, M.; Kim, E.-S.; Kim, S.W.; Lee, Y.J.; Choi, S.J.; Choi, B.; Park, S.; Ju, Y.S.; et al. 4-1bb co-stimulation further enhances anti-pd-1-mediated reinvigoration of exhausted cd39⁺ cd8 t cells from primary and metastatic sites of epithelial ovarian cancers. *J. Immunol. Ther. Cancer* **2020**, *8*, e001650. [[CrossRef](#)] [[PubMed](#)]
63. Grönholm, M.; Feodoroff, M.; Antignani, G.; Martins, B.; Hamdan, F.; Cerullo, V. Patient-derived organoids for precision cancer immunotherapy. *Cancer Res.* **2021**, *81*, 3149–3155. [[CrossRef](#)] [[PubMed](#)]
64. Aisenbrey, E.A.; Murphy, W.L. Synthetic alternatives to matrigel. *Nat. Rev. Mater.* **2020**, *5*, 539–551. [[CrossRef](#)] [[PubMed](#)]
65. Kozłowski, M.T.; Crook, C.J.; Ku, H.T. Towards organoid culture without matrigel. *Commun. Biol.* **2021**, *4*, 1387. [[CrossRef](#)]
66. Ruifrok, A.C.; Johnston, D.A. Quantification of histochemical staining by color deconvolution. *Anal. Quant. Cytol. Histol.* **2001**, *23*, 291–299.

Appendix II:

Anderle, N., Schäfer-Ruoff, F., Staebler, A., Kersten, N., Koch, A., Önder, C., Keller, A-L., Liebscher, S., Hartkopf, A., Hahn, M., Templin, M., Brucker, SY., Schenke-Layland, K., Schmees, C. *Breast cancer patient-derived microtumors resemble tumor heterogeneity and enable protein-based stratification and functional validation of individualized drug treatment.* (PREPRINT available at Research Square, 2023; <https://doi.org/10.21203/rs.3.rs-2781727/v1>) - **Accepted:** 28 July 2023; **Published:** 18 August 2023: *J Exp Clin Cancer Res* **42**, 210 (2023). <https://doi.org/10.1186/s13046-023-02782-2>

Breast cancer patient-derived microtumors resemble tumor heterogeneity and enable protein-based stratification and functional validation of individualized drug treatment

Nicole Anderle^{1*}, Felix Schäfer-Ruoff¹, Annette Staebler², Nicolas Kersten^{3,4}, André Koch⁵, Cansu Önder⁵, Anna-Lena Keller¹, Simone Liebscher⁶, Andreas Hartkopf^{5,7}, Markus Hahn⁵, Markus Templin¹, Sara Y. Brucker^{5,8}, Katja Schenke-Layland^{1,6,8}, Christian Schmees^{1*}

¹NMI Natural and Medical Sciences Institute at the University of Tuebingen, 72770 Reutlingen, Germany

²Institute of Pathology and Neuropathology, Eberhard Karls University Tuebingen, 72076 Tuebingen, Germany

³Interfaculty Institute for Bioinformatics and Medical Informatics (IBMI), University of Tuebingen, 72076 Tuebingen, Germany

⁴FZI Research Center for Information Technology, 76131 Karlsruhe, Germany

⁵Department of Women's Health, University Women's Hospital, Eberhard Karls University Tuebingen, 72076 Tuebingen, Germany

⁶Institute of Biomedical Engineering, Department for Medical technologies and Regenerative Medicine, Eberhard Karls University Tuebingen, 72076 Tuebingen, Germany

⁷Department of Gynecology and Obstetrics, University Hospital of Ulm, 89081 Ulm, Germany

⁸Cluster of Excellence iFIT (EXC2180) "Image-Guided and Functionally Instructed Tumor Therapies", Eberhard Karls University Tuebingen, 72076 Tuebingen, Germany

*Email: nicole.anderle@nmi.de; christian.schmees@nmi.de

1. Abstract

Despite tremendous progress in deciphering breast cancer at the genomic level, the pronounced intra- and intertumoral heterogeneity remains a major obstacle to the advancement of novel and more effective treatment approaches. Frequent treatment failure and the development of treatment resistance highlight the need for patient-derived tumor models that reflect the individual tumors of breast cancer patients and allow a comprehensive analyses and parallel functional validation of individualized and therapeutically targetable vulnerabilities in protein signal transduction pathways. Here, we introduce the generation and application of breast cancer patient-derived 3D microtumors (BC-PDMs). Residual fresh tumor tissue specimens were collected from n=102 patients diagnosed with breast cancer and subjected to BC-PDMs isolation. BC-PDMs retained histopathological characteristics, and extracellular matrix (ECM) components together with key protein signaling pathway signatures of the corresponding primary tumor tissue. Accordingly, BC-PDMs reflect the inter- and intratumoral heterogeneity of breast cancer and its key signal transduction properties. DigWest®-based protein expression profiling of identified treatment responder and non-responder BC-PDMs enabled the identification of potential resistance and sensitivity markers of individual drug treatments, including markers previously associated with treatment response and yet undescribed proteins. The combination of individualized drug testing with comprehensive protein profiling analyses of BC-PDMs may provide a valuable complement for personalized treatment stratification and response prediction for breast cancer.

2. Keywords

Preclinical tumor model, tumor heterogeneity, therapy resistance, therapy sensitivity, protein profiling, breast cancer, anti-cancer drug efficacy

3. Background

According to the SEER (The Surveillance, Epidemiology, and End Results - Program) database, breast cancer (BC) remains the most common cancer in women. Despite a 5-year survival rate of 90% (all cancer stages), BC is the 2nd leading cause of cancer death in women. Since 1989, BC mortality rates have been reduced by 43%, primarily through early detection by mammography, improved local treatment, and increasingly effective systemic adjuvant therapies in early stages of cancer (1). Based on the genetic, morphologic, and clinical intertumoral heterogeneity, BC is classified into different subtypes. The WHO distinguishes 19 different histological subtypes including invasive BC, which infiltrate the stroma and surrounding breast tissue, and non-invasive, in-situ carcinomas, which are the preinvasive counterparts. If they arise in the mammary ducts, they are referred to as invasive ductal carcinomas (IDC) or ductal carcinoma in-situ (DCIS). Whereas invasive lobular carcinomas (ILC) and lobular carcinomas in-situ (LCIS) arise from the lobules of the mammary glands (2). The most common invasive subtype is IDC of no special type (NST) showing no distinct architectural features (3). IDC subtypes with defined, distinctive architectural features are less common. Global gene expression analyses have further classified BC into four molecular subtypes with distinct gene expression patterns: the hormone receptor-related luminal-A and luminal B tumors versus the hormone receptor-negative, HER2-enriched and basal-like tumors (4-6). These reflect different phenotypes, disease prognosis, treatment paradigms and responses to therapies (7-11). In clinical practice, BC stratification is performed by the immunohistochemical determination of routine pathologic markers such as estrogen receptor α (ER α), progesterone receptor (PgR) and human epidermal growth factor receptor 2 (HER2), and by semiquantitative evaluation of Ki-67. In this regard, BC is pathologically classified as ER α /PR-positive, HER2-positive or as triple-negative breast cancer (TNBC), which lack the expression of these receptors and can themselves be considered a very heterogeneous group of cancers (12, 13). Besides this intertumoral heterogeneity, enormous diversity of tumor cell profiles is also observed within the same tumor, termed intratumoral heterogeneity (14). Alterations in genome, epigenome/transcriptome, and proteome, in invasive capacity, proliferation, stemness, cell plasticity but also the extrinsic interplay with the tumor microenvironment (15) contribute to the heterogeneity of individual tumor cell subpopulations. This leads to diverse disease manifestations in individual patients and failure of systematic treatment (16). With regard to the TME, we are only at the beginning of our understanding of its interaction with the tumor and how it influences the response to therapy (17, 18). Apparently, different TME gene expression patterns alter BC phenotypes (19, 20). Despite the success of genomic expression analysis in classifying BC according to different gene signatures or revealing gene alterations, a comprehensive understanding of treatment failures due to extensive

tumor heterogeneity is still lacking (21, 22). Therefore, more effective therapies need to be developed and the mechanisms of resistance better understood. In particular, a personalized treatment approach based on functional analysis of protein expression data could help to improve treatment efficacy and patient outcome.

Here, we demonstrate the applicability of patient-derived microtumors (PDM) isolated from residual fresh mammary carcinoma tissue samples as an *ex vivo* 3D breast cancer model that not only consists of tumor cells but also of TME and extracellular matrix (ECM) components of the corresponding patient tumor. We successfully generated microtumor samples of different BC subtypes with histopathological features and ECM components corresponding to those of the original primary tumor tissue. Protein profiling of BC-PDMs by DigiWest™ revealed heterogeneous signaling pathway activity similar to the patient's tumor and reflected the intertumoral heterogeneity of BC. We combined functional drug testing with signaling pathway analyses in BC-PDMs to evaluate therapy responses and identified markers of treatment sensitivity/resistance.

4. Materials and Methods

4.1. Human specimen

Non-processed human breast tumor samples were collected after surgery and completion of pathological examination from patients with primary breast cancer as part of the publicly funded PRIMO project (Personalized medicine for tailored cancer therapies). Written informed consent was obtained from all participants prior to surgery. The research project was approved by the ethics commission at the Medical Faculty Tuebingen (project number #788/2018BO2). Clinical patient data for the above-mentioned samples were submitted in pseudonymized form. A total of $n = 102$ samples were obtained from consenting participants, who underwent surgery at Center for Women's Health, University Hospital Tuebingen. Inclusion criteria were individuals > 18 years of age who had given informed consent to participate in the project, with unilateral invasive primary and recurrent breast carcinomas regardless of ER-/PgR- and HER2-status, tumor size, nodal-status and grading. Enrolled patients did not receive neoadjuvant treatment. Patients with distant metastatic disease were excluded.

4.2. Generation of patient-derived microtumors from residual fresh breast tumor tissue

Fresh dissected breast tumor tissues were transported within DMEM/F12 culture media (Gibco) and subsequently processed as previously described (2022) (23). The isolation of patient-derived microtumors was adapted from Kondo et al. (24). Briefly, tumors were washed in HBSS (Gibco), fragmented with forceps, and digested with Liberase DH (Roche) for 2 hours at 37°C. The digested tissue was filtered through a 500 μm stainless steel mesh (VWR) followed by a 40 μm cell strainer (Corning). Tumor fragments retained by the cell strainer were washed in HBSS and cultured in suspension in StemPro® hESC SFM (Gibco) supplemented with 8 ng/ml FGF-basic (Gibco), 0.1 mM β -mercaptoethanol (Gibco), 1.8% BSA (Gibco) and 100 $\mu\text{g}/\text{ml}$ Primocin (Invivogen) in a cell-repellent culture dish (60x15mm) (Corning). The single-cell filtrate was used for the expansion of tumor-infiltrating lymphocytes in Advanced RPMI 1640 (GIBCO) supplemented with 2 mM glutamine (Gibco), 1% MEM vitamins (Gibco), 5% human serum (SigmaAldrich) and 100 $\mu\text{g}/\text{ml}$ primocin (Invivogen). IL-2 (100 U/ml), IL-7 (10 U/ml) and IL-15 (23.8 U/ml) (Peprotech) were freshly added to the culture media. CD3/CD28 Dynabeads (Milteny Biotech) were added for expansion.

4.3. Viability measurement of BC-PDMs using Calcein-AM live cell and SYTOX™ Orange dead cell stain

Viability of BC-PDMs was assessed by live/dead-cell staining using 6.6 μM Calcein-AM™ (Invitrogen) live cell stain and 5 μM SYTOX™ Orange nucleic acid dead cell stain

(Invitrogen). To visualize nuclei 1 $\mu\text{g}/\text{mL}$ of Hoechst 33258 (Invitrogen) was added. BC-PDMs were directly picked from the suspension culture and resuspended in staining solution consisting of DMEM/F12 phenol-red free media (Gibco) supplemented with StemPro® hESC supplement (Gibco), 8 ng/ml FGF-basic (STEMCELL Technologies), 0.1 mM 2-mercaptoethanol (Gibco), 1.8 % BSA (Gibco) and 100 $\mu\text{g}/\text{mL}$ primocin (Invivogen). After 30 min of incubation, z-stack images were taken using the Zeiss CellObserver Z1 (Carl Zeiss). Maximum intensity projections of the 3D z-stacks were generating using the ZEN software (Version 2.6). Imaris software (version 8.0) was used to create 3D surface masks for viable and dead cells in the FITC and TRITC channel. For each surface mask, the fluorescent intensity sums and the volume was measured. Fluorescent intensities were normalized to the total (BC-PDMs) volume (μm^3).

4.4. Histology and immunohistochemistry

For histology BC-PDMs were fixed for 1 hour in 4% Roti® Histofix (Carl Roth) at RT and incubated for 5 min in Harris Hematoxylin (Leica Biosystems), shortly washed in dH_2O and dehydrated in an ethanol series (2x 50% ethanol, 2x 70% ethanol, each for 15 min). Using Tissue-Tek® Cryomolds® (Sakura), BC-PDMs were embedded in Richard-Allan Scientific™ HistoGel™ (Thermo Fisher Scientific). Tissue processing was performed using the HistoCore PEARL (Leica Biosystems). After processing, BC-PDMs histogel-blocks were paraffin-embedded for sectioning. Three micrometer sections of FFPE BC-PDMs samples were cut. In contrast, corresponding PTT were snap frozen on dry ice and cut as cryosections (5-7 μm). PTT-cryosections were immersed in ice-cold 4% Roti® Histofix (Carl Roth) for 10 min at 2-4°C and washed afterwards 3x with PBS. Hematoxylin and eosin (H&E) as well as Movat-pentachrome staining was performed on BC-PDMs-FFPE and PTT-cryosections.

Immunohistochemical staining of BC-PDMs was performed using the Autostainer Link 48 (Agilent) in combination with the Dako PT Link (Agilent) for antigen-retrieval according to the manufacturer's recommendations. Detailed information of the used antibodies is listed below (Table 1). Stained FFPE/cryosections were imaged with Axio Scan Z1. All primary antibodies were validated in normal, healthy tissues as well as in FFPE and cryosections. DAB and collagen staining (Movat-pentachrome staining) was semi-quantified using ImageJ Fiji software. The color deconvolution plugin was used to separate stains using Ruifrok and Johnston's method for DAB stains (25), and manual deconvolution for collagen stain. The percentage of area positive for DAB/collagen was determined. Percent area fraction was measured as the percentage of pixels in the image or selection to which thresholds were applied. The certified pathologist was blinded for evaluation of microtumor H&E stainings.

Table 1. Antibodies for IHC staining.

Antibody	Manufacturer	Product No.	Additional reagents	Usage
rabbit anti-human ERalpha	Abcam	ab16660	Rb Linker Enhancer	1:30
rabbit anti-human HER2/ErbB2	Cell Signaling Technology	4290	Rb Linker Enhancer	1:80
mouse anti-human PgR	Dako	IR068	Ms Linker	R.T.U
rabbit anti-human cytokeratin 5	Abcam	ab64081	Rb Linker Enhancer	1:200
rabbit anti-human cytokeratin 6	Abcam	ab93279	Rb Linker Enhancer	1:50
mouse anti-human cytokeratin 18	Dako	IR618	Ms Linker Enhancer	R.T.U
rabbit anti-human FAPalpha	BioRad	AHP1322	Rb Linker	1:50
rabbit anti-human CD163	Abcam	ab182422	Rb Linker	1:200
mouse anti-human PD-L1	Dako	22C3	Ms Linker Enhancer	1:50
mouse anti-human CD8	Dako	IR623	-	R.T.U

4.5. Multiplex protein profiling via DigiWest

DigiWest was performed as described previously (26). Western blot was carried out using the NuPAGE system (Life Technologies) with a 4-12% Bis-Tris gel and PVDF membranes. Membranes were washed with PBST and proteins were biotinylated by adding 50 μ M NHS-PEG12-Biotin in PBST for 1 h. The membranes were washed with PBST and dried overnight. Each protein (Western-Blot) lane was cut into 96 strips of 0.5 mm each. Western Blot-strips were sorted by molecular weight into a 96-well plate (Greiner Bio-One). Proteins were eluted using a 10 μ l of elution buffer (8 M Urea, 1% Triton-X100 in 100 mM Tris-HCl pH 9.5). Proteins of each 96-well representing a distinct molecular weight fraction were coupled overnight to Neutravidin-coated MagPlex beads (Luminex) of a distinct color ID. Non-bound binding sites were blocked with 500 μ M deactivated NHS-PEG12-Biotin for 1 h. To reconstruct the original Western blot lane, the beads were pooled, with the color IDs representing the molecular weight fraction of the proteins. For antibody incubation 5 μ l of the DigiWest bead mixes were added to 50 μ l assay buffer (Blocking Reagent for ELISA (Roche) supplemented with 0.2% milk powder, 0.05% Tween-20 and 0.02% sodium azide) in a 96-well plate. In the next step, the assay buffer was discarded, 30 μ l of primary antibody solution was added per well to the DigiWest bead mixes and incubated overnight at 15°C on a shaker (for primary antibody list, see SI Materials). Bead mixes were washed 2x with PBST before adding 30 μ l secondary antibody (labeled with phycoerythrin – PE) solution. After 1h of incubation at 23°C, the bead mixes were washed 2x in PBST. Read-outs were performed using the Luminex FlexMAP 3D instrument. Protein bands were displayed as peaks by plotting the molecular weight against the corresponding median signal intensity. To integrate peaks of an expected molecular weight, a macro-based algorithm created in excel was

applied. The local background was subtracted and for each peak the integral of the area was calculated (averaged fluorescent intensities – AFI). The resulting signals were normalized to total protein amount loaded onto the beads, if applicable centered on median of all BC-PDMs/PTT or only BC-PDMs samples. Subsequently, weak protein signals were determined as “lower detection limit minus one”. Further data processing is described in the figures.

4.6. Drug testing in BC-PDMs using CellTox Green™ Cytotoxicity Assay

To assess cell killing effects of different anti-cancer therapies and targeted therapies for breast cancer in BC-PDMs, the real-time CellTox™ Green Cytotoxicity assay (Promega) was performed according to manufacturer’s protocol. After the isolation of BC-PDMs from breast carcinoma specimen, the BC-PDMs were cultured for 1-2 weeks prior efficacy compound testing. The assays were performed according to manufacturer’s protocol. For each treatment, three to five replicates each with $n = 15$ BC-PDMs were prepared in phenol-red free BC-PDMs culture medium with a total volume of 150 μ l. A proprietary cyanine dye binds to DNA in compromised cells leading to enhanced fluorescent signal. The dye is excluded from viable cells and thereby shows no increase in fluorescence. The fluorescent signal produced by the dye binding to DNA is therefore proportional to cell death. The dye was diluted 1:1000 and signals were measured as relative fluorescent unit (RFU) (485–500 nm Excitation / 520–530 nm Emission) using the Envision Multilabel Plate Reader 2102 and Tecan Spark Multimode Plate Reader. RFU values were background-corrected and treatment to DMSO (H_2O) control fold changes were calculated for each measured time point. Outliers were excluded using Iglewicz and Hoaglin’s robust test for multiple outliers applying a recommended Z-score of ≥ 3.5 (27).

4.7. Statistical analysis

Statistical analysis was performed using GraphPad Prism software. Statistical methods are illustrated in the respective figure legends. For Boxplot data, whiskers represent quartiles with minimum and maximum values and the median. Datasets with no normal distribution were analyzed with unpaired, two-tailed Mann-Whitney-U-test, otherwise as indicated. For all analyses, p values < 0.05 were considered statistically significant. Recommended post-hoc tests were applied for multiple comparisons. Data is analyzed as mean with standard error of the mean (SEM).

5. Results

5.1. BC-PDMs can be isolated from breast tumor tissues of different types with high viability

We previously established a novel 3D platform consisting of patient-derived microtumors (PDM) and tumor infiltrating lymphocytes (TILs) to identify treatment responses and therapeutic vulnerabilities in ovarian cancer and glioblastoma (23, 28, 29). Here, we aimed to extend the PDM and TIL isolation (Figure S1) method to BC. Isolation and expansion of TIL populations was successful in >95% of analyzed tissue samples with an average TIL viability of >90% (Figure S1A-B). Multicolor flow cytometry analyses identified the presence of heterogenous subpopulations of regulatory and exhausted T cell populations (Figure S1C-H). The study enrolled patients over 18 years of age diagnosed with BC of all molecular subtypes. In total, we obtained $n = 102$ residual fresh mammary carcinoma tissue samples from debulking surgeries conducted at the University Hospital Tuebingen (Table S1). To analyze the viability of BC-PDMs after the isolation from BC specimen, we combined live-dead cell staining with 3D spinning disc confocal microscopy. As shown in Figure 1A, viable cells were stained with Calcein-AM, dead cells with SYTOX™ Orange and nuclei with Hoechst dye. Comparing the fluorescent intensities of viable and dead cells normalized to the total measured volume (μm^3) in $n = 27$ BC-PDMs models (Figure 1B), the number of viable cells was significantly higher than that of dead cells (Wilcoxon signed rank test, $p < 0.001$). Within the $n = 27$ BC-PDMs samples, microtumors had variable sizes, with an average area of $59261 \mu\text{m}^2$, a maximum area of $888481 \mu\text{m}^2$ and a minimum area of $7003 \mu\text{m}^2$ (Figure 1C, Table S2). The overall success rate of BC-PDMs isolation from $n = 102$ breast carcinomas was > 75%. We were able to isolate more than 100 PDM per sample from 50% of the tissue samples obtained (Figure 1D). In 25.5% of cases, PDM were generated with less than $n = 100$ PDM per sample, while in the remaining 24.5%, no PDM were recovered from the tissue sample. In total, we successfully established $n = 77$ BC microtumor samples. Depending on the number of PDM recovered per sample, different downstream analyses could be performed such as immunohistochemistry (IHC), anti-cancer drug efficacy testing and/or protein profiling (see below). To determine whether the success rate of BC-PDMs isolation was related to specific clinical features of the original primary tumor, we correlated the available clinical data of the corresponding tumor samples and the obtained BC-PDMs models (including samples with > 100 isolated PDM) (Figure 1E). The success rate of BC-PDMs isolation appeared to be largely independent of clinical features of the corresponding primary tumor tissue (PTT). BC-PDMs were successfully isolated from breast tumor tissue samples regardless of tumor grade, histological tumor type and hormone receptor status.

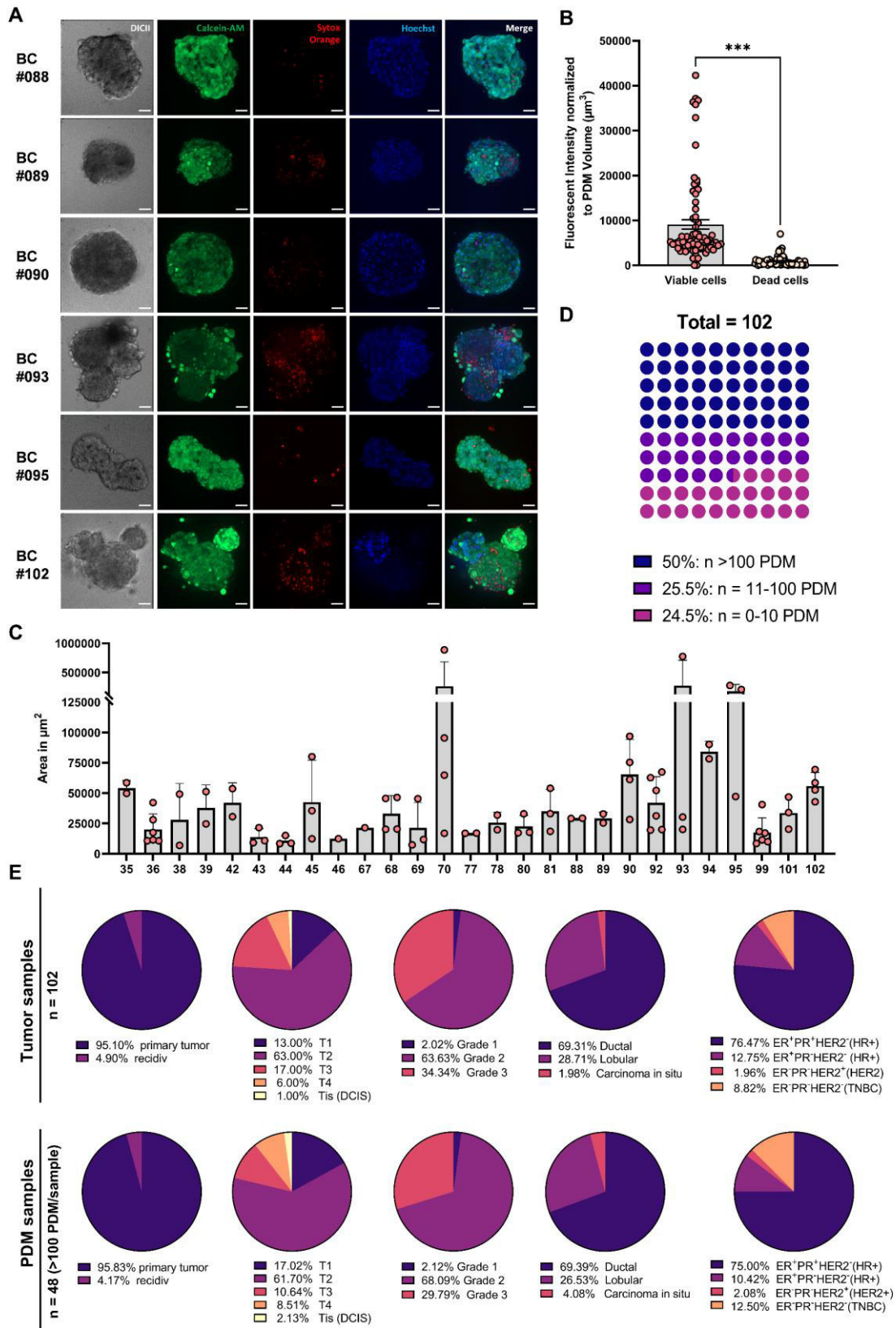


Figure 1. Isolation success of BC-PDMs. (A) Live-dead cell staining of isolated breast cancer (BC) BC-PDMs from representative breast carcinoma tissue samples. BC-PDMs were stained with Calcein-AM (viable cells), SYTOX™ Orange (dead cells) and Hoechst 33258 (nuclei). Scale bars 50 μm . (B) Quantification of viable and dead cells in $n = 27$ BC models (on average three BC-PDMs per model) reveals high viability of BC-PDMs. Fluorescent intensities and volumes (μm^3) were assessed using the Imaris Software. Wilcoxon paired signed rank test, $***p < 0.001$. (C) Area measurement of BC-PDMs from $n = 27$ BC models. Data are shown as mean values with SD. (D) Success rate of microtumor isolation from $n = 102$ breast carcinomas. 50% of BC BC-PDMs models reached a total number of more than 100 single microtumors. (E) Correlation of BC-PDMs isolation success rate and clinical characteristics of corresponding breast carcinomas tissue samples.

5.2. Histotype-specific pathological characteristics of breast tumor tissue are conserved in corresponding BC-PDMs.

Breast carcinomas form a heterogeneous group of tumors and show high variability in morphologic features, e.g. degree of pleomorphism, cellular atypia, mitotic activity or stromal circumference. Yet, there are morphological features characteristic of different histologic subtypes. Among others, tumor cells form nests, clusters, cords, trabeculae, or single file lines ("Indian File") (30) depending on the specific sub-type. Using H&E staining, a certified pathologist compared the histopathological and cytological characteristics of the isolated BC-PDMs and the corresponding PTT. We divided the specimens according to histological classification into invasive ductal carcinomas of no special type (NST) and invasive lobular carcinomas (ILC) with or without in-situ components. Tumor cells of NST-PTT formed irregular invasive nests/clusters, cords, and sheets within the stroma, in some tissues with glandular features (Figure 2A). PTT further displayed distinct ascitic structures filled with tumor cells (#33, #68), tubular structures (#58, #68) with small lumina, papillary structures or no distinct architecture. Similar to corresponding PTT, tumor cells of NST-BC-PDMs formed solid (cohesive), papillary nests with closely spaced cells (BC-PDMs/PTT: #33, #42, #58, #68, #90) and a clear separation from the ECM compartment. In addition, glandular structures were also evident within NST-BC-PDMs (#31 and #45). The histopathologic architecture of ILCs with in-situ sites is more specific than that of IDC. The lobular ascites of in-situ lesions retained their overall structure in PTT and were filled with small, round, monomorphic epithelial cells almost without lumen (e.g. #70, #86). Infiltrating cells within ILCs were dispersed with poor cohesion and grew in slender strands or single files (so called "Indian Files") or concentrically around ducts or lobules (PTT e.g. #25, #70, #86). Tumor cells of ILC-BC-PDMs were mostly discohesive and dissociated in the surrounding stromal tissue (#25, #53, #86, #92, #102), thus resembling primary infiltrating tumor lesions (Figure 2B). This histological feature was also found in NST-BC-PDMs #96. Overall, pathological evaluation of BC-PDMs specimens revealed histological similarity to breast tumor tissue in 97.5% of cases (n = 39/40) and to histological tumor type (IDC/NST) in 95% of cases (n = 36/38) (Figure 2C). Stromal compartments were present in 57.5% of cases (n = 23/40). In result of comparison of the cytopathology of BC-PDMs and corresponding PTT, similar cellular atypia was found. While some BC-PDMs consisted of small, rather homogenous cells without prominent nucleoli (e.g. #25, #29, #45, #53), other samples exhibited moderate (#31, #33, #58, #96) to strong nuclear pleomorphism (#68, #70, #86, #90, #92, #102) with large, hyperchromatic nuclei and prominent nucleoli. Most BC-PDMs resembled a moderate nuclear grade (n = 21) with moderate hyperchromasia (n = 19). While 20.5% (n = 8/39) of samples had a similar nuclear grade of BC-PDMs and corresponding PTT, the majority

(59%) of BC-PDMs had a nuclear grade decreased by 1 degree (Figure S2A). In summary, BC-PDMs largely resemble the histopathology of the corresponding primary tumor tissue.

5.3. BC-PDMs contain extracellular matrix components of the original tumor tissue

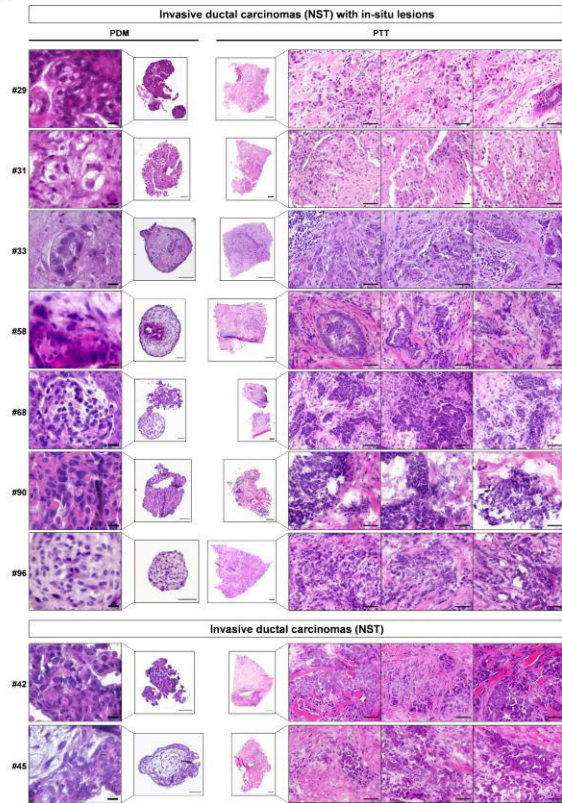
The ECM, representing a complex network of tissue fibers, glycoproteins (e.g. elastin, laminin, fibronectin), proteoglycans (PGs), and glycosaminoglycans (GAGs), not only provides stability and a reservoir for e.g. growth factors, but also plays a role in breast tumorigenesis, invasiveness (31, 32) and therapy response (33). Furthermore, ECM stiffness and density were found to correlate with prognosis in breast cancer (34) (35). To evaluate and compare the ECM within BC-PDMs and corresponding PTT, we used the Movat-pentachrome staining to visualize different components of connective tissue on a single slide (36). In PTT sections, the predominant ECM components were PGs/GAGs (cyan blue) and collagen fibers (yellow), which mostly overlapped (green) (Figure 2D). In all PTT, dense collagen networks were detected in close proximity to the tumor masses due to increased collagen deposition. This leads to the “stiffening” of the tissue (31). The collagen fibers exhibited different morphologies: short and wavy (e.g. PTT #29), thin and linear (e.g. PTT #31) or thick and linear (e.g. #36, #53). Most notable were dense and thick collagen fibers wrapped around tumor masses (e.g. PTT #31, 58), especially in stromal areas adjacent to in-situ lesions (e.g. PTT #36, #86, #102). Tumor borders were either relatively smooth, with collagen fibers drawn at a tangential angle around the tumor (e.g. PTT #86) or oriented perpendicular in the direction of cell invasion (e.g. PTT #58) (Provenzano, 2006 #522). Corresponding BC-PDMs exhibited ECM components to a lesser extent compared to primary tissue. Despite limited enzymatic tissue disruption during BC-PDMs isolation with collagenase I and II, we detected collagen expression (yellow/green) in the corresponding BC-PDMs (e.g. BC-PDMs #29, #36, #58, #53, #70). Compared to tumor masses in the PTT, which are surrounded by thick collagen fibers, the arrangement of collagen in BC-PDMs was less specific. In BC-PDMs, the collagen rather formed a backbone structure for the tumor cells. In general, BC-PDMs appeared like small tumor fragments excised from tumor masses of the corresponding primary tumor tissue and consisted of the inner tumor cell mass with its ECM components, but without the framing collagen fibers. In addition to cross-linked collagen-fibers, PGs/GAGs (cyan blue) were found within tumor masses/islets of the PTT (e.g. #29, #58, #53, #70) and demarcated tumor masses from the stroma as a single layer separated from collagen fibers (e.g. PTT #58, #86, #102). PGs/GAGs were found in BC-PDMs when their expression within tumor masses in corresponding PTT was high (e.g., BC-PDMs #29, 31, #58). Elastic fibers (black) were mostly attached to collagen fibers (e.g. PTT #53, #86, #102) and were more abundant in ILC compared to IDC (NST) tissues. In contrast to other BC-PDMs, the ECM of BC-PDMs #102 exhibited elastic fibers, as in the

corresponding primary tumor. Further, mucin (blue/gray) secreted by tumor cells was found in sections of PTT #31 and #86 and in the corresponding BC-PDMs. Different amounts of collagen were observed between ILC and NST tumors, both in PTT and PDM samples (Figure 2E). Within ILC-PTT, significant higher amounts of collagen fibers were detected compared to NST-PTT (Figure 2F), as previously reported (37). Collagen deposition in PDM was reduced as compared to corresponding PTT sections as expected due to the restricted amount of BC-PDM available for these analyses. Data showed a non-significant trend towards higher collagen deposition in ILC BC-PDM (Figure 2E-F). In conclusion, the Movat-pentachrome staining allowed the visualization of different ECM components of the primary tumor within BC-PDMs. Compared to whole tumor masses in tumor tissues, the ECM compartments in BC-PDMs occur to a lesser extent and in slightly different arrangement.

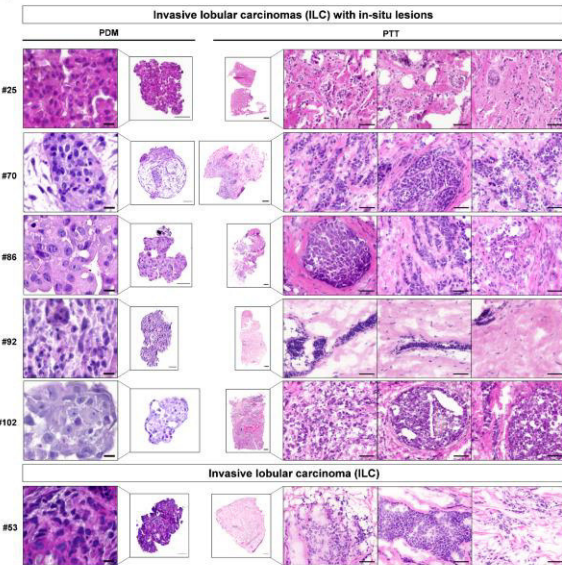
5.4. Immunohistochemical analysis of hormone receptor expression enables distinction of BC-PDMs isolated from hormone receptor positive and TNBC primary tumors.

To further characterize BC-PDMs, we performed immunohistochemistry (IHC) analysis of FFPE-BC-PDMs sections. We examined the expression of hormone receptors, cytokeratins as well as cancer-associated fibroblasts (CAFs) and immune cell markers using DAB staining. To analyze the expression of clinical molecular markers, we stained BC-PDMs sections for ER α , PgR and HER2. BC-PDMs were classified as hormone receptor positive (HR+) or triple negative (TNBC) as determined by pathologic evaluation of the primary tumor (Figure 3A). TNBC is an aggressive type of BC usually with higher grade, higher rate of early recurrence and a worse 5-year prognosis (38-41). It is defined by lacking expression of hormone receptors and HER2. For each tissue sample, the corresponding immunoreactive scores (IRS) and HER2 scores (0-3) were determined (Table S1). ER α and PgR staining of BC-PDMs was consistent with the corresponding clinical classification and was increased in BC-PDMs originating from HR+ PTT (Figure 3B). The level of ER α and PgR expression varied within HR+ BC-PDMs. In contrast, HR expression was strongly reduced in TNBC-PDMs. HER2 was detectable in HR+ BC-PDMs sample #10 and #37. However, HER2 expression in BC-PDMs #37 did not resemble its clinical HER2 score, which was reported to be zero. In conclusion, IHC staining enabled the identification of BC-PDMs isolated from clinical HR+ breast tumors and those isolated from clinical TNBC tumors based on hormone receptor expression.

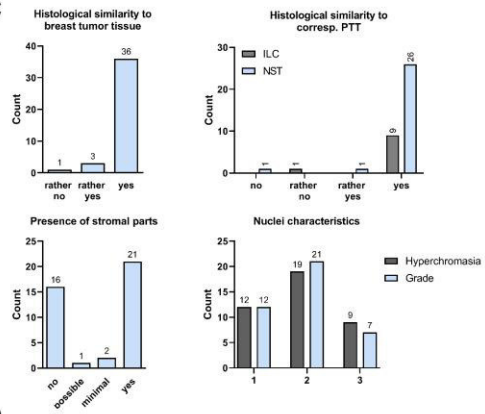
A



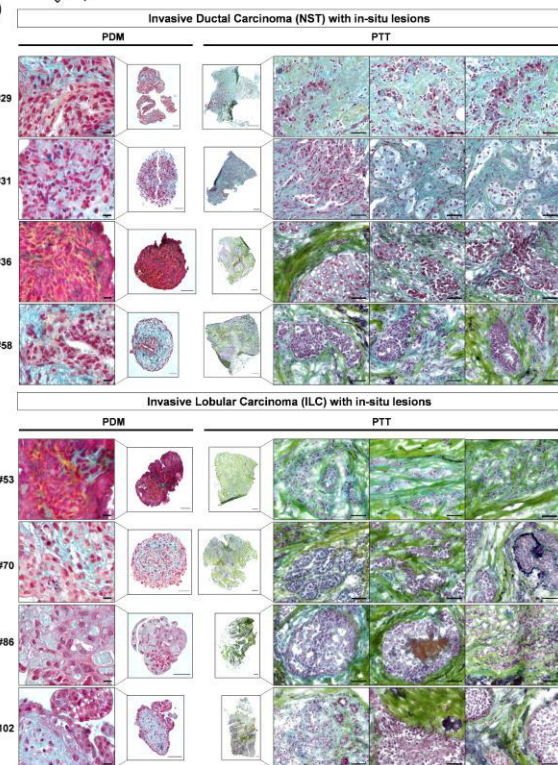
B



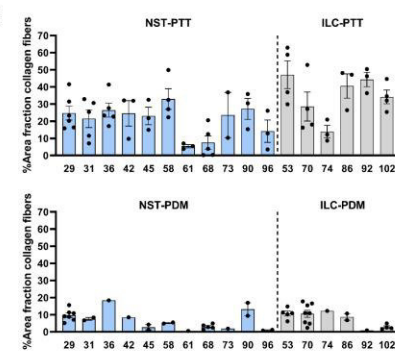
C



D



E



F

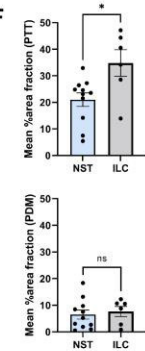


Figure 2. Histopathology and cytology of BC-PDMs and corresponding PTT. H&E staining of BC-PDMs and corresponding primary, (A) invasive ductal breast carcinomas (NST) with/without ductal in-situ (DCIS) lesions and (B) invasive lobular breast carcinomas (ILC) with/without lobular in-situ (LCIS) lesions. (C) Pathological evaluation of BC-PDMs. $n = 39/40$ BC-PDMs resembled histopathology of breast carcinomas, $n = 36/38$ of the corresponding primary tumor histotype (NST/ILC; NST/ILC histology not available for one sample; one other sample classified as medullary carcinoma and excluded from comparison of NST and ILC BC-PDMs) and $n = 23/40$ BC-PDMs displayed stromal parts. Histopathological tumor characteristics of BC-PDMs were assessed such as hyperchromasia and nuclei differentiation (nuclear grade 1: nuclei with little variation in size and shape; grade 3: large nuclei with high variation in size and shape; grade 2: nuclei show features between 1 and 3. (D) Movat-pentachrome staining revealed connective tissue compartments in BC-PDMs and PTT e.g. collagen fibers (yellow), PGs/GAGs (cyan blue), collagen/PGs/GAGs-superimposition (green), mucins (blue) and elastin (black; representative images shown for $n = 8$ matched pairs of BC-PDMs and corresponding PTT). (E) Amount of collagen fibers within BC-PTT and BC-PDMs. Collagen fibers are measured semi-quantitatively as %-area fraction. RGB images were unmixed by subtractive mixing (color deconvolution) via ImageJ. (F) Averaged %-area fraction of BC-PTT and BC-PDM ($n = 17$) samples shown in (E). Data are mean with SEM. * $p < 0.05$, ** $p < 0.01$, *** $p < 0.001$. Unpaired, parametric t-test. Scale bars BC-PDMs: $50 \mu\text{m}/10 \mu\text{m}$ (zoom); PTT: $500 \mu\text{m}/50 \mu\text{m}$ (zoom; paired sections of BC-PDMs and corresponding PTT specimen were available from $n=17$ samples displaying stromal parts for Movat-pentachrome stainings).

5.5. BC-PDMs display differential expression of luminal and basal cytokeratins

Since cytokeratin (CK) expression is thought to be stable throughout carcinogenesis (42), CKs are studied as differentiation markers in precancerous breast lesions. Breast tissue normally consists of a stratified epithelium with luminal epithelial cells surrounded by a basement membrane composed of myoepithelial cells, both with different CK phenotypes (43, 44). Breast carcinomas are found to express different CKs, such as the luminal subtype expressing luminal epithelial CKs (CK8/CK18/CK19) or the basal subtype expressing basal myoepithelial high molecular weight (HMW) CKs (CK5/CK6/ CK7/CK14) (4, 45, 46). Nevertheless, some breast tumors were shown to express both types of CKs (44, 47). Here, we analyzed CK5, CK6 and CK18 staining of HR+ and TNBC-PDMs. We found highly heterogenous staining of CKs in HR+ and TNBC -PDM. The heterogenous CK expression allowed us to subdivide the BC-PDMs based on CK expression. Thus, we divided HR+ BC-PDMs into four groups based on the evaluated CK expression: CK5-/CK18+ (luminal, differential glandular phenotype), CK5+ (basal), CK5/6+ (basal, stem cell phenotype) and CK5/6/18+ (intermediate glandular phenotype) (48)(Figure 3C). CK5-/CK18+-PDM showed significantly higher CK18 expression compared to CK5 (** $p = 0.004$) or CK6 (** $p = 0.005$) (Figure 3D). The abundances of CK5 and CK6 were significantly higher in the CK5+ ($p = 0.006$) and CK5/6+ ($p = 0.020$) groups compared to the CK5-/CK18+ group. Some HR+ BC-PDMs were positive for all three CKs. Comparing the CK expression between HR+ BC-PDMs and TNBC -PDM, we found significantly increased CK18 expression ($p = 0.006$), a marker for luminal carcinomas, in HR+ BC-PDMs (Figure 3D). TNBC BC-PDMs did not show CK18 expression, but moderate expression of CK5/6. This is consistent with the literature (44). As a hallmark of EMT, lack of CK18 expression has been associated with tumor progression (49) as it promotes cancer cell migration (50). Two of the four TNBC -PDM analyzed here showed strong CK5 expression, and BC-PDMs #38 also displayed high CK6 expression. Due to high CK5/6 positivity correlating with poorer prognosis (51), TNBC -PDM #38 was defined as a basal-like subtype of TNBC. Overall, CK5/6 expression was not

significantly different among HR+ and TNBC -PDMs (Figure 3D). When ILC and NST BC-PDM were compared, ILC BC-PDM showed a non-significant trend towards higher expression of the HMW cytokeratins (CK5/6), whereas NST BC-PDM showed a non-significant trend towards higher expression of luminal CK18 (Figure 3E). We next analyzed additional markers such as FAP α , associated with CAFs (cancer-associated fibroblasts), and immune cell markers CD163, CD8 and PD-L1 (Figure 3F). PD-L1, a T cell inhibitory checkpoint marker, and CD8, a marker for cytotoxic T cells, were mostly absent from BC-PDMs except for BC-PDMs #70. CD8⁺ T cells were detected in BC-PDMs #78. Sporadic expression of CD163 indicating the presence of M2 macrophages was found in BC-PDMs

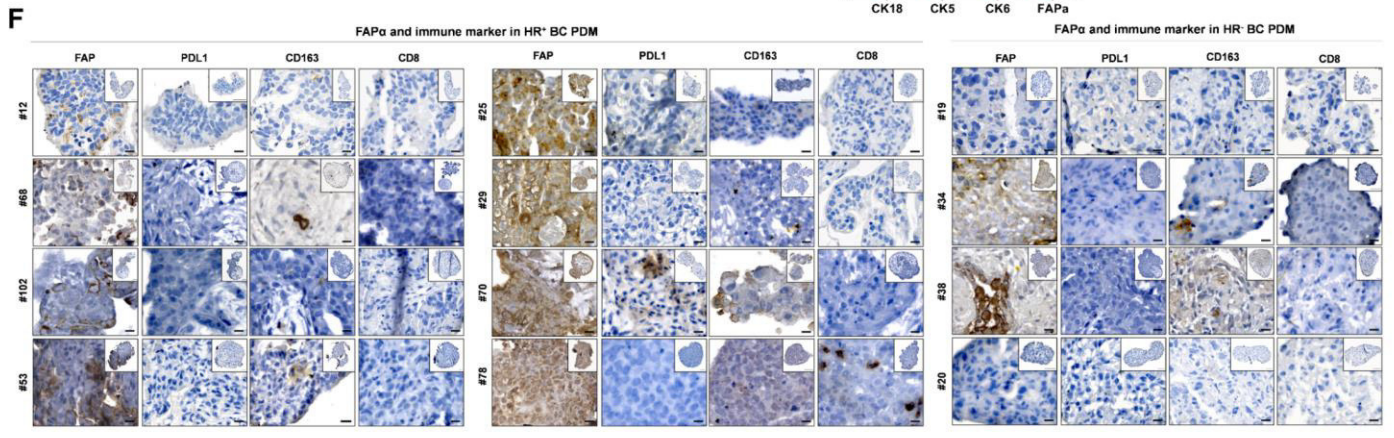
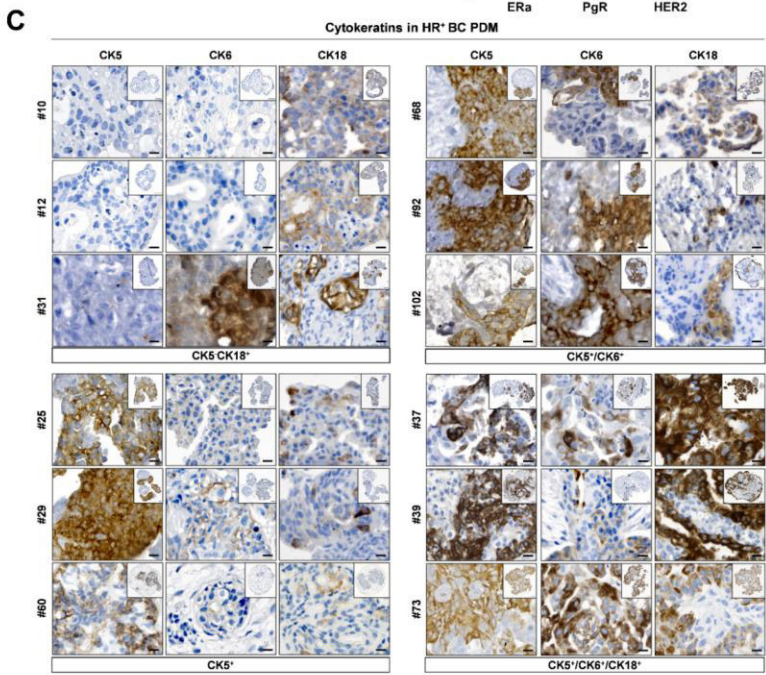
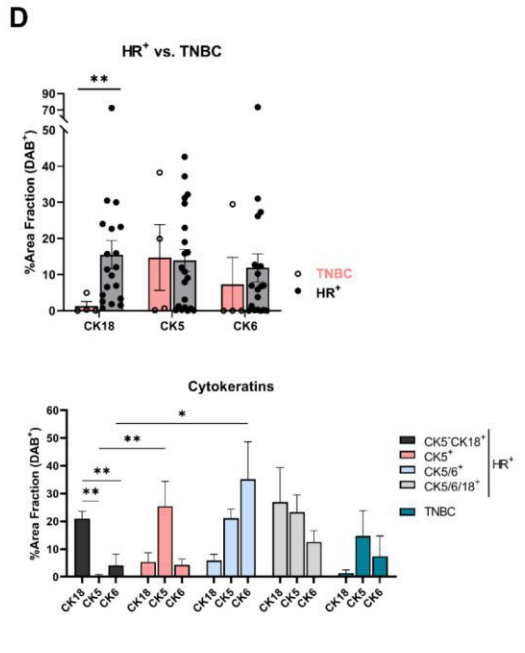
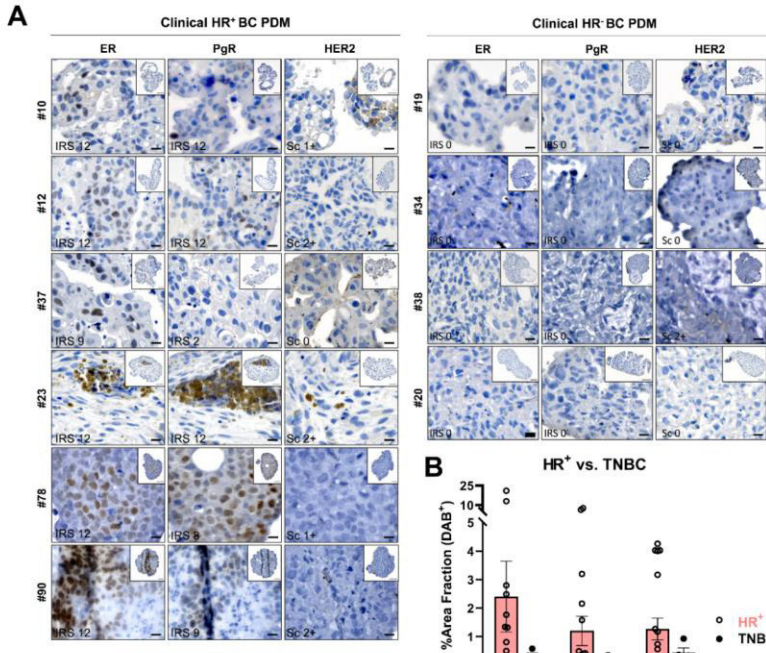


Figure 3. Immunohistochemical analysis of breast cancer specific and immune cell markers in BC-PDMs.

DAB staining was analyzed semi-quantitatively as %-area fraction of a BC-PDMs. RGB images were unmixed by subtractive mixing (color deconvolution) using ImageJ software. (A) Hormone receptor (HR) DAB staining of clinically classified HR+ BC-PDMs vs. TNBC BC-PDMs. Clinically assessed immunoreactive scores (IRS) from primary tumor are indicated. HR+ BC-PDMs were arranged in ascending order of ER α expression (B) HR+ BC-PDMs have increased HR expression (ER α , PgR, HER2) compared to TNBC BC-PDMs. (C) DAB staining of luminal cytokeratin (CK18) and basal cytokeratins (CK5 and CK6). BC-PDMs were grouped into four groups according to CK staining: CK5-CK18⁺, CK5⁺, CK5/6⁺ and CK5/6/18⁺. (D) Significantly elevated expression of luminal CK18 vs. basal CK5/CK6 in HR+ compared to TNBC BC-PDMs. Mann-Whitney U test, ** $p = 0.006$. Differences in CK18, CK5 and CK6 expression in HR+ and TNBC BC-PDMs according to their classification into the previously determined groups. Within group: One-way ANOVA, Holm-Šidák's multiple comparisons test. Different group comparison: Two-way ANOVA, Holm-Šidák's multiple comparisons test. (E) Differences in CK and FAP α expression in ILC BC-PDMs vs. NST BC-PDMs. NST-BC-PDMs show higher levels of CK18, while ILC-BC-PDMs show significant higher levels of FAP α . Mann-Whitney U-test, * $p = 0.028$. Both ILC/NST-BC-PDMs express basal CK5 and 6. (F) DAB staining of FAP α and immune markers in BC BC-PDMs grouped into HR+ and TNBC. For HR+ BC-PDMs, BC-PDMs were arranged in ascending order of FAP α expression. Data are mean with SEM. * $p < 0.05$, ** $p < 0.01$, *** $p < 0.001$. ER α : estrogen receptor alpha; PgR: progesterone receptor; HER2: HER2/neu-ErbB2 receptor.

(e.g. #68, #53, #70, #34). In contrast, FAP α was detectable in all stained BC-PDMs, to varying degrees. Among them, ILC-BC-PDMs showed significantly stronger FAP α staining (Figure 3E, $p = 0.028$) in accordance with the literature (52). Significant differences between TNBC and HR+ BC-PDMs were not identified. In conclusion, BC-PDMs largely reflect the hormone receptor status of the corresponding tumor tissue and exhibit heterogeneous expression of CKs and FAP α , which are markedly different in HR+ and TNBC and ILC-NST BC-PDMs. In addition, immune cell markers could be identified sporadically in BC-PDMs and independent of hormone receptor status.

5.6. Protein expression and signaling pathway activity of BC-PDMs correlate with corresponding primary tumors

Following histological characterization, we extended the comparison of BC-PDMs with corresponding primary tumor tissues by in-depth quantitative protein profiling analyses. We therefore measured protein expression and activity of key signal transduction pathways in $n = 20$ matched BC-PDMs-PTT pairs employing the DigiWest® technology (26). In this way, we generated protein profiling datasets covering 142 total and phosphorylated proteins (raw data: Table S3; BC-PDMs-PTT data: Table S4). The analyzed profiling panel comprised proteins from the cell cycle, Jak/STAT, MAPK, RTK, PI3K/Akt, EMT/cytoskeleton and Wnt signaling pathways. Pearson correlation revealed an overall high, positive correlation of averaged protein signals between matched BC-PDMs and PTT with $P_r = 0.856$ ($p < 0.001$; Figure 4A). Furthermore, comparison of signaling pathway activity and expression of breast cancer-related proteins, resulted in no significant differences. Overall, the average protein expression of BC-PDMs resembled that of matched breast cancer tissue (Figure 4B, Table S5). Subsequently, changes in protein abundance were determined between BC-PDMs and PTT pairs. In total, $n = 18$ analytes displayed significant differences in expression ($-\log_{10}(q) > 1.3$) and a \log_2 fold change of at least $|1|$ (Figure 4C-D). BC-PDMs had increased protein levels of the cytoskeletal protein cytokeratin 5 and 6 (CK5/6), while expression of immune cell markers CD11c, CD16, CD68, CD8 alpha, CD25, PD1 and PD-L1 were decreased. This is consistent with our IHC data, demonstrating that BC-PDMs are small tumor fragments

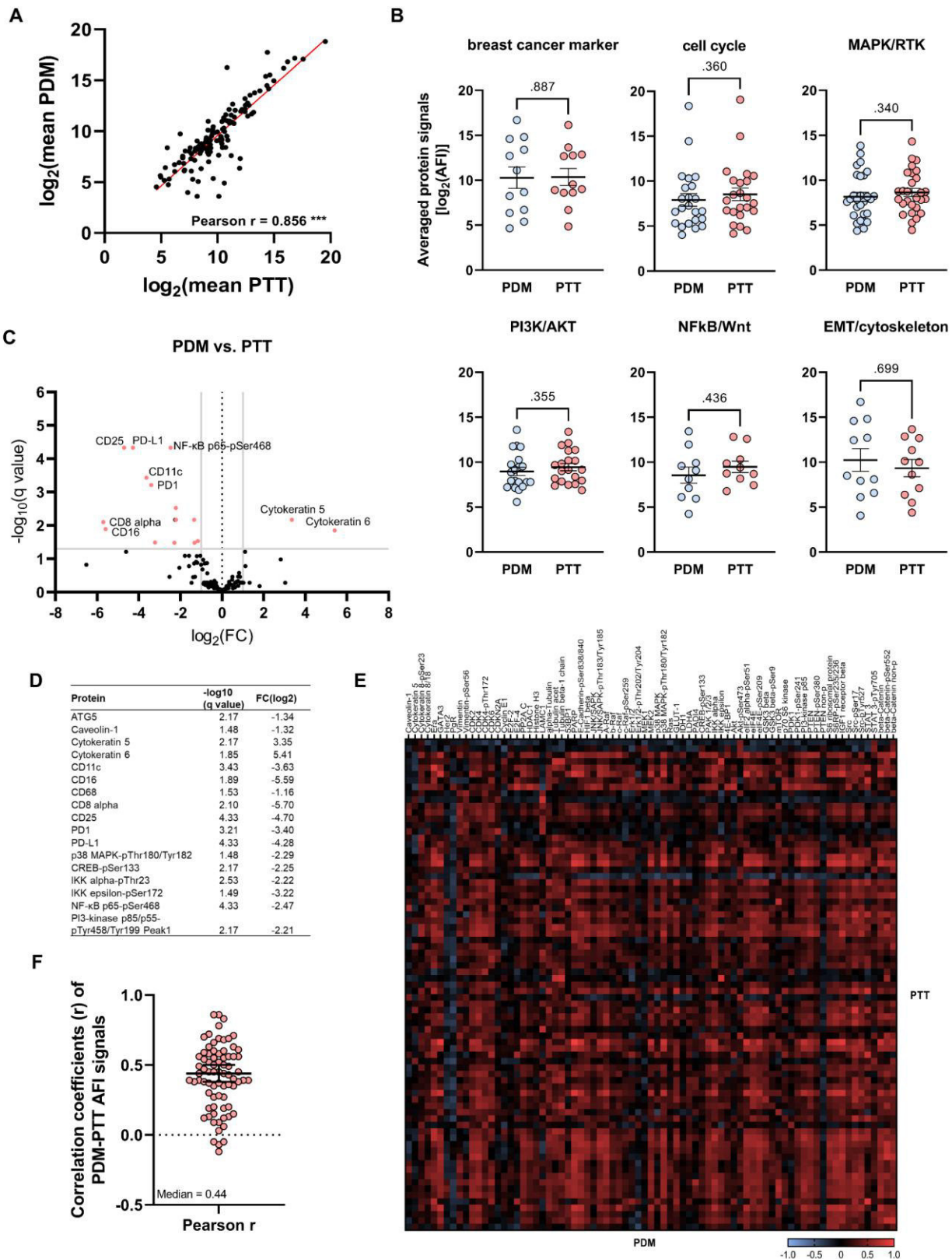


Figure 4. Comparison of protein profiles from BC-PDMs and corresponding primary tumor tissue. $N = 20$ matched BC-PDMs and PTT-pairs were analyzed. (A) X-Y plot of correlated protein means of BC-PDMs and PTT. Protein signals of measured BC-PDMs-PTT samples were correlated using Pearson correlation. DigiWest AFI protein signals were averaged for BC-PDMs/ PTT and \log_2 transformed. Each dot represents one protein. Pearson $r = 0.856$; $***p < 0.001$. (B) Overall signaling pathway activity in BC-PDMs resembled that of primary BC tumors. Proteins were sorted by pathway affiliation. Shown are AFI protein signals, averaged for BC-PDMs/PTT and \log_2 transformed. Mann-Whitney test; p values as indicated. (C-D) Differently expressed proteins of matched BC-PDMs-PTT samples. Volcano plot shows proteins with significantly decreased or increased expression in BC-PDMs with an adjusted FDR p -value ($-\log_{10}(q)$) > 1.3 and a \log_2 fold change $> |1|$; multiple t -test with Welch correction; Benjamini, Krieger, and Yekutieli FDR. Exact values are shown in D. (E) Heatmap of unclustered Pearson correlation coefficients (r) shows moderate correlation of AFI protein signals over BC-PDMs and matched PTT samples. (F) Pearson correlation coefficients (r) displayed as scatter plot with a median correlation of $r = 0.44$. Data are mean with SEM. AFI: averaged fluorescent intensities.

composed of tumor cells, ECM proteins and partially stromal cells of the corresponding tumor tissue, with immune cell infiltrates in a few cases. Other proteins displaying reduced expression in BC-PDMs as compared to matched PTT belong to different signaling pathways. Among them were mainly phospho-proteins of the MAPK pathway (p38 MAPK-pThr180/Tyr163), the PI3K pathway (PI3K p85/p55-pTyr458/199) and the NFkB pathway (NFkB p65-pSer172, IKK alpha-pThr23, IKK epsilon-pSer172). Correlation data of individual proteins showed a general, positive correlation between protein signals of matched BC-PDMs/PTT-pairs (Figure 4E) with a median coefficient of $r = 0.44$ (Figure 4F). Table S6 lists the proteins whose signal levels correlated significantly with those of the primary tumors. Significant positive correlations were found across all signaling pathways. Among them, ER α protein expression was significantly correlated between BC-PDMs and matched PTT ($r = 0.86$, $***p < 0.001$). ER α is clinically relevant for the classification of breast tumors. In addition to the histological assessment, we demonstrated at the protein level that the protein signaling pathway profiles of BC-PDMs are similar to those of the original tumor tissue across several signaling pathways. In individual cases, differences between the results of protein profiling analyses and histopathological assessment were observed. The corresponding tumor of BC-PDM #81 was classified as TNBC according to histopathology, whereas the result of protein profiling identified this model as ER α positive. In contrast, tumor sample #36 showed expression of ER according to histopathology, but not according to protein profiling. Overall, protein expression of PTT is reflected in BC-PDMs with high correlation.

5.7. Cross-comparison of protein profiling data among individual BC-PDMs identifies personalized pathway activation signatures

To classify the BC-PDMs samples based on their individual protein profiles, we analyzed signaling pathway activity of $n = 42$ BC-PDMs samples using hierarchical cluster linkage (HCL) analysis (Figure 5; Table S7). In addition, samples were assigned according to clinical data as HR+, TNBC or HER2-positive (HER2+) (illustrated in Table S1). Cluster analysis of cell cycle-related proteins resulted in four sample groups with different levels of cell cycle regulator expression (Figure 5A). In addition to cluster 1, which included the BC-PDMs sample #38, all HR+ BC-PDMs samples with either weak or mixed expression levels were grouped into cluster 2 ($n = 8$) and 3 ($n = 17$). Clusters differed mainly in the expression of transcriptional activators E2F-1, E2F-2, transcriptional repressor E2F-4 and p53. TNBC, HER2+ and the remaining HR+ BC-PDMs samples were grouped into cluster 4 ($n = 16$) and showed overall increased expression of cell cycle regulatory proteins. HCL of MAPK-RTK pathway proteins distinguished three sample groups separating $n = 19$ HR+ BC-PDMs with overall decreased protein abundances from $n = 19$ TNBC-, HER2+- and HR+ BC-PDMs with elevated expression levels (Figure 5B). Notably c-Met, RSK1-pThr573, NF1 and c-Raf were

upregulated in the latter group compared with the HR+ -only group. When comparing PI3K/Akt pathway activity among individual BC-PDMs models, samples were divided into two groups, too, with one group again consisting of HR+ samples and the other containing all TNBC and HER2+ samples (Figure 5C). Here, BC-PDMs were characterized by enhanced levels of beta-catenin, FoxO3a, Akt-pSer473, CREB, CREB-pSer133, PDK1 and IKKalpha-pThr23.

Next, we visualized the median-centered protein profiling data of BC-PDMs in box-whisker plots. This allowed us to identify individual BC-PDMs samples with increased expression of proteins belonging to cell cycle, MAPK/RTK and/or PI3K/AKT signaling pathways, respectively (Figure 5D). Of interest were BC-PDMs samples with median-centered protein expression \log_2 AFI ≥ 1 , corresponding to a fold change ≥ 2 (Table S8). Upregulated cell cycle activity was identified in $n = 8$ BC-PDMs, whereas MAPK/RTK signaling was amplified in $n = 11$ BC-PDMs with median expression levels ≥ 1 . Higher PI3K/Akt pathway activity was present in $n = 7$ BC-PDMs. Interestingly, all three signaling pathways were concomitantly upregulated in the four BC-PDMs samples #20, #78, #92 and #96. At the same time other BC-PDMs models showed simultaneous downregulation of all analyzed signaling pathways as indicated by \log_2 AFI values ≤ -1 (e.g. BC-PDMs #15, #18, #60, #89, #99). Pathway analysis thus allowed the classification of individual BC-PDMs samples based on specific protein expression profiles. Histopathologic phenotypes were not observed to correlate with pathway activity.

5.8. TNBC-PDMs exhibit increased PI3K/AKT and MAPK/RTK pathway activity

DigiWest-based protein profiling of BC-PDMs also enabled the differentiation of TNBC -PDM from HR+ BC-PDMs samples. TNBCs are known to be characterized by altered oncogenic signaling pathways such as PI3K/Akt and MAPK/Erk (53). Genetic aberrations of upstream regulators, such as activating mutations of PI3K, Ras, b-Raf, loss of function mutations of PTEN, overexpression of EGFR, have been shown to be common in breast cancer and play an important role in its dysregulation (54-59). These changes can cause the development of chemoresistance in TNBC patients (60-62). In line with these findings, we found PI3K/AKT ($p = 0.006$) and MAPK/RTK ($p = 0.032$) pathways significantly upregulated within TNBC -PDM as compared to HR+ BC-PDMs (Figure 5E). Proteins with significantly elevated abundance included AKT ($p = 0.022$), eIF2 α -pSer51 ($p = 0.009$), eIF4E ($p = 0.049$), GSK3beta ($p = 0.006$), GSK3beta-pSer9 ($p = 0.007$), PTEN ($p = 0.040$), PTEN non-p ($p = 0.044$), p70S6K ($p = 0.009$), CREB-pSer133 ($p = 0.041$). All these regulators have previously been associated with TNBC. Furthermore, we were able to assign additional proteins with elevated abundance in TNBC -PDM to the MAPK/RTK pathway. Parallel to the PI3K signaling, the MAPK pathway is another driving force in TNBC (63) and correlates with high disease

recurrence rates in patients with TNBC (64). We observed significant upregulation for Erk1/2 ($p = 0.022$), MEK2 ($p = 0.002$), Src-pSer17 ($p = 0.012$) and Src-pTyr527 ($p = 0.014$) (Figure 5F). Other signaling pathways (e.g. cell cycle, NF κ B-Wnt) did not show a significant distinction in expression between TNBC- and HR+ BC-PDMs. However, we identified upregulation of individual proteins related to the cell cycle: CDK2 ($p = 0.022$),

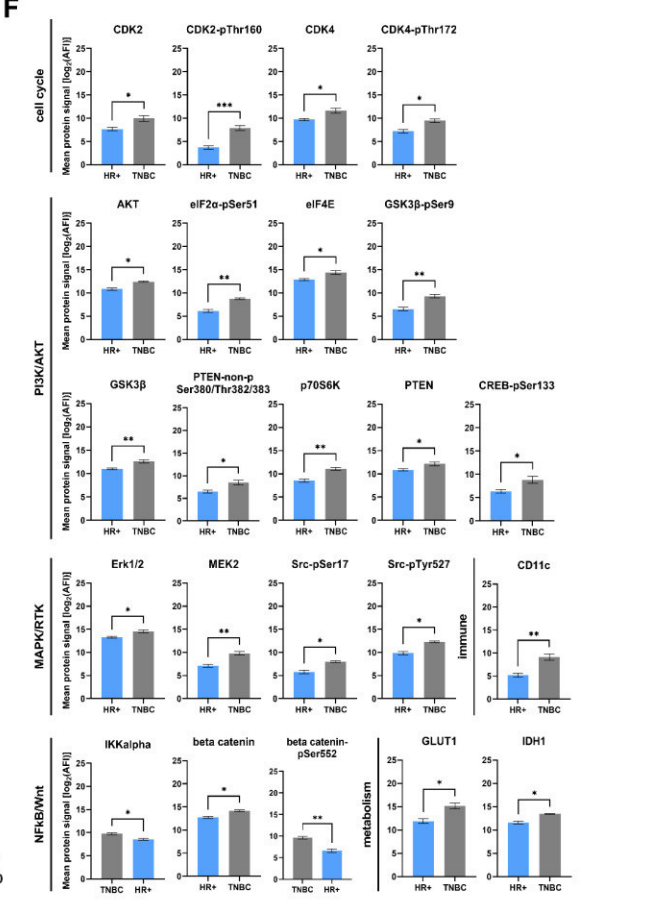
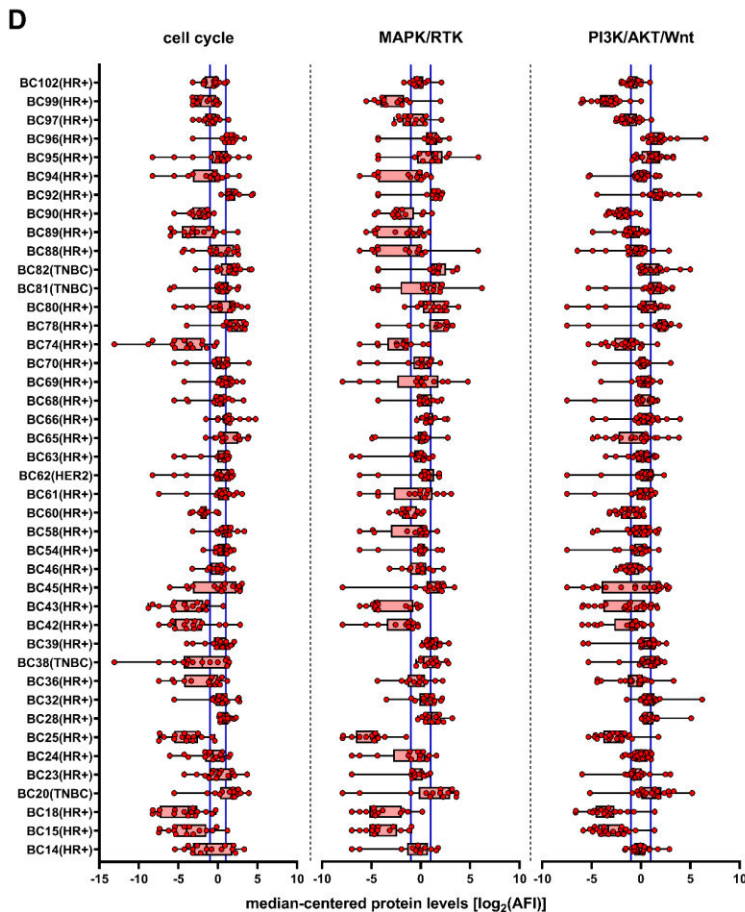
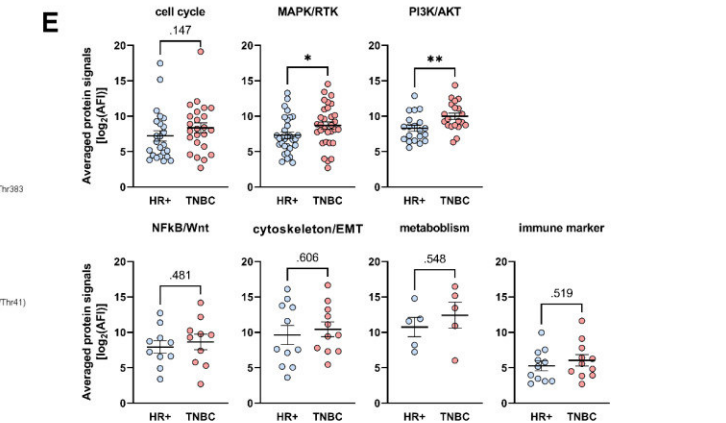
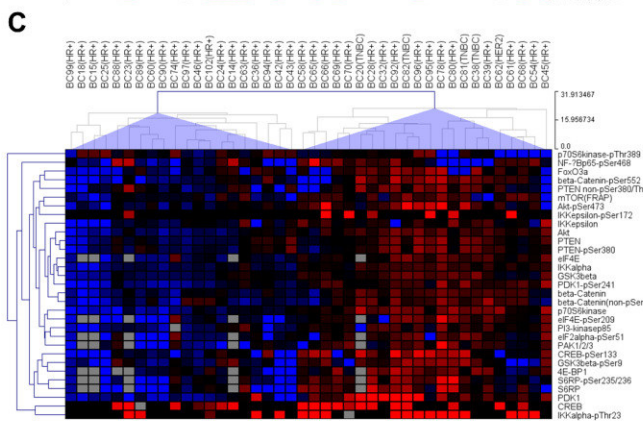
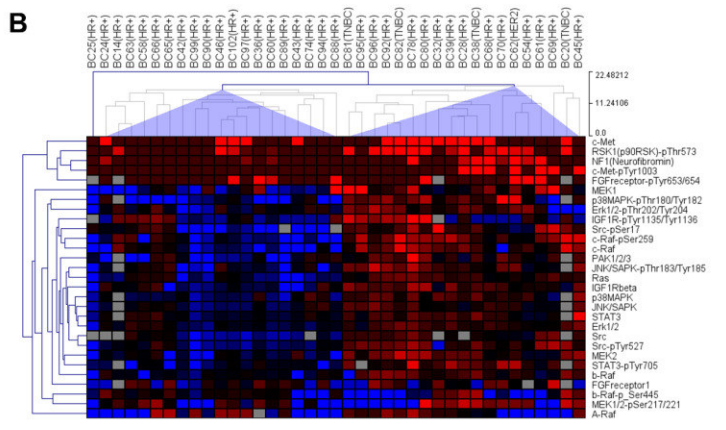
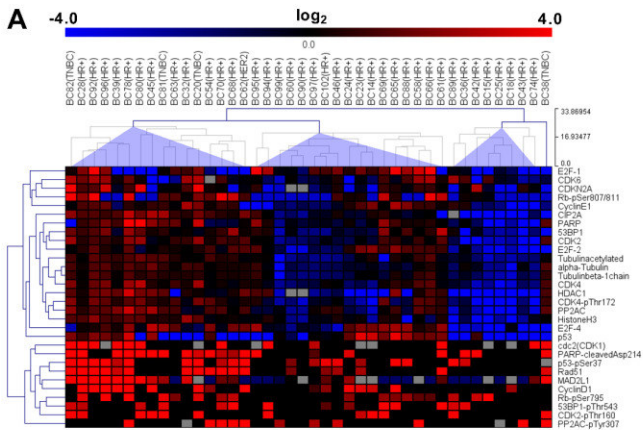


Figure 5 DigiWest-based protein pathway profiling of BC BC-PDMs. Hierarchical cluster linkage analysis (HCL) of median-centered, \log_2 transformed AFI protein signals of $n = 42$ BC BC-PDMs samples, divided into cell cycle, MAPK/RTK and PI3K/Akt pathways. Molecular subtype classifications of BC BC-PDMs samples as indicated. (A) HCL of sample and cell cycle-related analytes with complete linkage. Four sample clusters were identified based on differential expression levels. (B) HCL of sample and MAPK/RTK-related analytes with average linkage. There are two main sample clusters (excl. BC BC-PDMs #25) that separate samples with high MAPK/PI3K protein expression from those with low expression. (C) HCL of sample and PI3K/AKT-related analytes with complete linkage. Two main sample clusters were identified: "high-expression" and "low-expression". (D) Differences in signal transduction in BC BC-PDMs samples. Box-whisker plots show median-centered, \log_2 transformed AFI protein signals of different pathways. Data distribution within samples is illustrated by lines connecting min. and max. values. Each red dot represents a protein. Black lines in box plots indicate the "median" of measured proteins within a sample. Blue lines delineate the values $> |1|$ corresponding to a fold change > 0.5 . (E) TNBC BC-PDMs showing elevated PI3K/AKT- and MAPK/RTK- pathway activity. The averaged, \log_2 transformed protein signals are compared between TNBC and HR+ BC-PDMs within different pathways. Mann-Whitney U test, PI3K: $p = 0.006$, MAPK/RTK: $p = 0.032$. (F) Differentially expressed proteins in TNBC BC-PDMs. Comparison of mean protein expression in TNBC vs. HR+ BC BC-PDMs. Enhanced protein abundances in TNBC BC-PDMs were found for several proteins associated with cell cycle, metabolism, immune system, PI3K/AKT, MAPK/RTK and NF κ B pathway. Mann-Whitney U test, * $p < 0.05$, ** $p < 0.01$, *** $p < 0.001$. Data are mean with SEM.

CDK2-pThr160 ($p < 0.001$), CDK4 ($p = 0.025$) and CDK4-pThr172 ($p = 0.019$). While CDK2 hyperactivation is linked to basal-like breast cancer tumors (65), aberrant expression of CDK4 is linked to drug resistance (66). Consistent with increased eIF2 α -phosphorylation in TNBC -PDM and the associated upregulation of aerobic glycolysis (67-69), we also found an upregulation of metabolism-related proteins including GLUT1 ($p = 0.029$) and IDH1 ($p = 0.029$). When comparing BC-PDMs derived from NST and ILC tumors, we detected no differences in overall signaling pathway activity (Figure S3A). However, we observed differential expression for individual proteins such as E-Cadherin-pSer838/840, CK8-pSer23 and ER α (Figure S3B). Decreased E-Cadherin levels in ILC-BC-PDMs are in accordance with inactivating *CDH1* (E-Cadherin) mutations that are frequently observed in ILC tumors and disrupt cellular adhesion/epithelial integrity (70, 71). In accordance with G. Ciriello et al. (72), we discovered lower GATA 3 protein levels in ILC tumors. Reduced ER α signal in ILC-BC-PDMs may be explained by decreased GATA3 expression, as it plays a pivotal role in the recruitment of the ER transcription complex (73). In summary, identified overexpressed signaling proteins in TNBC -PDM affect many different cellular processes in cancer cells, including proliferation, differentiation, migration, cell growth and survival. Our results are consistent with previous findings in TNBC and show that BC-PDMs reflect protein signaling pathway activation characteristics of corresponding primary breast tumors.

5.9. Identification of marker panels for individualized responses towards hormone- and chemotherapy using combined cytotoxicity and protein profiling analyses of BC-PDMs

BC-PDMs responses to four anti-cancer drugs were evaluated by a microplate-based cytotoxicity assay. Microtumors derived from different patients were treated with the selective estrogen receptor modulator (74) tamoxifen (TAM), the taxane chemotherapeutics docetaxel (DTX) and paclitaxel (PTX), and the CDK4/6 inhibitor palbociclib (75). Samples were not differentiated according to receptor status since differences regarding the receptor status

determined by histopathology and by protein profiling analysis, respectively, were observed in individual cases (see Section 5.6). Treatment-induced cell death was measured in a time series (24h, 48h and 72h) and compared to the respective vehicle control (Table S9). A significant treatment effect, defined as a significant fold change in cell death between vehicle control and treatment, was considered a response, whereas a nonsignificant effect was considered a non-response or treatment resistance. (Mixed-effects model, Fisher's uncorrected LSD test). This approach allowed to divide the samples into responder (R) and non-responder (Non-R) groups (Figure 6A). BC-PDMs responded heterogeneously to the applied drug treatment. Most frequently they responded to treatment with DTX (9/29). Four samples showed a response to TAM (4/29), six samples to PTX (6/29) and five samples to PAB (5/29). Next, we compared the protein expression profiles (median-centered, log₂ transformed data) of the previously determined responder and non-responder BC-PDMs groups. Using DigiWest® analysis, we generated resistance/sensitivity protein marker panels that clearly distinguished responder from non-responder BC-PDMs (Figure 6). For each treatment, we selected proteins that are associated with therapy response/resistance according to literature and are significantly differentially expressed in responder vs. non-responder BC-PDMs or are involved in therapy-related signaling pathways (Table 2, Figure S4).

In the TAM responder group, we identified a panel of nine proteins with significantly decreased abundances (Figure 6B, Mann Whitney U test, ***p < 0.001). Phosphorylated proteins that were elevated in the treatment-resistant BC-PDMs group (Table 2) included ERα-pSer167, FGFR-pTyr653/654, PI3-kinase p85/p55-pTyr458/199, and IKKepsilon-pSer172, all of which are directly or indirectly related to TAM resistance according to the literature (76-81). The panel further contained regulators of the cell cycle (CDK6, Cyclin B1)

Table 2. Treatment-resistance and -sensitivity panel of BC derived microtumors

	Tamoxifen	Docetaxel	Paclitaxel	Palbociclib
resistance panel	ERα-pSer167	Caveolin-1	Caveolin-1	Cytokeratin6
	FGFreceptor-pTyr653/654	Vimentin-pSer56	PgR	Vimentin-pSer56
	IGF1Rbeta	CyclinE1	Cytokeratin5	CDK6
	Src-pSer17	B-Raf-pSer445	Cytokeratin6	CyclinE1
	PI3-kinase p85/p55-pTyr458/199	IKKε-pSer172	Vimentin-pSer56	Erk1/2-pThr202/Tyr204
	CDK6	NF-κB p100/p52	MEK1/2-pSer217/221	FGFRpTyr653/654
	Cyclin B1	Cyp1B1	mTOR(FRAP)	eIF4E-pSer209
	IKKepsilon-pSer172		IKKα-pThr23	
	beta-Catenin(non-pSer33/37/Thr41)		Tau	
		ERα	GATA3	CDK2-pThr160
sensitivity panel	E2F-4	E2F-4	Cytokeratin8/18	CyclinD1
	Src-pTyr527	CIP2A	E-Cadherin	ER
	αTubulin	Cytokeratin8/18	Tubulin-ac	Her2
	Tubulin-ac	Tau-pSer202	Tubulin beta-1chain	c-Raf-pSer259
	eIF2α-pSer51	Erk1/2-pThr202/Tyr204	cdc2(CDK1)	JNK/SAPK-pThr183/Tyr185
	GLUT-1	beta-Catenin-pSer552	CDK4-pThr172	p38MAPK-pThr180/Tyr182
	LDHA		Cyclin B1	E-Cadherin-pSer838/840
	PDK1-pSer241		E2F-2	
			Rb-pSer807/811	
			NF1(Neurofibromin)	
		c-Met-pTyr1003		
		beta-Catenin-pSer552		

and the Wnt-signaling pathway (non-phosphorylated beta-catenin). Within this panel, CDK6 expression was significantly different in non-responder versus responder BC-PDMs (Figure 6C, Mann-Whitney U test, * $p = 0.035$). In simple logistic regression analysis, CDK6 was found to negatively affect the likelihood of response to TAM with a 50% decrease in the odds (OR = 0.5, 95% CI 0.21-0.82) (Figure S4B; Table S10; $p < 0.05$ [Wald, LRT]). A panel of nine proteins with increased abundance was found to correlate with TAM sensitivity (Figure 6D, Mann Whitney U test, *** $p < 0.001$). This included ER α , the transcriptional repressor protein E2F-4, the microtubule protein α Tubulin and proteins involved in cancer cell metabolism (GLUT1, LDHA and PDK1-pSer241) and stress responses (eIF2A-pSer51).

Using a 7-protein resistance panel, we were able to significantly distinguish DTX non-responder from DTX responder BC-PDMs (Figure 6E, Mann Whitney U-test, *** $p < 0.001$). This panel included proteins associated with EMT induction (Vimentin-pSer56, NF κ B p100/p52 and IKK ϵ -pSer172) or drug metabolism (CYP1B1), which are also known to induce drug resistance to DTX and PTX in cancer cells (82, 83) (Table 2). In addition, higher Caveolin-1, Cyclin E1 and b-Raf-pSer445 protein levels contributed to DTX resistance of BC-PDMs. We found Caveolin-1 (* $p = 0.029$) and the MAPK-pathway related protein b-Raf-pSer445 (*** $p < 0.001$) to be significantly enriched in non-responder BC-PDMs (Figure 6F, Mann Whitney U-test). Figure 6G shows the protein panel predicting sensitivity of BC-PDMs to DTX treatment (Mann Whitney U-test, * $p = 0.017$) with increased expression of e.g. ER α , luminal-cell marker (Cytokeratin 8/18), inactive beta-catenin-pSer552 and microtubule associated protein Tau-pSer202 (Table 2). In this panel, we identified Cytokeratin 8/18 (Figure 6H, Mann Whitney U-test, *** $p < 0.001$) and Tau-pSer202 (Figure 6H, Mann Whitney U-test, $p = 0.028$) to be significantly enriched. By logistic regression analysis, expression of Caveolin-1 and b-Raf-pSer445 was shown to decrease the odds of DTX response of BC-PDMs by 44% (OR = 0.56, 95% CI: 0. 0.32-0.88) and 54% (OR = 0.46, 95% CI: 0.25 to 0.72) and thus contribute to DTX resistance. In contrast, elevated Tau-pSer202 (OR = 1.46, 95% CI: 1.06 to 2.22) and CK8/18 (OR = 1.54, 95% CI: 1.06 to 2.67) levels were significantly associated with DTX treatment response in BC -PDM (Figure S4D; Table S10; $p < 0.05$ [Wald, LRT]).

Paclitaxel treatment resistance of BC-PDMs was determined by a heterogenous panel of 9 proteins enriched in non-responder BC-PDMs (Figure 6I, Mann Whitney U-test, *** $p < 0.001$). Resistance-associated proteins were Caveolin-1, PgR, mTOR, phosphorylated MEK1/2 (pSer217/221) of the Erk/MAPK signaling pathway, phosphorylated IKK α (pThr23) of the NF κ B pathway, the microtubule-associated protein Tau and the basal breast cancer markers Cytokeratin 5, Cytokeratin 6 and Vimentin-pSer56 (Table 2). Moreover, we identified Vimentin-pSer56 to be significantly enriched in the PTX non-responder BC-PDMs (Figure 6J, Mann Whitney U-test, ** $p = 0.004$). Using a 13-protein panel, we could differentiate PTX

sensitive from resistant BC-PDMs (Mann Whitney U-test, $***p < 0.001$). We discovered several cell cycle-associated proteins (e.g. CDK1, CDK4-pThr172), luminal epithelial cell markers (e.g. E-Cadherin, Cytokeratin 8/18), the microtubule-forming protein Tubulin (acetylated Tubulin, Tubulin beta-chain), the Ras-inhibitor NF1 (Neurofibromin), c-Met-pTyr1003 and beta-Catenin-pSer55, whose expression affected BC-PDMs sensitivity to PTX treatment. Protein abundances differed significantly for GATA3 (Figure 6L, Mann Whitney U-test, $**p = 0.009$), NF1 (Figure 6L, Mann Whitney U-test, $**p = 0.005$) and c-Met-pTyr1003 (Figure 6L, Mann Whitney U-test, $*p = 0.020$). The probability of BC-PDMs response to PTX was doubled by increased GATA3 (OR = 2.34, 95% CI: 1.24-6.2) and NF1 (OR = 2.15, 95% CI: 1.25-4.5) expression and decreased levels of Vimentin-pSer56 (OR = 0.72, 95% CI: 0.51-0.93) (Figure S4F; Table S10; $p < 0.01$ [Wald, LRT]). To the best of our knowledge, there are no studies to date that have reported a link between the expression of these proteins and PTX treatment response.

For PAB treatment, we identified a resistance panel including proteins previously associated with PAB resistance: CDK6, Cyclin E1 and FGFR. Combined with basal breast cancer markers Cytokeratin 6 and Vimentin, the MAPK-signaling protein Erk1/2- pThr202/Tyr204 and the active mTOR signaling protein eIF4E-pSer209, these proteins could differentiate PAB resistant from PAB sensitive BC-PDMs (Figure 6M, Mann Whitney U-test, $***p < 0.001$). In contrast, sensitivity to PAB was predicted by a 8-protein panel (Figure 6N and 6O, Mann Whitney U-test, $***p < 0.001$) with increased ER α ($**p = 0.003$), HER2 ($**p = 0.003$), CDK2-pThr160 ($**p = 0.004$), E-Cadherin-pSer838/840 ($*p = 0.014$), Cyclin D1, c-Raf-p259, JNK/SAPK-pThr183/Tyr185 and p38MAPK-pThr180/Tyr182 signals in responder BC-PDMs. An increase of ER α (OR = 2.15, 95% CI: 1.2-5.91), HER2 (OR = 72.48, 95% CI: 2.36-14948598) and E-Cadherin-pSer838/840 (OR = 1.84, 95% CI: 1.15 to 3.55) by one level more than doubled the odds of BC-PDMs responding to PAB therapy (Figure S4H; Table S10; $p < 0.01$ [Wald, LRT]).

In summary, we identified heterogeneous responses to anti-cancer drug treatment in BC-PDMs. Through comprehensive molecular protein signaling pathway analysis of treatment-responsive and -resistant BC-PDMs, we gained insights into the treatment response mechanisms of breast cancer cells in microtumors, which were shown to resemble histopathological and protein expression profile characteristics of the corresponding primary breast tumor. Our data confirmed several proteins known to play a role in treatment resistance and/or sensitivity, and also identified novel markers that significantly correlate with individualized treatment responses.

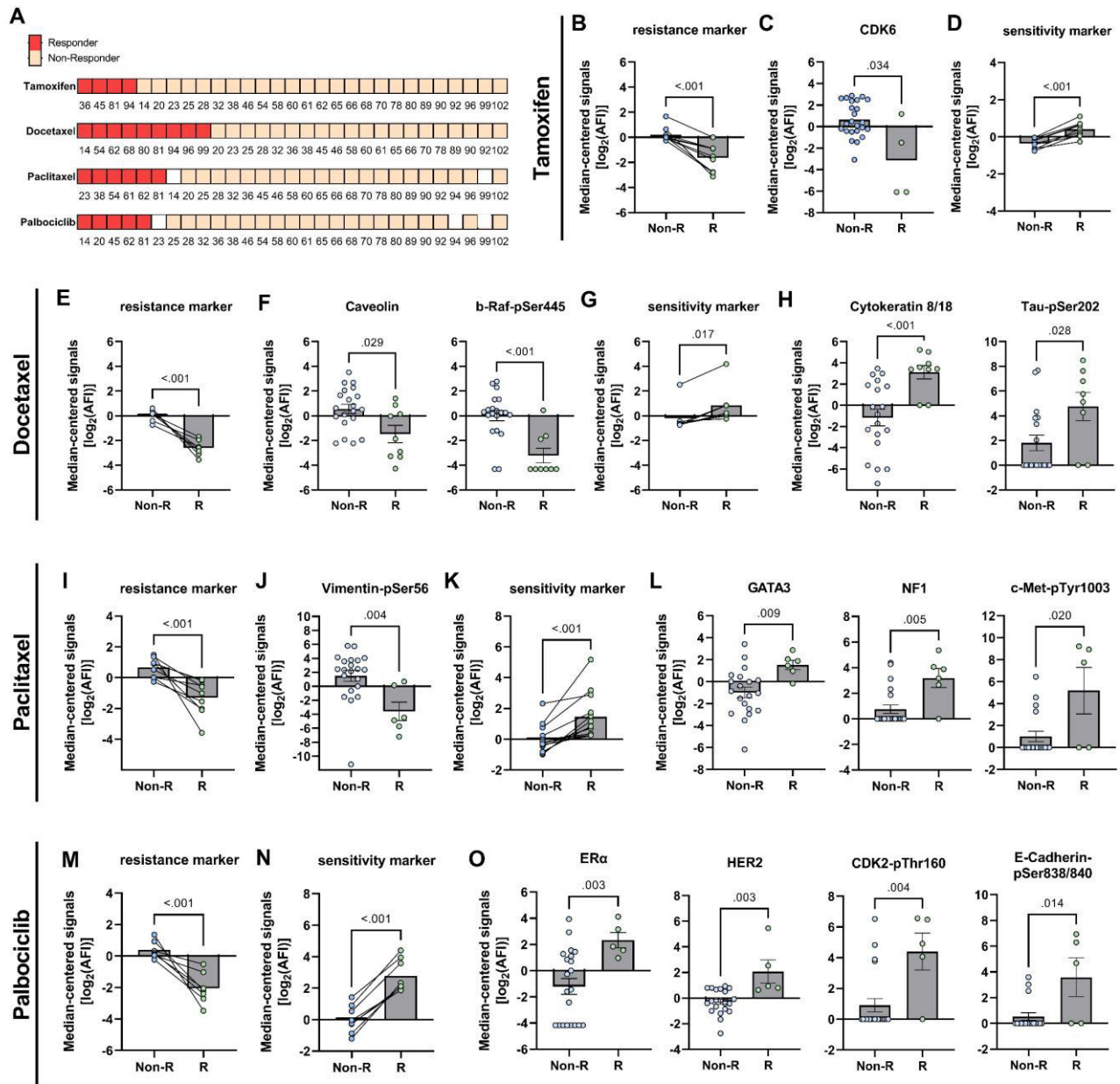


Figure 6. Treatment responses analyzed in BC-PDMs and identification of resistance and sensitivity marker panels. (A) Treatment response of breast cancer (BC) PDM to anti-cancer drugs. Microtumors were classified as “responder” and non-responder” based on the results of cytotoxicity measurements (Celltox Green™ assay; Promega). Cytotoxicity was determined in a time series (24h, 48h and 72h). Treatment effects were analyzed as fold change of the respective control for each measurement time point using a mixed-effects model (REML) and Fisher’s uncorrected LST test. Statistically significant fold changes were defined as “response” and BC-PDMs were accordingly classified as “responders”. The numbers indicate BC sample number. (B-D) TAM, (E-H) DTX, (I-L) PTX and (M-O) PAB resistance and sensitivity marker panels. Median-centered, \log_2 -transformed DigiWest AFI protein signals were compared between R and Non-R groups. Each data point within the scatter bar plots represents the same protein in R and Non-R. Lines connect protein data points between Non-R and R. Therapy resistance and sensitivity panels were identified including up to thirteen proteins (for detailed protein list see Table 1.). Comparison of R and Non-R protein “panel” signals by non-parametric, unpaired Mann-Whitney U test. Within these protein panels individual, differentially expressed proteins are depicted (non-parametric, unpaired Mann-Whitney U test). * $p < 0.05$, ** $p < 0.01$ and *** $p < 0.001$. Shown are mean with SEM. AFI: average fluorescent intensities; Non-R: non-responder; R: responder; TAM: tamoxifen (100 nM), DTX: docetaxel (5.5 μ M), PTX: paclitaxel (4 μ M), PAB: Palbociclib (150 nM).

6. Discussion

Breast cancer is a highly heterogeneous disease with profound morphological, genetic and phenotypical variability resulting in multiple disease manifestations with different response to treatment (16). Gene expression analysis and classical immunohistochemical analysis has enabled the differentiation of BC subtypes and subsequently served to guide treatment selection and patient stratification in BC (4-6). Still, development of treatment resistance remains a major challenge in the management of this malignancy, largely due to the pronounced intra-tumoral heterogeneity that characterizes BC beyond genetic profiles (16). Apart from the intrinsic changes and interactions of tumor cells, also the crosstalk of tumor cells with the complex TME impacts the BC phenotypic manifestation and thus the development of treatment resistance (19, 20). In this context, the use of tumor models accurately representing the complexity of patient tumors, while at the same time being applicable for a variety of readout methods, is becoming increasingly important. To date, a number of different *ex vivo* platforms and model systems have been described in this context, such as patient-derived tumor organoids, tumor explants, tumor slices, and others (84-86). In this study, we successfully generated a repertoire of microtumor samples from different BC subtypes representing disease heterogeneity. We applied previously published protocols for isolating microtumors from primary tumor tissues (23, 28, 29). BC-PDMs recapitulate general histological features and tumor-type specific features of NST (IDC) and ILC like growth patterns, cellular pleomorphism and atypia of the corresponding primary tumor tissue. Using Movat-pentachrome stainings, we found the most abundant BC-related ECM proteins (37, 87), collagen and PGs/GAGs, also present in BC-PDMs and show a tendency for increased collagen deposition within ILC-type PDM comparable to PTT. Studies demonstrated that collagen deposition, which increases ECM stiffness, and the density and orientation of collagen fibers affect tumor aggressiveness, invasiveness, therapy responses and correlates with prognosis in BC (88-90). Hence, BC tumor models that comprise ECM structures of native tumors like BC-PDMs represent relevant test systems to investigate disease biology and therapy resistance.

Moreover, our results highlight other features in BC-PDMs characteristic of different BC subtypes as previously described, including hormone-receptor expression in HR+ BC-PDMs compared with TNBC -PDM, increased collagen deposition in ILC-derived BC-PDMs (37), heterogeneous expression profiles of luminal (CK18) and basal cell markers (CK5 and CK6) (44) with decreased CK18 expression in TNBC -PDM (49), and high FAP α expression in ILC-BC-PDMs (52). Regarding the CK expression in BC-PDM, we observed similar cellular profiles as described previously by Abd El-Rehim, D.M. et al (44), i.e. the differentiated glandular phenotype (CK18⁺), the stem cell phenotype (CK5/6⁺) and an intermediate glandular phenotype (CK5/6⁺, CK18⁺) (48). In contrast to this study, we did further

differentiate CK5⁺ BC-PDMs from CK5⁺/CK6⁺ BC-PDMs. According to several reports, 17% of ILCs express basal CKs (91). In our study, ILC-BC-PDMs expressed relatively high levels of CK5/6 compared to NST-BC-PDMs, which is therefore somewhat surprising. In order to provide a more precise statement on this, BC-PDMs established from a larger cohort of ILC samples would need to be evaluated. However, differential protein expression analysis revealed an overall higher expression of CK5 and CK6 in BC-PDMs regardless of breast tumor type compared to primary tumors. Overexpressed CK5 could be attributable to low estrogen concentrations during culture of BC-PDMs as described before (92-94). Similar results have been observed in organoids derived from BC patients (95). We cannot exclude the possibility that the culture conditions for BC-PDMs may favor the selection and outgrowth of BC subclones with a basal epithelial phenotype (CK5/CK6⁺), which are often associated with *BRCA-1* mutated BC (96, 97) and are underrepresented in the primary tumor. This observation warrants further investigation in future studies.

Compared to frequently employed gene expression analysis of tumor models, our study investigated BC microtumors on the protein level using the DigiWest® method covering 142 total and phosphoproteins. Thereby, breast cancer-related protein expression levels and signaling pathway profiles largely correlated with those of corresponding primary tumors. Hierarchical cluster analysis grouped BC-PDMs according to their classification and molecular protein expression signature. Further, our DigiWest® data confirmed protein signatures of TNBC-PDMs consistent with those in the literature, characterized by upregulated PI3K/Akt and MAPK/RTK signaling (53, 63, 64, 98) with overexpressed proteins associated with integrated stress response (99-102), higher relapse rates, mortality (64, 103, 104), tumor growth and EMT (29, 105-107). When comparing BC-PDMs and primary tumor profiles, we found decreased expression of NFκB signaling pathway proteins NFκB regulates processes of immune and inflammatory responses and is part of the immune defense against transformed cells (108, 109). Because the protein data also showed diminished expression of immune cell markers in BC-PDMs, the attenuated presence of immune cells in microtumors might explain the observed, decreased NFκB-related signals as compared to PTT.

Our study validates the application of BC-PDM for *in vitro* functional drug testing, as demonstrated previously for ovarian cancer and glioblastoma microtumors (23, 28, 29), to functionally complement molecular and histopathological analyses. Protein profiling analysis combined with functional drug testing allowed us to identify phenotypic hallmarks of treatment resistance and sensitivity, as opposed to genetic alterations that may not correlate with clinical benefit (21). As the growth of some types of BC is driven by increased signaling from estrogen and progesterone receptors, hormone therapies have been developed that prevent hormones from binding to these receptors. TAM is a competitive inhibitor of the

estrogen receptor known as a selective modulator, while fulvestrant is a selective ER degrader (110). It has been reported that overexpressed CDK6 inhibits fulvestrant-mediated (ER-down regulation-induced) apoptosis and thus induces fulvestrant-resistance (111). Our data implicates that TAM resistance may also be characterized by high CDK6 levels in BC-PDMs illustrating the possibility of resistance mechanisms similar to fulvestrant. Furthermore, it is known that ER α activation through phosphorylation of Ser167 in an estrogen-independent manner and FGFR activation can cause TAM resistance: both proteins were identified within our BC-PDMs TAM resistance panel (76, 80, 112). In line with the clinical application of TAM in HR+ BC (113), increased total ER α levels contribute to TAM sensitivity in BC-PDMs.

Drug treatment assays with BC-PDMs were conducted independently of hormone receptor status. In individual cases, differences in the result of histopathological analysis of hormone receptor expression in tumor tissue compared to protein analysis were evident. Residual fresh tumor tissue specimens received for BC-PDM isolation and protein expression analyses were inherently not identical to the sample of the corresponding tumor tissue examined by histopathology. Breast carcinoma is characterized by marked intratumoral heterogeneity, with consequences previously described in the literature, including reduced concordance rates in receptor expression between core and excisional biopsies (114-117). In addition, a minority of approximately 10% ER-negative breast carcinomas together with a molecularly defined subset of TNBC have been described in the literature to show response to tamoxifen (118, 119).

The chemotherapeutic agent DTX has shown high activity as an antimicrotubular agent in both neoadjuvant and adjuvant application in advanced and metastatic breast cancer (120). It also had the strongest effect on BC-PDMs treatment response as compared to other anti-cancer drugs tested. In line with previous studies, BC-PDMs generated from less invasive BC, luminal-like CK8/18 high BC-PDMs with inactive β -catenin signaling and thus lower EMT-transition, and BC-PDMs with high ER expression were sensitive to treatment (121-123). Contrary, we confirmed that high expression of EMT-related and EMT-inducible proteins, high expression of DTX-metabolizing CYP1B1 and increased Caveolin-1 in BC-PDMs predict DTX resistance (82, 83, 124, 125). Surprisingly we did identify Ser202 phosphorylated Tau to positively and b-Raf-pSer445 to negatively influence DTX sensitivity of BC-PDMs. To date, there are no reports on either protein or their potential impact on response to taxane treatment. However, there are conflicting data on whether the expression of tau correlates with taxane response (126, 127).

As the first taxane compound discovered, PTX has a similar function to DTX as antimicrotubular agent (128). The critical role of the EMT process in PTX resistance, (83), is

well represented indicated by the resistance and sensitivity marker panel we identified in BC-PDMs, including EMT-regulator proteins such as Vimentin-pSer56, CK5, CK6, E-Cadherin, CK8/18, IKK α -pThr23, beta-Catenin-pSer55. Contrary to DTX, our results regarding PTX resistance of BC-PDMs indicate that increased total Tau protein levels correlate with treatment resistance. Further studies are warranted to further investigate the importance of Tau protein expression in taxane treatment response of breast cancer. In line with previous *in vitro* studies our data suggest a correlation between high PgR levels and decreased PTX sensitivity (129). Interestingly, we found three proteins being significantly elevated in PTX sensitive BC-PDMs: GATA3, NF1 and c-Met-pTyr1003. So far, these proteins have not been linked to taxane sensitivity, but have generally been associated with breast cancer development (130-133).

In addition to endocrine and chemotherapy, we also tested the CDK4/6 inhibitor palbociclib (75). The emergence of several intrinsic and acquired resistance mechanisms has been described preclinically, however without verification in the clinical setting (134). Our comparison of responder and non-responder BC-PDMs protein expression profiles provided intriguing results regarding PAB treatment. We identified several proteins in our BC-PDMs resistance/sensitivity panel to be predictive for PAB response that have been linked to PAB resistance/sensitivity in previous studies, such as CDK6, Cyclin E1, FGFR, Cyclin D1 and ER α (134). Surprisingly, our data also suggest Vimentin, CK6, CDK2-p and HER2 protein expression as novel PAB-treatment response markers. Increased Vimentin and CK6 levels may define a more aggressive and invasive tumor type that is resistant to PAB (51, 135). Our analyses identified phosphorylated CDK2 to contribute to PAB-sensitivity of BC-PDMs, while other studies reported the opposite, as the cyclin E-CDK2 pathway is an important bypass mechanism of the cyclin D1-CDK4/6 axis in acquired PAB-resistance (134). Both CDK4/6-Cyclin D and CDK2-Cyclin E complexes are decisive for the transition of G1- to S-phase and thus required for cell cycle progression. Further studies are warranted to evaluate this differential response in BC-PDMs.

In summary, we have shown that a salient feature of BC-PDMs, in addition to their histopathological and molecular similarity to the corresponding patient tumor, is the representation of native ECM components that collectively represent the disease heterogeneity of BC. Limitations of this novel patient-derived model system are the restricted number of microtumors available for downstream analyses, the reduced expression of immune cell markers and NF κ B signaling proteins, as well as the enhanced expression of CK5 and CK6 as compared to corresponding primary tumor tissue. Further evaluation in additional sample cohorts will be needed to understand the underlying mechanism and to assess the long-term stability of HR-expression in BC-PDMs cultures. In this context, a subtype-specific analysis of drug treatment effects in BC-PDMs, with a particular focus on

TNBC cases, would also be of special interest for future studies. Moreover, the application of BC-PDMs in patient-derived xenograft mouse models would allow the study of long-term growth kinetics as well as processes of tumor metastasis as recently described (136). Regarding the application of BC-PDMs for assessment of immune cell interaction and immune-oncological treatment responses, we have previously shown functional drug testing of immune checkpoint inhibitors in co-cultures of ovarian cancer and glioblastoma PDM and autologous immune cells (23, 28, 29).

7. Conclusion

Based on comprehensive protein profiling analyses in combination with functional drug testing assays in BC-PDMs our study highlights the potential of identifying patient-tumor specific, differentially expressed proteins to discriminate treatment responders from non-responders and warrants further, confirmatory studies in larger sample cohorts. Specifically, future studies will focus on the comparison of functional drug testing and protein profiling data from BC-PDMs with clinical treatment response in respective patients. As a complement to genomic mutation analysis and standard subtype classification, the combination of individual histopathologic analysis, preclinical drug testing, and parallel protein profiling analyses of BC-PDMs may hold promise for identifying predictive markers of treatment resistance and sensitivity to personalize breast cancer therapies.

8. List of abbreviations

BC	breast cancer
CAFs	cancer-associated fibroblasts
CK	cytokeratin
DAB	3,3'-Diaminobenzidin
DCIS	ductal carcinoma in-situ
DMSO	Dimethyl sulfoxide
DTX	docetaxel
ECM	extracellular matrix
EMT	epithelial-to-mesenchymal transition
ER	estrogen receptor
FAP α	fibroblast-associated protein α
FC	fold change
FFPE	formalin-fixed paraffin-embedded
GAGs	glycosaminoglycans
H&E	hematoxylin and eosin staining
HCL	hierarchical clustering
HER2	human epidermal growth factor receptor 2
HR	hormone receptor
IDC	invasive ductal carcinoma
IHC	immunohistochemistry
ILC	invasive lobular carcinoma
IRS	immunoreactive score
LCIS	lobular carcinoma in-situ
NST	invasive ductal carcinoma of no special type
PAB	palbociclib
PDM	patient-derived microtumors
PgR	progesterone receptor
PGs	proteoglycans
PTT	primary tumor tissue
PTX	paclitaxel
RFU	relative fluorescent units
TAM	tamoxifen
TIL	tumor infiltrating lymphocytes
TME	tumor microenvironment
TNBC	triple-negative breast cancer

9. Declarations

Institutional Review Board Statement: The study was conducted in accordance with the Declaration of Helsinki and approved by the Institutional Review Board (or Ethics Committee) of the University Hospital Tuebingen, Germany (788/2018BO2, November 15th 2018).

Consent Statement: The use of human samples was approved by the local Ethics Commission at the Medical Faculty Tuebingen under the reference number 788/2018BO2 (15 November 2018). All patients enrolled gave their informed consent to participate in the study prior to surgery.

Data Availability Statement: The data that support the findings of this study are available from the corresponding authors upon reasonable request and after signature of an MTA from the corresponding authors.

Competing interests: A.H. received consulting and speaking fees from AstraZeneca, Amgen, Clovis, Daichii Synkyo, Eisai, ExactScience, Gilead, GSK, Hexal, Lilly, MSD, Novartis, Pfizer, Roche, Pierre-Fabre and Seagen. N.A., F.S-R., N.K, A.K., A.-L.K., B.G., A.S., S.L., M.P., M.H., S.Y.B., K.S-L., M.T. and C.S. declare no competing interest.

Funding: This work received financial support from the Ministry of Baden-Wuerttemberg for Economic Affairs, Labor, and Tourism (grant 3-4332.62-HSG/84).

Author Contributions: Conceptualization and design of the study, C.S., M.T., N.A., A.K., A.H., S.Y.B, and K.S-L.; data collection, data analysis, investigation and interpretation, N.A., F.S-R., S.L., A.K., A.-L.K., A.S., N.K. and C.S.; writing—original draft, N.A. and C.S.; writing—review and editing, N.A., C.S., A.-L.K., K.S-L., A.K., S.Y.B., A.H. and A.S.; visualization, N.A., C.S.; supervision, C.S., S.Y.B., K.S-L.; project administration: N.A., C.S. and A.K. All authors have read and agreed to the published version of the manuscript.

Acknowledgments: We gratefully acknowledge Prof. Dr. Diethelm Wallwiener (Department of Women's Health, University Women's Hospital, Tübingen University Hospital) for his excellent support, helpful discussions and providing fresh tumor tissue biopsies. We thank all patients and healthy volunteers enrolled for giving their informed consent for secondary use of residual tissue, respectively.

10. References

1. Caswell-Jin JL, Plevritis SK, Tian L, Cadham CJ, Xu C, Stout NK, et al. Change in Survival in Metastatic Breast Cancer with Treatment Advances: Meta-Analysis and Systematic Review. *JNCI Cancer Spectr.* 2018;2(4):pky062.
2. Lakhani SR, Ellis IO, Schnitt S, Tan PH, van de Vijver M. *WHO Classification of Tumours of the Breast.* 2012.
3. Tavassoli FA. Pathology and genetics of tumours of the breast and female genital organs. *World Health Organization Classification of Tumours.* 2003.
4. Perou CM, Sørlie T, Eisen MB, Van De Rijn M, Jeffrey SS, Rees CA, et al. Molecular portraits of human breast tumours. *Nature.* 2000;406(6797):747-52.
5. Sørlie T, Perou CM, Tibshirani R, Aas T, Geisler S, Johnsen H, et al. Gene expression patterns of breast carcinomas distinguish tumor subclasses with clinical implications. *Proc Natl Acad Sci U S A.* 2001;98(19):10869-74.
6. Sørlie T, Tibshirani R, Parker J, Hastie T, Marron JS, Nobel A, et al. Repeated observation of breast tumor subtypes in independent gene expression data sets. *Proc Natl Acad Sci U S A.* 2003;100(14):8418-23.
7. Tsang JYS, Tse GM. *Molecular Classification of Breast Cancer.* *Adv Anat Pathol.* 2020;27(1):27-35.
8. Carey LA, Dees EC, Sawyer L, Gatti L, Moore DT, Collichio F, et al. The triple negative paradox: primary tumor chemosensitivity of breast cancer subtypes. *Clin Cancer Res.* 2007;13(8):2329-34.
9. Rouzier R, Perou CM, Symmans WF, Ibrahim N, Cristofanilli M, Anderson K, et al. Breast cancer molecular subtypes respond differently to preoperative chemotherapy. *Clinical cancer research.* 2005;11(16):5678-85.
10. Martin M, Romero A, Cheang MC, López García-Asenjo JA, García-Saenz JA, Oliva B, et al. Genomic predictors of response to doxorubicin versus docetaxel in primary breast cancer. *Breast Cancer Res Treat.* 2011;128(1):127-36.
11. Glück S, Ross JS, Royce M, McKenna EF, Jr., Perou CM, Avisar E, et al. TP53 genomics predict higher clinical and pathologic tumor response in operable early-stage breast cancer treated with docetaxel-capecitabine ± trastuzumab. *Breast Cancer Res Treat.* 2012;132(3):781-91.
12. Lehmann BD, Bauer JA, Chen X, Sanders ME, Chakravarthy AB, Shyr Y, et al. Identification of human triple-negative breast cancer subtypes and preclinical models for selection of targeted therapies. *J Clin Invest.* 2011;121(7):2750-67.
13. Lehmann BD, Jovanović B, Chen X, Estrada MV, Johnson KN, Shyr Y, et al. Refinement of Triple-Negative Breast Cancer Molecular Subtypes: Implications for Neoadjuvant Chemotherapy Selection. *PLoS One.* 2016;11(6):e0157368.
14. Koren S, Bentires-Alj M. Breast Tumor Heterogeneity: Source of Fitness, Hurdle for Therapy. *Mol Cell.* 2015;60(4):537-46.
15. Hong SP, Chan TE, Lombardo Y, Corleone G, Rotmensz N, Bravaccini S, et al. Single-cell transcriptomics reveals multi-step adaptations to endocrine therapy. *Nature Communications.* 2019;10(1):3840.
16. Lüönd F, Tiede S, Christofori G. Breast cancer as an example of tumour heterogeneity and tumour cell plasticity during malignant progression. *Br J Cancer.* 2021;125(2):164-75.
17. Heindl A, Sestak I, Naidoo K, Cuzick J, Dowsett M, Yuan Y. Relevance of Spatial Heterogeneity of Immune Infiltration for Predicting Risk of Recurrence After Endocrine Therapy of ER+ Breast Cancer. *JNCI: Journal of the National Cancer Institute.* 2017;110(2):166-75.
18. Natrajan R, Sailem H, Mardakheh FK, Arias Garcia M, Tape CJ, Dowsett M, et al. Microenvironmental Heterogeneity Parallels Breast Cancer Progression: A Histology-Genomic Integration Analysis. *PLoS Med.* 2016;13(2):e1001961.
19. Glajcar A, Szpor J, Pacek A, Tyrak KE, Chan F, Streb J, et al. The relationship between breast cancer molecular subtypes and mast cell populations in tumor microenvironment. *Virchows Arch.* 2017;470(5):505-15.

20. Bareche Y, Buisseret L, Gruosso T, Girard E, Venet D, Dupont F, et al. Unraveling Triple-Negative Breast Cancer Tumor Microenvironment Heterogeneity: Towards an Optimized Treatment Approach. *J Natl Cancer Inst.* 2020;112(7):708-19.
21. Pezo RC, Chen TW, Berman HK, Mulligan AM, Razak AA, Siu LL, et al. Impact of multi-gene mutational profiling on clinical trial outcomes in metastatic breast cancer. *Breast Cancer Res Treat.* 2018;168(1):159-68.
22. Pauli C, Hopkins BD, Prandi D, Shaw R, Fedrizzi T, Sboner A, et al. Personalized In Vitro and In Vivo Cancer Models to Guide Precision Medicine. *Cancer Discov.* 2017;7(5):462-77.
23. Anderle N, Koch A, Gierke B, Keller A-L, Staebler A, Hartkopf A, et al. A Platform of Patient-Derived Microtumors Identifies Individual Treatment Responses and Therapeutic Vulnerabilities in Ovarian Cancer. *Cancers (Basel).* 2022;14(12):2895.
24. Kondo J, Endo H, Okuyama H, Ishikawa O, Iishi H, Tsujii M, et al. Retaining cell-cell contact enables preparation and culture of spheroids composed of pure primary cancer cells from colorectal cancer. *Proc Natl Acad Sci U S A.* 2011;108(15):6235-40.
25. Ruifrok AC, Johnston DA. Quantification of histochemical staining by color deconvolution. *Anal Quant Cytol Histol.* 2001;23(4):291-9.
26. Treindl F, Ruprecht B, Beiter Y, Schultz S, Döttinger A, Staebler A, et al. A bead-based western for high-throughput cellular signal transduction analyses. *Nature Communications.* 2016;7(1):12852.
27. Iglewicz B, Hoaglin DC. How to detect and handle outliers. Milwaukee, Wis.: Milwaukee, Wis. : ASQC Quality Press; 1993. ix, 87 p. p.
28. Przystal JM, Becker H, Canjuga D, Tsiami F, Anderle N, Keller A-L, et al. Targeting CSF1R Alone or in Combination with PD1 in Experimental Glioma. *Cancers (Basel).* 2021;13(10):2400.
29. Walter B, Canjuga D, Yüz SG, Ghosh M, Bozko P, Przystal JM, et al. Argyrin F Treatment-Induced Vulnerabilities Lead to a Novel Combination Therapy in Experimental Glioma. *Advanced Therapeutics.* 2021:2100078.
30. McCart Reed AE, Kalinowski L, Simpson PT, Lakhani SR. Invasive lobular carcinoma of the breast: the increasing importance of this special subtype. *Breast Cancer Res.* 2021;23(1):6.
31. Lepucki A, Orlińska K, Mielczarek-Palacz A, Kabut J, Olczyk P, Komosińska-Vashev K. The Role of Extracellular Matrix Proteins in Breast Cancer. *Journal of Clinical Medicine.* 2022;11(5):1250.
32. Klimonda Z, Karwat P, Dobruch-Sobczak K, Piotrkowska-Wróblewska H, Litniewski J. Breast-lesions characterization using Quantitative Ultrasound features of peritumoral tissue. *Sci Rep.* 2019;9(1).
33. Henke E, Nandigama R, Ergün S. Extracellular matrix in the tumor microenvironment and its impact on cancer therapy. *Frontiers in molecular biosciences.* 2020;6:160.
34. Bergamaschi A, Tagliabue E, Sørlie T, Naume B, Triulzi T, Orlandi R, et al. Extracellular matrix signature identifies breast cancer subgroups with different clinical outcome. *The Journal of pathology.* 2008;214(3):357-67.
35. Riaz M, Sieuwerts AM, Look MP, Timmermans MA, Smid M, Foekens JA, et al. High TWIST1 mRNA expression is associated with poor prognosis in lymph node-negative and estrogen receptor-positive human breast cancer and is co-expressed with stromal as well as ECM related genes. *Breast Cancer Res.* 2012;14(5):1-15.
36. Movat HZ. Demonstration of all connective tissue elements in a single section; pentachrome stains. *AMA Arch Pathol.* 1955;60(3):289-95.
37. Natal RdA, Paiva GR, Pelegati VB, Marenco L, Alvarenga CA, Vargas RF, et al. Exploring Collagen Parameters in Pure Special Types of Invasive Breast Cancer. *Sci Rep.* 2019;9(1):7715.
38. Carey L, Winer E, Viale G, Cameron D, Gianni L. Triple-negative breast cancer: disease entity or title of convenience? *Nature Reviews Clinical Oncology.* 2010;7(12):683-92.
39. Dent R, Trudeau M, Pritchard KI, Hanna WM, Kahn HK, Sawka CA, et al. Triple-negative breast cancer: clinical features and patterns of recurrence. *Clin Cancer Res.* 2007;13(15 Pt 1):4429-34.

40. Yin W-J, Lu J-S, Di G-H, Lin Y-P, Zhou L-H, Liu G-Y, et al. Clinicopathological features of the triple-negative tumors in Chinese breast cancer patients. *Breast Cancer Res Treat.* 2009;115(2):325-33.
41. Dignam JJ, Dukic V, Anderson SJ, Mamounas EP, Wickerham DL, Wolmark N. Hazard of recurrence and adjuvant treatment effects over time in lymph node-negative breast cancer. *Breast Cancer Res Treat.* 2009;116(3):595-602.
42. Moll R, Franke WW, Schiller DL, Geiger B, Krepler R. The catalog of human cytokeratins: patterns of expression in normal epithelia, tumors and cultured cells. *Cell.* 1982;31(1):11-24.
43. Taylor-Papadimitriou J, Stampfer M, Bartek J, Lewis A, Boshell M, Lane EB, et al. Keratin expression in human mammary epithelial cells cultured from normal and malignant tissue: relation to in vivo phenotypes and influence of medium. *J Cell Sci.* 1989;94 (Pt 3):403-13.
44. Abd El-Rehim DM, Pinder SE, Paish CE, Bell J, Blamey R, Robertson JF, et al. Expression of luminal and basal cytokeratins in human breast carcinoma. *The Journal of Pathology.* 2004;203(2):661-71.
45. Wetzels R, Kuijpers H, Lane EB, Leigh IM, Troyanovsky S, Holland R, et al. Basal cell-specific and hyperproliferation-related keratins in human breast cancer. *The American journal of pathology.* 1991;138(3):751.
46. Birnbaum D, Bertucci F, Ginestier C, Tagett R, Jacquemier J, Charafe-Jauffret E. Basal and luminal breast cancers: basic or luminous? *Int J Oncol.* 2004;25(2):249-58.
47. Böcker W, Moll R, Poremba C, Holland R, Van Diest PJ, Dervan P, et al. Common adult stem cells in the human breast give rise to glandular and myoepithelial cell lineages: a new cell biological concept. *Lab Invest.* 2002;82(6):737-46.
48. Korsching E, Packeisen J, Agelopoulos K, Eisenacher M, Voss R, Isola J, et al. Cytogenetic Alterations and Cytokeratin Expression Patterns in Breast Cancer: Integrating a New Model of Breast Differentiation into Cytogenetic Pathways of Breast Carcinogenesis. *Lab Invest.* 2002;82(11):1525-33.
49. Woelfle U, Sauter G, Santjer S, Brakenhoff R, Pantel K. Down-Regulated Expression of Cytokeratin 18 Promotes Progression of Human Breast Cancer. *Clinical Cancer Research.* 2004;10(8):2670-4.
50. Fortier A-M, Asselin E, Cadrin M. Keratin 8 and 18 Loss in Epithelial Cancer Cells Increases Collective Cell Migration and Cisplatin Sensitivity through Claudin1 Up-regulation. *J Biol Chem.* 2013;288(16):11555-71.
51. Rodríguez-Pinilla SM, Sarrió D, Honrado E, Hardisson D, Calero F, Benitez J, et al. Prognostic significance of basal-like phenotype and fascin expression in node-negative invasive breast carcinomas. *Clin Cancer Res.* 2006;12(5):1533-9.
52. Park CK, Jung WH, Koo JS. Expression of cancer-associated fibroblast-related proteins differs between invasive lobular carcinoma and invasive ductal carcinoma. *Breast Cancer Res Treat.* 2016;159(1):55-69.
53. Zhao JJ, Liu Z, Wang L, Shin E, Loda MF, Roberts TM. The oncogenic properties of mutant p110alpha and p110beta phosphatidylinositol 3-kinases in human mammary epithelial cells. *Proc Natl Acad Sci U S A.* 2005;102(51):18443-8.
54. The Cancer Genome Atlas N. Comprehensive molecular portraits of human breast tumours. *Nature.* 2012;490(7418):61-70.
55. Liu T, Yacoub R, Taliaferro-Smith LD, Sun S-Y, Graham TR, Dolan R, et al. Combinatorial Effects of Lapatinib and Rapamycin in Triple-Negative Breast Cancer Cells. *Mol Cancer Ther.* 2011;10(8):1460-9.
56. Cossu-Rocca P, Orrù S, Mironi MR, Sanges F, Sotgiu G, Ena S, et al. Analysis of PIK3CA Mutations and Activation Pathways in Triple Negative Breast Cancer. *PLoS One.* 2015;10(11):e0141763.
57. Ooms LM, Binge LC, Davies EM, Rahman P, Conway JR, Gurung R, et al. The Inositol Polyphosphate 5-Phosphatase PIPP Regulates AKT1-Dependent Breast Cancer Growth and Metastasis. *Cancer Cell.* 2015;28(2):155-69.
58. Stephens P, Hunter C, Bignell G, Edkins S, Davies H, Teague J, et al. Lung cancer: intragenic ERBB2 kinase mutations in tumours. *Nature.* 2004;431(7008):525-6.

59. Lynch TJ, Bell DW, Sordella R, Gurubhagavatula S, Okimoto RA, Brannigan BW, et al. Activating mutations in the epidermal growth factor receptor underlying responsiveness of non-small-cell lung cancer to gefitinib. *N Engl J Med*. 2004;350(21):2129-39.
60. LoPiccolo J, Blumenthal GM, Bernstein WB, Dennis PA. Targeting the PI3K/Akt/mTOR pathway: effective combinations and clinical considerations. *Drug Resist Updat*. 2008;11(1-2):32-50.
61. McCubrey JA, Steelman LS, Kempf CR, Chappell WH, Abrams SL, Stivala F, et al. Therapeutic resistance resulting from mutations in Raf/MEK/ERK and PI3K/PTEN/Akt/mTOR signaling pathways. *J Cell Physiol*. 2011;226(11):2762-81.
62. Steelman LS, Navolanic PM, Sokolosky ML, Taylor JR, Lehmann BD, Chappell WH, et al. Suppression of PTEN function increases breast cancer chemotherapeutic drug resistance while conferring sensitivity to mTOR inhibitors. *Oncogene*. 2008;27(29):4086-95.
63. Umemura S, Yoshida S, Ohta Y, Naito K, Osamura RY, Tokuda Y. Increased phosphorylation of Akt in triple-negative breast cancers. *Cancer Sci*. 2007;98(12):1889-92.
64. Eralp Y, Derin D, Ozluk Y, Yavuz E, Guney N, Saip P, et al. MAPK overexpression is associated with anthracycline resistance and increased risk for recurrence in patients with triple-negative breast cancer. *Ann Oncol*. 2008;19(4):669-74.
65. Sviderskiy VO, Blumenberg L, Gorodetsky E, Karakousi TR, Hirsh N, Alvarez SW, et al. Hyperactive CDK2 Activity in Basal-like Breast Cancer Imposes a Genome Integrity Liability that Can Be Exploited by Targeting DNA Polymerase ϵ . *Mol Cell*. 2020;80(4):682-98.e7.
66. Hamilton E, Infante JR. Targeting CDK4/6 in patients with cancer. *Cancer Treat Rev*. 2016;45:129-38.
67. Warburg O, Wind F, Negelein E. THE METABOLISM OF TUMORS IN THE BODY. *J Gen Physiol*. 1927;8(6):519-30.
68. Alluri P, Newman LA. Basal-like and triple-negative breast cancers: searching for positives among many negatives. *Surg Oncol Clin N Am*. 2014;23(3):567-77.
69. Pelicano H, Zhang W, Liu J, Hammoudi N, Dai J, Xu RH, et al. Mitochondrial dysfunction in some triple-negative breast cancer cell lines: role of mTOR pathway and therapeutic potential. *Breast Cancer Res*. 2014;16(5):434.
70. Vlug E, Ercan C, van der Wall E, van Diest PJ, Derksen PWB. Lobular Breast Cancer: Pathology, Biology, and Options for Clinical Intervention. *Arch Immunol Ther Exp (Warsz)*. 2014;62(1):7-21.
71. Christgen M, Derksen PWB. Lobular breast cancer: molecular basis, mouse and cellular models. *Breast Cancer Res*. 2015;17(1):16.
72. Ciriello G, Michael, Andrew, Matthew, Suhm, Pastore A, et al. Comprehensive Molecular Portraits of Invasive Lobular Breast Cancer. *Cell*. 2015;163(2):506-19.
73. Liu Z, Merkurjev D, Yang F, Li W, Oh S, Friedman MJ, et al. Enhancer activation requires trans-recruitment of a mega transcription factor complex. *Cell*. 2014;159(2):358-73.
74. Shah SP, Roth A, Goya R, Oloumi A, Ha G, Zhao Y, et al. The clonal and mutational evolution spectrum of primary triple-negative breast cancers. *Nature*. 2012;486(7403):395-9.
75. Shu CA, Gainor JF, Awad MM, Chiuzan C, Grigg CM, Pabani A, et al. Neoadjuvant atezolizumab and chemotherapy in patients with resectable non-small-cell lung cancer: an open-label, multicentre, single-arm, phase 2 trial. *Lancet Oncol*. 2020;21(6):786-95.
76. Campbell RA, Bhat-Nakshatri P, Patel NM, Constantinidou D, Ali S, Nakshatri H. Phosphatidylinositol 3-Kinase/AKT-mediated Activation of Estrogen Receptor α : A NEW MODEL FOR ANTI-ESTROGEN RESISTANCE *. *J Biol Chem*. 2001;276(13):9817-24.
77. Ghayad SE, Vendrell JA, Larbi SB, Dumontet C, Bieche I, Cohen PA. Endocrine resistance associated with activated ErbB system in breast cancer cells is reversed by inhibiting MAPK or PI3K/Akt signaling pathways. *Int J Cancer*. 2010;126(2):545-62.
78. Guo JP, Shu SK, Esposito NN, Coppola D, Koomen JM, Cheng JQ. IKKepsilon phosphorylation of estrogen receptor alpha Ser-167 and contribution to tamoxifen resistance in breast cancer. *J Biol Chem*. 2010;285(6):3676-84.
79. Kastrati I, Joosten SEP, Semina SE, Alejo LH, Brovkovych SD, Stender JD, et al. The NF- κ B Pathway Promotes Tamoxifen Tolerance and Disease Recurrence in Estrogen Receptor-Positive Breast Cancers. *Mol Cancer Res*. 2020;18(7):1018-27.

80. Lv Q, Guan S, Zhu M, Huang H, Wu J, Dai X. FGFR1 Is Associated With Tamoxifen Resistance and Poor Prognosis of ER-Positive Breast Cancers by Suppressing ER Protein Expression. *Technol Cancer Res Treat*. 2021;20:15330338211004935.
81. Wang W, Nag SA, Zhang R. Targeting the NF κ B signaling pathways for breast cancer prevention and therapy. *Curr Med Chem*. 2015;22(2):264-89.
82. McFadyen MC, McLeod HL, Jackson FC, Melvin WT, Doehmer J, Murray GI. Cytochrome P450 CYP1B1 protein expression: a novel mechanism of anticancer drug resistance. *Biochem Pharmacol*. 2001;62(2):207-12.
83. Ashrafizadeh M, Mirzaei S, Hashemi F, Zarrabi A, Zabolian A, Saleki H, et al. New insight towards development of paclitaxel and docetaxel resistance in cancer cells: EMT as a novel molecular mechanism and therapeutic possibilities. *Biomed Pharmacother*. 2021;141:111824.
84. Foo MA, You M, Chan SL, Sethi G, Bonney GK, Yong W-P, et al. Clinical translation of patient-derived tumour organoids- bottlenecks and strategies. *Biomarker Research*. 2022;10(1):10.
85. He L, Deng C. Recent advances in organotypic tissue slice cultures for anticancer drug development. *Int J Biol Sci*. 2022;18(15):5885-96.
86. Templeton AR, Jeffery PL, Thomas PB, Perera MPJ, Ng G, Calabrese AR, et al. Patient-Derived Explants as a Precision Medicine Patient-Proximal Testing Platform Informing Cancer Management. *Front Oncol*. 2021;11:767697.
87. Troup S, Njue C, Kliewer EV, Parisien M, Roskelley C, Chakravarti S, et al. Reduced expression of the small leucine-rich proteoglycans, lumican, and decorin is associated with poor outcome in node-negative invasive breast cancer. *Clin Cancer Res*. 2003;9(1):207-14.
88. Conklin MW, Eickhoff JC, Riching KM, Pehlke CA, Eliceiri KW, Provenzano PP, et al. Aligned Collagen Is a Prognostic Signature for Survival in Human Breast Carcinoma. *The American Journal of Pathology*. 2011;178(3):1221-32.
89. Provenzano PP, Inman DR, Eliceiri KW, Knittel JG, Yan L, Rueden CT, et al. Collagen density promotes mammary tumor initiation and progression. *BMC Med*. 2008;6(1):11.
90. Walsh AJ, Cook RS, Lee JH, Arteaga CL, Skala MC. Collagen density and alignment in responsive and resistant trastuzumab-treated breast cancer xenografts. *Journal of biomedical optics*. 2015;20(2):026004.
91. Fadare O, Wang SA, Hileeto D. The expression of cytokeratin 5/6 in invasive lobular carcinoma of the breast: evidence of a basal-like subset? *Hum Pathol*. 2008;39(3):331-6.
92. Fettig LM, McGinn O, Finlay-Schultz J, LaBarbera DV, Nordeen SK, Sartorius CA. Cross talk between progesterone receptors and retinoic acid receptors in regulation of cytokeratin 5-positive breast cancer cells. *Oncogene*. 2017;36(44):6074-84.
93. Kabos P, Haughian JM, Wang X, Dye WW, Finlayson C, Elias A, et al. Cytokeratin 5 positive cells represent a steroid receptor negative and therapy resistant subpopulation in luminal breast cancers. *Breast Cancer Res Treat*. 2011;128(1):45-55.
94. McGinn O, Ward AV, Fettig LM, Riley D, Ivie J, Paul KV, et al. Cytokeratin 5 alters β -catenin dynamics in breast cancer cells. *Oncogene*. 2020;39(12):2478-92.
95. Campaner E, Zannini A, Santorsola M, Bonazza D, Bottin C, Cancila V, et al. Breast Cancer Organoids Model Patient-Specific Response to Drug Treatment. *Cancers (Basel)*. 2020;12(12).
96. Foulkes WD, Brunet J-Sb, Stefansson IM, Straume O, Chappuis PO, Bégin LR, et al. The Prognostic Implication of the Basal-Like (Cyclin Ehigh/p27low/p53+/Glomeruloid-Microvascular-Proliferation+) Phenotype of BRCA1-Related Breast Cancer. *Cancer Res*. 2004;64(3):830-5.
97. Foulkes WD, Stefansson IM, Chappuis PO, Bégin LR, Goffin JR, Wong N, et al. Germline BRCA1 Mutations and a Basal Epithelial Phenotype in Breast Cancer. *JNCI: Journal of the National Cancer Institute*. 2003;95(19):1482-5.
98. Bartholomeusz C, Gonzalez-Angulo AM, Liu P, Hayashi N, Lluch A, Ferrer-Lozano J, et al. High ERK protein expression levels correlate with shorter survival in triple-negative breast cancer patients. *Oncologist*. 2012;17(6):766-74.

99. Bai X, Ni J, Beretov J, Wasinger VC, Wang S, Zhu Y, et al. Activation of the eIF2 α /ATF4 axis drives triple-negative breast cancer radioresistance by promoting glutathione biosynthesis. *Redox Biol.* 2021;43:101993.
100. Pakos-Zebrucka K, Koryga I, Mnich K, Ljubic M, Samali A, Gorman AM. The integrated stress response. *EMBO Rep.* 2016;17(10):1374-95.
101. Pouysségur J, Dayan F, Mazure NM. Hypoxia signalling in cancer and approaches to enforce tumour regression. *Nature.* 2006;441(7092):437-43.
102. Sonenberg N, Hinnebusch AG. Regulation of translation initiation in eukaryotes: mechanisms and biological targets. *Cell.* 2009;136(4):731-45.
103. Bhat M, Robichaud N, Hulea L, Sonenberg N, Pelletier J, Topisirovic I. Targeting the translation machinery in cancer. *Nature Reviews Drug Discovery.* 2015;14(4):261-78.
104. Flowers A, Chu QD, Panu L, Meschonat C, Caldito G, Lowery-Nordberg M, et al. Eukaryotic initiation factor 4E overexpression in triple-negative breast cancer predicts a worse outcome. *Surgery.* 2009;146(2):220-6.
105. McCawley LJ, Li S, Wattenberg EV, Hudson LG. Sustained activation of the mitogen-activated protein kinase pathway. A mechanism underlying receptor tyrosine kinase specificity for matrix metalloproteinase-9 induction and cell migration. *J Biol Chem.* 1999;274(7):4347-53.
106. Wei Y, Chen YH, Li LY, Lang J, Yeh SP, Shi B, et al. CDK1-dependent phosphorylation of EZH2 suppresses methylation of H3K27 and promotes osteogenic differentiation of human mesenchymal stem cells. *Nat Cell Biol.* 2011;13(1):87-94.
107. Yang CC, LaBaff A, Wei Y, Nie L, Xia W, Huo L, et al. Phosphorylation of EZH2 at T416 by CDK2 contributes to the malignancy of triple negative breast cancers. *Am J Transl Res.* 2015;7(6):1009-20.
108. Oeckinghaus A, Ghosh S. The NF-kappaB family of transcription factors and its regulation. *Cold Spring Harb Perspect Biol.* 2009;1(4):a000034.
109. Chen F, Castranova V. Nuclear Factor-kB, an Unappreciated Tumor Suppressor. *Cancer Res.* 2007;67(23):11093-8.
110. Nathan MR, Schmid P. A Review of Fulvestrant in Breast Cancer. *Oncology and Therapy.* 2017;5(1):17-29.
111. Alves CL, Elias D, Lyng M, Bak M, Kirkegaard T, Lykkesfeldt AE, et al. High CDK6 Protects Cells from Fulvestrant-Mediated Apoptosis and is a Predictor of Resistance to Fulvestrant in Estrogen Receptor-Positive Metastatic Breast Cancer. *Clinical Cancer Research.* 2016;22(22):5514-26.
112. Yamnik RL, Digilova A, Davis DC, Brodt ZN, Murphy CJ, Holz MK. S6 Kinase 1 Regulates Estrogen Receptor β ; in Control of Breast Cancer Cell Proliferation *. *J Biol Chem.* 2009;284(10):6361-9.
113. Early Breast Cancer Trialists' Collaborative G. Relevance of breast cancer hormone receptors and other factors to the efficacy of adjuvant tamoxifen: patient-level meta-analysis of randomised trials. *The Lancet.* 2011;378(9793):771-84.
114. Andrade VP, Gobbi H. Accuracy of typing and grading invasive mammary carcinomas on core needle biopsy compared with the excisional specimen. *Virchows Arch.* 2004;445(6):597-602.
115. Burge CN, Chang HR, Apple SK. Do the histologic features and results of breast cancer biomarker studies differ between core biopsy and surgical excision specimens? *Breast.* 2006;15(2):167-72.
116. Ough M, Velasco J, Hieken TJ. A comparative analysis of core needle biopsy and final excision for breast cancer: histology and marker expression. *Am J Surg.* 2011;201(5):692-4.
117. Richter-Ehrenstein C, Müller S, Noske A, Schneider A. Diagnostic accuracy and prognostic value of core biopsy in the management of breast cancer: a series of 542 patients. *Int J Surg Pathol.* 2009;17(4):323-6.
118. Manna S, Holz MK. Tamoxifen Action in ER-Negative Breast Cancer. *Sign Transduct Insights.* 2016;5:1-7.

119. Scarpetti L, Oturkar CC, Juric D, Shellock M, Malvarosa G, Post K, et al. Therapeutic Role of Tamoxifen for Triple-Negative Breast Cancer: Leveraging the Interaction Between ER β and Mutant p53. *Oncologist*. 2023;28(4):358-63.
120. Nowak AK, Wilcken NRC, Stockler MR, Hamilton A, Ghersi D. Systematic review of taxane-containing versus non-taxane-containing regimens for adjuvant and neoadjuvant treatment of early breast cancer. *The Lancet Oncology*. 2004;5(6):372-80.
121. Kim K, Lu Z, Hay ED. DIRECT EVIDENCE FOR A ROLE OF β -CATENIN/LEF-1 SIGNALING PATHWAY IN INDUCTION OF EMT. *Cell Biol Int*. 2002;26(5):463-76.
122. Shi R, Liu L, Wang F, He Y, Niu Y, Wang C, et al. Downregulation of cytokeratin 18 induces cellular partial EMT and stemness through increasing EpCAM expression in breast cancer. *Cell Signal*. 2020;76:109810.
123. Tham Y-L, Gomez LF, Mohsin S, Gutierrez MC, Weiss H, Hilsenbeck SG, et al. Clinical response to neoadjuvant docetaxel predicts improved outcome in patients with large locally advanced breast cancers. *Breast Cancer Res Treat*. 2005;94(3):279-84.
124. Marín-Aguilera M, Codony-Servat J, Reig Ò, Lozano JJ, Fernández PL, Pereira MV, et al. Epithelial-to-Mesenchymal Transition Mediates Docetaxel Resistance and High Risk of Relapse in Prostate Cancer EMT Role in Docetaxel Resistance. *Mol Cancer Ther*. 2014;13(5):1270-84.
125. Yang C-PH, Galbiati F, Volonté D, Horwitz SB, Lisanti MP. Upregulation of caveolin-1 and caveolae organelles in Taxol-resistant A549 cells. *FEBS Lett*. 1998;439(3):368-72.
126. Barbolina MV. Dichotomous role of microtubule associated protein tau as a biomarker of response to and a target for increasing efficacy of taxane treatment in cancers of epithelial origin. *Pharmacol Res*. 2021;168:105585.
127. Puzstai L, Jeong J-H, Gong Y, Ross JS, Kim C, Paik S, et al. Evaluation of Microtubule-Associated Protein-Tau Expression As a Prognostic and Predictive Marker in the NSABP-B 28 Randomized Clinical Trial. *J Clin Oncol*. 2009;27(26):4287-92.
128. Verweij J, Clavel M, Chevalier B. Paclitaxel (Taxol) and docetaxel (Taxotere): not simply two of a kind. *Ann Oncol*. 1994;5(6):495-505.
129. Schmidt M, Bremer E, Hasenclever D, Victor A, Gehrman M, Steiner E, et al. Role of the progesterone receptor for paclitaxel resistance in primary breast cancer. *Br J Cancer*. 2007;96(2):241-7.
130. Beviglia L, Matsumoto K, Lin C-S, Ziober BL, Kramer RH. Expression of the C-Met/HGF receptor in human breast carcinoma: Correlation with tumor progression. *Int J Cancer*. 1997;74(3):301-9.
131. Edakuni G, Sasatomi E, Satoh T, Tokunaga O, Miyazaki K. Expression of the hepatocyte growth factor/c-Met pathway is increased at the cancer front in breast carcinoma. *Pathol Int*. 2001;51(3):172-8.
132. Mehra R, Varambally S, Ding L, Shen R, Sabel MS, Ghosh D, et al. Identification of GATA3 as a Breast Cancer Prognostic Marker by Global Gene Expression Meta-analysis. *Cancer Res*. 2005;65(24):11259-64.
133. Pearson A, Proszek P, Pascual J, Fribbens C, Shamsher MK, Kingston B, et al. Inactivating NF1 Mutations Are Enriched in Advanced Breast Cancer and Contribute to Endocrine Therapy Resistance. *Clinical Cancer Research*. 2020;26(3):608-22.
134. Pandey K, An H-J, Kim SK, Lee SA, Kim S, Lim SM, et al. Molecular mechanisms of resistance to CDK4/6 inhibitors in breast cancer: A review. *Int J Cancer*. 2019;145(5):1179-88.
135. Gravdal K, Halvorsen OJ, Haukaas SA, Akslen LA. A Switch from E-Cadherin to N-Cadherin Expression Indicates Epithelial to Mesenchymal Transition and Is of Strong and Independent Importance for the Progress of Prostate Cancer. *Clinical Cancer Research*. 2007;13(23):7003-11.
136. Vilgelm AE, Bergdorf K, Wolf M, Bharti V, Shattuck-Brandt R, Blevins A, et al. Fine-Needle Aspiration-Based Patient-Derived Cancer Organoids. *iScience*. 2020;23(8):101408.

Supplementary Information

SI Materials:

SI Materials 1. Antibodies used in DigiWest protein profiling analysis.

Supplementary Figures:

Figure S1. Multicolor flow cytometry analysis of isolated and expanded TILs from BC specimen

Figure S2. Correlation of nuclear grade in PDM and PTT.

Figure S3. Proteomic comparison of NST and ILC-derived BC PDM.

Figure S4. Identification of resistance and sensitivity marker panels in treatment responder and non-responder microtumors and regression analysis of differently expressed proteins.

Supplementary Tables:

Table S1. Clinical patient data of the patient cohort.

Table S2. Descriptive statistics of “area” and “fluorescent intensity live/dead” measurements in PDM.

Table S3. Raw data of DigiWest® protein signals in PDM and PTT samples and total measured protein amounts.

Table S4. DigiWest®-based AFI protein signals in matched PDM-PTT pairs DigiWest®-based AFI protein signals in matched PDM-PTT pairs.

Table S5. DigiWest®-based AFI protein signals of matched PDM-PTT pairs sorted by pathway affiliation

Table S6. Pearson correlation of protein abundances in PDM and corresponding PTT (PDM/PTT pairs).

Table S7. DigiWest®-based AFI protein signals of n = 42 PDM samples.

Table S8. Descriptive statistics of averaged, median-centered and log2 transformed protein signals for cell cycle, MAPK/RTK and PI3K/AKT pathway in n = 42 PDM samples.

Table S9. Celltox™ Green assay RFU (relative fluorescent unit) values of BC microtumors treated with TAM, DTX, PTX and PAB.

Table S10. Descriptive statistics of simple logistic regression analysis of differentially expressed proteins in treatment responder and non-responder groups.

SI Materials

SI Materials 1. Antibodies used in DigiWest protein profiling analysis.

Analyte	Uniprot	Product_No	Supplier
4E-BP1	Q13541	1557-1	Abcam
53BP1	Q12888	4937	Cell Signaling
53BP1-pThr543	Q12888	3428	Cell Signaling
Akt	P31749	4685	Cell Signaling
Akt-pSer473	P31749	4060	Cell Signaling
alpha-SMA	P62736	14968	Cell Signaling
alpha-Tubulin	P68366	302211	Synaptic Systems
A-Raf	P10398	4432	Cell Signaling
ATG5	Q9H1Y0	12994	Cell Signaling
Beclin-1	Q14457	3738	Cell Signaling
beta-Catenin	P35222	8480	Cell Signaling
beta-Catenin(non-pSer33/37/Thr41)	P35222	8814	Cell Signaling
beta-Catenin-pSer552	P35222	9566	Cell Signaling
b-Raf	P15056	14814	Cell Signaling
b-Raf-p-Ser445	P15056	2696	Cell Signaling
BRCA1	P38398	9010	Cell Signaling
Caveolin-1	Q03135	3238	Cell Signaling
CD11c	P20702	45581	Cell Signaling
CD16	P08637	80006	Cell Signaling
CD25	P01589	13517	Cell Signaling
CD3epsilon	P07766	4443	Cell Signaling
CD4	P01730	PA5-87425	Thermo Fisher Scientific
CD56	P13591	3576	Cell Signaling
CD68	P34810	86985	Cell Signaling
CD8alpha	P01732	85336	Cell Signaling
cdc2(CDK1)	P06493	9112	Cell Signaling
CDK2	P24941	2546	Cell Signaling
CDK2-pThr160	P24941	2561	Cell Signaling
CDK4	P11802	12790	Cell Signaling
CDK4-pThr172	P11802	PA-64482	Invitrogen
CDK6	Q00534	sc-7961	Santa Cruz
CDKN2A	P42771	10883-1-AP	Protein Tech Group
CIP2A	Q8TCG1	A301-454A	Bethyl
c-Met	P08581	3148	Cell Signaling
c-Met-pTyr1003	P08581	3135	Cell Signaling
c-Raf	P04049	9422	Cell Signaling
c-Raf-pSer259	P04049	9421	Cell Signaling
CREB	P16220	9197	Cell Signaling
CREB-pSer133	P16220	9198	Cell Signaling
CTMP	Q96KR2	4612	Cell Signaling
CyclinD1	P24385	2978	Cell Signaling
CyclinE1	P24864	4129	Cell Signaling
Cyp1B1	Q16678	sc-374228	Santa Cruz
Cytokeratin5	P13647	M3270	Spring Bioscience
Cytokeratin6	P02538	2302-1	Abcam
Cytokeratin8/18	P05783	4546	Cell Signaling
Cytokeratin8-pSer23	P05787	2147-1	abcam (Epitomics)
E2F-1	Q01094	3742	Cell Signaling
E2F-2	Q14209	DR1095-100UG	Millipore
E2F-4	Q16254	orb10571	Biorbyt

E-Cadherin	P12830	sc-59778	Santa Cruz
E-Cadherin-pSer838/840	P12830	2239-1	Abcam
eIF2alpha-pSer51	P05198	3398	Cell Signaling
eIF4E	P06730	2067	Cell Signaling
eIF4E-pSer209	P06730	9741	Cell Signaling
ER	P03372	RM-9101-S	Thermo Fisher Scientific
ERalpha-pSer167	#NV	2514	Cell Signaling
Erk1/2	P28482	4695	Cell Signaling
Erk1/2-pThr202/Tyr204	P28482	4370	Cell Signaling
FGFreceptor1	P11362	9740	Cell Signaling
FGFreceptor-pTyr653/654	P11362	3476	Cell Signaling
FLOWER(C9orf7)	Q9UGQ2	orb164624	Biorbyt
FoxO3a	O43524	2497	Cell Signaling
GATA3	P23771	5852	Cell Signaling
GLUT-1	P11166	07-1401	Millipore
GSK3beta	P49841	9315	Cell Signaling
GSK3beta-pSer9	P49841	9336	Cell Signaling
HDAC1	Q13547	2062	Cell Signaling
Her2	P04626	A0485	Dako
HIF1beta(ARNT)	P27540	5537	Cell Signaling
HistoneH3	P68431	9715	Cell Signaling
HLA-A,B,C	n.a.		AG Stevanovic
IDH1	O75874	8137	Cell Signaling
IGF1Rbeta	P08069	3018	Cell Signaling
IGF1R-pTyr1135/Tyr1136	P08069	3024	Cell Signaling
IKKalpha	O15111	2682	Cell Signaling
IKKalpha-pThr23	O15111	ab38515	Abcam
IKKepsilon	Q14164	2905	Cell Signaling
IKKepsilon-pSer172	Q14164	8766	Cell Signaling
JNK/SAPK	P45983	9252	Cell Signaling
JNK/SAPK-pThr183/Tyr185	P45983	4668	Cell Signaling
Ki-67	P46013	K1700-05D	US Biologicals
LAMC1	P11047	92921	Cell Signaling
LDHA	P00338	2012	Cell Signaling
MAD2L1	Q13257	4636	Cell Signaling
MEK1	Q02750	9124	Cell Signaling
MEK1/2-pSer217/221	Q02750	9154	Cell Signaling
MEK2	P36507	9125	Cell Signaling
mTOR(FRAP)	P42345	2983	Cell Signaling
NF1(Neurofibromin)	P21359	14623	Cell Signaling
NF-kBp65-pSer468	Q04206	3039	Cell Signaling
p38MAPK	Q16539	9212	Cell Signaling
p38MAPK-pThr180/Tyr182	Q16539	4511	Cell Signaling
p53	P04637	9282	Cell Signaling
p53-pSer37	P04637	9289	Cell Signaling
p70S6kinase	P23443	2708	Cell Signaling
p70S6kinase-pThr389	P23443	9206	Cell Signaling
PADI4	Q9UM07	sc-365369	Santa Cruz
PAK1/2/3	Q13153	2604	Cell Signaling
PARP	P09874	9532	Cell Signaling
PARP-cleavedAsp214	P09874	9541	Cell Signaling
PD1	Q15116	86163	Cell Signaling
PDK1	Q15118	3062	Cell Signaling
PDK1-pSer241	Q15118	3061	Cell Signaling
PD-L1	Q9NZQ7	13684	Cell Signaling
PI3-kinase p85	P27986	4292	Cell Signaling

PP2AC	P67775	2259	Cell Signaling
PP2AC-pTyr307	P67775	AF3989	R&D
PgR	P06401	8757	Cell Signaling
PTEN	P60484	9552	Cell Signaling
PTEN non- pSer380/Thr382/Thr383	P60484	7960	Cell Signaling
PTEN-pSer380	P60484	9551	Cell Signaling
Rad51	Q06609	ab109107	Abcam
Ras	P01116	8955	Cell Signaling
Rb-pSer795	P06400	9301	Cell Signaling
Rb-pSer807/811	P06400	8516	Cell Signaling
RSK1(p90RSK)-pThr573	Q15418	ab62324	Abcam
S6RP	P62753	2217	Cell Signaling
S6RP-pSer235/236	P62753	2211	Cell Signaling
Snail	O95863	3879	Cell Signaling
Src	P12931	2109	Cell Signaling
Src-pSer17	P12931	5473	Cell Signaling
Src-pTyr527	P12931	2105	Cell Signaling
STAT3	P40763	4904	Cell Signaling
STAT3-pTyr705	P40763	9145	Cell Signaling
Tau	P10636	sc-32274	Santa Cruz
Tau-pSer202	P10636	39357	Cell Signaling
Tubulin acetylated	P68366	T6793	Cell Signaling
Tubulinbeta-1chain	Q9H4B7	MAB16676	Abnova
Vimentin	P08670	5741	Cell Signaling
Vimentin-pSer56	P08670	7391	Cell Signaling

Supplementary Figures

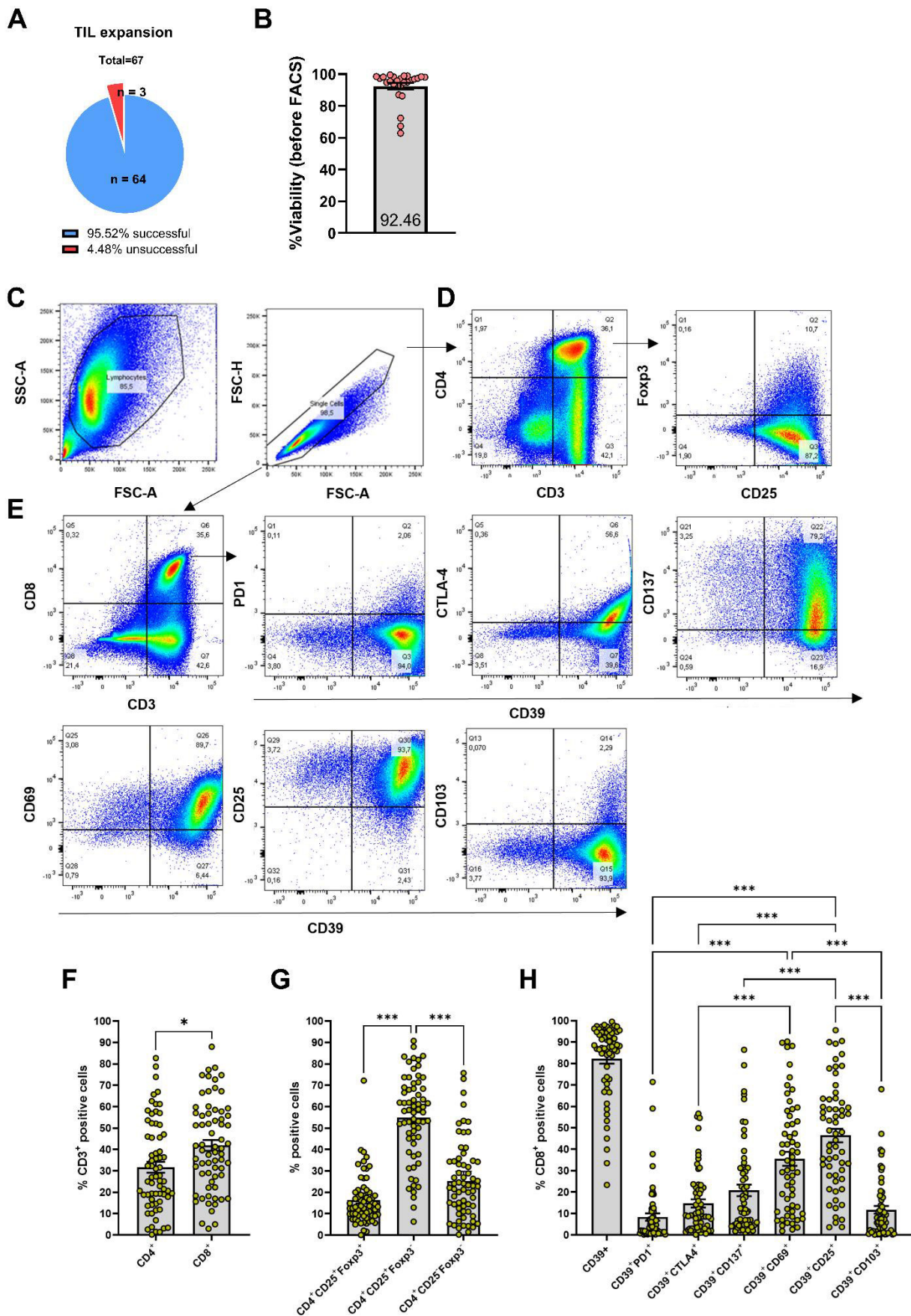


Figure S2. Multicolor flow cytometry analysis of isolated and expanded TILs from BC specimen. TILs were isolated in parallel to PDM isolation as a filtered single cell fraction from digested tumor samples. (A) TILs derived from $n = 67$ tissue samples were subsequently cultured, expanded and characterized by flow cytometry. BC-TIL expansion was highly successful with a 95.52% success rate (B) Viability of expanded TILs measured by NucleoCounter® NC-200™ prior to FACS staining. Average viability was 92.46%. (C) Gating strategy for lymphocyte and single cells. (D) Lymphocytes gated for $CD3^+CD4^+$ and regulatory T cells. (E) Lymphocytes gated for $CD3^+CD8^+$ cells. Cells are further differentiated into tumor-specific $CD39^+$ cells expressing activation markers (PD1, CLTA-4, CD137, CD69, CD25) or the tissue-residence marker (CD103). (F-H) Cell frequencies of $n = 67$, $n = 65$ and $n = 60$ expanded BC-TIL samples; Paired t-test or Friedman test with Dunn's multiple comparison test; * $p < 0.05$, ** $p < 0.01$, *** $p < 0.001$. Data are mean with SEM.

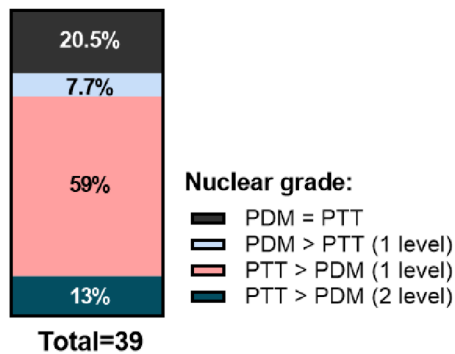


Figure S1. Correlation of nuclear grade in PDM and PTT. Nuclear grading of $n = 39$ PDM and PTT was assessed by a pathologist. In 20.5% of the specimen, nuclear grading of PTT was reflected by PDM. In 59% of the cases, PDM resembled a one-degree lower nuclear grade.

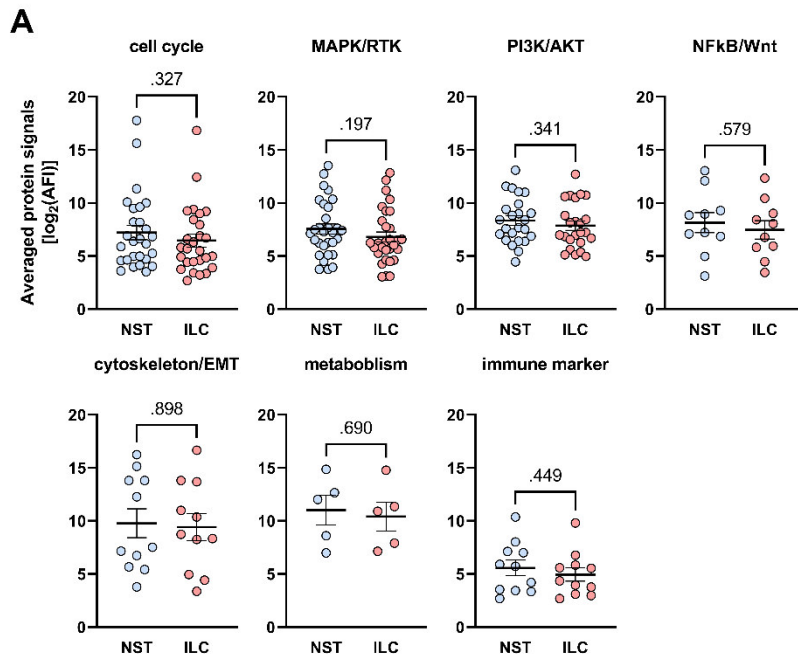
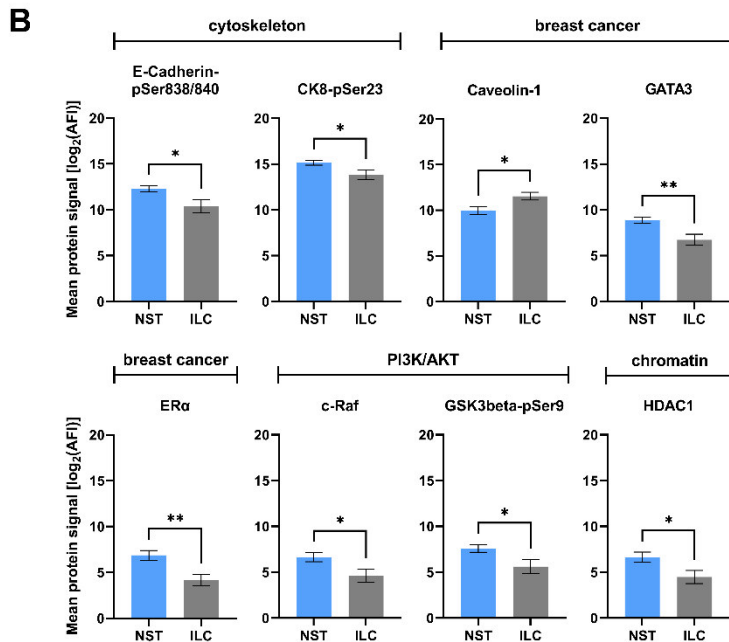


Figure S3. Proteomic comparison of NST and ILC-derived BC PDM. (A) Signaling pathway comparison of NST- and ILC-derived BC PDM. Normalized protein signals (AFI) in NST-/ILC-BC PDM were averaged and log₂ transformed. No significant differences were detected. Mann-Whitney U test, $p < 0.05$. (B) Differentially expressed proteins in NST-/ILC-BC PDM. Enhanced protein abundances in NST- BC PDM were identified for several proteins associated with cell cytoskeleton, PI3K/AKT pathway and chromatin regulation, and with general breast cancer markers. Mann-Whitney U test, * $p < 0.05$, ** $p < 0.01$, *** $p < 0.001$. Data are mean with SEM.



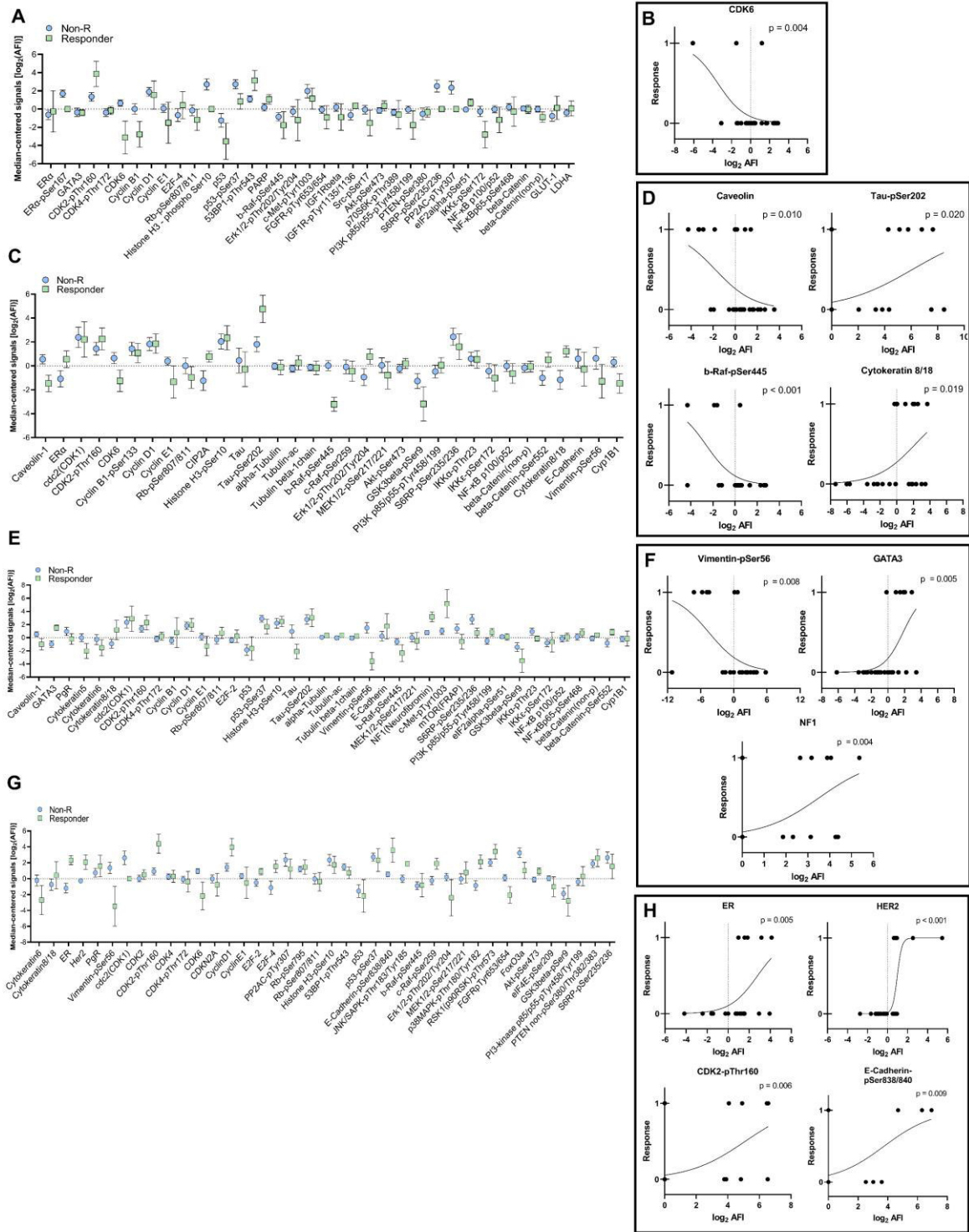


Figure S4. Identification of resistance and sensitivity marker panels in treatment responder and non-responder microtumors and regression analysis of differently expressed proteins. Microtumors were treated with four anti-cancer drugs and grouped into treatment responder and non-responders based on the results of cell death assays (CellTox™ green cytotoxicity assay, Promega). DigiWest AFI protein signals of microtumors were median-centered, log₂-transformed and compared between R and Non-R groups. Proteins that are associated with response/resistance to therapy according to literature, are differentially expressed, or are involved in therapy-related signaling pathways were plotted as interleaved scatter plots for tamoxifen (A), docetaxel (C), paclitaxel (E), and palbociclib (G) treatment. Blue symbols indicate the mean protein signal of the non-responder group, green symbols indicate the mean protein signal of the responder group. Simple logistic regression of differentially expressed proteins are depicted in (B) for tamoxifen, (D) for docetaxel, (F) for paclitaxel and (H) for palbociclib responses (1 = response; 0 = no response). Protein signals are displayed as log₂ transformed AFI signals. As indicated by p-values (LRT) < 0.05, the amount of the shown proteins (predictor variables) significantly affected the likelihood of response to treatment. Descriptive statistics of simple logistic regressions are shown in Table S10. *p < 0.05, **p < 0.01 and ***p < 0.001. Shown are mean with SEM. Non-R and R. AFI: average fluorescent intensities; Non-R: non-responder; R: responder.

Supplementary Tables

Table S1. Clinical patient data of the patient cohort.

Sample ID#	Study-ID#	Age	Tumor status	Histological type	Tumor grade	ER	ER-IRS	PR	PR-IRS	Her2	Her2-IHC-Score	pT	pN	cM	pL	pV	pPn
BC1	#001	77	primary carcinoma	ILC	2	1	12	0	0	0	0	2	2	0	0	0	0
BC2	#002	92	primary carcinoma	NST	3	0	0	0	0	1	3+	3	X	X	1	0	0
BC3	#003	57	primary carcinoma	NST	2	1	12	0	0	0	1+	3	3a	1	1	0	0
BC4	#004	62	primary carcinoma	NST	3	1	12	0	0	0	1+	2	1a	0	1	0	1
BC5	#005	62	primary carcinoma	ILC	2	1	12	1	12	0	2+	2	3a	0	0	0	1
BC6	#006	49	primary carcinoma	ILC	2	1	8	1	2	0	0	3	2a	0	0	0	0
BC7	#007	56	primary carcinoma	NST	2	1	12	1	12	0	1+	4b	3a	0	1	0	1
BC8	#008	55	primary carcinoma	NST	2	1	12	1	12	0	0	3	1a	1	0	0	0
BC8	#008	55	primary carcinoma	NST	2	1	12	1	12	0	0	3	1a	1	0	0	0
BC9	#009	61	primary carcinoma	NST	3	1	4	1	1	0	0	4d	3b	1	1	0	0
BC10	#010	83	primary carcinoma	NST	2	1	12	1	12	0	1+	4b	1a	0	0	0	0
BC11	#011	54	primary carcinoma	NST	3	1	12	0	0	0	2+	3	0	0	0	0	0
BC12	#012	84	primary carcinoma	NST	1	1	12	1	12	0	2+	1c	1a	0	0	0	0
BC13	#013	54	primary carcinoma	NST	3	1	9	1	6	0	2+	2	0	0	1	0	0
BC14	#014	78	primary carcinoma	NST	2	1	0	0	0	0	1+	2	0	0	0	0	0
BC15	#015	50	primary carcinoma	ILC	2	1	12	1	12	0	2+	2	1	0	0	0	0
BC16	#016	74	primary carcinoma	NST	2	1	12	1	4	0	1+	1c	1a	0	1	0	0
BC17	#017	87	primary carcinoma	NST	3	1	12	1	12	0	2+	2	1a	1	1	0	0
BC18	#018	48	primary carcinoma	NST	3	1	12	1	9	0	2+	2	0	0	0	0	0
BC19	#019	70	second primary carcinoma	NST	3	0	0	0	0	0	0	1c	0	0	0	0	0
BC20	#020	64	primary carcinoma	NST	3	0	0	0	0	0	0	3	0	0	0	0	0
BC21	#021	82	primary carcinoma	NST	2	1	12	1	12	0	2+	1c	0	0	0	0	0
BC22	#022	54	primary carcinoma	NST	1	1	12	1	12	0	1+	1c	0	0	0	0	0
BC23	#023	56	primary carcinoma	mucinous	2	1	12	1	12	0	2+	2	1a	0	0	0	0
BC24	#024	54	primary carcinoma	NST	2	1	12	1	12	0	2+	2	1	0	0	0	0
BC25	#025	69	primary carcinoma	ILC	2	1	12	1	12	0	1+	2	0	0	0	0	0
BC26	#026	81	primary carcinoma	NST	3	1	12	1	6	0	2+	2	1	0	0	0	0
BC27	#027	77	primary carcinoma	ILC	2	1	12	1	4	0	0	3	1a	0	0	0	0
BC28	#028	66	primary carcinoma	NST	2	1	12	1	9	0	1+	2	1a	1	0	0	0
BC29	#029	87	primary carcinoma	NST	2	1	12	0	2	0	1+	2	2a	X	0	0	1
BC30	#030	48	primary carcinoma	NST	3	1	12	1	6	0	2+	2	0	0	0	0	0
BC31	#031	74	primary carcinoma	NST	3	1	4	0	0	0	0	2	0	0	0	0	0
BC32	#032	61	primary carcinoma	NST	3	1	12	1	9	0	2+	0	0	0	0	0	0
BC33	#033	82	primary carcinoma	NST	2	1	12	1	12	0	0	2	0	X	0	0	0
BC34	#034	83	primary carcinoma	NST	3	0	0	0	0	0	0	3	0	0	0	1	0
BC35	#035	66	primary carcinoma	NST	2	1	12	1	2	0	1+	1c	0	1	0	0	0
BC36	#036	81	primary carcinoma	NST	3	1	3	0	0	1	3+	2	1	X	0	0	0
BC37	#037	34	primary carcinoma	NST	3	1	9	1	2	0	0	3	3a	x	0	0	0
BC38	#038	87	primary carcinoma	NST	3	0	0	0	0	0	2+	2	2a	X	0	0	1
BC39	#039	51	primary carcinoma	medullary	3	1	6	0	0	0	0	2	0	0	0	0	0
BC40	#040	51	primary carcinoma	NST	3	1	1	1	0	0	1+	2	1a	1	0	0	0
BC41	#041	84	primary carcinoma	NST	3	1	12	1	2	0	1+	2	3a	x	1	1	0
BC42	#042	60	primary carcinoma	NST	3	1	12	1	12	0	1+	2	2a	0	0	0	0
BC43	#043	42	primary carcinoma	ILC	2	1	12	1	12	0	1+	2	1a	x	0	0	0
BC44	#044	76	primary carcinoma	ILC	2	1	12	1	6	0	0	2	1a	0	0	0	0
BC45	#045	66	primary carcinoma	NST	3	1	12	1	4	0	1+	2	1a	0	0	0	0
BC46	#046	51	primary carcinoma	DCIS	3	1	9	0	0	0	0	is	x	0	0	0	0
BC47	#047	75	primary carcinoma	NST	3	1	12	1	2	0	0	2	3a	x	1	0	0
BC48	#048	62	primary carcinoma	NST	3	0	0	0	1	0	0	1c	0	0	0	0	0
BC49	#049	79	primary carcinoma	NST	2	1	12	1	12	0	2+	2	0(+)	x	0	0	0
BC50	#050	80	primary carcinoma	ILC	2	1	12	1	3	0	0	1c	0(-)	X	0	0	0
BC51	#051	62	primary carcinoma	ILC	2	1	12	1	9	0	0	2	1a	X	0	0	0
BC52	#052	57	primary carcinoma	NST	3	0	0	0	0	0	1+	2	X	0	0	0	0
BC53	#053	55	primary carcinoma	ILC	2	1	12	1	9	0	1+	2	2a	0	0	0	0
BC54	#054	79	primary carcinoma	SPC	2	1	12	1	8	0	0	2	1	1	0	0	0
BC55	#055	70	primary carcinoma	NST	3	1	8	1	0	0	2+	2	1a	0	0	0	0
BC56	#056	52	primary carcinoma	ILC	1	1	12	1	12	0	0	3	1a	X	0	0	0
BC57	#057	72	primary carcinoma	NST	2	1	12	1	8	0	2+	2	0	0	0	0	0
BC58	#058	48	primary carcinoma	NST	2	1	12	1	12	0	2+	2	1a	0	0	0	0
BC59	#059	74	primary carcinoma	ILC	2	1	12	1	12	0	2+	2	0	0	0	0	0
BC60	#060	40	primary carcinoma	NST	2	1	1	1	0	0	1+	2	1	X	1	0	0
BC61	#061	63	primary carcinoma	NST	1	1	12	1	9	0	1+	2	0	X	0	0	0
BC62	#062	79	primary carcinoma	NST	0	0	0	0	0	1	3+	2	0	0	0	0	0
BC63	#063	64	primary carcinoma	micropapillary	2	1	12	1	4	0	2+	1c	1a	1	0	1	0
BC64	#064	80	primary carcinoma	NST	3	1	12	1	12	0	1+	2	1a	x	0	0	0
BC65	#065	79	primary carcinoma	NST	3	1	12	1	8	0	2+	2	1a	x	0	0	0
BC66	#066	64	primary carcinoma	ILC	2	1	12	1	12	0	1+	1c	0	0	0	0	0
BC66	#066	64	primary carcinoma	ILC	2	1	12	1	6	0	1+	2	1a	x	0	0	0
BC67	#067	85	primary carcinoma	NST	2	0	0	0	0	0	2+	2	0	x	0	0	0
BC68	#068	47	primary carcinoma	NST	2	1	1	1	0	0	0	2	0	0	0	0	0
BC69	#069	79	primary carcinoma	ILC	2	1	12	1	9	0	2+	2	1a	1	0	0	0
BC70	#070	48	primary carcinoma	ILC	2	1	12	1	12	0	2+	1c	0	x	0	0	0
BC71	#071	61	recidiv	NST	2	1	12	1	12	0	1+	1c	0	x	0	0	0
BC72	#072	61	recidiv	ILC	2	1	12	1	3	0	2+	2	0(-)	0	0	0	0
BC73	#073	49	primary carcinoma	NST	2	1	12	1	8	0	2+	2	0	0	0	0	0
BC74	#074	84	primary carcinoma	ILC	2	1	12	1	9	0	1+	1c	1a	1	0	0	0
BC75	#075	54	primary carcinoma	NST	2	1	12	1	12	0	2+	2	1a	x	0	0	0
BC76	#076	64	primary carcinoma	ILC	2	1	12	1	3	0	2+	3	1a	x	0	0	0
BC77	#077	71	primary carcinoma	NST	2	1	12	1	8	0	1+	2	1a	0	0	0	0
BC78	#078	66	recidiv	NST	3	1	12	1	8	0	1+	2	0	0	0	0	0
BC79	#079	73	primary carcinoma	ILC	2	1	12	1	9	0	2+	2	0	0	0	0	0
BC80	#080	88	primary carcinoma	NST	2	1	12	1	12	0	1+	2	x	x	0	0	0
BC81	#081	75	primary carcinoma	NST	3	0	0	0	0	0	0	4b	0	0	0	0	0
BC82	#082	59	primary carcinoma	NST	3	0	0	0	0	0	0	2	1a	0	0	0	0
BC83	#083	59	primary carcinoma	ILC	2	1	12	0	0	0	1+	2	0(-)	0	0	0	0
BC84	#084	87	primary carcinoma	NST	3	1	12	0	1	0	2+	3	X	X	0	0	0
BC85	#085	79	primary carcinoma	ILC	2	1	12	1	8	0	2+	3	0	x	1	0	0
BC86	#086	77	recidiv	ILC	2	1	12	1	9	0	2+	2	0(-)	0	0	0	0
BC87	#087	43	primary carcinoma	NST	2	1	12	1	12	0	1+	2	0	1	0	0	0
BC88	#088	80	primary carcinoma	NST	3	1	12	1	6	0	1+	4b	3a	1	0	0	0
BC89	#089	71	primary carcinoma	ILC	2	1	12	1	12	0	1+	2	0(-)	0	0	0	0
BC90	#090	82	primary carcinoma	NST	2	1	12	1	9	0	2+	2	0	0	0	0	0
BC91	#091	61	primary carcinoma	ILC	2	1	12	1	6	0	1+	3	0(-)	x	0	0	1
BC92	#092	68	primary carcinoma	ILC	2	1	12	1	12	0	0	1c	0	x	0	0	0
BC93	#093	78	primary carcinoma	NST	2	1	12	1	9	0	1+	1c	0	x	0	0	0
BC94	#094	51	primary carcinoma	NST	2	1	12	1	12	0	2+	4b	1a	x	1	0	0
BC95	#095	71	primary carcinoma	NST	2	1	9	1	9	0	0	2	1a	x	0	0	0
BC96	#096	48	primary carcinoma	NST	2	1	12	1	12	0	0	3	3a	1	0	0	0
BC97	#097	49	primary carcinoma	ILC	2	1	12	1	12	0	2+	3	1a	0	0	0	0
BC98	#098	54	primary carcinoma	NST	2	1	?	0	0	0	0	2	1a	x	1	0	0
BC99	#099	61	primary carcinoma	NST	2	1	12	1									

Table S2. Descriptive statistics of “area” and “fluorescent intensity live/dead” measurements in PDM.

	Area	Calcein-AM FI / Total Volume	Sytox Orange FI / Total Volume
Number of values	81	80	80
Minimum	7003	1	0
Maximum	888481	42306	6973
Range	881478	42305	6973
Mean	59261	9081	909.7
Std. Deviation	130386	9396	1097
Std. Error of Mean	14487	1051	122.7
Lower 95% CI of mean	30430	6990	665.6
Upper 95% CI of mean	88092	11172	1154
Coefficient of variation	220.0%	103.5%	120.6%

Table S3. Raw data of DigiWest® protein signals in PDM and PTT samples and total measured protein amounts.

Table S4. DigiWest®-based AFI protein signals in matched PDM-PTT pairs DigiWest®-based AFI protein signals in matched PDM-PTT pairs.

Table S5. DigiWest®-based AFI protein signals of matched PDM-PTT pairs sorted by pathway affiliation

Table S6. Pearson correlation of protein abundances in PDM and corresponding PTT (PDM/PTT pairs).

	Pearson r	p-value	
Cytokeratin 8-pSer23	0.55	0.013	*
ERa	0.86	<0.001	***
GATA3	0.83	<0.001	***
CDK4	0.52	0.019	*
CDKN2A	0.66	0.002	**
E2F-4	0.45	0.048	*
PP2A C	0.58	0.007	**
HDAC1	0.56	0.010	*
alpha-Tubulin	0.63	0.003	**
53BP1	0.72	<0.001	***
PARP	0.45	0.048	*
E-Cadherin-pSer838/840	0.69	<0.001	***
HIF1 beta (ARNT)	0.49	0.029	*
JNK/SAPK	0.47	0.037	*
JNK/SAPK-pThr183/Tyr185	0.61	0.004	**
p38 MAPK	0.56	0.010	*
GLUT-1	0.70	<0.001	***
PAK 1/2/3	0.63	0.003	**
IKK alpha	0.68	<0.001	**
eIF4E	0.56	0.010	**
eIF4E-pSer209	0.71	<0.001	***
GSK3 beta	0.60	0.005	**
mTOR (FRAP)	0.58	0.008	**
PDK1	0.52	0.020	*
PDK1-pSer241	0.45	0.046	*
PI3-kinase p85	0.69	<0.001	***
PTEN	0.56	0.011	*
S6 ribosomal protein	0.49	0.027	*
S6RP-pSer235/236	0.60	0.005	**
IGF1 receptor beta	0.59	0.006	**
Src	0.50	0.029	*
Src-pSer17	0.54	0.014	*
Src-pTyr527	0.55	0.011	*
STAT 3	0.86	<0.001	***
beta-Catenin	0.50	0.024	*
beta-Catenin-pSer552	0.78	<0.001	***

Table S7. DigIWest®-based AFI protein signals of n = 42 PDM samples.

Table S8. Descriptive statistics of averaged, median-centered and log2 transformed protein signals for cell cycle, MAPK/RTK and PI3K/AKT pathway in n = 42 PDM samples.

cell cycle										MAPK/RTK										PI3K/AKT									
Sample	Number	Min.	Max.	25% Percentile	75% Percentile	Median	Range	Lower 95% CI of mean	Upper 95% CI of mean	Sample	Number	Min.	Max.	25% Percentile	75% Percentile	Median	Range	Lower 95% CI of mean	Upper 95% CI of mean	Sample	Number	Min.	Max.	25% Percentile	75% Percentile	Median	Range	Lower 95% CI of mean	Upper 95% CI of mean
BC14(HR+)	15	-5.44	3.32	-3.18	1.85	-1.45	8.76	-2.584	0.4253	BC14(HR+)	15	-5.44	3.32	-3.18	1.85	-1.45	8.76	-2.584	0.4253	BC14(HR+)	21	-1.62	2.87	-0.665	0.335	-0.19	4.49	-0.4901	0.4472
BC15(HR+)	15	-7.48	1.2	-5.53	-1.46	-3.95	8.88	-5.18	-2.269	BC15(HR+)	15	-7.48	1.2	-5.53	-1.46	-3.95	8.68	-5.18	-2.269	BC15(HR+)	21	-5.85	1.37	-4.32	-1.85	-3.29	7.22	-3.765	-2.178
BC18(HR+)	15	-8.27	-0.28	-7.39	-2.61	-3.75	7.99	-5.788	-2.857	BC18(HR+)	15	-8.27	-0.28	-7.39	-2.61	-3.75	7.99	-5.788	-2.857	BC18(HR+)	21	-6.62	1.39	-4.605	-2.665	-3.56	8.01	-4.325	-2.653
BC20(TNBC)	15	-5.53	3.9	0.25	2.43	1.89	9.43	-0.1528	2.359	BC20(TNBC)	15	-5.53	3.9	0.25	2.43	1.89	9.43	-0.1528	2.359	BC20(TNBC)	21	-5.16	5.19	0.03	2.065	1.17	10.35	0.09399	1.926
BC23(HR+)	15	-4.27	3.69	-1.12	1.78	-0.04	7.96	-1.117	1.119	BC23(HR+)	15	-4.27	3.69	-1.12	1.78	-0.04	7.96	-1.117	1.119	BC23(HR+)	21	-5.96	2.99	-0.93	0.07	-0.65	8.95	-1.231	0.3114
BC24(HR+)	15	-6.09	1.57	-1.65	0.55	-0.64	7.66	-2.246	0.1737	BC24(HR+)	15	-6.09	1.57	-1.65	0.55	-0.64	7.66	-2.246	0.1737	BC24(HR+)	21	-1.86	1.09	-0.66	0.645	0	2.95	-0.4791	0.2858
BC25(HR+)	15	-7.48	-0.4	-5.53	-2.51	-3.98	7.08	-5.295	-2.866	BC25(HR+)	15	-7.48	-0.4	-5.53	-2.51	-3.98	7.08	-5.295	-2.866	BC25(HR+)	21	-5.32	1.77	-3.795	-1.78	-2.43	7.09	-3.351	-1.894
BC28(HR+)	15	0.16	2.28	0.32	1.29	0.94	2.12	0.6103	1.347	BC28(HR+)	15	0.16	2.28	0.32	1.29	0.94	2.12	0.6103	1.347	BC28(HR+)	21	0.05	5.08	0.42	1.285	0.57	5.03	0.5325	1.488
BC32(HR+)	15	-5.53	2.72	-0.29	1.2	0.56	8.25	-0.7142	1.458	BC32(HR+)	15	-5.53	2.72	-0.29	1.2	0.56	8.25	-0.7142	1.458	BC32(HR+)	21	-1.44	6.2	0.325	1.395	0.84	7.64	0.3218	1.597
BC36(HR+)	15	-7.48	1.18	-4.27	0.03	-0.95	8.66	-3.401	-0.4483	BC36(HR+)	15	-7.48	1.18	-4.27	0.03	-0.95	8.66	-3.401	-0.4483	BC36(HR+)	21	-4.44	3.31	-1.305	0.175	-0.16	7.75	-1.567	0.1052
BC38(TNBC)	15	-13.11	1.43	-4.36	1.17	-2	14.54	-4.809	-0.3056	BC38(TNBC)	15	-13.11	1.43	-4.36	1.17	-2	14.54	-4.809	-0.3056	BC38(TNBC)	21	-5.32	2.4	0.17	1.665	1	7.72	-0.1621	1.368
BC39(HR+)	15	-3.95	2.06	-0.55	1.1	0.34	6.01	-0.9878	0.8892	BC39(HR+)	15	-3.95	2.06	-0.55	1.1	0.34	6.01	-0.9878	0.8892	BC39(HR+)	21	-5.85	2.58	0.075	1.305	0.85	8.43	-0.6886	1.184
BC42(HR+)	15	-7.48	2.8	-5.44	-2.01	-3.11	10.28	-4.628	-1.562	BC42(HR+)	15	-7.48	2.8	-5.44	-2.01	-3.11	10.28	-4.628	-1.562	BC42(HR+)	21	-5.96	1.08	-2.71	-0.285	-0.86	7.04	-2.419	-0.5609
BC43(HR+)	15	-8.8	0.65	-5.74	-1.88	-3.95	9.45	-5.651	-2.612	BC43(HR+)	15	-8.8	0.65	-5.74	-1.88	-3.95	9.45	-5.651	-2.612	BC43(HR+)	21	-5.96	1.68	-3.795	0.445	-1.14	7.64	-2.615	-0.3798
BC45(HR+)	15	-6.09	3.05	-3.18	2.38	0.54	9.14	-1.705	1.425	BC45(HR+)	15	-6.09	3.05	-3.18	2.38	0.54	9.14	-1.705	1.425	BC45(HR+)	21	-7.48	2.86	-3.975	1.825	0.86	10.34	-2.083	0.8826
BC46(HR+)	15	-3.25	1.91	-0.87	0.48	0	5.16	-0.7778	0.5685	BC46(HR+)	15	-3.25	1.91	-0.87	0.48	0	5.16	-0.7778	0.5685	BC46(HR+)	21	-2.51	0.89	-1.59	-0.14	-1.05	3.4	-1.314	-0.5334
BC54(HR+)	14	-1.86	2	-0.1125	1.263	0.725	3.86	-0.006738	1.154	BC54(HR+)	14	-1.86	2	-0.1125	1.263	0.725	3.86	-0.006738	1.154	BC54(HR+)	21	-7.48	1.81	-0.695	0.34	0.04	9.29	-1.356	0.3466
BC58(HR+)	15	-3.18	3.34	0.41	1.49	0.93	6.52	0.0843	1.676	BC58(HR+)	15	-3.18	3.34	0.41	1.49	0.93	6.52	0.0843	1.676	BC58(HR+)	21	-4.89	1.82	-0.82	0.79	0.09	6.71	-1.028	0.5189
BC60(HR+)	13	-3.52	0.09	-2.23	-1.385	-1.82	3.61	-2.401	-1.199	BC60(HR+)	13	-3.52	0.09	-2.23	-1.385	-1.82	3.61	-2.401	-1.199	BC60(HR+)	21	-3.19	0.29	-2.035	-0.31	-1.19	3.48	-1.691	-0.6923
BC61(HR+)	15	-7.48	3.06	-0.03	1.42	0.77	10.54	-1.343	1.552	BC61(HR+)	15	-7.48	3.06	-0.03	1.42	0.77	10.54	-1.343	1.552	BC61(HR+)	21	-7.48	1.47	-0.46	0.985	0.24	8.95	-1.251	0.6418
BC62(HER2)	15	-8.27	1.91	-0.23	1.36	0.41	10.18	-2.146	1.193	BC62(HER2)	15	-8.27	1.91	-0.23	1.36	0.41	10.18	-2.146	1.193	BC62(HER2)	21	-7.48	2.35	-0.045	0.97	0.55	9.83	-0.9415	0.9539
BC63(HR+)	15	-5.53	1.43	-0.07	1.15	0.82	6.96	-1.335	1.025	BC63(HR+)	15	-5.53	1.43	-0.07	1.15	0.82	6.96	-1.335	1.025	BC63(HR+)	21	-3.56	1.59	-0.485	0.59	0	5.15	-0.6611	0.4535
BC65(HR+)	15	-1.54	3.87	0.36	2.59	0.76	5.41	0.4103	2.144	BC65(HR+)	15	-1.54	3.87	0.36	2.59	0.76	5.41	0.4103	2.144	BC65(HR+)	21	-4.89	3.85	-2.29	0.63	0.08	8.74	-1.493	0.5491
BC66(HR+)	15	-1.52	4.76	0.88	1.76	1.12	6.28	0.5321	2.231	BC66(HR+)	15	-1.52	4.76	0.88	1.76	1.12	6.28	0.5321	2.231	BC66(HR+)	21	-4.89	3.97	-0.285	1.235	0.56	8.86	-0.5272	1.18
BC68(HR+)	15	-5.53	3.24	-0.49	0.83	0.26	8.77	-1.632	0.9548	BC68(HR+)	15	-5.53	3.24	-0.49	0.83	0.26	8.77	-1.632	0.9548	BC68(HR+)	21	-7.48	1.67	-0.265	1.065	0.15	9.15	-1.125	0.8076
BC69(HR+)	15	-4.27	3.16	0.21	1.67	1.04	7.43	-0.1099	1.715	BC69(HR+)	15	-4.27	3.16	0.21	1.67	1.04	7.43	-0.1099	1.715	BC69(HR+)	21	-4.03	1.97	-0.085	0.72	0.15	6	-0.3726	0.6669
BC70(HR+)	15	-5.53	3.91	-0.36	1.15	0.29	9.44	-1.253	1.189	BC70(HR+)	15	-5.53	3.91	-0.36	1.15	0.29	9.44	-1.253	1.189	BC70(HR+)	21	-4.67	3.02	-0.03	0.495	0.23	7.69	-0.4791	0.6925
BC74(HR+)	15	-13.11	-0.15	-5.74	-1.96	-3.95	12.96	-6.452	-2.582	BC74(HR+)	15	-13.11	-0.15	-5.74	-1.96	-3.95	12.96	-6.452	-2.582	BC74(HR+)	20	-5.32	1.67	-2.698	-0.515	-1.29	6.99	-2.351	-0.8206
BC78(HR+)	15	-3.95	3.56	1.39	3.27	2.24	7.51	0.8144	2.867	BC78(HR+)	15	-3.95	3.56	1.39	3.27	2.24	7.51	0.8144	2.867	BC78(HR+)	21	-7.48	3.9	1.705	2.545	2.31	11.38	0.1737	2.651
BC80(HR+)	15	-5.53	3.76	-1.05	1.91	1.5	9.29	-1.183	1.796	BC80(HR+)	15	-5.53	3.76	-1.05	1.91	1.5	9.29	-1.183	1.796	BC80(HR+)	21	-7.48	2.73	-0.02	1.54	0.53	10.21	-1.083	1.223
BC81(TNBC)	15	-6.09	2.59	-0.05	1.36	0.48	8.68	-1.383	1.386	BC81(TNBC)	15	-6.09	2.59	-0.05	1.36	0.48	8.68	-1.383	1.386	BC81(TNBC)	21	-5.32	3.18	0.83	2.045	1.24	8.5	0.09048	1.904
BC82(TNBC)	15	-2.85	4.25	0.34	2.48	2.05	7.1	0.6467	2.596	BC82(TNBC)	15	-2.85	4.25	0.34	2.48	2.05	7.1	0.6467	2.596	BC82(TNBC)	21	-0.19	4.99	0.21	1.895	0.93	5.18	0.692	1.917
BC88(HR+)	15	-4.49	2.6	-1.02	2.01	-0.2	7.09	-1.48	1.118	BC88(HR+)	15	-4.49	2.6	-1.02	2.01	-0.2	7.09	-1.48	1.118	BC88(HR+)	21	-6.44	2.84	-1.26	0.245	-0.5	9.28	-1.749	0.09642
BC89(HR+)	14	-6.01	2.53	-4.585	-0.4675	-2.9	8.54	-3.996	-1.015	BC89(HR+)	14	-6.01	2.53	-4.585	-0.4675	-2.9	8.54	-3.996	-1.015	BC89(HR+)	21	-4.89	0.64	-1.445	-0.095	-1.05	5.53	-1.525	-0.4046
BC90(HR+)	13	-5.53	-0.5	-3.23	-1.265	-2.31	5.03	-3.127	-1.515	BC90(HR+)	13	-5.53	-0.5	-3.23	-1.265	-2.31	5.03	-3.127	-1.515	BC90(HR+)	21	-3.5	-0.05	-2.515	-1.38	-1.78	3.45	-2.298	-1.484
BC92(HR+)	15	0.4	4.44	1.32	2.23	1.65	4.04	1.353	2.566	BC92(HR+)	15	0.4	4.44	1.32	2.23	1.65	4.04	1.353	2.566	BC92(HR+)	21	-4.44	5.91	1.185	2.125	1.95	10.35	0.8762	2.544
BC94(HR+)	15	-8.27	2.69	-3.18	0	-0.42	10.96	-2.905	0.177	BC94(HR+)	15	-8.27	2.69	-3.18	0	-0.42	10.96	-2.905	0.177	BC94(HR+)	21	-5.32	1.9	-0.44	0.61	0.04	7.22	-1.041	0.6011
BC95(HR+)	15	-8.27	3.93	-0.84	1.25	0.36	12.2	-2.122	1.319	BC95(HR+)	15	-8.27	3.93	-0.84	1.25	0.36	12.2	-2.122	1.319	BC95(HR+)	21	-0.88	3.27	0.06	1.97	1.01	4.15	0.5648	1.688
BC96(HR+)	15	-3.18	3.32	0.91	1.93	1.5	6.5	0.5196	2.092	BC96(HR+)	15	-3.18	3.32	0.91	1.93	1.5	6.5	0.5196	2.092	BC96(HR+)	21	0.2	6.55	1.045	2.21	1.77	6.35	1.288	2.504
BC97(HR+)	15	-3.18	1.33	-1.61	-0.25	-0.9	4.51	-1.498	-0.2954	BC97(HR+)	15	-3.18	1.33	-1.61	-0.25	-0.9	4.51	-1.498	-0.2954	BC97(HR+)	21	-2.53	1.06	-1.92	-0.37	-1.17	3.59	-1.569	-0.7107
BC99(HR+)	15	-3.24	0.14	-3.09	-0.24	-2.17	3.38	-2.406	-0.9967	BC99(HR+)	15	-3.24	0.14	-3.09	-0.24	-2.17	3.38	-2.406	-0.9967	BC99(HR+)	21	-6.05	0.02	-4.16	-2.53	-3.07	6.07	-4.054	-2.677
BC102(HR+)	15	-3.18	1.14	-1.68	-0.21	-0.48	4.32	-1.331	-0.08369	BC102(HR+)	15	-3.18	1.14	-1.68	-0.21	-0.48	4.32	-1.331	-0.08369	BC102(HR+)	21	-1.97	0.91	-1.15	-0.32	-1.01	2.88</		

Table S10. Descriptive statistics of simple logistic regression analysis of differentially expressed proteins in treatment responder and non-responder groups.






	Tamoxifen	Docetaxel				Paclitaxel			Palbociclib			
	CDK6	Caveolin-1	b-Raf-pSer445	CK8/18	Tau-pSer202	Vimentin-pSer56	NF1	GATA3	ER α	HER2	CDK2-pThr160	E-Cadherin-pSer838/840
Best-fit values												
β_0	-2.412	-1.047	-2.026	-0.9766	-2.318	-1.478	-2.71	-1.559	-2.141	-4.158	-2.853	-2.283
β_1	-0.6962	-0.574	-0.7759	0.4319	0.3803	-0.3253	0.7651	0.8498	0.7645	4.283	0.5589	0.6073
X at 50%	-3.464	-1.824	-2.611	2.261	6.094	-4.544	3.542	1.834	2.8	0.9709	5.106	3.759
Std. Error												
β_0	0.7999	0.4884	0.7463	0.5074	0.8766	0.5781	0.9364	0.6658	0.9107	2.906	0.9945	0.8229
β_1	0.3181	0.2512	0.2636	0.2291	0.1808	0.145	0.3106	0.3956	0.3939	3.702	0.234	0.2736
X at 50%	1.408	0.9346	0.7265	1.306	1.778	2.224	0.864	0.7744	0.9501	0.2443	1.301	1.319
95% CI (profile likelihood)												
β_0	-4.432 to -1.120	-2.138 to -0.1641	-3.846 to -0.7921	-2.139 to -0.06383	-4.479 to -0.8688	-2.822 to -0.4622	-5.118 to -1.213	-3.196 to -0.4431	-4.484 to -0.7581	-14.05 to -1.355	-5.492 to -1.296	-4.325 to -0.9220
β_1	-1.570 to -0.1940	-1.139 to -0.1283	-1.393 to -0.3247	0.05950 to 0.9818	0.05628 to 0.7967	-0.6691 to -0.07848	0.2238 to 1.504	0.2120 to 1.825	0.1825 to 1.777	0.8570 to 16.52	0.1507 to 1.128	0.1393 to 1.268
X at 50%	-10.26 to -1.538	-7.251 to -0.3149	-4.628 to -1.293	0.1759 to 15.32	3.438 to 23.33	-17.40 to -1.343	2.159 to 7.748	0.6087 to 6.184	1.340 to 8.557	0.6588 to 2.421	3.069 to 12.26	1.814 to 11.11
Odds ratios												
β_0	0.08968	0.3509	0.1319	0.3766	0.0985	0.2281	0.06651	0.2104	0.1176	0.01563	0.05765	0.102
β_1	0.4985	0.5633	0.4603	1.54	1.463	0.7223	2.149	2.339	2.148	72.48	1.749	1.836
95% CI (profile likelihood) for odds ratios												
β_0	0.01189 to 0.3262	0.1179 to 0.8487	0.02136 to 0.4529	0.1178 to 0.9382	0.01134 to 0.4195	0.05946 to 0.6299	0.005986 to 0.2972	0.04092 to 0.6421	0.01129 to 0.4685	7.894e-007 to	0.004120 to 0.2735	0.01324 to 0.3977
β_1	0.2081 to 0.8236	0.3201 to 0.8796	0.2484 to 0.7227	1.061 to 2.669	1.058 to 2.218	0.5122 to 0.9245	1.251 to 4.502	1.236 to 6.201	1.200 to 5.914	2.356 to 14948598	1.163 to 3.088	1.149 to 3.552
Is slope significantly non-zero?												
Z	2.189	2.285	2.943	1.885	2.104	2.243	2.464	2.148	1.941	1.157	2.389	2.219
P value	0.029	0.022	0.003	0.059	0.035	0.025	0.014	0.032	0.052	0.247	0.017	0.026
Deviation from zero?	Significant	Significant	Significant	Not Significant	Significant	Significant	Significant	Significant	Not Significant	Not Significant	Significant	Significant
Likelihood ratio test												
Log-likelihood ratio (G squared)	8.095	6.646	13.4	5.477	5.38	7.061	8.115	7.79	8.004	13.31	7.511	6.739
P value	0.004	0.01	<.001	0.019	0.02	0.008	0.004	0.005	0.005	<.001	0.006	0.009
Reject Null Hypothesis?	Yes	Yes	Yes	Yes	Yes	Yes	Yes	Yes	Yes	Yes	Yes	Yes
P value summary	**	**	***	*	*	**	**	**	**	***	**	**
Area under the ROC curve												
Area	0.8333	0.7556	0.8722	0.7697	0.7963	0.873	0.8254	0.85	0.8952	0.9095	0.8429	0.7647
Std. Error	0.1374	0.09898	0.07769	0.09002	0.1123	0.07197	0.1048	0.07929	0.06615	0.06314	0.1171	0.151
95% confidence interval	0.5640 to 1.000	0.5616 to 0.9495	0.7199 to 1.000	0.5933 to 0.9462	0.5762 to 1.000	0.7320 to 1.000	0.6199 to 1.000	0.6946 to 1.000	0.7656 to 1.000	0.7858 to 1.000	0.6133 to 1.000	0.4688 to 1.000
P value	0.036	0.03	0.002	0.029	0.033	0.006	0.017	0.011	0.007	0.005	0.019	0.078
Goodness of Fit												
Tjur's R squared	0.4062	0.222	0.4362	0.1655	0.2243	0.2832	0.3125	0.2767	0.2826	0.4946	0.3221	0.3582
Cox-Snell's R squared	0.2511	0.2048	0.37	0.1836	0.2008	0.2301	0.2596	0.2589	0.265	0.4006	0.2509	0.2639
Model deviance. G squared	14.87	29.28	22.52	27.34	21.61	21.54	20.49	20.3	17.45	12.15	17.95	16.84

Appendix III:

Przystal JM, Becker H, Canjuga D, Tsiami F, **Anderle N**, Keller A-L, Pohl A, Ries CH, Schmittnaegel M, Korinetska N, Koch M, Schittenhelm J, Tatagiba M, Schmees C, Beck SC, Tabatabai G. *Targeting CR Alone or in Combination with PD-1 in Experimental Glioma*. *Cancers*. 2021; 13(10):2400.

Article

Targeting CSF1R Alone or in Combination with PD1 in Experimental Glioma

Justyna M. Przystal ^{1,2,†}, Hannes Becker ^{1,2,†} , Denis Canjuga ¹, Foteini Tsiami ^{1,2}, Nicole Anderle ³, Anna-Lena Keller ³ , Anja Pohl ³, Carola H. Ries ⁴, Martina Schmittnaegel ⁴, Nataliya Korinetska ¹, Marilyn Koch ¹, Jens Schittenhelm ^{2,5} , Marcos Tatagiba ^{1,6}, Christian Schmees ³ , Susanne C. Beck ^{1,2} and Ghazaleh Tabatabai ^{1,2,7,*} 

- ¹ Department of Neurology & Interdisciplinary Neuro-Oncology, Hertie Institute for Clinical Brain Research, Center for Neuro-Oncology, Comprehensive Cancer Center, University Hospital Tübingen, Eberhard Karls University Tübingen, 72076 Tübingen, Germany; przystal@kispi.uzh.ch (J.M.P.); hannes.becker@student.uni-tuebingen.de (H.B.); denis.canjuga@gmx.net (D.C.); foteini.tsiami@student.uni-tuebingen.de (F.T.); nataliya.korinetska@med.uni-tuebingen.de (N.K.); Marilyn.Koch@med.uni-tuebingen.de (M.K.); marcos.tatagiba@med.uni-tuebingen.de (M.T.); su.beck@uni-tuebingen.de (S.C.B.)
- ² German Translational Cancer Consortium (DKTK), DKFZ Partner Site Tübingen, 72076 Tübingen, Germany; jens.schittenhelm@med.uni-tuebingen.de
- ³ NMI, Natural and Medical Sciences Institute, University of Tübingen, 72770 Reutlingen, Germany; Nicole.Anderle@nmi.de (N.A.); anna-lena.keller@nmi.de (A.-L.K.); anja.pohl@nmi.de (A.P.); Christian.Schmees@nmi.de (C.S.)
- ⁴ Roche Innovation Center Munich, Oncology Division, Roche Pharmaceutical Research and Early Development, 82377 Penzberg, Germany; riescarola@gmx.de (C.H.R.); martina.schmittnaegel@roche.com (M.S.)
- ⁵ Institute for Neuropathology, University Hospital Tübingen, 72076 Tübingen, Germany
- ⁶ Department of Neurosurgery, University Hospital Tübingen, Eberhard Karls University Tübingen, 72076 Tübingen, Germany
- ⁷ Cluster of Excellence iFIT (EXC 2180) “Image Guided and Functionally Instructed Tumor Therapies”, Eberhard Karls University Tübingen, 72076 Tübingen, Germany
- * Correspondence: ghazaleh.tabatabai@uni-tuebingen.de; Tel.: +49-(0)7071-298-5018; Fax: +49-(0)7071-292-5167
- † Contributed equally to this work.



Citation: Przystal, J.M.; Becker, H.; Canjuga, D.; Tsiami, F.; Anderle, N.; Keller, A.-L.; Pohl, A.; Ries, C.H.; Schmittnaegel, M.; Korinetska, N.; et al. Targeting CSF1R Alone or in Combination with PD1 in Experimental Glioma. *Cancers* **2021**, *13*, 2400. <https://doi.org/10.3390/cancers13102400>

Academic Editors: Donat Kögel, Christel Herold-Mende, Benedikt Linder and Frank A.E. Kruyt

Received: 2 March 2021
Accepted: 10 May 2021
Published: 15 May 2021

Publisher’s Note: MDPI stays neutral with regard to jurisdictional claims in published maps and institutional affiliations.



Copyright: © 2021 by the authors. Licensee MDPI, Basel, Switzerland. This article is an open access article distributed under the terms and conditions of the Creative Commons Attribution (CC BY) license (<https://creativecommons.org/licenses/by/4.0/>).

Simple Summary: Glioblastomas are incurable tumors of the central nervous system. Currently, treatment strategies combine neurosurgical intervention, radiation therapy, and chemotherapy. Yet, clinical experience shows that tumors acquire escape mechanisms. Furthermore, the tumor-associated microenvironment, including macrophages expressing the receptor CSF1R, promote and nourish tumor cells. The so-called PD1/PDL1 axis is a major reason why tumors can grow with a “magic hat”; i.e., unrecognized from the immune system. The aim of our study was to assess treatment strategies that target macrophages in the microenvironment by blocking CSF1R alone or in combination with PD1 blockade. Using an immune competent mouse model and an ex vivo microtumor model using freshly resected glioblastoma material, we observed prolonged survival of treated mice and an improved “attack” of the immune system. We conclude that targeting CSF1R is a promising strategy that should be explored in clinical trials, potentially in combination with PD1 blockade.

Abstract: Glioblastoma is an aggressive primary tumor of the central nervous system. Targeting the immunosuppressive glioblastoma-associated microenvironment is an interesting therapeutic approach. Tumor-associated macrophages represent an abundant population of tumor-infiltrating host cells with tumor-promoting features. The colony stimulating factor-1/ colony stimulating factor-1 receptor (CSF-1/CSF1R) axis plays an important role for macrophage differentiation and survival. We thus aimed at investigating the antiglioma activity of CSF1R inhibition alone or in combination with blockade of programmed death (PD) 1. We investigated combination treatments of anti-CSF1R alone or in combination with anti-PD1 antibodies in an orthotopic syngeneic glioma mouse model, evaluated post-treatment effects and assessed treatment-induced cytotoxicity in a coculture model of patient-derived microtumors (PDM) and autologous tumor-infiltrating lymphocytes (TILs) ex

vivo. Anti-CSF1R monotherapy increased the latency until the onset of neurological symptoms. Combinations of anti-CSF1R and anti-PD1 antibodies led to longterm survivors in vivo. Furthermore, we observed treatment-induced cytotoxicity of combined anti-CSF1R and anti-PD1 treatment in the PDM/TILs cocultures ex vivo. Our results identify CSF1R as a promising therapeutic target for glioblastoma, potentially in combination with PD1 inhibition.

Keywords: CSF1R; PD1; glioblastoma; sequential therapy; immunotherapy

1. Introduction

Glioblastoma is an incurable aggressive primary brain tumor. The median overall survival is still in the range of 1.5 years despite multimodal therapy even in selected clinical trial population [1–5], and 5-year survival rates are only approximately 5% [6]. Glioblastomas efficiently reprogram their microenvironment towards an immunosuppressive milieu [7] by altered surface molecule expressions, e.g., human leucocyte antigen (HLA)-E and lectin-like transcript-1 (LLT-1) [8,9]. Moreover, upregulated signal transducer and activator of transcription 3 (STAT3) induces the production of immunosuppressive cytokines like transforming growth factor (TGF)-beta and interleukin (IL)-6 [10,11]. Consequently, immunotherapeutic strategies aimed at overcoming this glioblastoma-associated immunosuppressive signature are considered promising. Various approaches are currently in clinical development, e.g., peptide vaccination, cellular therapies, and immune checkpoint blockade. Immune checkpoint blockade with antibodies targeting the programmed cell death (PD)1 led to promising results in several metastatic cancers [12]. They act by interfering with the interaction between PD1 and the respective ligands and thereby disrupting the inhibitory effects on T cell-mediated immune reaction [13]. However, PD1 inhibition did not led to the same clinical outcome in glioblastoma. In progressive glioblastoma, nivolumab was not superior compared with bevacizumab (NCT02017717). Investigations of the efficacy of nivolumab in newly diagnosed glioblastoma are currently ongoing (NCT02617589, NCT02667587). Postoperative treatment with PD1 antibody and radiation therapy in *O*⁶-methylguanine DNA methyltransferase (MGMT)-unmethylated newly diagnosed glioblastoma did not improve overall survival compared with radiation therapy and temozolomide (NCT02617589).

A potential strategy for enhancing the efficacy of PD1 in glioblastoma might be the design of rational combination therapies. In melanoma, mining of publicly available transcriptomic data sets indicated a coenrichment of CD8⁺ T cells with colony stimulating factor (CSF)1 and other macrophage-specific markers, which were associated with nonresponsiveness to PD1 blockade [14]. In human gliomas, expression of CSF1 is present in glial fibrillary acidic protein (GFAP)-positive cells [15]. Cultured glioblastoma sphere-forming cells release CSF1 [16]. Moreover, CSF1 has an oncogenic role in gliomagenesis [17]. Yet, a Phase II study investigating the compound PLX3397, an oral small molecule inhibitor targeting CSF1R and KIT, in 37 patients, suggested that the compound is well-tolerated, but monotherapy has no efficacy [18]. The inhibition of CSF1R in a preclinical study using the RCAS-hPDGF-B/Nestin-Tv-a; Ink4a/Arf^{-/-} model led to prolonged overall survival [19]. Moreover, microenvironmental alterations by CSF1R blockade rendered tumor cells susceptible to receptor tyrosine kinase inhibitors dovitinib and vatalinib in preclinical studies [20].

Based on these facts, we hypothesized that CSF1R blockade might be a promising therapeutic strategy, either as monotherapy or in combination with PD1 inhibition [21].

2. Results

2.1. Expression of CSF1R, CD204, CD163, PD1, and PD-L1 in Primary and Progressive Glioblastoma

We investigated paired human glioblastoma samples from primary and subsequent progressive disease for the presence of CSF1R, CD204, CD163, PD1, PD-L1, CD3, CD4, and CD8 (as illustrated in Figure 1). Six patients received radiotherapy only between first diagnosis and progression, and 28 of 34 (82.4%) patients were treated with radiation therapy and concomitant and adjuvant temozolomide [22]. For the analysis of the immunohistochemical stainings, expression levels of tissue-dependent markers were assessed. The expression of all markers was observed in most cases with usually low to intermediate levels (as illustrated in Supplementary Table S2). We used the established immunoreactive score (IRS) to link semiquantitative staining frequency and intensity pattern. IRS calculations demonstrate the presence and strong staining signal particularly of CD204 and CSF1R in both primary and corresponding progressive tissue (as illustrated in Supplementary Figure S1). Highest mean IRS values were observed for tumor-associated macrophages marker CD204 ($\text{mean}_{\text{CD204}}: 7.16$) and T cell marker CD4 ($\text{mean}_{\text{CD4}}: 5.74$). Additionally, the treatment target CSF1R was consistently present ($\text{mean}_{\text{CSF1R}}: 4.57$), and PD1 IRS were rather less seen in this cohort ($\text{mean}_{\text{PD1}}: 0.29$). Furthermore, the frequency of tumor-infiltrating lymphocytes (TILs) and tumor-associated macrophages (TAMs) was stable in progressive compared with that of newly diagnosed tumor tissue.

Inpatient expression patterns reveal rather stable expression of tumoral microenvironmental markers (as illustrated in Supplementary Table S3). As an example, 57.1% and 60% of the samples show the same expression levels for CSF1R and PD1 in primary and recurrent tumor situations (as illustrated in Supplementary Table S3).

Next, we performed correlation analysis of tissue-based parameters. Potential correlation of TAMs and TILs markers were of particular interest to link presence of both compartments inside the tumor microenvironment in newly diagnosed and progressive glioblastoma tissue (as illustrated in Supplementary Figure S2). Strongest positive linear correlation was found between CD204 and PD-L1 (correlation coefficient $r_{\text{recurr}} = 0.843$, $p_{\text{recurr}} < 0.0001$). PD-L1 expression revealed intermediate to strong association with CD163 expression ($r_{\text{prim}} = 0.459$, $p_{\text{prim}} < 0.006$; $r_{\text{recurr}} = 0.643$, $p_{\text{recurr}} < 0.0001$) and CSF1R ($r_{\text{prim}} = 0.492$, $p_{\text{prim}} < 0.005$). CSF1R showed moderate correlation with TAM-marker CD204, too ($r_{\text{prim}} = 0.381$, $p < 0.003$). We detected a correlation between PD1 and CD4 ($r_{\text{prim}} = 0.323$, $p_{\text{prim}} < 0.047$). CD163 revealed intermediate association with CSF1R ($r_{\text{prim}} = 0.492$, $p_{\text{prim}} < 0.005$), as well as with CD4 and CD8 ($r_{\text{prim}} = 0.373$, $p_{\text{prim}} < 0.025$).

T cell specific markers showed either strong or intermediate positive linear correlation; for instance, general T cell marker CD3 correlated with CD4 and CD8 ($r_{\text{prim}} = 0.548$, $p_{\text{prim}} < 0.001$; $r_{\text{recurr}} = 0.569$; $p_{\text{recurr}} < 0.003/0.039$) (as illustrated in Supplementary Figure S2). The remaining subgroups and tissue-dependent markers did not reveal significant effect sizes and correlations.

Taken together, our stainings detected CSF1R and markers for TAM and TILs in newly diagnosed and corresponding progressive glioblastoma samples. Our correlation analysis mainly revealed an association between immunosuppressive signature (PD1 and PD-L1) and TAMs/TILs markers. Our data further suggest that CSF1R and PD1 stainings are comparable (as illustrated in Supplementary Table S2) in newly diagnosed and corresponding progressive disease.

2.2. Monotherapies with PD1 Antibody and CSF1R Antibody Prolong the Latency until the Onset of Neurological Symptoms In Vivo and Lead to an Altered Immune Signature in the Microenvironment

We first investigated the efficacy of monotherapies with PD1 or CSF1R antibody in a syngeneic mouse model. We implanted SMA-560 tumor cells into the right striatum of VM/Dk mice (day 0) and started the treatment on day 14 with the anti-CSF1R antibody 2G2, or the anti-PD1 antibody RMP1.14 or the respective control antibodies. The median survival time in the control group was 18 days, in the anti-CSF1R group 22 days, and in

the anti-PD1 group 23 days (as illustrated in Figure 2A). The survival time refers to the experimental endpoint as outlined in material/methods.

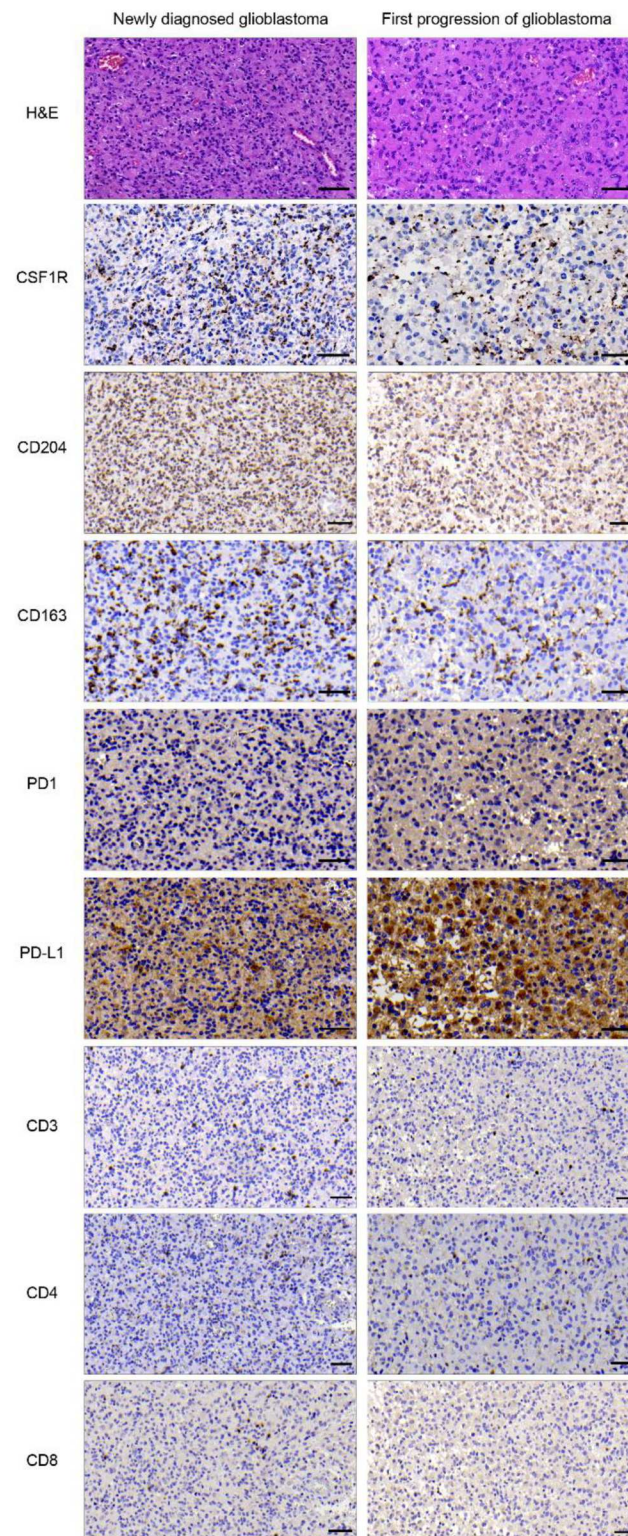


Figure 1. CSF1R and PD1 are present in primary and progressive glioblastoma. Representative tumor areas from matched pairs of newly diagnosed and progressive glioblastoma. H&E staining (top row) and immunohistochemical staining of CSF1R ($n = 28$), CD204 ($n = 27$), CD163 ($n = 31$), PD1 ($n = 30$), PD-L1 ($n = 31$), CD3 ($n = 28$), CD4 ($n = 30$), and CD8 ($n = 28$). Scale bars 50 μm .

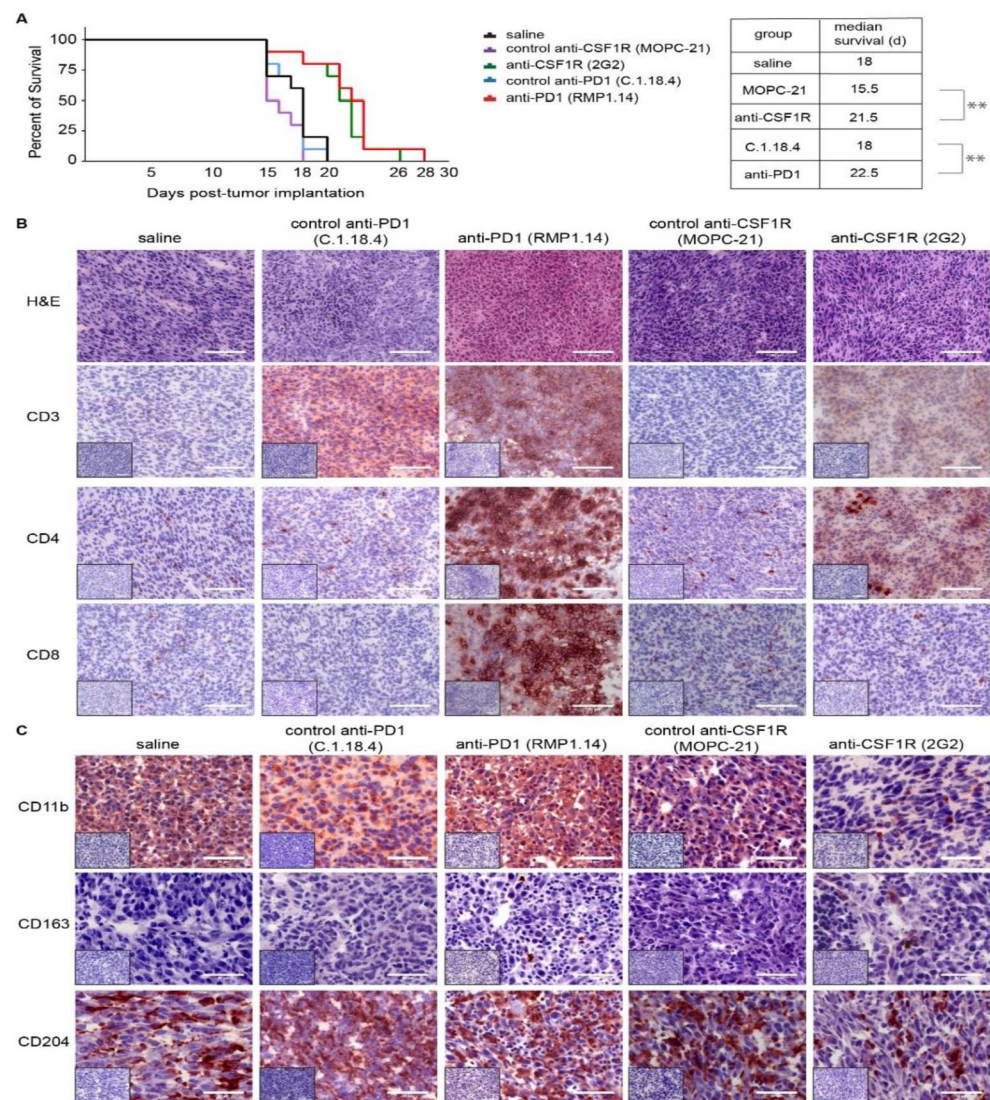


Figure 2. Monotherapies with PD1 and CSF1R blockade in experimental syngeneic SMA-560 glioma in vivo. **(A):** Kaplan–Meier plot showing symptom-free survival. Experimental groups ($n = 10$ in each group) include control treatment (saline), anti-CSF1R (2G2) antibody, anti-PD1 (RPM1.14) antibody, and respective control antibodies. Treatments started on day 14 post-tumor implantation. Tukey–Kramer post hoc test was used after performing Log-rank (Mantel–Cox) test ($p < 0.001$). $** p < 0.001$ Survival time depicted in Kaplan–Meier plot refers to experimental endpoint as described in detail in material/methods section and in Supplementary Table S1. **(B,C):** Immunohistochemical analysis in post-treatment SMA-560 gliomas of one representative animal per group ($n = 1$). Small inserts show staining control without application of primary antibody. (scale bars in **(B)**: 100 μm ; scale bars in **(C)**: 50 μm).

We performed immunohistochemical analyses on post-treatment brains of each experimental group and investigated infiltrations of tumor tissues by T cells and macrophages/microglia using CD3, CD4, CD8 (as illustrated in Figure 2B), CD11b, CD163, CD204 (as illustrated in Figure 2C), and PD1 and PD-L1 (as illustrated in Supplementary Figure S4). In the control (saline treatment) group, CD3, CD4, CD8 stainings revealed decreased staining distribution with only few single positive cells (as illustrated in Figure 2B, first column). Of note, CD11b and CD204 stainings showed strong signals (as illustrated in Figure 2C, first column). This pattern was similar in the control antibody-treated tissues (as illustrated in Figure 2A,B, second and fourth column). In contrast, the tumor tissue after a treatment with the anti-PD1 antibody showed strong stainings for CD3-, CD4-, and CD8-positive cells (as illustrated in

Figure 2B, third column) and unaltered strong CD204 positivity (as illustrated in Figure 2C, third column). The treatment with the anti-CSF1R antibody led to an increase of CD4-positive cells (as illustrated in Figure 2A, last column) and a reduction of CD11b- and CD204-positive cells (as illustrated in Figure 2C, last column).

2.3. Combinations of Anti-CSF1R and Anti-PD1 Antibodies Lead to Longer Term Surviving Animals In Vivo If Applied Simultaneously or Sequentially, but Only If PD1 Blockade Follows CSF-1R Blockade

Next, we investigated the impact of simultaneous and sequential combination treatments in vivo (as illustrated in Figure 3A). Monotherapies with anti-CSF1R, anti-PD1, and respective control antibodies served as control groups in the experimental setup. The survival times refer to the experimental endpoint as outlined above and in Supplementary Table S1. Median overall survival was prolonged with each monotherapy compared with that of the respective control group (as illustrated in Figure 3B).

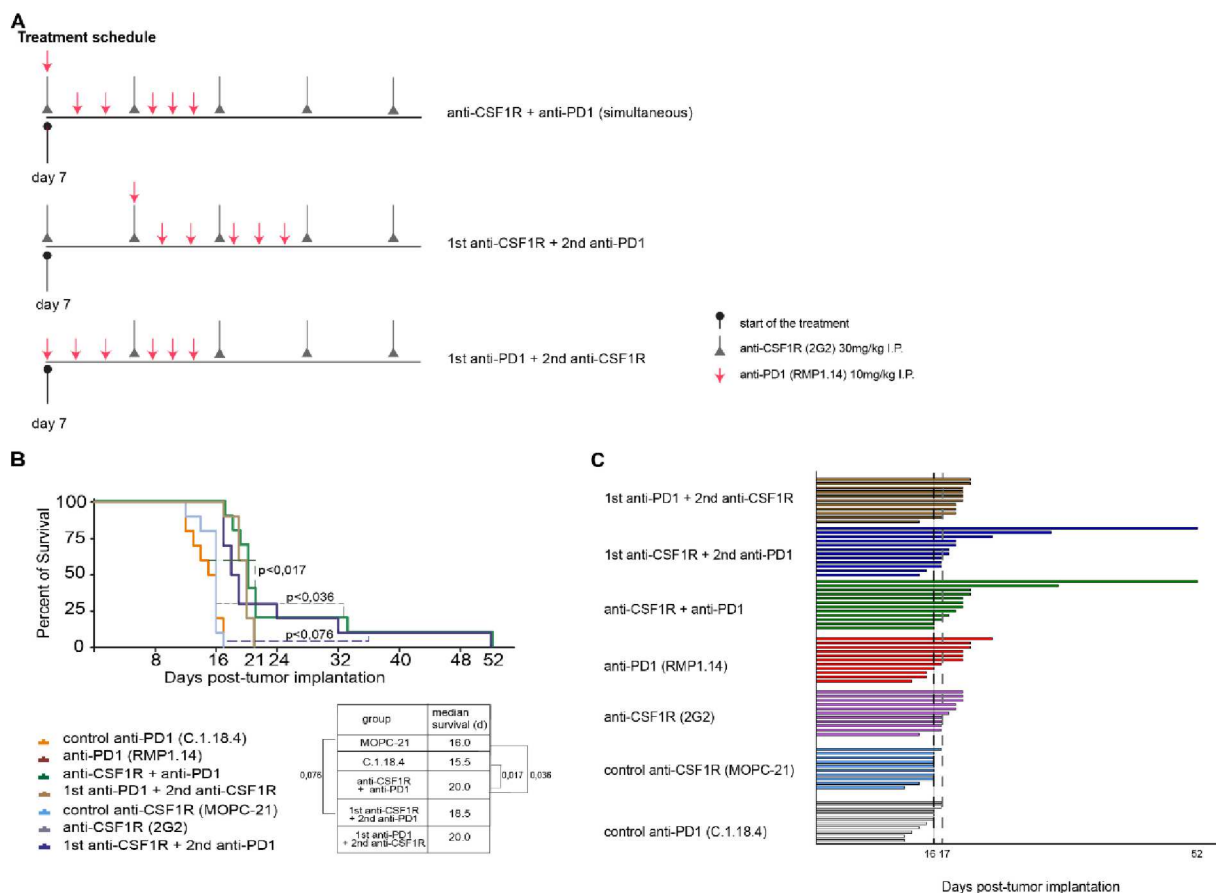


Figure 3. Simultaneous and sequential combinations of PD1 and CSF1R blockade in vivo. (A): Schematic overview of experimental design. (B): Kaplan–Meier plots: combination therapies vs. monotherapies vs. controls. Experimental groups ($n = 10$ in each group) are as indicated: Blue dashed line shows p -value between combination therapy group starting with anti-CSF1R treatment and CSF1R control group. Green dashed lines show p -value between both control groups vs. simultaneous combination group. P-values were calculated by using Tukey–Kramer post hoc test after performing Log-rank (Mantel–Cox) test ($p < 0.0001$). (C): Symptom-free survival graph displaying each single mouse per experimental group. Experimental groups are: control anti-PD1, control anti-CSF1R, anti-PD1, anti-CSF1R, anti-CSF1R plus anti-PD1, anti-CSF1R and then anti-PD1, and anti-PD1 and then 2nd anti-CSF1R. Dashed line on day 16 represents median latency until experimental endpoint in control group. Dashed line on day 17 shows time point where last animal of control group reached experimental endpoint. Day 52 indicates last surviving animals. Experimental endpoints are described in detail in the material/methods section and in Supplementary Table S1.

Simultaneous treatment with anti-CSF1R and anti-PD1 antibody led to a durable tail of longer-term surviving animals. The sequential treatments only led to longer-term surviving animals when anti-CSF1R antibody was administered before anti-PD1 antibody (as illustrated in Figure 3C). The median overall survival, however, was not significantly prolonged.

2.4. Combined Anti-CSF1R and PD1 Antibodies Lead to Decreased CSF1R and Increased CD8/CD4 and CD8/FoxP3 Ratios in Post-Treatment Tissues

To further understand the treatment effects of anti-CSF1R and anti-PD1 antibodies, we investigated the immune signature in post-treatment tissues. First, we investigated the post-treatment immune signature after 2 injections of anti-CSF1R and 3 injections of anti-PD1 antibodies, i.e., around day 10 after the onset of treatment. The analysis of macrophage/microglia markers (as illustrated in Figure 4) revealed a reduction of CD11b- and CD204-positive cells with anti-CSF1R antibody monotherapy and combined treatments.

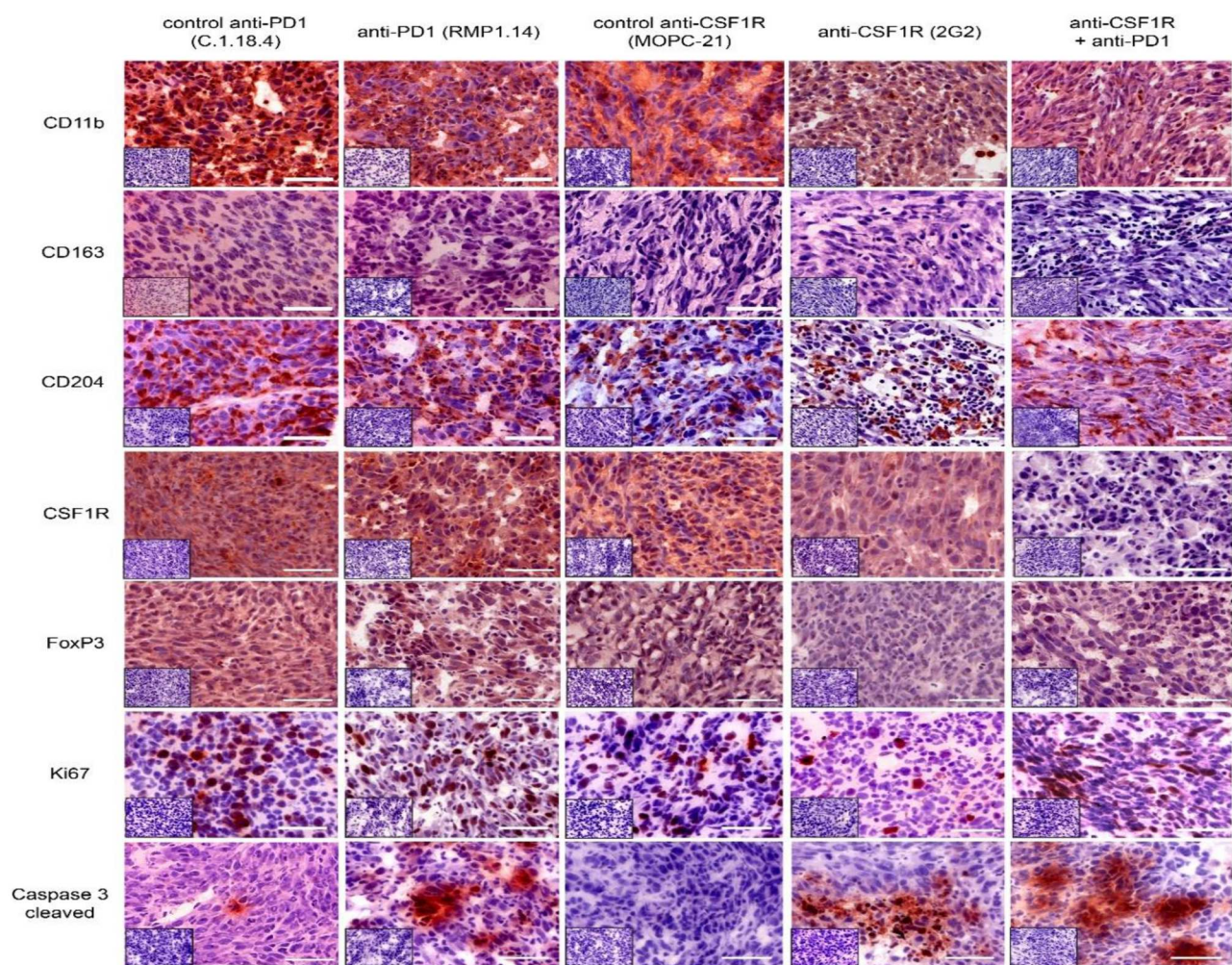


Figure 4. Immunohistochemical analysis in post-treatment tissues ($n = 3$ in each group were analysed). Representative IHC staining patterns of tumor tissues with indicated antibodies after 2 injections of CSF1R antibodies and 3 injections of PD1 antibodies. Small inserts show staining control without application of primary antibody. Scale bars 50 μm .

Of note, the staining intensity of CSF1R was only reduced after anti-CSF1R antibody monotherapy and combined treatments (as illustrated in Figure 4). Ki67 staining did not significantly change after treatments. Treatments with anti-PD1 antibody and anti-CSF1R antibody and their combinations led to a strong signal for cleaved caspase 3. Of note, PD1 and its ligand PD-L1 were present in all treatment groups (as illustrated in Supplementary Figure S4). Quantifications indicated a lack of difference in Ki67 between treatment groups

(as illustrated in Figure 5A), an increase of cleaved caspase 3 after anti-CSF1R monotherapy (as illustrated in Figure 5B), and increased CD8⁺/CD4⁺ ratio and CD8⁺/FoxP3⁺ ratio as monotherapy and in combination with anti-PD1 (as illustrated in Figure 5C-F and Supplementary Figure S3). Moreover, quantification of macrophage/microglia marker showed generally weak CD163 staining signal (as illustrated in Figure 5G) and CD204 reduction after anti-CSF1R monotherapy and after combination therapy with an anti-PD1-antibody (as illustrated in Figure 5H).

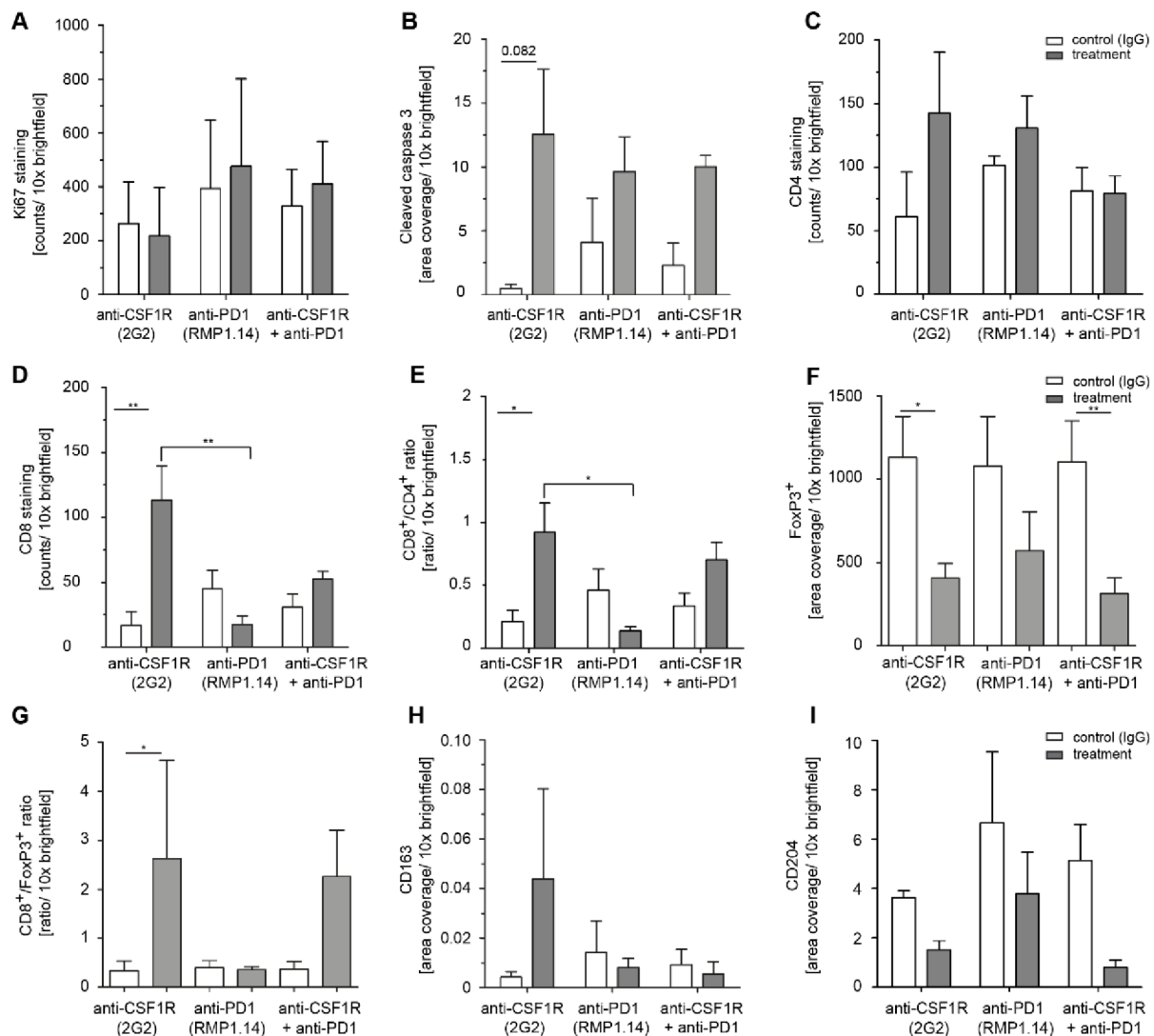


Figure 5. Quantification of Ki67, cleaved caspase 3, CD4, CD8 as well as CD8/CD4, and CD8/FoxP3 ratios in post-treatment tissue. Quantification of Ki67 (A), cleaved caspase 3 (B), CD4 (C), CD8⁺ (D), CD8⁺/CD4⁺ ratio (E), FoxP3⁺ (F), CD8/FoxP3 ratio (G), CD163 (H), and CD204 (I) in tumor tissues after 2 injections of CSF1R and 3 injections of PD1 antibodies. Three animals (n = 3) in each group were analysed. Statistical analysis was done using one-way ANOVA followed by Tukey's multiple comparison test. ** $p < 0.01$, * $p < 0.05$.

We performed a thorough immunohistochemical analysis on post-tumor tissues from simultaneous versus sequential treatments involving CD3, CD4, CD8 (as illustrated in Figure 6A), CD11b, CD163, CD204 (as illustrated in Figure 6B), and PD1, PD-L1 (as illustrated in Supplementary Figure S4). Furthermore, we quantified the effects on CD4 (data not shown), CD8, CD8/CD4 ratio, and CD204 (as illustrated in Figure 6C). Anti-CSF1R alone and in combination with anti-PD1 led to 3-fold and 2-fold increased infiltration with CD8⁺ cells (as illustrated in Figure 6C (1,2)), and 6-fold and 1.5-fold higher CD8/CD4

ratio compared with that of respective IgG controls (as illustrated in Figure 6C(3)). The influx of CD4⁺ cells was similar in all treatment groups compared with that of controls (data not shown). CD204⁺ cells decreased after treatments with anti-CSF1R blockade alone (as illustrated in Figure 6B,C). Of note, the reduction of CD204⁺ cells is particularly pronounced after combined treatments of anti-PD1 and anti-CSF1R blockade (as illustrated in Figure 6B, last row, columns 3–5; Figure 6C (3)). We also observed a decrease in CD204⁺ cells after anti-PD1 blockade alone. Yet, this reduction was significantly lower compared to that of the other treatment groups (as illustrated in Figure 6B,C).

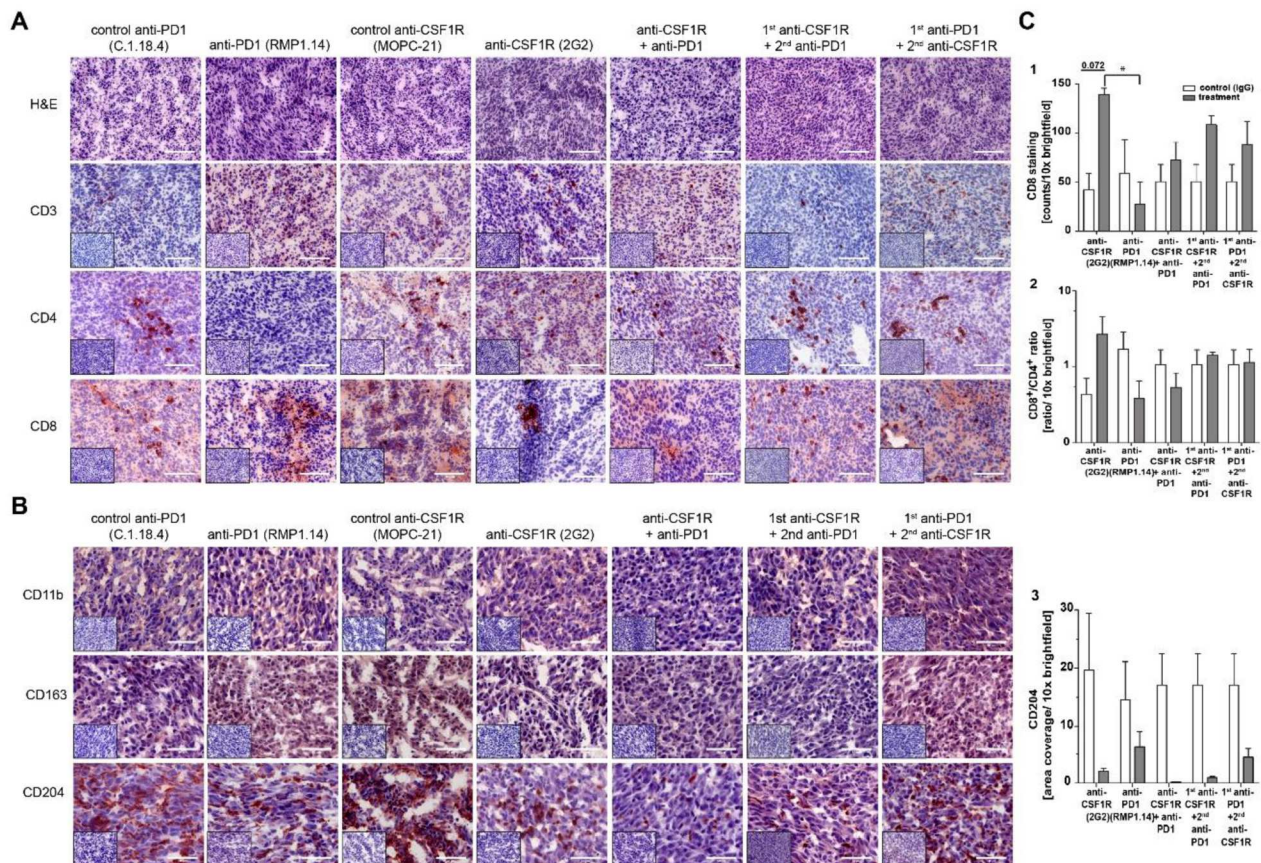


Figure 6. Immunohistochemical analysis of one representative animal per group ($n = 1$) of tumor-infiltrating host cells in simultaneous versus sequential combinations of PD1 and CSF1R blockade in vivo. (A), H&E and immunohistochemical analysis in representative tumor tissues. Scale bar 100 μ m. (B), Immunohistochemical analysis in representative tumor tissues. Scale bars 50 μ m. Small inserts show staining control without application of primary antibody. (C), Quantification of CD8⁺ (1), CD8⁺/CD4⁺ ratio (2), and CD204⁺ (3) cells. For quantification, three tissue samples of different tumor depth per animal were analysed. Statistical analysis was done using one-way ANOVA followed by Tukey’s multiple comparison test. $p < 0.05$.

2.5. Coinhibition of CSF1R and PD1 Enhances Cytotoxicity in Glioblastoma PDM/TILs Co-Cultures Ex Vivo

Based on our results so far, we concluded that anti-CSF1R antibodies reshape the glioma-associated microenvironment by decreasing CD204⁺ cells and increasing the influx of CD8⁺ cells. We aimed at understanding the functional consequence of this observation regarding a combination therapy with anti-PD1 antibody. To this end, we used a patient-derived microtumor (PDM)/ tumor-infiltrating lymphocytes (TILs) coculture model derived from fresh residual tissue of glioblastoma resection by enzymatic tissue digestion (as illustrated in Figure 7B). Isolated autologous TILs were expanded and subsequently used in a coculture experiment with respective PDMs. We further characterized the isolated TILs population by multicolor flow cytometry (as illustrated in Supplementary

Figure S5) and detected CD8 and CD4 positive T cells. Further T cell subpopulations widely expressed T cell activation markers like CD107 or CD137 (as illustrated in Supplementary Figure S5).

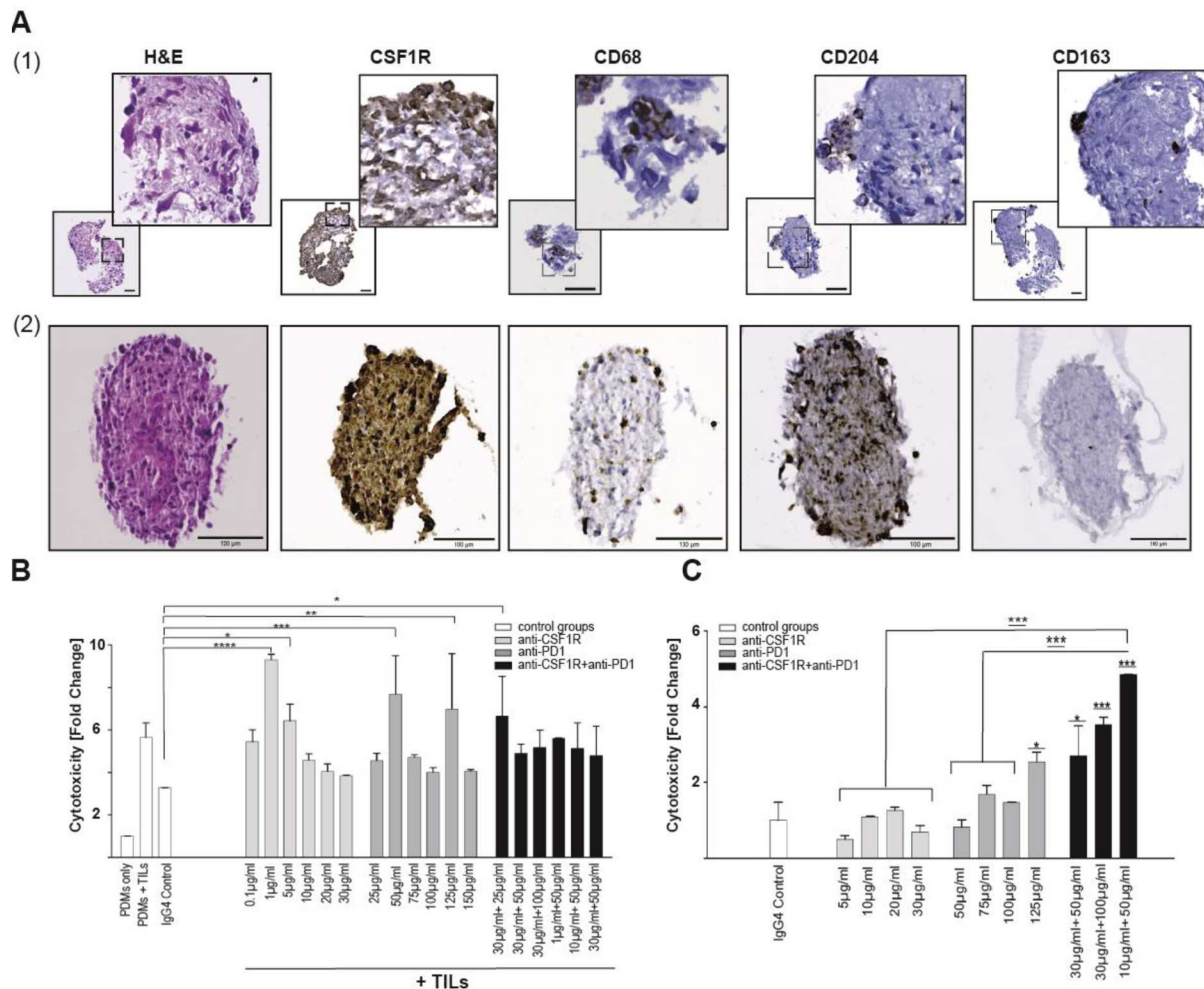


Figure 7. Treatment-induced cytotoxicity in PDMs and PDM/TILs coculture. (A) Immunohistochemistry staining of (1) PDM model 1 and (2) PDM model 2 for markers of macrophages (CD68), tumor-associated macrophages markers (CD204 and CD163), and CSF1R. Scale bars 100 µm. (B) PDM model 1, coculture with autologous TILs, treatments and concentrations as indicated after 72 h ($n = 3$ per concentration). Fold changes were normalized to PDMs only. Two-way ANOVA followed by Dunnett's multiple comparison test was used. PDMs+IgG4-Control served as control group. **** $p < 0.0001$, *** $p < 0.001$, ** $p < 0.01$, * $p < 0.05$. (C): PDM model 2 was treated in the absence of TILs with either CSF1R/PD1 or combination treatments and concentrations as indicated. Cytotoxicity was measured after 72 h. Fold changes were normalized to isotype control; significance above bars refer to control group. Two-way ANOVA followed by Dunnett's multiple comparison test was used. PDMs +IgG4-Control served as control group. *** $p < 0.001$, * $p < 0.05$.

For monotherapies or combination treatments, we used different concentrations of anti-CSF1R [21] and anti-PD1 antibodies and measured the extent of treatment-induced cytotoxicity (as illustrated in Figure 7C). We did not observe any changes in the treatment-naïve control groups, i.e., PDMs only and PDM + TILs (as illustrated in Figure 7B,C). Anti-CSF1R antibody alone led to increased treatment-induced cytotoxicity at 1 µg and 5 µg/mL. Anti-PD1 antibody alone led to increased treatment-induced cytotoxicity at 50 µg/mL and 125 µg/mL (as illustrated in Figure 7B). Using different concentrations for combination treatments, we observed an increased treatment-induced cytotoxicity already with 25 µg/mL anti-PD1 combined with anti-CSF1R. Immunohistochemical staining of

PDM model 1 showed low amounts of infiltrated CD204- and CD163-macrophages together with prominent expression of target protein CSF1R (as illustrated in Figure 7A (1)).

Next, we generated another PDM model (PDM 2) derived from a different tumor sample. Immunohistochemical analysis of PDM model 2 using CSF1R, CD68, CD204, and CD163 revealed the presence of tumor-associated macrophage markers (as illustrated in Figure 7A (2)). Of note, the treatment target CSF1R was strongly present inside PDM 2.

We treated this PDM model 2 without the addition of autologous TILs to investigate the effects of anti-CSF1R and anti-PD1 antibodies on the compartment of tumor-associated macrophages infiltrated into respective PDMs (as illustrated in Figure 7A (2),C).

In contrast to PDM model 1 (as illustrated in Figure 7B), all three tested combination therapy regimes revealed significantly higher cytotoxicity in PDM model 2 (as illustrated in Figure 7C). The most effective treatment regime was the combination of 10 µg/mL anti-CSF1R with 50 µg/mL anti-PD1. It showed significantly higher cytotoxicity compared with vehicle and both monotherapies. Monotherapy with anti-PD1 only led to increased cytotoxicity with the highest anti-PD1 concentration (125 µg/mL) (as illustrated in Figure 7C). Yet, by combining CSF1R and anti-PD1, already low concentrations of both compounds led to an increased cytotoxicity in PDM 2. To further validate this result, we investigated the combination therapy in a third PDM model (PDM model 3, as illustrated in Supplementary Figure S6) with positive immunohistochemical CSF1R staining and moderate presence of further TAM markers (as illustrated in Supplementary Figure S6A). Similar to previously tested PDM models, the combination therapy showed highest cytotoxicity in PDM model 3 (as illustrated in Supplementary Figure S6B).

3. Discussion

Treatment strategies involving targets in the immunosuppressive glioma-associated microenvironment could be a promising strategy to improve the currently available therapeutic options for glioblastoma patients [23]. Glioma-associated macrophages display distinct tumor-promoting features [24] and contribute to resistance in glioma immunotherapy [25]. In melanoma, for example, macrophage-associated markers including CSF1 were associated with nonresponsiveness to PD1 inhibition [14]. Thus, we investigated anti-CSF1R either alone or in combination with anti-PD1 in experimental glioma. A comprehensive immunophenotyping of newly diagnosed versus progressive glioblastoma investigating tumor-infiltrating leukocytes (TILs) and peripheral blood leukocytes demonstrated an exhaustion signature of TILs in progressive glioblastoma [26]. Of note, this study analysed primary and progressive glioblastoma with matching age-related healthy donors. Immunohistochemical staining in matched paired tumor tissues from primary and corresponding progressive glioblastoma from our center indicated that the relevant targets of the anti-CSF1R and anti-PD1 combination regimen, i.e., CSF1R, the macrophage markers CD204, CD163, and PD1 and PD-L1, were present in patient-derived tissue of newly diagnosed and progressive disease (as illustrated in Figure 1, Supplementary Table S2). Our data confirm previous studies that detected these markers in glioblastoma tissue [17,27]; yet, these studies did not investigate potential treatment-associated alterations between newly diagnosed and progressive disease, nor did they correlate the presence of TILs and TAMs inside the tumor microenvironment. In this context, the performed spearman correlation analysis might suggest that mainly the PD1/PD-L1 axis correlates with histological markers for TAMs (CD204/CD163) and TILs (CD4) in primary and recurrent tissue samples. Our findings might further indicate that TILs infiltration remained comparable in newly diagnosed and corresponding progressive tissue in our cohort (as illustrated in Supplementary Table S3), but larger sample studies will be necessary to validate this finding. A noteworthy observation was that the molecular targets of our compounds, i.e., CSF1R and PD-1, were detected in newly diagnosed and progressive glioblastoma (as illustrated in Figure 1). We conclude that a combined targeting of CSF1R and PD1 in future clinical trials might be feasible in newly diagnosed and as well as in RT/TMZ-treated progressive glioblastoma.

Interestingly, CSF1R blockade alone led to a prolonged latency until the onset of neurological symptoms (as illustrated in Figure 2). As indicated by reduced staining distribution in post-treatment tissues from SMA-560 tumors for CSF1R, CD204, and CD11b after CSF1R monotherapy, the target population is efficiently diminished by the anti-CSF1R antibody in our experimental setup (as illustrated in Figure 2). These results are comparable with other studies combining glioma-associated microenvironment targets with an anti-PD1 checkpoint inhibitor. For example, combinations of C-X-C chemokine receptor type 4 (CXCR-4)/ C-X-C chemokine Ligand (CXCL-12)-axis and led to reduced microglial infiltration and improved PD1 efficacy [28].

We observed that combined treatments with CSF1R and PD1 antibodies altered the immune signature in immunohistochemically analysed post-treatment tissues; in particular, increased T cell infiltration and elevated CD8⁺/CD4⁺ and CD8⁺/FoxP3⁺ ratios (as illustrated in Figures 5 and 6). Higher CD8⁺/CD4⁺ ratios were also observed with anti-CXCR4 and anti-PD1 combination [28]. A recent study on 66 patients [29] highlighted molecular determinants of response to nivolumab. One of the features of nonresponding PTEN-mutant tumors was a markedly reduced immune cell infiltration. Thus, the increased immune cell infiltration by anti-CSF1R observed here might indicate a promising signal for improving the treatment efficacy of PD1 inhibition in glioblastoma. Our data interpretation is further supported by a recent study demonstrating that the combination of anti-PD1 and anti-CSF1R antibodies prolonged the survival of BRAFV600E-driven mouse melanoma [14]. The combination of a CSF1R inhibitor and PD1 reversed the development of immune resistance in a dendritic cell vaccination model [30]. Combinations of PD1 antibodies with inhibition of the T cell exhaustion marker LAG-3 or an inhibition of the tryptophan catabolic enzyme IDO showed comparable results, i.e., increased efficacy of anti-PD1 treatment, later onset of neurological symptoms, and recomposition of the tumor associated microenvironment [31,32]. In our combination treatments, we only observed long-term surviving animals after simultaneous combination treatments or in sequential treatments when PD1 blockade followed CSF1R blockade (as illustrated in Figure 3). This might reflect that the CSF1R blockade-mediated reduction of activated macrophages in post-treatment staining contributes to a better efficacy of subsequent PD1 blockade as indicated by a reduction of CD204+ cells in post-treatment tissues (as illustrated in Figure 2, Figures 4–6). Of note, anti-CSF1R also led to increased influx of CD8⁺ cells (as illustrated in Figure 6). This might further contribute to an efficacy of PD1 blockade. Of course, the limitations of these results need to be considered too; we only observed two long-term surviving mice upon sequential treatments with anti-CSF1R followed by PD1 antibodies. This indicates that further underlying factors determine the efficacy of this combination therapy that need to be investigated in more detail in upcoming studies. Yet, our observations in the PDM culture and PDM/TILs coculture model further support the potential of a combined anti-CSF1R and anti-PD1 strategy: a combined inhibition of PD1 and CSF1R enhanced treatment-induced cytotoxicity (as illustrated in Figure 7B) already at a low concentration of 25 µg/mL of anti-PD1, whereas 25 µg/mL of anti-PD1 monotherapy did not lead to increased treatment-related cytotoxicity (as illustrated in Figure 7B).

Taken together, our study indicates that CSF1R inhibition might be a promising therapeutic strategy for clinical translation in glioblastoma. Furthermore, our data indicate that anti-CSF1R antibody might enhance the efficacy of anti-PD1 antibody even at lower concentrations. Thus, for combinations of anti-CSF1R and anti-PD1, it will be necessary to investigate its sequence and dosage in early phase clinical trials. Recent phase I clinical trials using neoadjuvant dosing of PD1 antibody in progressive glioblastoma suggest that the timing of anti-PD1 antibody needs further consideration [33,34]. Thus, a thorough investigation of novel combinatorial approaches, including anti-CSF1R and anti-PD1, in early phase clinical trials will also have to consider their dosage and timing.

4. Materials and Methods

4.1. SMA-560 Cell Implantation into Syngeneic VM/Dk Mice

All animal experiments were performed in accordance with the local authorities and the German laws governing the use of experimental animals. All procedures are approved by The Institute of Animal Welfare and the Veterinary Office at the University of Tübingen and the Regional Council Tübingen. We used the syngeneic SMA-560/VM/Dk mouse model that was described before [35–37]).

Five thousand SMA-560 cells were implanted as described previously [38,39]. In brief, adult mice were anesthetized with 3-component anesthesia (fentanyl, midazolam, and medetomidin) before intracranial injection to the right striatum using a fixed stereotactic apparatus. SMA-560 mouse cells were resuspended in $1 \times$ PBS, and 5×10^3 cells in a volume of 2 μ L were injected into female or male VM/Dk mice. Glioma-bearing mice were randomized to the experimental groups and were carefully monitored and euthanized at the onset of moderate clinical symptoms, which were evaluated according to a defined scoring system that is outlined in detail in Supplementary Table S1.

4.2. Treatment Schedules In Vivo

The CSF1R (2G2), anti-PD1 antibodies and control antibodies (C.1.18.4 and MOPC-21) were provided by Roche Diagnostics (Penzberg, Germany) [21]. Treatments with anti-CSF1R and the control antibody were performed once weekly, 30 mg/kg by intraperitoneal injection. The treatments with anti-PD1 and the control antibody were performed 3 times per week for 2 weeks, 10 mg/kg by intraperitoneal injection.

4.3. Scoring of Experimental Animals

After surgery, the animals were closely monitored, and the clinical symptoms were evaluated according to a defined scoring scheme (Supplementary Table S1). The endpoint of the experiments was set at moderate distress. As soon as moderate clinical symptoms were observed, the experimental animals were euthanized conforming to local standards (Regional Council Tübingen).

4.4. Immunohistochemistry of Murine Tumor Samples

The following antibodies were used: CD3, CD4, CD8, CD11b, CD163, FoxP3, Ki67 (Abcam, Cambridge, UK), CD204 (ThermoFisher, Waltham, MA, USA), and cleaved caspase 3 (Cell Signaling, Frankfurt am Main, Germany). Eight μ m thick sections were prepared using a Leica CM3050S cryostat and stored at -80 °C. Frozen sections were air-dried at room temperature for 10 min, fixed in ice-cold acetone at -20 °C for 10 min or 4% PFA for 15 min. Bloxall (Vector Laboratories, Peterborough, UK) was used to quench endogenous peroxidase activity. Slides were incubated with 10% bovine serum albumin (BSA) in PBS-Tween 0.3% for 1 h at room temperature and then incubated with primary antibody in a humidity chamber overnight at 4 °C. The following day, slides were incubated for 1 h at room temperature with biotinylated secondary antibodies, and positive staining was detected using Vector NovaRED (Vector Laboratories, Burlingame, CA, USA). Stained tissue sections were investigated under Carl Zeiss Axioplan2 Imaging brightfield microscope. Staining analyses and picture processing were performed using Fiji ImageJ (National Institutes of Health, Bethesda, MA, USA).

4.5. Immunohistochemistry of Human Glioblastoma Samples

We obtained the approval by the ethical board of the University Hospital Tübingen (permission number 077/2016BO2). We identified 34 patients who were treated at our Neuro-oncology Centre where samples were available from the newly diagnosed treatment-naïve tissue and from first progression. All samples were classified as glioblastoma, IDH-wildtype, WHO grade IV according to the current WHO classification of central nervous system (CNS) tumors. Formalin-fixed, paraffin-embedded tissue microarray sections were stained for CD3 (1:500, 40 min CC1 pretreatment, clone SP7, ThermoFisher, Waltham,

MA, USA), CD4 (1:2, 24 min CC1, clone SP35, Ventana Medical Systems, Roche Group, Indianapolis, IN, USA), CD8 (RTU, 64 min CC1, clone SP57, Ventana Medical Systems, Roche Group, USA), CD163 (RTU, MRQ-26, Ventana Medical Systems, Roche Group, USA), CSF1R (dilution 1:2500, 32 min CC1, clone 29, Roche Diagnostics GmbH, Penzberg, Germany), PD1 (1:100, 64 min CC2, Clone MRQ-22, Zytomed, Berlin, Germany), PD-L1 (1:100, 64 min CC1, ab205921, Abcam, Cambridge, UK), and CD204 (1:2500, 32 min CC1, HPA000272, Sigma Aldrich, St. Louis, MI, USA) on the Ventana Benchmark XT immunohistochemistry system with a 32 min antibody incubation time each. The slides were scanned at 20x using either the Ventana iScan HT or the Hamamatsu Nanozoomer[®] bright field scanner, and positively stained cells within tumor tissue were evaluated and quantified manually or by a semiautomated staining quantification using ImageJ (National Institutes of Health, Bethesda, MA, USA, <https://imagej.nih.gov/ij1997--2018/>, (accessed on 1 September 2020) as follows: none (<1% positive cells), low ($\leq 25\%$), intermediate ($\leq 50\%$), high ($\leq 75\%$), very high ($>75\%$).

Expression levels (as outlined in Supplementary Table S2) represent stained area percentage of whole tissue cores and were evaluated either manually or by a semiautomated staining quantification using ImageJ. Expression levels were grouped in 4 or 5 interval-based subgroups, groups were represented by values 0 to 4, and mean values were calculated. Additionally, an established immunoreactive score (IRS) was generated (as shown in Supplementary Figure S1). [40,41] The staining intensity of tissue samples was primarily semi-quantitatively scored as 0 (absent staining signal), 1 (weak expression), 2 (moderate expression), and 3 (strong expression). IRS was formed by multiplication of the intensity score and semiquantitative staining quantification (score 0–4, as outlined above). Difference in sample numbers is caused by incomplete transfer of tissue cores on the tissue microarray and number of matched pair sample sets.

4.6. Patient-Derived Microtumors (PDMs) and Tumor Infiltrating Lymphocytes (TILs)

We used fresh residual tumor tissue from glioblastoma resections and generated microtumors. The ethical board of the University Hospital Tübingen approved this study. We kept tumor tissue in DMEM F12 (Sigma Aldrich, St. Louis, MO, USA) plus 1% Primocin (Invivogen, San Diego, CA, USA), and washed samples with Hank's Balanced Salt Solution (HBSS; Thermo Fisher, Waltham, MA, USA). Tissue fragments were crushed into small (1–2 mm) pieces and were washed again. A digestion step was performed using a medium containing 0.28 U/mL Liberase DH (Sigma Aldrich, St. Louis, MO, USA) solution and incubated at 37 °C. Afterwards, the medium was discarded, and samples were washed and sequentially filtered through a stainless-steel wire mesh (500 μm hole size; Fisher Scientific, Waltham, MA, USA) and a 40 μm cell strainer (pluri Select Life Science, Leipzig, Germany). For TILs isolation, single cells of the flow-through were collected and stored in liquid nitrogen.

PDMs were carefully collected and cultured in StemPro[®] hESC SFM medium (Thermo Fisher, Waltham, MA, USA) with bFGF (10 $\mu\text{g}/\text{mL}$; Peprotech, Rocky Hill, NJ, USA) and 1% Primocin (Invivogen, San Diego, CA, USA) at 5% CO_2 and 37 °C. Isolated cells of the flow-through were resuspended for TILs expansion in T cell medium (Advanced RPMI (Sigma Aldrich, St. Louis, MO, USA), containing Glutamine (200 mM; Thermo Fisher, Waltham, MA, USA), 1 \times MEM Vitamins (Thermo Fisher, Waltham, MA, USA), human AB serum (5%; Sigma Aldrich, St. Louis, MO, USA), Primocin (1%; Invivogen, San Diego, CA, USA) containing IL-15 (23.8 U/mL; Peprotech, Rocky Hill, NJ, USA), IL-2 (100 U/mL; Peprotech, Rocky Hill, NJ, USA), IL-7 (10U/mL, Peprotech, Rocky Hill, NJ, USA), and CD3-/CD28-coated magnetic beads (Dynabeads Human T-Activator CD3/CD28, Thermo Fisher, Waltham, MA, USA). TILs were expanded at 5% CO_2 and 37 °C.

PDM viability was assessed by costaining with Calcein-AM (Thermo Fisher Scientific; green channel) for highlighting viable cells and SyTOX Orange (Thermo Fisher Scientific; red channel) for identification of dead cells.

4.7. Flow Cytometry for the Characterization of PDM-Derived TILs

We used FIX&PERM Cell Permeabilization Kit (Thermo Fisher, Waltham, MA, USA) for fixation and permeabilization. TILs immune phenotypes were analyzed on an LSR Fortessa cytometer (Beckton, Dickinson & Company, Franklin Lakes, NJ, USA) using the following antibodies: Anti-CD4-BV510, Anti-CD107a-BV605, Anti-CD8-PerCP/Cy5.5, Anti-CD3-FITC, Anti-CD137-APC/Cy7, and Anti-CD25-Alexa Fluor 700 (all antibodies purchased from BioLegend, San Diego, CA, USA). Data analysis was performed using FlowJo v10.6.2.

4.8. Coculture Cytotoxicity Assay

PDMs were cultured in 96-well plates together with autologous TILs at an effector: target cell ratio of 4:1 with the CellTox™ Green Cytotoxicity Assay reagent (Promega, Madison, WI, USA) [42]. Treatments included anti-CSF1R antibody [21], anti-PD1 antibody (Absource Diagnostics GmbH, Munich, Germany), and the respective human IgG4 isotype control (Invivogen, San Diego, CA, USA) at indicated concentrations and time points (each measured in triplicates). Fluorescence assay signal was measured using a multimode microplate reader (Excitation filter: 485 (20) nm, Emission filter: 535 (20) nm; Tecan, Männedorf, Switzerland). Measured fluorescence units were background corrected and plotted, and the resulting fold change values normalized to isotype treated controls.

4.9. Immunohistochemistry of PDMs

PDMs were isolated as described above (4.6), collected using 40 µm cell strainers (Corning, Glendale, AZ, USA), washed twice in HBSS (Thermo Fisher Scientific), and fixed in 4% phosphate-buffered formaldehyde solution at pH7 (Carl Roth, Karlsruhe, Germany) for 1 h at room temperature. Next, PDMs were stained with hematoxylin (Leica Biosystems, Nußloch, Germany) for 5 min, washed briefly in H₂O, and incubated twice in 50% EtOH and 70% EtOH for 15 min each. PDMs were then embedded into a gel matrix (Richard–Allan Scientific HistoGel, Fisher Scientific, Waltham, MA, USA) using a cryomold (Sakura Finetek, Staufen im Breisgau, Germany) according to manufacturer’s instructions. The gel matrix containing PDMs was stored in 70% EtOH for up to 2 weeks until further processing for immunohistochemistry. For immunohistochemistry analyses, gel-embedded PDMs were embedded into paraffin blocks. 5 µm sections were subjected to H&E staining (Leica Biosystems) as well as IHC staining using a DAB (3,3'-Diaminobenzidine) staining solution (Leica Biosystems). The following antibodies were used for IHC staining of PDM sections: CSF1R (used at 1:200 dilution; Catalog Number: 25949-1-AP, Proteintech, Manchester, UK), MSR1/CD204 (used at 1:1000 dilution; Catalog Number: HPA000272, Atlas Antibodies AB, Bromma, Sweden), CD68 (used at 1:400 dilution, clone D4B9C, Catalog number: 76,437, Cell Signaling Technology, Danvers, MA, USA), and CD163 (used at 1:500 dilution, clone D6U1J, Catalog number: 93,498, Cell Signaling Technology). Stained sections were imaged on an Axio Scan.Z1 Slide Scanner (Carl Zeiss, Oberkochen, Germany) and equipped with an EC Plan-Neofluar 20×/0.5 objective (Carl Zeiss) and a Hitachi HV-F203SCL CCD color camera (Hitachi, Tokyo, Japan).

4.10. Statistics

P values of IHC quantification were generated by using one-way Analysis of variance (ANOVA) with Tukey’s multiple comparison test (GraphPad Prism 9). In *in vivo* survival studies, Kaplan–Meier method (Kaplan–Meier survival fractions) was used to generate *p* values and calculate the Log–rank (Mantel–Cox). Moreover, the Tukey–Kramer post hoc test was used. Error bars represent standard error of the mean (SEM). For the analysis of the immunohistochemical staining, a correlation of tissue-dependent markers was assessed using spearman’s rank correlation. Correlation coefficient *r* was calculated and results showing *r* > 0.30 with related *p*-values were included in Supplementary Figure S2. Effect sizes were interpreted referring to Cohen’s standard, which describes *r* ≥ 0.1 as small association, *r* ≥ 0.3 as moderate association, and *r* ≥ 0.5 as strong association [43].

Statistical significance in the coculture experiment was primarily tested with a two-way ANOVA test followed by an Dunnett multiple comparison test (GraphPad Prism 8).

5. Conclusions

In summary, we report here data for a targeting of anti-CSF1R alone or in combination with anti-PD1 *in vivo* and *ex vivo*. We conclude that our data contribute a novel therapeutic strategy for clinical translation in future early phase clinical trials for glioblastoma patients.

Supplementary Materials: The following are available online at <https://www.mdpi.com/article/10.3390/cancers13102400/s1>, Figure S1: frequency of alternative quantification of human brain tissue samples by a calculated immunoreactive score (IRS); Figure S2: scatter plots outlining statistical correlation analysis of immunohistochemical markers in tissue samples from newly diagnosed and corresponding progressive glioblastoma; Figure S3: immunohistochemical analysis in post treatment tissue (CD3, CD4, and CD8); Figure S4: immunohistochemical analysis of PD1 and PD-L1; Figure S5: PDM morphology and TILs characterization of PDM model 1; Figure S6: treatment-induced cytotoxicity in PDM model 3; Table S1: parameter for scoring of the experimental animals; Table S2: semiquantitative analysis of immunohistochemical staining; Table S3: expression changes between primary and recurrent tumor tissue samples.

Author Contributions: Conceptualization: G.T.; design of animal experiments: J.M.P., S.C.B., G.T.; formal analysis, investigation, and data curation: J.M.P., H.B., D.C., F.T., N.A., A.-L.K., A.P., C.H.R., C.S., M.S., N.K., J.S., M.K., and M.T.; writing—original draft preparation: G.T.; writing—review and editing: all authors; visualization: H.B., J.M.P. with help of J.S. and N.K.; supervision: G.T.; project administration, S.C.B., G.T.; funding acquisition: G.T. All authors have read and agreed to the published version of the manuscript.

Funding: Parts of this research were funded by a research grant from German Scholars Organisation (GSO/EKFS05), by a research grant from Roche Diagnostics, by the Else Kröner Forschungskolleg (2015_Kolleg_14) to G.T., and by the Sigmund–Kiener–Stipendium to H.B. This work received financial support from the State Ministry of Economics, Labor, and Housing Baden-Wuerttemberg (35-4223.10/8, 3-4332.62-NMI/69) and the European Union (EFRE 415-021179.7).

Institutional Review Board Statement: The study was conducted according to the guidelines of the Declaration of Helsinki, and approved by the respective Institutional Review Board and regulatory bodies (i.e., Ethics Committee of the University Hospital Tübingen and the Regierungspräsidium Tübingen), Germany. The protocol codes are 077/2016BO2, approved 07.03.2016 and N14/15, approved 15.02.2016.

Informed Consent Statement: The Ethics Committee approved this study. It involved investigations on archived tumor samples only.

Data Availability Statement: The data presented in this study are available in this article.

Acknowledgments: We thank Heike Pfrommer, Sarah Hendel, and Yeliz Donat for excellent technical assistance.

Conflicts of Interest: J.M.P., H.B., D.C., N.K., J.S., M.T., and S.C.B. declare no conflicts of interest. M.K. received the Scholarship for Interdisciplinary Oncology including accommodation costs from medac GmbH as well as travel and accommodation costs from Roche for neuro-oncology training. C.H.R. is a former Roche employee and an inventor on granted and pending patent applications for therapeutic CSF1R antibodies. M.S. is a current member of Roche Diagnostics GmbH. G.T. reports personal fees from B.M.S., AbbVie, Novocure, Medac, and Bayer, and grants from B.M.S., Novocure, Roche Diagnostics, and Medac outside the submitted work. The funders had no role in the design of the study; in the collection, analyses, or interpretation of data; in the writing of the manuscript, or in the decision to publish the results.

References

1. Stupp, R.; Hegi, M.E.; Mason, W.P.; Bent, M.J.V.D.; Taphoorn, M.J.B.; Janzer, R.C.; Ludwin, S.K.; Allgeier, A.; Fisher, B.; Belanger, K.; et al. Effects of radiotherapy with concomitant and adjuvant temozolomide versus radiotherapy alone on survival in glioblastoma in a randomised phase III study: 5-year analysis of the EORTC-NCIC trial. *Lancet Oncol.* **2009**, *10*, 459–466. [[CrossRef](#)]

2. Gilbert, M.R.; Dignam, J.J.; Armstrong, T.S.; Wefel, J.S.; Blumenthal, D.T.; Vogelbaum, M.A.; Colman, H.; Chakravarti, A.; Pugh, S.; Won, M.; et al. A randomized trial of bevacizumab for newly diagnosed glioblastoma. *N. Engl. J. Med.* **2014**, *370*, 699–708. [[CrossRef](#)] [[PubMed](#)]
3. Gilbert, M.R.; Wang, M.; Aldape, K.D.; Stupp, R.; Hegi, M.E.; Jaeckle, K.A.; Armstrong, T.S.; Wefel, J.S.; Won, M.; Blumenthal, D.T.; et al. Dose-Dense Temozolomide for Newly Diagnosed Glioblastoma: A Randomized Phase III Clinical Trial. *J. Clin. Oncol.* **2013**, *31*, 4085–4091. [[CrossRef](#)]
4. Chinot, O.L.; Wick, W.; Mason, W.; Henriksson, R.; Saran, F.; Nishikawa, R.; Carpentier, A.F.; Hoang-Xuan, K.; Kavan, P.; Cernea, D.; et al. Bevacizumab plus Radiotherapy–Temozolomide for Newly Diagnosed Glioblastoma. *N. Engl. J. Med.* **2014**, *370*, 709–722. [[CrossRef](#)] [[PubMed](#)]
5. Stupp, R.; Taillibert, S.; Kanner, A.; Read, W.; Steinberg, D.M.; Lhermitte, B.; Toms, S.; Idbaih, A.; Ahluwalia, M.S.; Fink, K.; et al. Effect of Tumor-Treating Fields Plus Maintenance Temozolomide vs. Maintenance Temozolomide Alone on Survival in Patients With Glioblastoma: A Randomized Clinical Trial. *JAMA* **2017**, *318*, 2306–2316. [[CrossRef](#)]
6. Ostrom, Q.T.; Gittleman, H.; Liao, P.; Vecchione-Koval, T.; Wolinsky, Y.; Kruchko, C.; Barnholtz-Sloan, J.S. CBTRUS Statistical Report: Primary brain and other central nervous system tumors diagnosed in the United States in 2010–2014. *Neuro-Oncology* **2017**, *19* (Suppl. 5), v1–v88. [[CrossRef](#)]
7. Kurz, S.C.; Wen, P.Y. Quo Vadis—Do Immunotherapies Have a Role in Glioblastoma? *Curr. Treat. Options Neurol.* **2018**, *20*, 14. [[CrossRef](#)]
8. Wischhusen, J.; Friese, M.A.; Mittelbronn, M.; Meyermann, R.; Weller, M. HLA-E Protects Glioma Cells from NKG2D-Mediated Immune Responses In Vitro: Implications for Immune Escape In Vivo. *J. Neuropathol. Exp. Neurol.* **2005**, *64*, 523–528. [[CrossRef](#)]
9. Roth, P.; Mittelbronn, M.; Wick, W.; Meyermann, R.; Tatagiba, M.; Weller, M. Malignant Glioma Cells Counteract Antitumor Immune Responses through Expression of Lectin-Like Transcript-1. *Cancer Res.* **2007**, *67*, 3540–3544. [[CrossRef](#)]
10. Kinjyo, I.; Inoue, H.; Hamano, S.; Fukuyama, S.; Yoshimura, T.; Koga, K.; Takaki, H.; Himeno, K.; Takaesu, G.; Kobayashi, T.; et al. Loss of SOCS3 in T helper cells resulted in reduced immune responses and hyperproduction of interleukin 10 and transforming growth factor- β 1. *J. Exp. Med.* **2006**, *203*, 1021–1031. [[CrossRef](#)]
11. Wei, J.; Barr, J.; Kong, L.-Y.; Wang, Y.; Wu, A.; Sharma, A.K.; Gumin, J.; Henry, V.; Colman, H.; Priebe, W.; et al. Glioblastoma Cancer-Initiating Cells Inhibit T-Cell Proliferation and Effector Responses by the Signal Transducers and Activators of Transcription 3 Pathway. *Mol. Cancer Ther.* **2010**, *9*, 67–78. [[CrossRef](#)]
12. Brahmer, J.R.; Tykodi, S.S.; Chow, L.Q.M.; Hwu, W.-J.; Topalian, S.L.; Hwu, P.; Drake, C.G.; Camacho, L.H.; Kauh, J.; Odunsi, K.; et al. Safety and Activity of Anti-PD-L1 Antibody in Patients with Advanced Cancer. *N. Engl. J. Med.* **2012**, *366*, 2455–2465. [[CrossRef](#)]
13. Ribas, A. Tumor Immunotherapy Directed at PD-1. *N. Engl. J. Med.* **2012**, *366*, 2517–2519. [[CrossRef](#)] [[PubMed](#)]
14. Neubert, N.J.; Schmittnaegel, M.; Bordry, N.; Nassiri, S.; Wald, N.; Martignier, C.; Tillé, L.; Homicsko, K.; Damsky, W.; Hajjami, H.M.-E.; et al. T cell-induced CSF1 promotes melanoma resistance to PD1 blockade. *Sci. Transl. Med.* **2018**, *10*, eaan3311. [[CrossRef](#)] [[PubMed](#)]
15. Bender, A.M.; Collier, L.S.; Rodriguez, F.J.; Tieu, C.; Larson, J.D.; Halder, C.; Mahlum, E.; Kollmeyer, T.M.; Akagi, K.; Sarkar, G.; et al. Sleeping Beauty—Mediated Somatic Mutagenesis Implicates CSF1 in the Formation of High-Grade Astrocytomas. *Cancer Res.* **2010**, *70*, 3557–3565. [[CrossRef](#)] [[PubMed](#)]
16. Wu, A.; Wei, J.; Kong, L.-Y.; Wang, Y.; Priebe, W.; Qiao, W.; Sawaya, R.; Heimberger, A.B. Glioma cancer stem cells induce immunosuppressive macrophages/microglia. *Neuro-Oncol* **2010**, *12*, 1113–1125. [[CrossRef](#)] [[PubMed](#)]
17. De, I.; Steffen, M.D.; Clark, P.A.; Patros, C.J.; Sokn, E.; Bishop, S.M.; Litscher, S.; Maklakova, V.I.; Kuo, J.S.; Rodriguez, F.J.; et al. CSF1 Overexpression Promotes High-Grade Glioma Formation without Impacting the Polarization Status of Glioma-Associated Microglia and Macrophages. *Cancer Res.* **2016**, *76*, 2552–2560. [[CrossRef](#)]
18. Butowski, N.; Colman, H.; de Groot, J.F.; Omuro, A.M.; Nayak, L.; Wen, P.Y.; Cloughesy, T.F.; Marimuthu, A.; Haidar, S.; Perry, A.; et al. Orally administered colony stimulating factor 1 receptor inhibitor PLX3397 in recurrent glioblastoma: An Ivy Foundation Early Phase Clinical Trials Consortium phase II study. *Neuro-Oncology* **2016**, *18*, 557–564. [[CrossRef](#)]
19. Quail, D.F.; Bowman, R.L.; Akkari, L.; Quick, M.L.; Schuhmacher, A.J.; Huse, J.T.; Holland, E.C.; Sutton, J.C.; Joyce, J.A. The tumor microenvironment underlies acquired resistance to CSF-1R inhibition in gliomas. *Science* **2016**, *352*, aad3018. [[CrossRef](#)]
20. Yan, D.; Kowal, J.; Akkari, L.; Schuhmacher, A.J.; Huse, J.T.; West, B.L.; Joyce, J.A. Inhibition of colony stimulating factor-1 receptor abrogates microenvironment-mediated therapeutic resistance in gliomas. *Oncogene* **2017**, *36*, 6049–6058. [[CrossRef](#)]
21. Ries, C.H.; Cannarile, M.A.; Hoves, S.; Benz, J.; Wartha, K.; Runza, V.; Rey-Giraud, F.; Pradel, L.P.; Feuerhake, F.; Klaman, I.; et al. Targeting Tumor-Associated Macrophages with Anti-CSF-1R Antibody Reveals a Strategy for Cancer Therapy. *Cancer Cell* **2014**, *25*, 846–859. [[CrossRef](#)] [[PubMed](#)]
22. Stupp, R.; Mason, W.P.; van den Bent, M.J.; Weller, M.; Fisher, B.; Taphoorn, M.J.B.; Belanger, K.; Brandes, A.A.; Marosi, C.; Bogdahn, U.; et al. Radiotherapy plus Concomitant and Adjuvant Temozolomide for Glioblastoma. *N. Engl. J. Med.* **2005**, *352*, 987–996. [[CrossRef](#)] [[PubMed](#)]
23. Filley, A.C.; Henriquez, M.; Dey, M. Recurrent glioma clinical trial, CheckMate-143: The game is not over yet. *Oncotarget* **2017**, *8*, 91779–91794. [[CrossRef](#)]

24. Szulzewsky, F.; Arora, S.; de Witte, L.; Ulas, T.; Markovic, D.; Schultze, J.L.; Holland, E.C.; Synowitz, M.; Wolf, S.A.; Kettenmann, H. Human glioblastoma-associated microglia/monocytes express a distinct RNA profile compared to human control and murine samples. *Glia* **2016**, *64*, 1416–1436. [[CrossRef](#)] [[PubMed](#)]
25. Zheng, Y.; Bao, J.; Zhao, Q.; Zhou, T.; Sun, X. A Spatio-Temporal Model of Macrophage-Mediated Drug Resistance in Glioma Immunotherapy. *Mol. Cancer Ther.* **2018**, *17*, 814–824. [[CrossRef](#)]
26. Mohme, M.; Schliffke, S.; Maire, C.L.; Rüniger, A.; Glau, L.; Mende, K.C.; Matschke, J.; Gehbauer, C.; Akyüz, N.; Zapf, S.; et al. Immunophenotyping of Newly Diagnosed and Recurrent Glioblastoma Defines Distinct Immune Exhaustion Profiles in Peripheral and Tumor-infiltrating Lymphocytes. *Clin. Cancer Res.* **2018**, *24*, 4187–4200. [[CrossRef](#)]
27. Berghoff, A.S.; Kiesel, B.; Widhalm, G.; Rajky, O.; Ricken, G.; Wöhrer, A.; Dieckmann, K.; Filipits, M.; Brandstetter, A.; Weller, M.; et al. Programmed death ligand 1 expression and tumor-infiltrating lymphocytes in glioblastoma. *Neuro-Oncology* **2015**, *17*, 1064–1075. [[CrossRef](#)]
28. Wu, A.; Maxwell, R.; Xia, Y.; Cardarelli, P.; Oyasu, M.; Belcaid, Z.; Kim, E.; Hung, A.; Luksik, A.S.; Garzon-Muvdi, T.; et al. Combination anti-CXCR4 and anti-PD-1 immunotherapy provides survival benefit in glioblastoma through immune cell modulation of tumor microenvironment. *J. Neuro-Oncol.* **2019**, *143*, 241–249. [[CrossRef](#)]
29. Zhao, J.; Chen, A.X.; Gartrell, R.D.; Silverman, A.M.; Aparicio, L.; Chu, T.; Bordbar, D.; Shan, D.; Samanamud, J.; Mahajan, A.; et al. Immune and genomic correlates of response to anti-PD-1 immunotherapy in glioblastoma. *Nat. Med.* **2019**, *25*, 462–469. [[CrossRef](#)]
30. Antonios, J.P.; Soto, H.; Everson, R.G.; Moughon, D.; Orpilla, J.R.; Shin, N.P.; Sedighim, S.; Treger, J.; Odesa, S.; Tucker, A.; et al. Immunosuppressive tumor-infiltrating myeloid cells mediate adaptive immune resistance via a PD-1/PD-L1 mechanism in glioblastoma. *Neuro-Oncology* **2017**, *19*, 796–807. [[CrossRef](#)]
31. Harris-Bookman, S.; Mathios, D.; Martin, A.M.; Xia, Y.; Kim, E.; Xu, H.; Belcaid, Z.; Polanczyk, M.; Barberi, T.; Theodoros, D.; et al. Expression of LAG-3 and efficacy of combination treatment with anti-LAG-3 and anti-PD-1 monoclonal antibodies in glioblastoma. *Int. J. Cancer* **2018**, *143*, 3201–3208. [[CrossRef](#)]
32. Ladomersky, E.; Zhai, L.; Lenzen, A.; Lauing, K.L.; Qian, J.; Scholtens, D.M.; Gritsina, G.; Sun, X.; Liu, Y.; Yu, F.; et al. IDO1 Inhibition Synergizes with Radiation and PD-1 Blockade to Durably Increase Survival Against Advanced Glioblastoma. *Clin. Cancer Res.* **2018**, *24*, 2559–2573. [[CrossRef](#)] [[PubMed](#)]
33. Schalper, K.A.; Rodriguez-Ruiz, M.E.; Diez-Valle, R.; López-Janeiro, A.; Porciuncula, A.; Idoate, M.A.; Inogés, S.; de Andrea, C.; de Cerio, A.L.-D.; Tejada, S.; et al. Neoadjuvant nivolumab modifies the tumor immune microenvironment in resectable glioblastoma. *Nat. Med.* **2019**, *25*, 470–476. [[CrossRef](#)] [[PubMed](#)]
34. Cloughesy, T.F.; Mochizuki, A.Y.; Orpilla, J.R.; Hugo, W.; Lee, A.H.; Davidson, T.B.; Wang, A.C.; Ellingson, B.M.; Rytlewski, J.A.; Sanders, C.M.; et al. Neoadjuvant anti-PD-1 immunotherapy promotes a survival benefit with intratumoral and systemic immune responses in recurrent glioblastoma. *Nat. Med.* **2019**, *25*, 477–486. [[CrossRef](#)]
35. Sampson, J.H.; Ashley, D.M.; Archer, G.E.; Fuchs, H.E.; Dranoff, G.; Hale, L.P.; Bigner, D.D. Characterization of a Spontaneous Murine Astrocytoma and Abrogation of Its Tumorigenicity by Cytokine Secretion. *Neurosurgery* **1997**, *41*, 1365–1372. [[CrossRef](#)]
36. Serano, R.D.; Pegram, C.N.; Bigner, D.D. Tumorigenic cell culture lines from a spontaneous VM/Dk murine astrocytoma (SMA). *Acta Neuropathol.* **1980**, *51*, 53–64. [[CrossRef](#)]
37. Oh, T.; Fakurnejad, S.; Sayegh, E.T.; Clark, A.J.; Ivan, M.E.; Sun, M.Z.; Safaee, M.; Bloch, O.; James, C.D.; Parsa, A.T. Immunocompetent murine models for the study of glioblastoma immunotherapy. *J. Transl. Med.* **2014**, *12*, 107. [[CrossRef](#)]
38. Miller, J.; Eisele, G.; Tabatabai, G.; Aulwurm, S.; von Kürthy, G.; Stitz, L.; Roth, P.; Weller, M. Soluble CD70: A novel immunotherapeutic agent for experimental glioblastoma. *J. Neurosurg.* **2010**, *113*, 280–285. [[CrossRef](#)]
39. Weller, M.; Tabatabai, G.; Hasenbach, K.; Herrmann, C.; Maurer, G.; Möhle, R.; Marini, P.; Grez, M.; Wick, W. Glioma tropism of lentivirally transduced hematopoietic progenitor cells. *Int. J. Oncol.* **2010**, *36*, 1409–1417. [[CrossRef](#)] [[PubMed](#)]
40. Remmele, W.; Stegner, H.E. Vorschlag zur einheitlichen Definition eines Immunreaktiven Score (IRS) für den immunhistochemischen Östrogenrezeptor-Nachweis (ER-ICA) im Mammakarzinomgewebe (Recommendation for uniform definition of an immunoreactive score (IRS) for immunohistochemical estrogen receptor detection (ER-ICA) in breast cancer tissue). *Pathologe* **1987**, *8*, 138–140.
41. Meyerholz, D.K.; Beck, A.P. Principles and approaches for reproducible scoring of tissue stains in research. *Lab. Invest.* **2018**, *98*, 844–855. [[CrossRef](#)] [[PubMed](#)]
42. Schönholzer, M.T.; Migliavacca, J.; Alvarez, E.; Kumar, K.S.; Neve, A.; Gries, A.; Ma, M.; Grotzer, M.A.; Baumgartner, M. Real-time sensing of MAPK signaling in medulloblastoma cells reveals cellular evasion mechanism counteracting dasatinib blockade of ERK activation during invasion. *Neoplasia* **2020**, *22*, 470–483. [[CrossRef](#)] [[PubMed](#)]
43. Cohen, J. A power primer. *Psychol. Bull.* **1992**, *112*, 155–159. [[CrossRef](#)] [[PubMed](#)]

Supplementary information

Targeting CSF1R Alone or in Combination with PD1 in Experimental Glioma

Justyna M. Przystal, Hannes Becker, Denis Canjuga, Foteini Tsiami, Nicole Anderle, Anna-Lena Keller, Anja Pohl, Carola H. Ries, Martina Schmittnaegel, Nataliya Korinetska, Marilyn Koch, Jens Schittenhelm, Marcos Tatagiba, Christian Schmees, Susanne C. Beck and Ghazaleh Tabatabai

Table S1. Parameter for scoring of the experimental animals.

Parameter	Phenotype	Score
General appearance	Clean skin and orifices, no pain, no weight loss	0
	Slight eye or nose discharge, slight pain, up to 10% weight loss	1
	Sticky eyes, moderate pain, up to 19% weight loss	2
	Cramps, dehydration, strong pain, max. 20% weight loss	3
Behavior and motion activity	Normal spontaneous-explorative behavior, normal activity	0
	Reduced spontaneous-explorative behavior, reduced activity	1
	Strongly reduced spontaneous-explorative behavior, strongly reduced activity	2
	Total inactivity	3
Posture, facial expression and assessment of pain with the "grimace score" (1)	Normal posture, normal facial expression	0
	Slightly hunched back, less than 5 facial attributes with score 1, little pain	1
	Moderately hunched back, grimace score: all facial attributes are moderate, moderate pain	2
	Strongly hunched back, grimace score: all facial attributes are severe, severe pain	3
Neurological symptoms (Behaviour in the cage and on the grid, left paw paralysis)	None	0
	Slight loss-of-balance, occasionally missed steps, slight paralysis	1
	Moderate loss-of-balance, every third step missed, moderate paralysis	2
	Strong loss-of-balance, total inactivity, strong paralysis	3

Table S2. Semi-quantitative analysis of immunohistochemical stainings.

	Newly Diagnosed Glioblastoma		Progressive Glioblastoma	
	N	%	n	%
CSF1R expression	n=28			
none (<1%)	2/28	7.1	2/28	7.1
low ($\leq 10\%$)	12/28	42.9	15/28	53.6
intermediate ($\leq 25\%$)	6/28	21.4	5/28	17.9
high ($> 25\%$)	8/28	28.6	6/28	21.4
Mean value	1.71		1.54	
CD204 expression	n= 27			
none (<1%)	0/27	0	0/27	0
low ($\leq 25\%$)	4/27	11.1	3/27	11.1
intermediate ($\leq 50\%$)	9/27	33.3	9/27	37.3
high ($\leq 75\%$)	8/27	33.3	8/27	25.9
very high ($> 75\%$)	6/27	22.2	7/27	25.9

Mean value		2.67		2.67
CD163 expression	n=31			
none (<1%)	8/31	25.8	2/31	3.2
low (≤25%)	9/31	29.0	17/31	58.0
intermediate (≤50%)	7/31	22.6	9/31	29.0
high (≤75%)	7/31	22.6	3/31	9.7
very high (>75%)	0/31	0	0/31	0
Mean value		1.42		1.45
PD1 expression	n=30			
none (<1%)	20/30	66.7	22/30	76.7
low (≤25%)	9/30	30.0	7/30	23.3
intermediate (≤50%)	1/30	3.3	1/30	0
high (≤75%)	0/30	0	0/30	0
very high (>75%)	0/30	0	0/30	0
Mean value		0.37		0.23
PD-L1 expression	n=31			
none (<1%)	5/31	16.1	1/31	3.2
low (≤25%)	16/31	51.6	17/31	54.8
intermediate (≤50%)	7/31	22.6	11/31	35.5
high (≤75%)	3/31	9.7	2/31	6.5
very high (>75%)	0/31	0	0/31	0
Mean value		1.26		1.45
CD3expression	n=28			
none (<1%)	4/28	14.3	4/28	14.3
low (≤5%)	17/28	60.7	15/28	57.1
intermediate (≤10%)	6/28	25.0	9/28	28.6
high (≤15%)	1/28	0	0/28	0
very high (>15%)	0/28	0	0/28	0
Mean value		1.11		1.14
CD4 expression	n=30			
none (<1%)	3/30	10.0	1/30	3.3
low (≤5%)	5/30	16.7	3/30	10.0
intermediate (≤10%)	9/30	30.0	10/30	33.3
high (≤15%)	6/30	20.0	7/30	23.3
very high (>15%)	7/30	23.3	9/30	30.0
Mean value		2.3		2.67
CD8 expression	n=28			
none (<1%)	5/28	17.9	2/28	7.1
low (≤5%)	17/28	60.7	20/28	71.4
intermediate (≤10%)	6/28	21.4	5/28	17.9
high (≤15%)	0/28	0	1/28	3.6
very high (>15%)	0/28	0	0/28	0
Mean value		1.04		1.21

Table S3. Expression changes between primary and recurrent tumor tissue samples.

Marker	n	Primary > Recurrent		Recurrent > Primary		Equal Expression	
		N	%	n	%	n	%
CSF1R	28	7	25	5	17.8	16	57.1
CD204	27	7	25.6	7	25.6	13	48.1
CD163	30	9	30.0	12	40.0	9	30.0
PD1	30	7	23.3	4	13.3	19	63.3
PD-L1	31	5	16.1	11	35.5	15	48.4

CD3	28	8	28.6	7	25.0	13	46.4
CD4	30	10	33.3	6	20.0	14	46.6
CD8	28	9	32.1	5	17.9	14	50

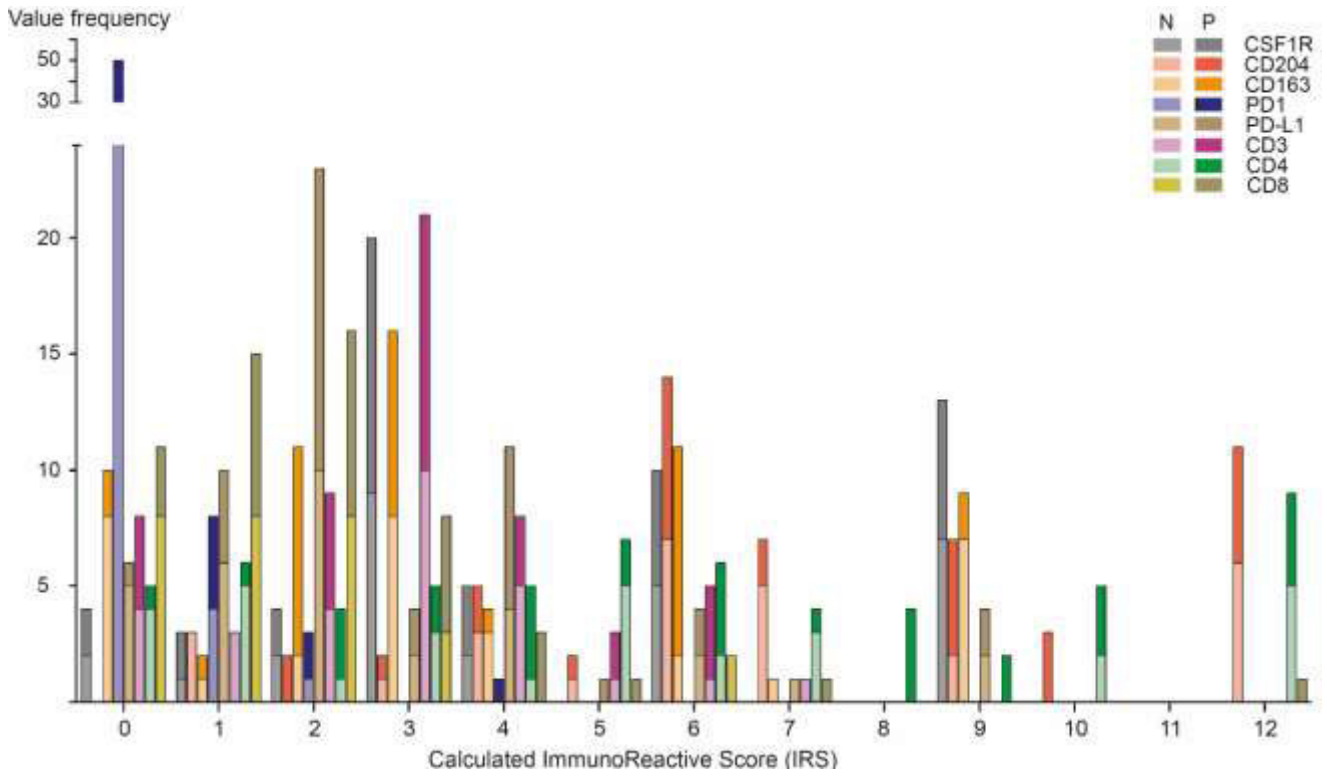


Figure S1. Frequency of alternative quantification of human tissue samples by a calculated immunoreactive score (IRS). IRS was obtained by multiplying staining intensity score with semi-quantitative score of Supplementary table 2 (range 0-12). Frequency of values are shown above. Sample numbers are as indicated in Supplementary table 2. Legend: "N": newly diagnosed Glioblastoma. "P": Progressive Glioblastoma.

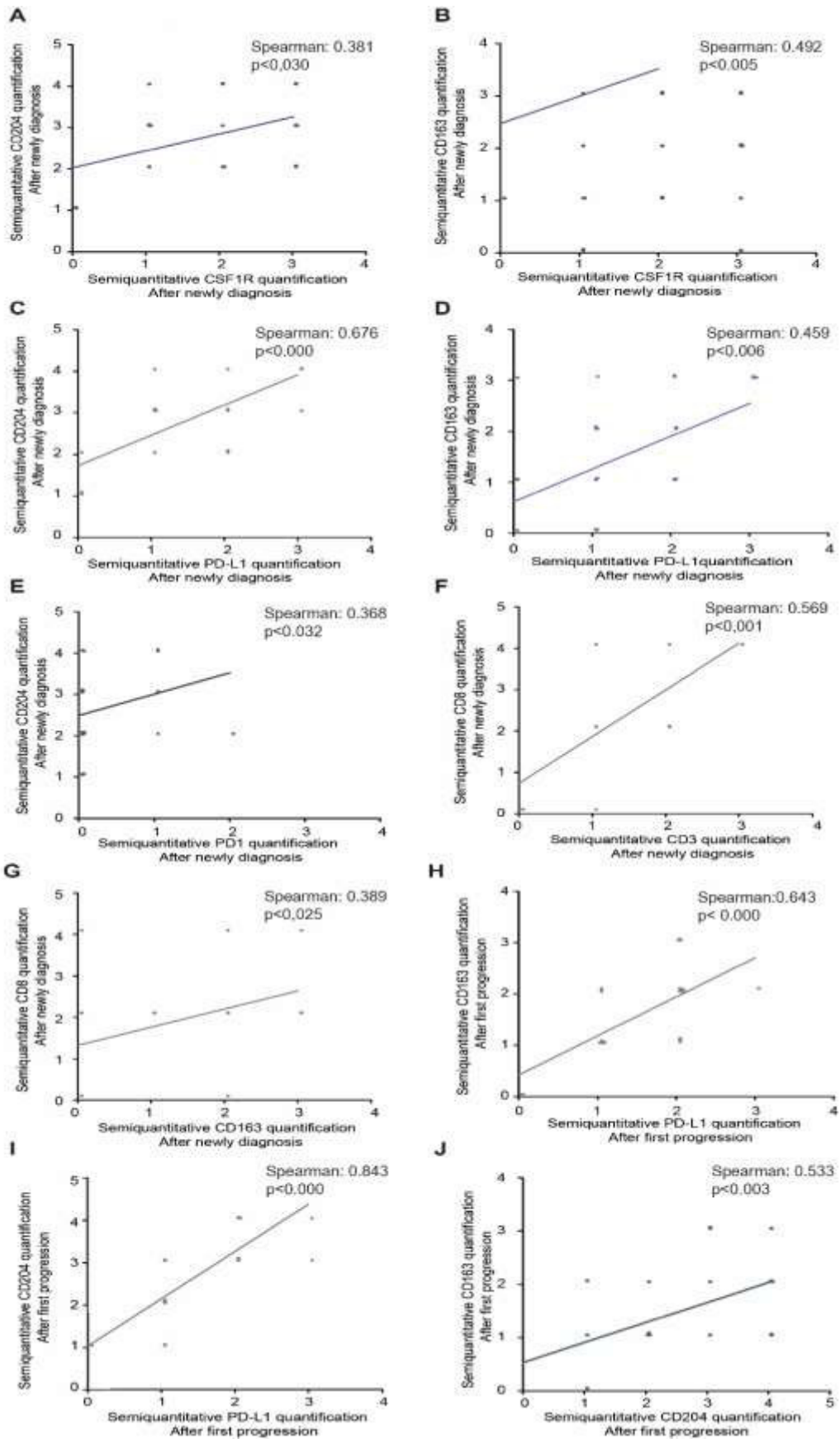
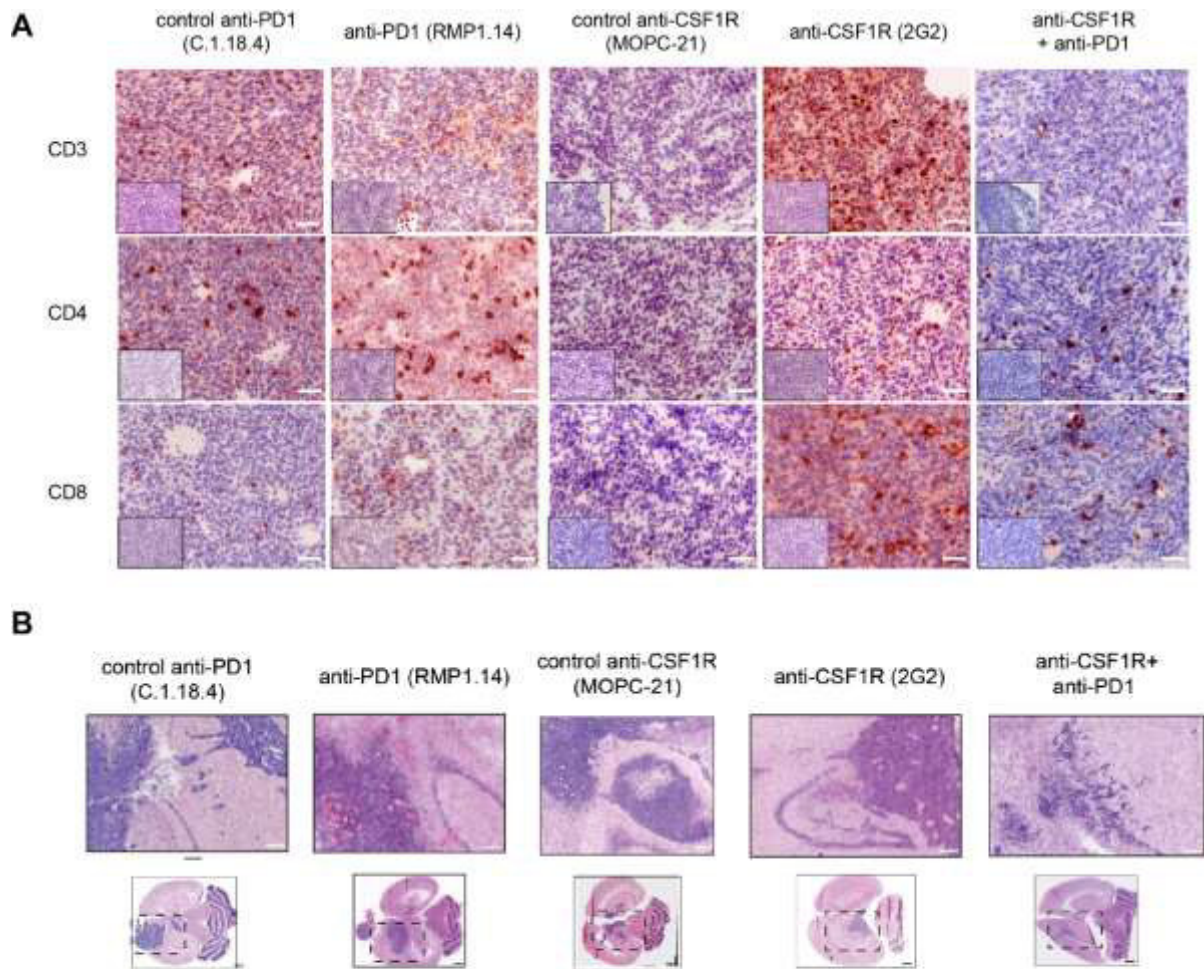


Figure S2. Scatter plots outlining statistical correlation analysis of immunohistochemical markers in tissue samples from newly diagnosed and corresponding progressive glioblastoma. Semiquantitative quantification of CSF-1R and CD204 (A), CSF1R and CD163 (B), PD-L1 and CD204 (C), PD-L1

and CD163 (D), PD1 and CD204 (E), CD3 and CD8 (F), CD163 and CD8 (G) in newly diagnosed glioblastoma. Semiquantitative quantification of PD-L1 and CD163 (H), PD-L1 and CD204 (I), CD204 and CD163 (J) at first progression of glioblastoma. The spearman correlation test was used for this analysis. Spearman correlation coefficient r and additional p -values as indicated. Sample numbers are as indicated in Supplementary table 2.



Sup. Fig.3

Figure S3. (A) Immunohistochemical analysis in post-treatment tissues ($n=3$ in each group were analysed). Immunohistochemical analysis in representative tumor tissues with the indicated antibodies after 2 injections of CSF1R antibodies and 3 injections of PD1 antibodies (as in Figure 4). Small inserts show staining control without application of primary antibody. Scale bars $50 \mu\text{m}$. (B) Whole brain HE sections illustrating the infiltrative growth of the SMA560 model. Sections of exemplary animals, of the respective treatment group as indicated above. Upper image, $5\times$ magnification, scale bar $200\mu\text{m}$. Bottom: overview image, scale bar $1000\mu\text{m}$.

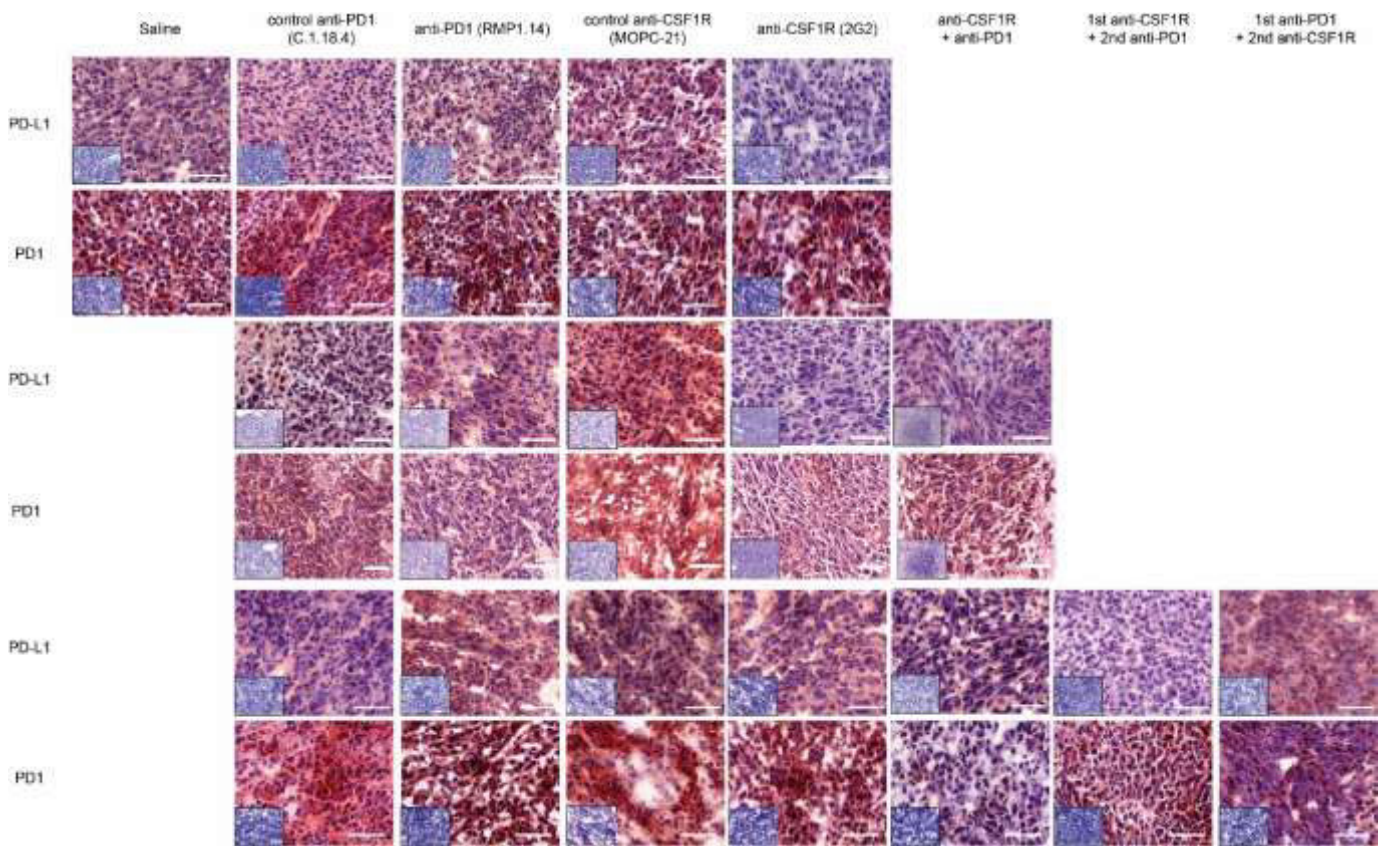


Figure S4. Immunohistochemical analysis of PD1 and PD-L1 expression in post-treatment tissues (in Figures 2, 5 and 6 in the main manuscript). Row 1 and 2, PD-L1 and PD1 expression refer to Figure 2; rows 3 and 4 refer to Figure 4; rows 5 and 6 row refer to Figure 6 (further details are outlined in the text). One animal (n=1) per group was analysed. Small inserts show staining control without application of primary antibody Scale bars 50 μ m.

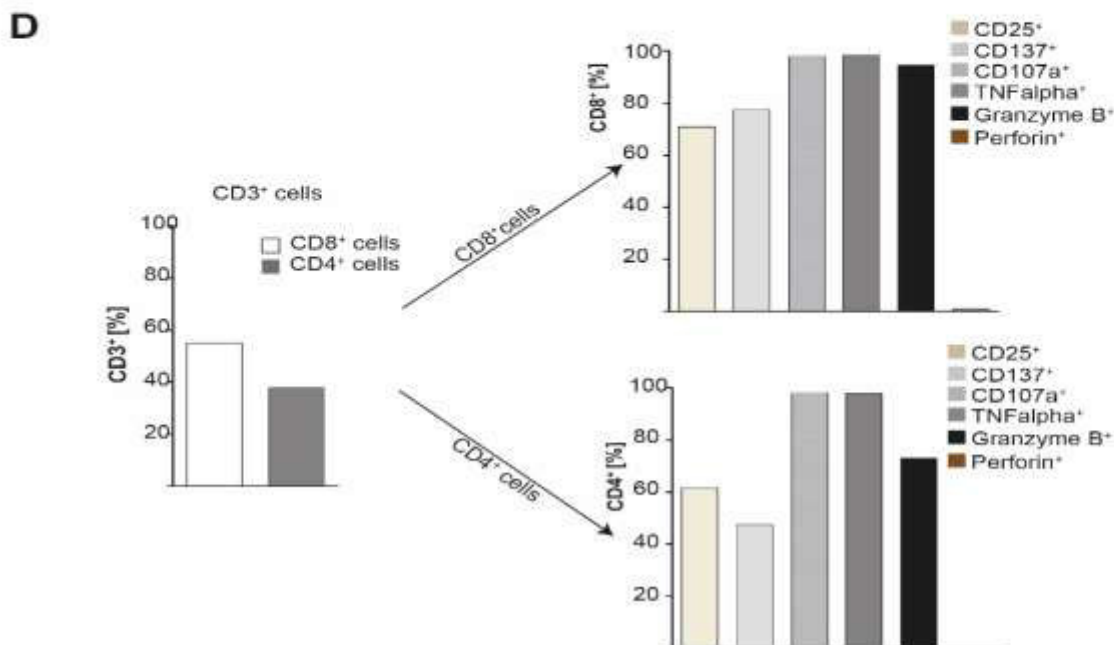
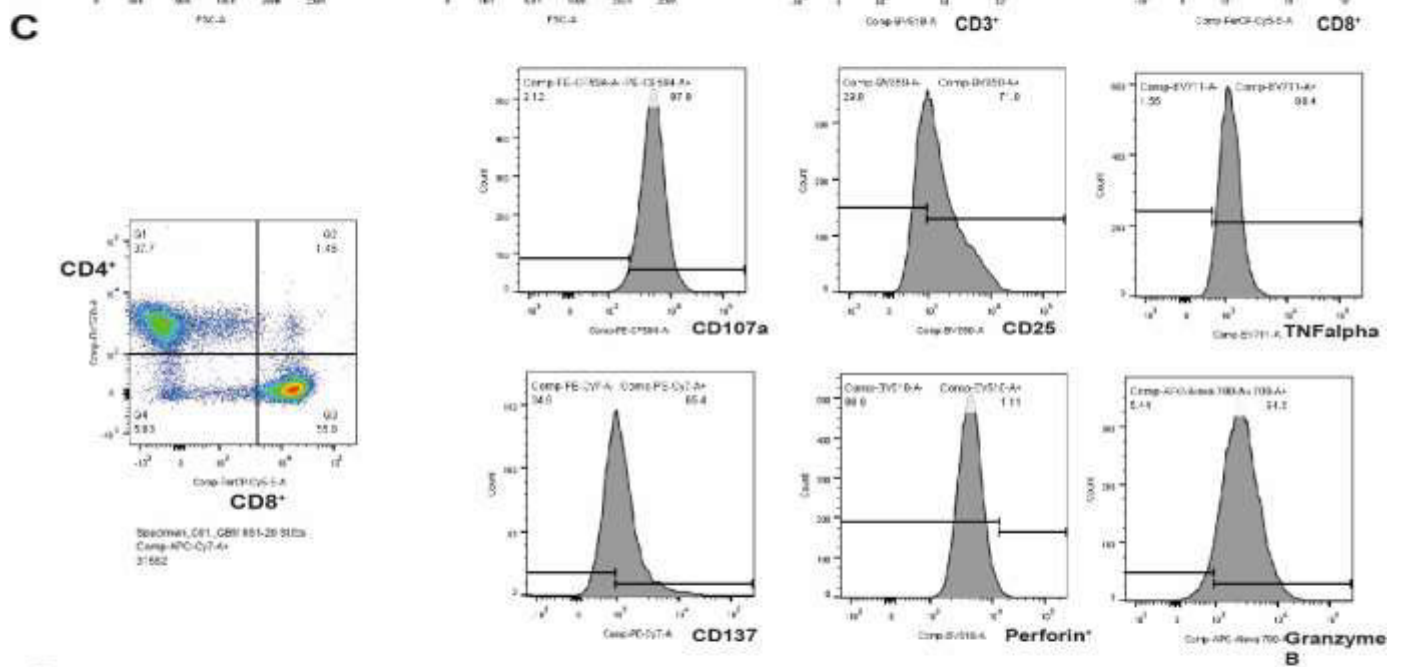
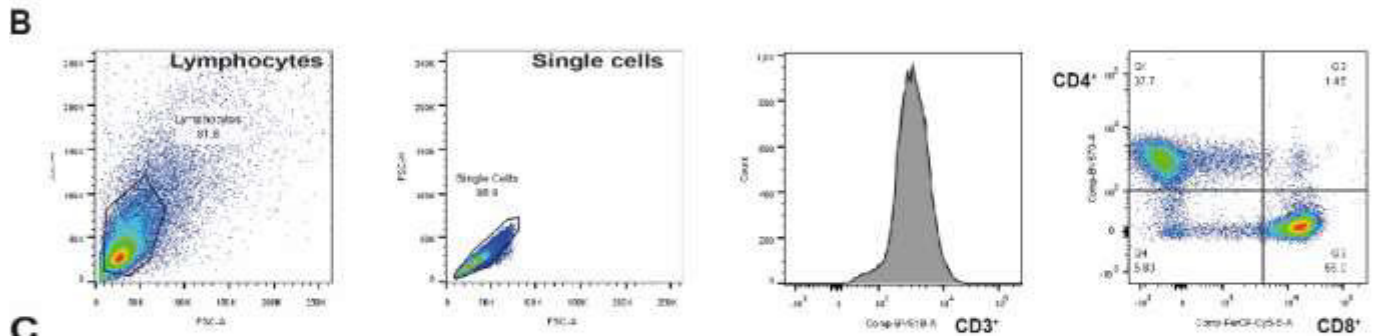
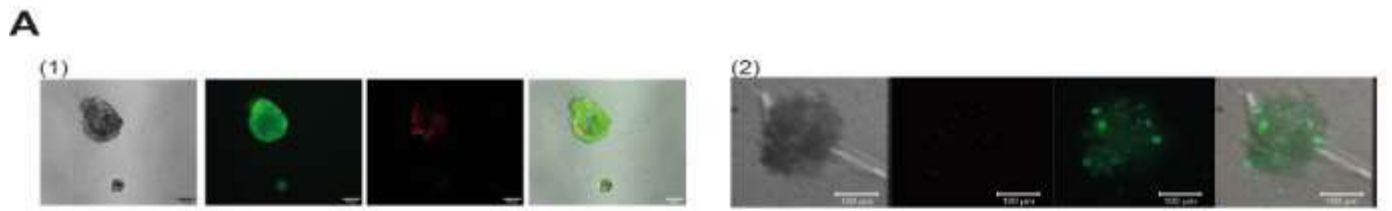


Figure S5. PDM morphology and TIL characterization of PDM model 1. (A) Representative fluorescent pictures highlighting viability of PDM model (1) 1 and (2) 2 following live-dead cell staining with calcein-AM (green channel, viable cells) and SyTOX Orange (red channel; dead cells). Scale bars 200 μ m. (B) T cell gating strategy using multi-color flow cytometry. Exemplary workflow for separating CD4+ and CD8+ cell population is shown. (C) Subpopulations of CD4+ and CD8+ cells are gated for T cell activation markers CD25, CD107a, CD137, Granzyme B and TNF α . (D) Quantification of T cell activation markers, characterizing TIL fraction of PDM model 1.

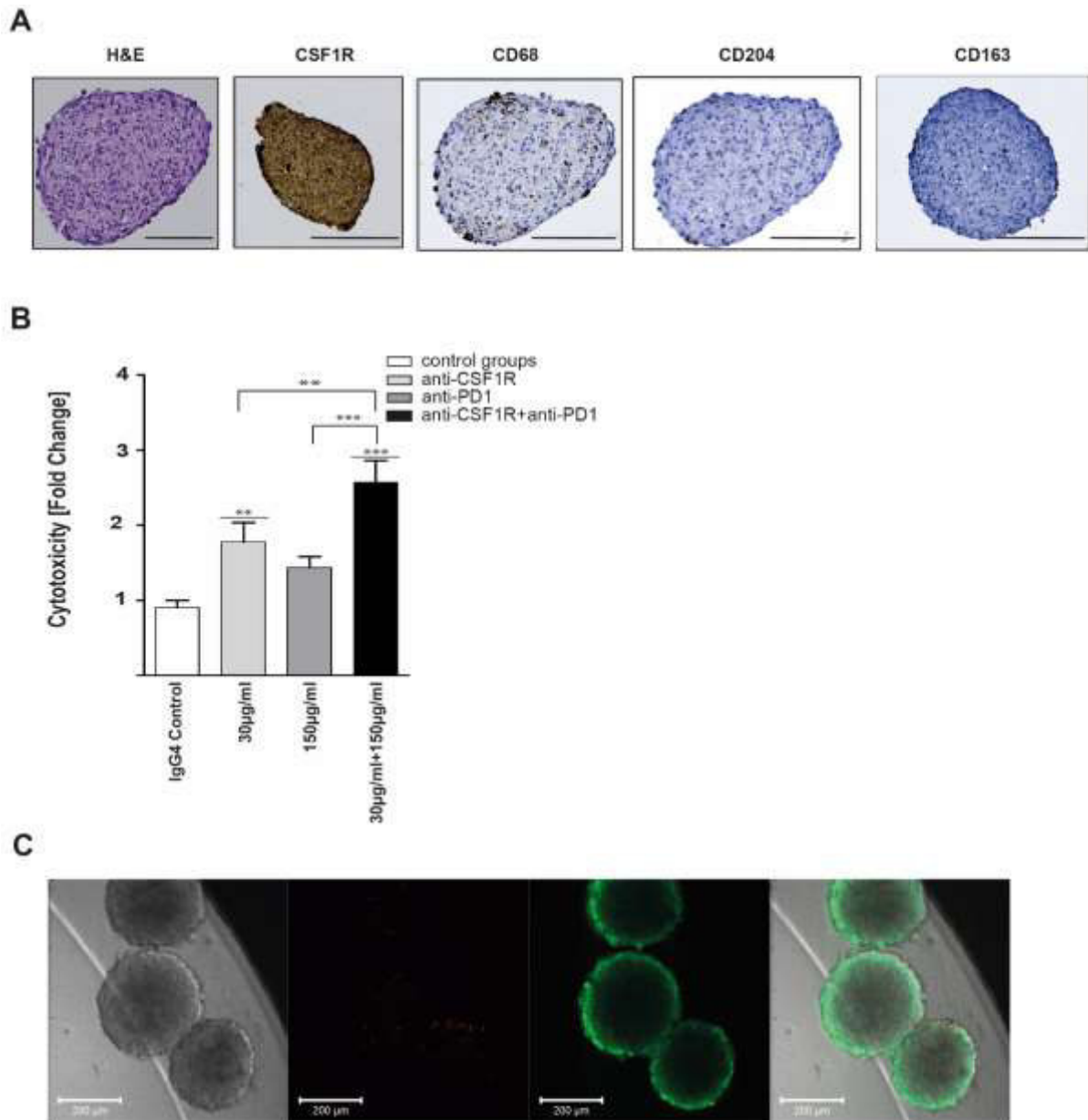


Figure S6. Treatment-induced cytotoxicity in PDM Model 3. (A) Immunohistochemistry staining of PDM model 3 for markers of macrophages (CD68), and tumor-associated macrophages (CD204 and CD163) as well as CSF1R. Scale bars 100 μ m. (B) PDM model 3 was treated in the absence of TILs with either CSF1R/ PD1 or combination, treatments and concentrations as indicated. Cytotoxicity was measured after 72h. Fold changes were normalized to isotype control, significance above bars refer to control group. Two-way ANOVA followed by Dunnett's multiple comparison test was used.

PDMs +IgG4-Control served as control group. ***P<0.001 and **P<0.01. (C) Representative fluorescent pictures of PDM model 3. Live dead cell staining with calcein-AM (green channel, viable cells) and SyTOX Orange (red channel; dead cells). Scale bars 200 μ m.

Reference

1. Langford, D.J.; Bailey, A.L.; Chanda, M.L.; Clarke, S.E.; Drummond, T.E.; Echols, S.; Glick, S.; Ingrao, J.; Klassen-Ross, T.; Lacroix-Fralish, M.L.; et al. Coding of facial expressions of pain in the laboratory mouse. *Nat. Methods* **2010**, *7*, 447–449.